Copolymerization, Aggregation and Thermoreversible Gelation of Polybenzimidazoles

A Thesis Submitted for the degree of

DOCTOR OF PHILOSOPHY

BY
Arindam Sannigrahi

School of Chemistry
University of Hyderabad
Hyderabad-500 046
INDIA

July 2010

Dedicated
to
Ma & Baba

DECLARATION

I hereby declare that the matter embodied in the thesis entitled "**Copolymerization, Aggregation and Thermoreversible Gelation of Polybenzimidazoles**" is the result of investigations carried out by me in the School of Chemistry, University of Hyderabad, Hyderabad, India under the supervision of **Dr. Tushar Jana** and it has not been submitted elsewhere for the award of any degree or diploma or membership, etc.

In keeping with the general practice of reporting scientific investigations, due acknowledgements have been made wherever the work described is based on the findings of other investigators. Any omission or error that might have crept in is regretted.

July 2010   **Arindam Sannigrahi**

UNIVERSITY OF HYDERABAD
Central University (P.O.), Hyderabad-500046, INDIA

Dr. Tushar Jana
Associate Professor
School of Chemistry

Tel: 91-40-23134808 (Office)
           91-9440127016 (Mobile)
Fax: 91-40-23012460
E-mail: tjsc@uohyd.ernet.in
         tjscuoh@gmail.com
Web: http://chemistry.uohyd.ernet.in/~tj/

CERTIFICATE

This is to certify that the work described in this thesis entitled "**Copolymerization, Aggregation and Thermoreversible Gelation of Polybenzimidazoles**" has been carried out by Mr. Arindam Sannigrahi under my supervision and the same has not been submitted elsewhere for any degree.

Dean   **Dr. Tushar Jana**
School of Chemistry   **(Thesis supervisor)**
University of Hyderabad
Hyderabad-500 046
India

PREFACE

The present thesis entitled *"Copolymerization, Aggregation and Thermoreversible Gelation of Polybenzimidazoles"* has been divided into seven chapters. ***Chapter 1*** provides a brief introduction on polybenzimidazoles type of heterocyclic polymers, common synthesis procedure, their various properties and applications. The most advanced application of phosphoric acid doped polybenzimidazole as an electrolyte in high temperature fuel cell application has also discussed. ***Chapter 2*** deals with synthesis and characterization of random polybenzimidazole copolymers consisting of m- and p-phenylene linkage. The architectural effects of dicarboxylic acid monomers on the copolymers properties are also discussed. In ***Chapter 3*** the structural isomeric effect of pyridine based dicarboxylic acid monomers on the copolymerizations of polybenzimidazoles and their properties are investigated. ***Chapter 4*** describes the aggregation behavior of meta-polybenzimidazole (m-PBI) in polar aprotic solvent like DMAc. The thermoreversible gelation of meta polybenzimidazole (*m*-PBI) in phosphoric acid (PA) is studied in ***Chapter 5***. ***Chapter 6*** addresses the thermoreversible gelation of meta polybenzimidazole (*m*-PBI) in phosphoric acid (PA) by varying the gel concentration and the polymer molecular weight. The thermo-mechanical properties and proton conductivities of the *m*-PBI gel membranes are also discussed. ***Chapter 7*** summarizes the findings of the present investigations, presents a concluding remark and the future scope and upcoming challenges.

July, 2010
School of chemistry,
University of Hyderabad   **Arindam Sannigrahi**
Hyderabad 500 046, India

Acknowledgement

July 2010   **Arindam Sannigrahi**
University of Hyderabad,
Hyderabad-500 046
India

Common Abbreviations

DSC	differential scanning calorimeter
DMSO	dimethyl sulphoxide
DMAc	N,N-dimethylacetamide
DMF	N,N-dimethylformamide
DMA	dynamic mechanical analyzer
FTIR	fourier transform infrared spectroscopy
IPA	isophthalic acid
NMR	nuclear magnetic resonance
M_n	number average molecular weight
M_w	weight average molecular weight
NMP	N-methyl-2-pyrrolidone
MEA	membrane electrode assembly
PA	phosphoric acid
PBI	polybenzimidazole
PDA	pyridine dicarboxylic acid
PVDF	poly (vinyledene fluoride)
PEMFC	polymer electrolyte membrane fuel cell
SEM	scanning electron microscopy
Tg	glass transition temperature
TAB	$3, 3^{'}, 4, 4^{'}$ – tetraaminobiphenyl
TGA	thermogravimetric analyzer
t	time
T	temperature
TEM	transmission electron microscopy
TPA	terephthalic acid
XRD	X-ray diffraction
Φ_f	fluorescence quantum yield

CONTENTS

xiii

Chapter 1

Introduction

1.1. Heterocyclic Polymers

Aromatic heterocyclic polymers were introduced at the beginning of 1960s in order to fulfill the thermal stability requirement for heat-resistant plastic for high temperature and military applications. Aromatic heterocyclic polymers have conjugated rigid structure with high glass transition temperature, strong linkages and display high resistance towards harsh environments owing to their aromatic and heterocyclic ring structures. Several varieties of these types of polymers were discovered during 1960-1972 and many reviews were published in the literature discussing mainly the synthesis and heat resistances properties.[1-3] The presence of direct linkage between the aromatic and heterocyclic ring nuclei makes the polymer chain very rigid which ensures the high glass transition temperatures (T_g) and leads to high mechanical strength at elevated temperature.[1] Due to presence of hetero aromatic nuclei, these polymers have high binding energy so that the macromolecules are very resistant towards chemical agents.[2] Depending on the more or less symmetrical structure of the heterocyclic macromolecules, it is possible to obtain crystalline or amorphous polymer. High glass transition temperature and poor solubility due to the rigid hetero aromatic structure of these types of polymers are the most frustrating drawbacks for their uses. Polyquinoline, polybenzimidazole (PBI), polybenzoxazoles and polybenzothaiazole etc. are the most important class of aromatic heterocyclic polymers. These types of polymer are most important for the practical application in numerous fields which include high temperature application, structural application, composite preparation, electrical, electronic and electro-optic applications.

1.2. Brief History of Polybenzimidazoles (PBIs)

In the middle of twentieth century, the U.S Air Force and NASA were looking for suitable materials for drogue chutes which could tolerate extreme high temperature and retain their mechanical strength over wide range of temperature. Hence a massive search begins for suitable materials concentrating mainly on the aromatic heterocyclic condensation polymers due to their valuable engineering properties such as flame retardation, radiative stability, excellent mechanical, thermal stabilities, strength

retention over wide range of temperatures, toughness, chemical inertness and adhesion characteristics. The finding came to the end in 1961 when Marvel and Vogel at the University of Illinois developed aromatic heterocyclic polybenzimidazoles (PBIs).[4-7] The exceptional thermal and oxidative stabilities and inherent nonflammability properties put them in a separate class in high temperature resistant polymer inventory. Polybenzimidazoles are   class of linear aromatic heterocyclic polymers with benzimidazole as a repeating unit which exhibit excellent thermal stability, resistance to chemicals.[4,5] Polybenzimidazoles from   3,3',4,4'-tetraaminobiphenyl and aliphatic diacids or derivatives were first appeared in U.S patent by Brinker and Rabinson in 1959.[8] One year later fully aromatic PBI having excellent thermal and chemical stabilities than aliphatic PBI was reported by Carl S. Marvel, one of the foremost researcher in the field of heterocyclic polymer chemistry.[4] The fundamental research work on these polymers in the early stage of development was carried out in Dupont and Hoechst Celanese Research Co by NASA and U.S. Air Force Materials Laboratory. Before the 1980s, the majority of PBI applications were restricted on fire-blocking applications, thermal protective clothing, high temperature matrix resins and reverse osmosis membranes. After the accident happened in Apollo space mission in which three astronauts died in flash fire, NASA and the U.S. Air Force strongly promoted the use of PBI textile fibers for making the garments for astronauts, fighter pilots and aerospace cabin accessories.[9-11] Polybenzimidazole with meta phenylene linkage, poly[2,2'-(m-phenylene)-5,5'-bibenzimidazole] was commercialized for the first time in the year 1983 by Celanese for the use in wide range of textile fibers and the fiber made from this polymer was trade marked as "**PBI**". In 1980s the low molecular weight PBI was marketed under the name of "**Celazole®**" as molding resins. The high performance PBI textile fibers have been used for several decades for high comfort, nonflammable fabrics used for protective clothing for astronauts and pilots flight suits, firemen clothing, gloves and protective layer for aircraft seats. Due to its outstanding applications in various fields the general chemistry of PBI and the development of different polybenzimidazole polymers have gained enormous interests and reviewed by many researchers.[4-7, 9-18]

1.3. Polybenzimidazole Synthesis Methods

Polybenzimidazoles are class of high-performance aromatic heterocyclic polymers with benzimidazole repeating units, generally synthesized by condensation reaction of utilizing aromatic bis(o-diamine)s and difunctional acids or its derivatives or by nucleophilic substitution reaction of AB type monomers.[4,5,9,13] The polycondensation reactions were generally carried out in two stages, under nitrogen atmosphere by taking equimolar amount of tetraamine with diphenyl isophthalate, isothalic acid, dimethyl isophthalate or isophthalonitrile followed by second stage heating of the solid prepolymer at an elevated temperature.[17,18] However, this procedure is inconvenient due to the formation of prepolymer in the 1st stage heating which has to be pulverized and discharged immediately before the second stage heating. A single stage molten polycondensation of 3,3',4,4'-tetraaminobiphenyl with diphenyl isophthalate or isopthalic acid was also reported by Choe et al. to synthesize high molecular weight PBI.[19] Polybenzimidazoles can also be synthesized by using two-stage solution polymerization technique in degassed phenol, veratrol, N, N-dimethylaniline and various amide solvent such as N, N-dimethylacetamide, N, N-dimethylformamide etc.[20-22] Currently the most widely used solvent for the production of PBIs is polyphosphoric acid (PPA) where PPA is being used as a solvent as well as condensing agent. Out of different types of polybenzimidazoles, most attention has been focused on poly [2,2'-(m-phenylene)-5,5'-bibenzimidazole] (meta-PBI or *m*-PBI here after) over last four decades. This is the only polybenzimidazole which has been commercialized by Hoechst Celanese Corporation under the trade name of PBI and extensive study was carried out on this polymer because of its unique characteristics like thermal and chemical stability, nonflammability and toughness and processability. In subsequent years, more than 18 different types of tetraamine and more than 50 varities of diacids have been used for the synthesis of numerous PBI backbone structures. Few representative tetraamine and dicarboxylic acid monomers which were used for the PBI synthesis are tabulated in Table 1.1 and Table 1.2.[9,16] In the following subsections, we have discussed different types of synthetic procedures which were followed in the literature for the PBI synthesis.

Table 1.1. *Aromatic Tetraamine monomers for PBI synthesis*
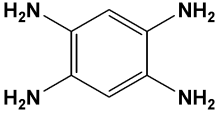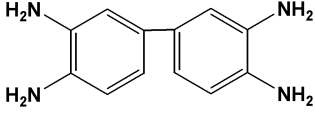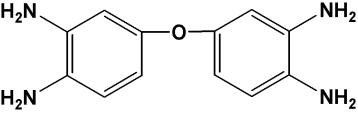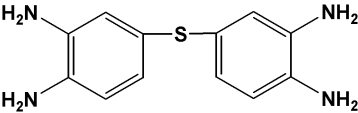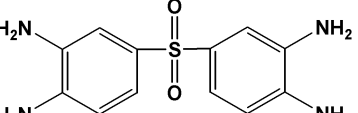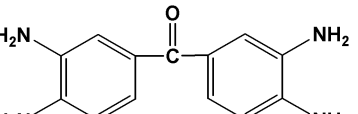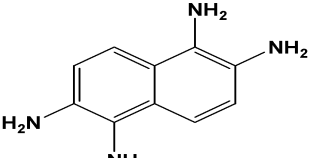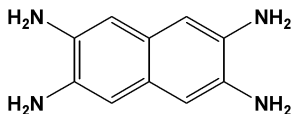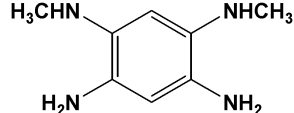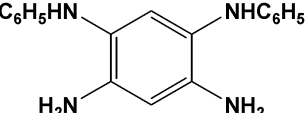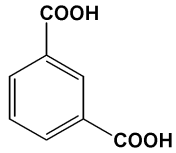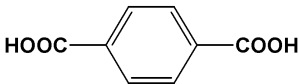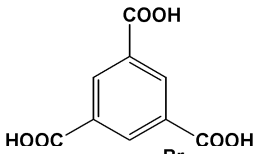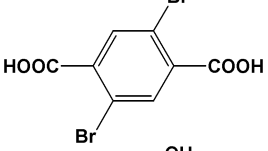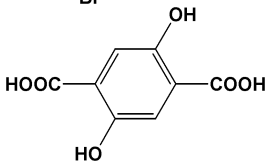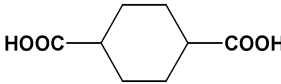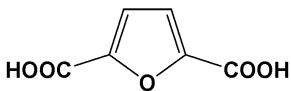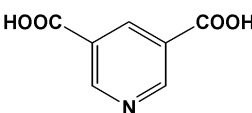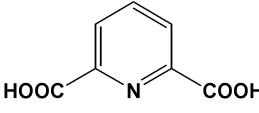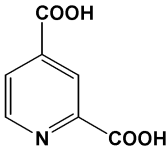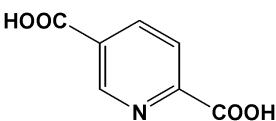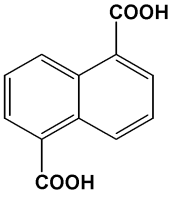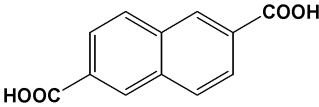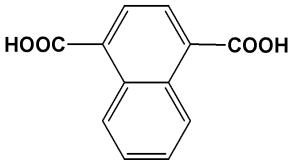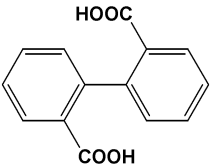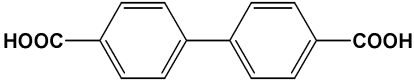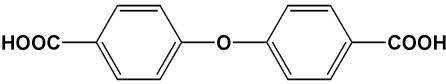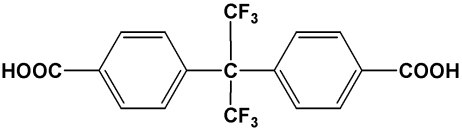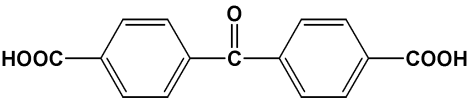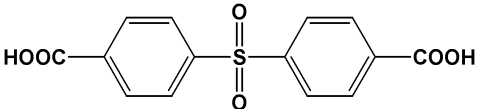
Structure	Name	M.P.(^{o}C)
	1,2,4,5-Tetraaminobenzene	274-276
	3,3',4,4'-tetraaminobiphenyl	178-179
	3,3',4,4'- tetraaminodiphenylether	150-151
	3,3',4,4'-tetraaminodiphenylsulfide	102-103
	3,3',4,4'-tetraaminodiphenylsulfone	174-175
	3,3',4,4'-tetraaminobenzophenone	217
	1,2,5,6-Tetraaminonaphthaline	-
	2,3,6,7- Tetraaminonaphthaline	-
	1,3-Dimethylamino-4,6-diaminobenzene	127-129
	1,3-Diphenylamine-4,6-diaminobenzene	210-211

Table 1.2. *Dicarboxylic acid monomers for PBI synthesis*

Structure	Name	M.P. (^{o}C)
	Benzene-1,3-dicarboxylic acid	341-343
	Benzene -1,4-dicarboxylic acid	>300
	Benzene -1,3, 5-tricarboxylic acid	>300
	2,5 dibromo -1,4- benzene dicarboxylic acid	-
	2,5 dihydroxy -1,4- benzene dicarboxylic acid	>300
	Cyclohexane- 1,4- dicarboxylic acid	164-167
	Furan- 2,5- dicarboxylic acid	>300
	Pyridine- 3,5- dicarboxylic acid	>300
	Pyridine- 2,6- dicarboxylic acid	248-250
	Pyridine- 2,4- dicarboxylic acid	246-247
	Pyridine- 2,5- dicarboxylic acid	242-247

Structure	Name	Value
	Naphthalene-1,5-dicarboxylic acid	>300
	Naphthalene-2,6-dicarboxylic acid	>300
	Naphthalene-1,4-dicarboxylic acid	>300
	Biphenyl-2,2$^/$ -dicarboxylic acid	-
	Biphenyl-4,4$^/$ -dicarboxylic acid	>300
	4,4$^/$ -Oxybis (benzoic acid)	-
	4,4$^/$ -(Hexafluoroisopropyledene) bis(benzoic acid)	272-274
	Benzophenone 4,4$^/$- dicarboxylic acid	-
	Diphenyl sulfone- 4,4$^/$ -dicarboxylic acid	>350

1.3.1. Melt /Solid State Polymerization

Pioneering approach by Vogel and Marvel[4-6] involved the solid state molten polycondensation of equimolar mixture of different tetraamines with the phenyl esters of different aromatic dicarboxylic acids. The reaction was carried out under nitrogen atmosphere by heating the equimolar amount of tetraamine and diphenyl ester (Scheme 1.1-1.3) and the temperature was gradually increased from about 200 to 300°C. The viscous melt which was formed initially changes quickly to solid cake or glassy foam. The initial low molecular weight materials were pulverized immediately and reheated under high vacuum for several hours at 350-400°C.
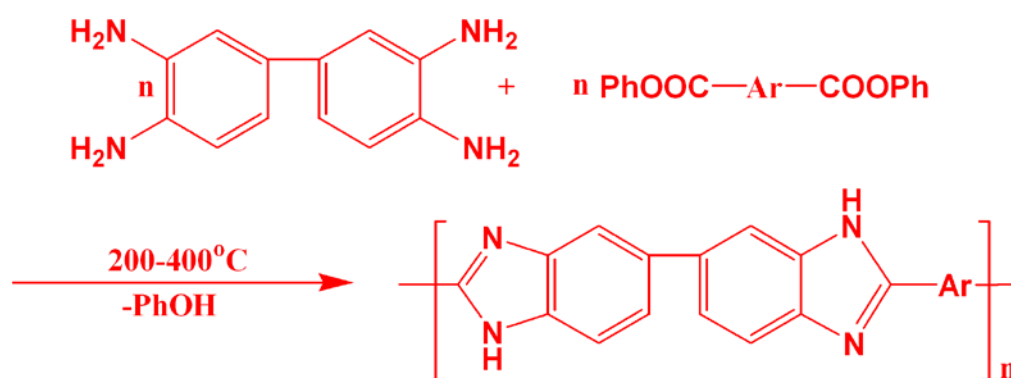
Scheme 1.1. *Melt condensation of 3,3',4,4'-tetraaminobiphenyl with aromatic dicarboxylic acid esters.*
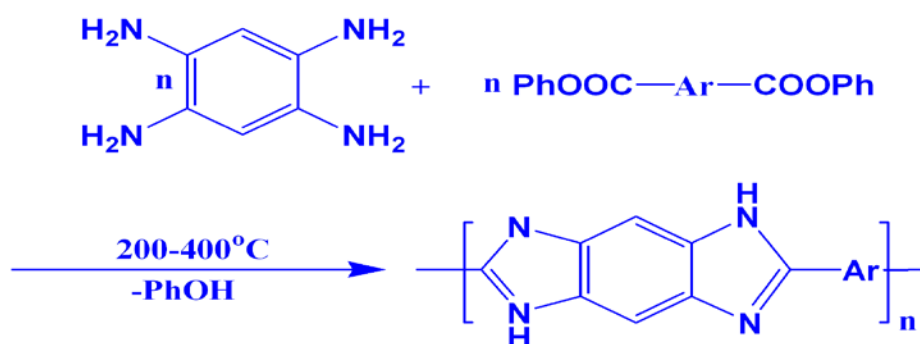
Scheme 1.2. *Melt condensation of tetraaminobenzene with aromatic dicarboxylic acid esters.*
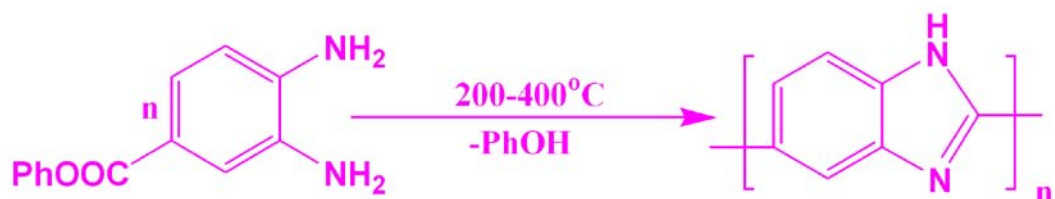
Scheme 1.3. *Melt condensation of diaminobenzoate.*

1.3.1.1. Two-stage Melt/Solid State Polymerization

Equimolar amounts of the 3,3',4,4'-tetraaminobiphenyl (TAB) and dicarboxylic acids or its derivative usually diphenyl ester of the dicarboxylic acid were taken in a round-bottomed flask equipped with mechanical stirrer and a condenser. The flask was evacuated and filled with oxygen free nitrogen gas and placed in a temperature controlled oil bath and heated under slow nitrogen flow at 220 to 260°C for next 1.5 h. The slow nitrogen gas flow was maintained through out the reaction because the 3,3',4,4'-tetraaminobiphenyl prone to oxidized at high temperature in presence of air. The resulting yellow colour prepolymer was cooled to room temperature, then it was pulverized to obtain low molecular weight PBI prepolymer. At this stage all the by-products like phenol and a part of water were evolved. When free dicarboxylic acid was used, water was the only by product. The ground powder prepolymer was placed in a three- necked flask equipped with a nitrogen inlet and outlet and a mechanical stirrer and the temperature was raised to 360 to 400°C for 1h.The resulting PBI exhibited higher molecular weight (Scheme 1.4). Various mechanistic pathways have been proposed for the formation of aromatic PBIs.
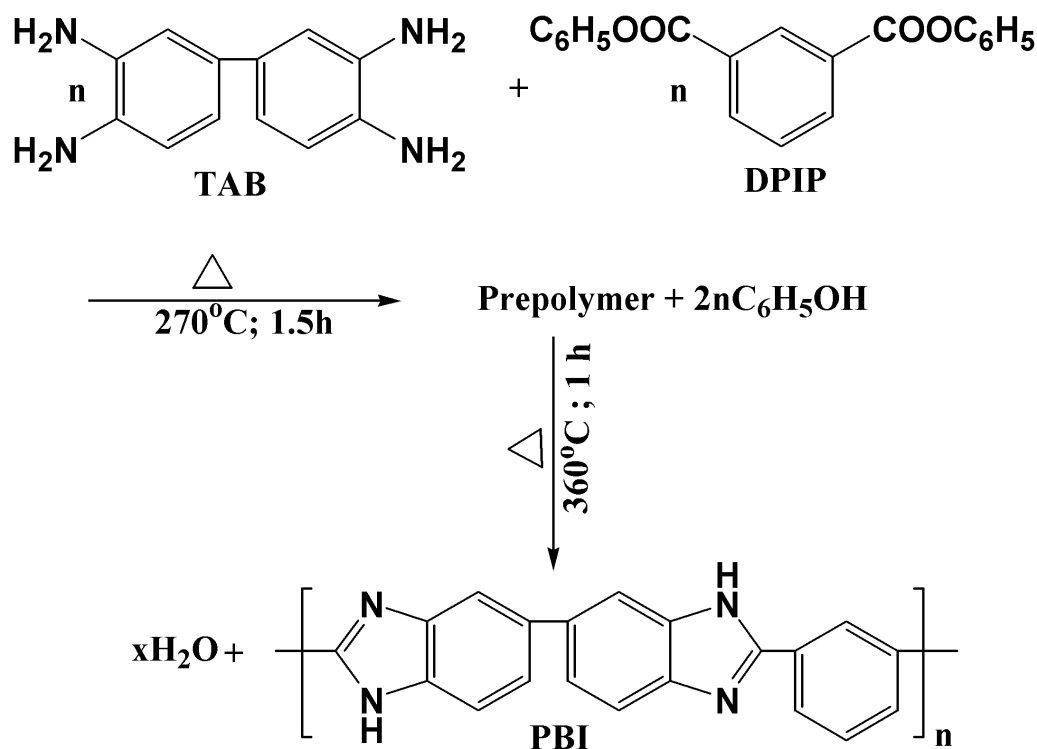
Scheme 1.4. *The two stage process for polybenzimidazole (PBI) synthesis.*[4]

However, an elaborate kinetic study carried out by Wrasidlo and Levine[23], suggested that condensation proceeds via a Schiff 's-base intermediate, which subsequently loses phenol to form PBI and it was the rate determining step of the reaction. The reaction proceeds via the addition of amine nucleophile to the carbonyl carbon of the ester followed by the elimination of water. The Schiff's-base thus generated were in equilibrium with cyclized benzimidazoline tautomer which was aromatized to the polybenzimidazole in the final step with the elimination of phenol (Scheme 1.5).[23]
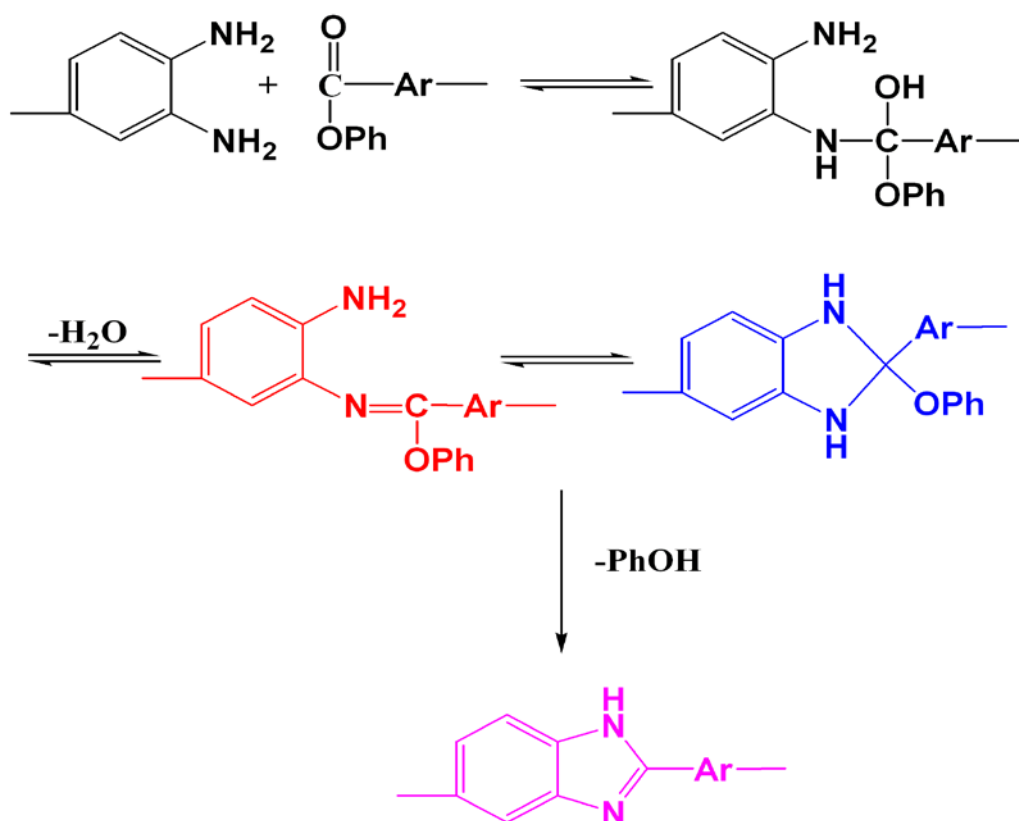
Scheme 1.5. *Mechanism of polybenzimidazole formation by solid state polymerization of 3,3',4,4'-tetraaminobiphenyl with aromatic dicarboxylic acid esters.*[23]

Using modern analytical techniques such as infrared/mass spectral techniques, other workers[24] have also found phenol is evolved before complete dehydration and they proposed that the condensation proceeds through poly(amino-amide)/ poly(hydroxybenzimidazoline) intermediate formation which above 260-280°C eliminate water and yield PBI polymer. This mechanistic study suggests that the PBI prepolymer may contain both amino-amide/hydroxybenzimidazoline and benzimidazole structures, which undergo complete conversion to PBI above 350°C (Scheme 1.6).[24]
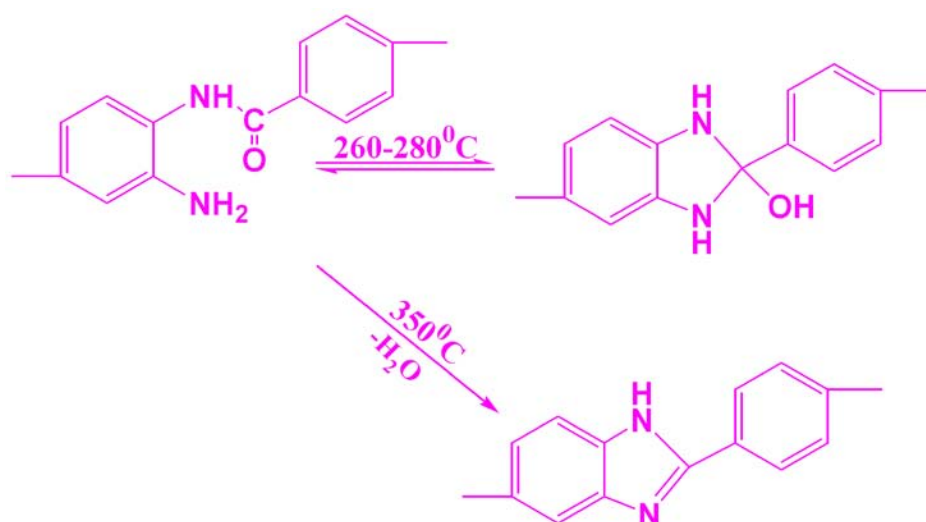
Scheme 1.6: *PBI synthesis from poly (amino-amide)/poly(hydroxybenzimidazoline) intermediate.*[24]

A novel approach for the PBI synthesis was developed by Gray et al[25] by allowing 3,3',4,4'-tetraaminobiphenyl (TAB) to undergo two stage low temperature melt condensation with 4-acetyleacetophenone at 250°C .This process involved (Scheme 1.7) formation of high molecular weight Schiff-base/benzimidazoline prepolymer at 250°C which was subsequently aromatized with elimination of methane by solid state heating at 300°C. The aromatization step involved elimination of methane rather than of the *p*-phenylene unit was further confirmed by mass spectroscopy and from the result of non polymeric model compound between the condensations of *o*-phenylenediamine with acetophenone. Other two-stage process for polybenzimidazole synthesis involved the solution polymerization of TAB with aromatic dialdehyde in N,N-dimethyl acetamide, with isophthalonitrile in N,N-dimethyl formamide, and with dialdehyde bis(bisulfate adduct) in dimethyl acetamide, followed by solid state polymerization at elevated temperature.[20-22]
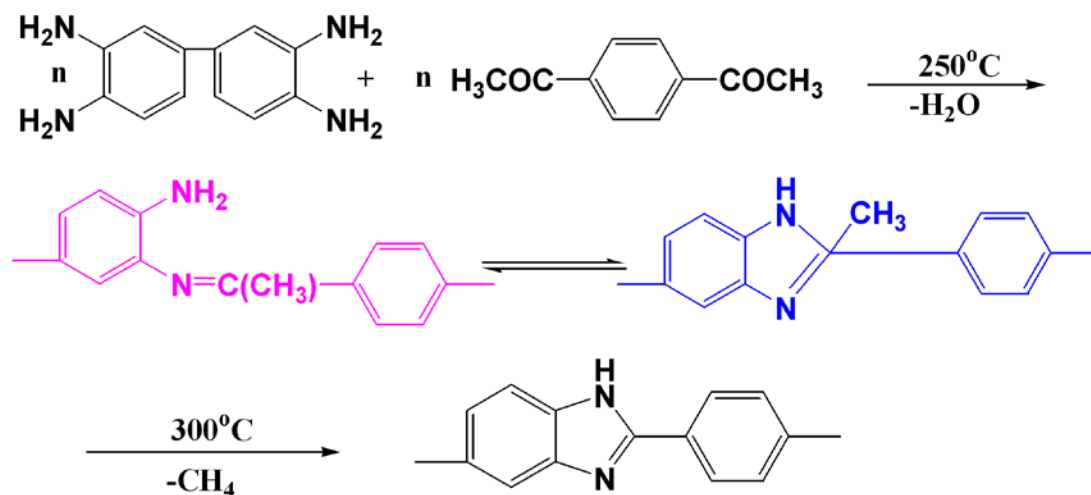
Scheme 1.7. *PBI synthesis from diaminobenzidine and 4-acetyleacetophenone.*[25]

1.3.1.2. Single Stage Melt/Solid Polymerization

Polybenzimidazoles were also synthesized by a single stage polycondensation in presence of catalyst.[9,19] This procedure is generally low-cost synthetic route for PBI synthesis. In this route moderately expensive diphenyl isophthalate (DPIP) was replaced by inexpensive isophthalic acid (IPA), dimethyl isophthalate, isophthalonitrile, or isophthaloyl dichloride. Equimolar amounts of the $3,3',4,4'$-tetraaminobiphenyl and isophthalic acid (IPA) and specified amount of catalyst (i.e., triphenyl phosphate) were taken into a three necked round-bottomed flask equipped with a nitrogen inlet and outlet, mechanical stirrer and a condenser. The flask was degassed and the process was repeated at least three times. The TAB and IPA mixture was heated rapidly from 200 to 310°C with high speed stirring for a period of 15 to 20 min. The stirring rate was slowly reduced at about 250°C and stopped at 310°C. The polymer was heated then for 45 min at elevated temperature (i.e. >400°C). The low molecular weight PBI polymers with inherent viscosity (I.V.) less than 0.2 dL/g were produced by reacting TAB with dimethyl isophthalate, isophthalonitrile, or isophthaloyl dichloride.[9] The high molecular weight PBI was prepared from TAB and IPA by melt condensation of the two

monomers in presence of catalyst at temperatures higher than the melting point of IPA (>340°C) (Scheme 1.8).[19] This single- stage polymerization has advantage over two-stage polymerization such as that the melt polymerization can be conduced in the absence of a solvent like polyphosphoric acid, N,N-dimethyl acetamide, N,N-dimethyl formamide and water is the only by-product formed in the new process which can be removed easily and the major advantage would be the estimated cost reduction.[19]
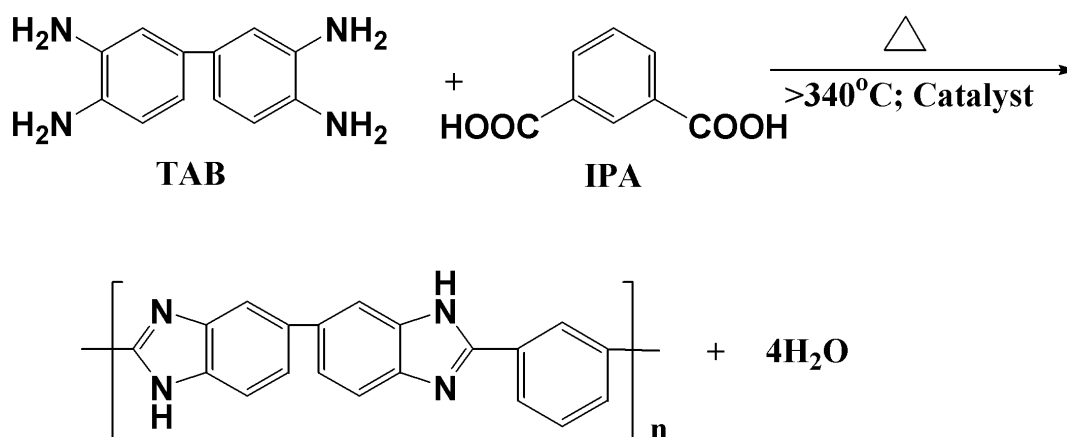
Scheme 1.8. *The single stage process for polybenzimidazole (PBI) synthesis.*[19]

1.3.2. Solution Polymerization

The polymerization of various tetraamine and dicarboxylic acids and its derivatives has been carried out using different high boiling solvents such as N,N-dimethyl acetamide, N,N-dimethyl formamide.[20-22] Most often use of these solvents leads to very low molecular weight PBIs, or often cyclization to benzimidazole structure has been incomplete. Various attempts have been made so far to overcome these problems by using an initial solution polymerization where the prepolymer is formed, followed by solid state polymerization at the elevated temperature at the final stage of the polymerization or by producing the prepolymer by solid state melting at 200 to 220°C, followed by completion of polymerization in the high boiling-point solvent. It has been reported[26-27] that aromatic diamines and aromatic dinitriles undergoes

polymerization in polar aprotic solvent where the intermediate polyamidines are formed which are subsequently cyclized to low molecular weight PBIs in the presence of NH$_4$Cl /HCl (Scheme 1.9).[26-27]
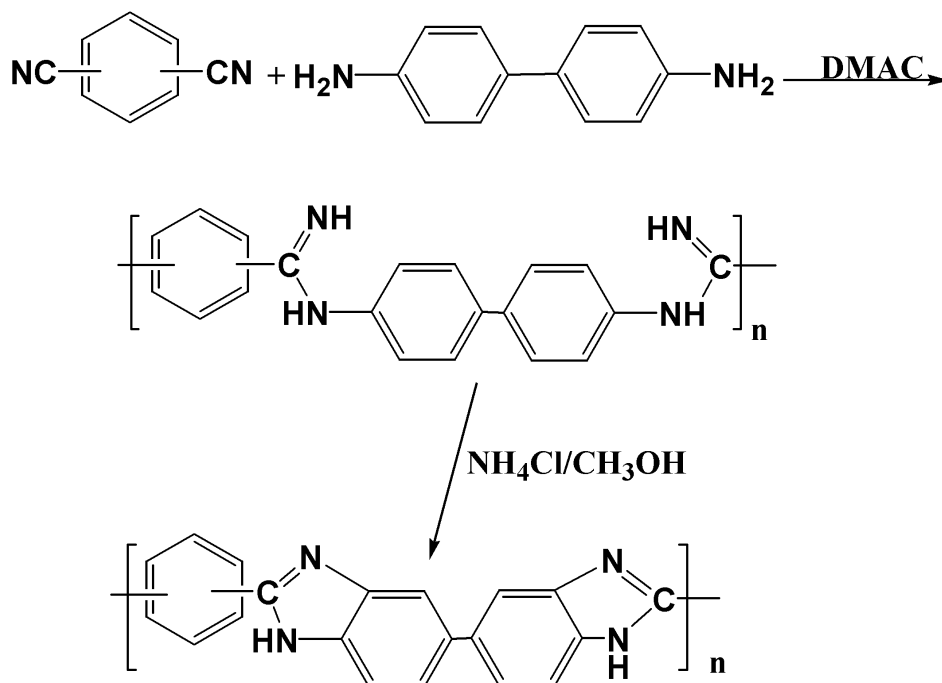
Scheme 1.9. *The synthesis of polybenzimidazole (PBI) in DMAc.*[26-27]

Relatively high molecular weight PBIs have been made from aromatic dicarboxylic acid chlorides and substituted tetraamine by initially low temperature polycondensation in polar solvent followed by aromatization in solution or film or after isolation of solid polymer by solid state polymerization.[28-30] This procedure is very useful for preparation of N-substituted PBIs. Korshak et al.[29,31-32] have also prepared PBIs by reductive cyclization at 180-200°C of poly (*o*-nitro) amides. The most widely used solvent for the production of PBIs is polyphosphoric acid (PPA) or polyphosphoric acid esters.[9,19,33-35] PPA has been used as a solvent or catalyst for a number of polyheterocyclization systems. PPA was introduced into the PBI chemistry in 1964 by Iwakura et al.[36] and since then number of workers has been started using it in various polymer laboratories. The main benefit is that the oxidation sensitive tetraamines can be

replaced by the more stable hydrochloride salt.[9] In this process not the prepolymer but fully cyclized and polymerized PBI has been formed by using aromatic dicarboxylic acids/dimethylesters, diamides, and dinitriles.In this procedure tetraamines and aromatic dicarboxylic acids or derivatives are dissolved in PPA at 140°C in a three necked round-bottomed flask equipped with a nitrogen inlet and outlet and mechanical stirrer. The reaction mixture is then heated to at 180-210°C for about 18-20 h with stirring and finally poured water and neutralized by alkaline solution and dried under vacuum oven. If tetraamine tetra hydrochloride salt is used, the dehydrochlorination in PPA is first carried out at 140°C to eliminate HCl gas.[9] After the elimination of HCl gas the dicarboxylic acid monomer is added and then the reaction mixture is heated to at 180-210°C for about 18-20 h.
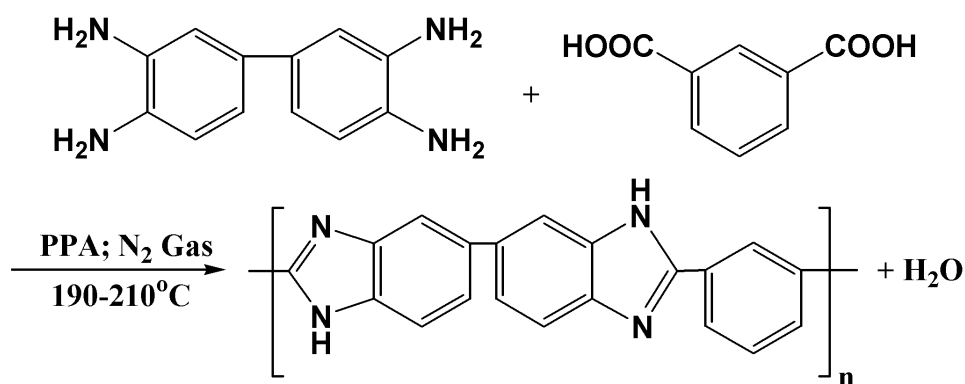
Scheme 1.10. *The synthesis of polybenzimidazole (PBI) in polyphosphoric acid (PPA) medium.*

1.3.3. Catalysts

Cheo et al. have shown the effect of different catalysts on the polymerization of 3,3',4,4'-tetraaminobiphenyl and isophthalic acid or diphenyl isophthalate and reported variation in the molecular weight of the polymer depending on the type of catalysts used for the polymerization.[9,19,37-42] Phosphorus containing catalysts such as triphenyl

phosphate, triphenyl phosphite and phosphoric acid are very effective for producing high molecular weight polymer. Catalysts such as dichlorophenylphosphine, chlorophenylphosphine, triphenyl phosphite diphenylphosphine oxide, diphenyl chlorophosphate, triphenyl phosphate, dimethoxyphenylphosphine, dibutoxyphenylphosphine, o-phenyl phosphorochloridite, phenyl N-phenylphosphoramidochloridate, and dichlorodimethylsilane produced PBI polymers with I.V greater than 0.7 dl/g.[19] It was also demonstrated that the I.V of PBI polymer increases with increasing catalyst concentration in the reaction mixture and saturates after 1% (by weight).[19]

1.4. Physical and Chemical Properties

The wide varieties of different PBI homopolymers structures were reported in the literature. A large number of copolymers obtained from various types of dicarboxylic acid monomers and TAB polymerization were also reported. Homopolymers and copolymers synthesized using 3,3',4,4'-tetraaminobiphenyl (TAB) and different dicarboxylic acids or its derivatives, are listed in Scheme 1.11 and 1.12, respectively. Very few of these structures have been used for practical purposees. Almost all aromatic benzimidazole polymers obtained by different synthetic procedures are remarkably similar in their general physical and chemical behavior. The PBIs powder is generally yellow to brown colour solid, and infusible up to 400°C and amorphous in nature but some degree of crystallinity was found in more symmetrical structures.[4,7,13,36] PBIs are highly hygroscopic in nature and it can take moisture 5 to 10% of its weight.[13, 43-44] The only polymer which has received much attention as a practical material is poly [2,2'-(m-phenylene)-5,5'-bibenzimidazole] (1 in Scheme 1.11) and most commonly known as *m*-PBI. Generally aromatic polybenzimidazoles are more thermally stable than aliphatic polybenzimidazoles due to its rigid backbone structure.[4-7] Most of the aromatic PBIs are soluble in limited number of organic polar aprotic solvents such as N,N-dimethyl acetamide(DMAc), N,N-dimethyl formamide(DMF) ,N,N-dimethyl sulfoxide (DMSO) and in acids like sulphuric acid, formic acid etc.[4,7,13,36]
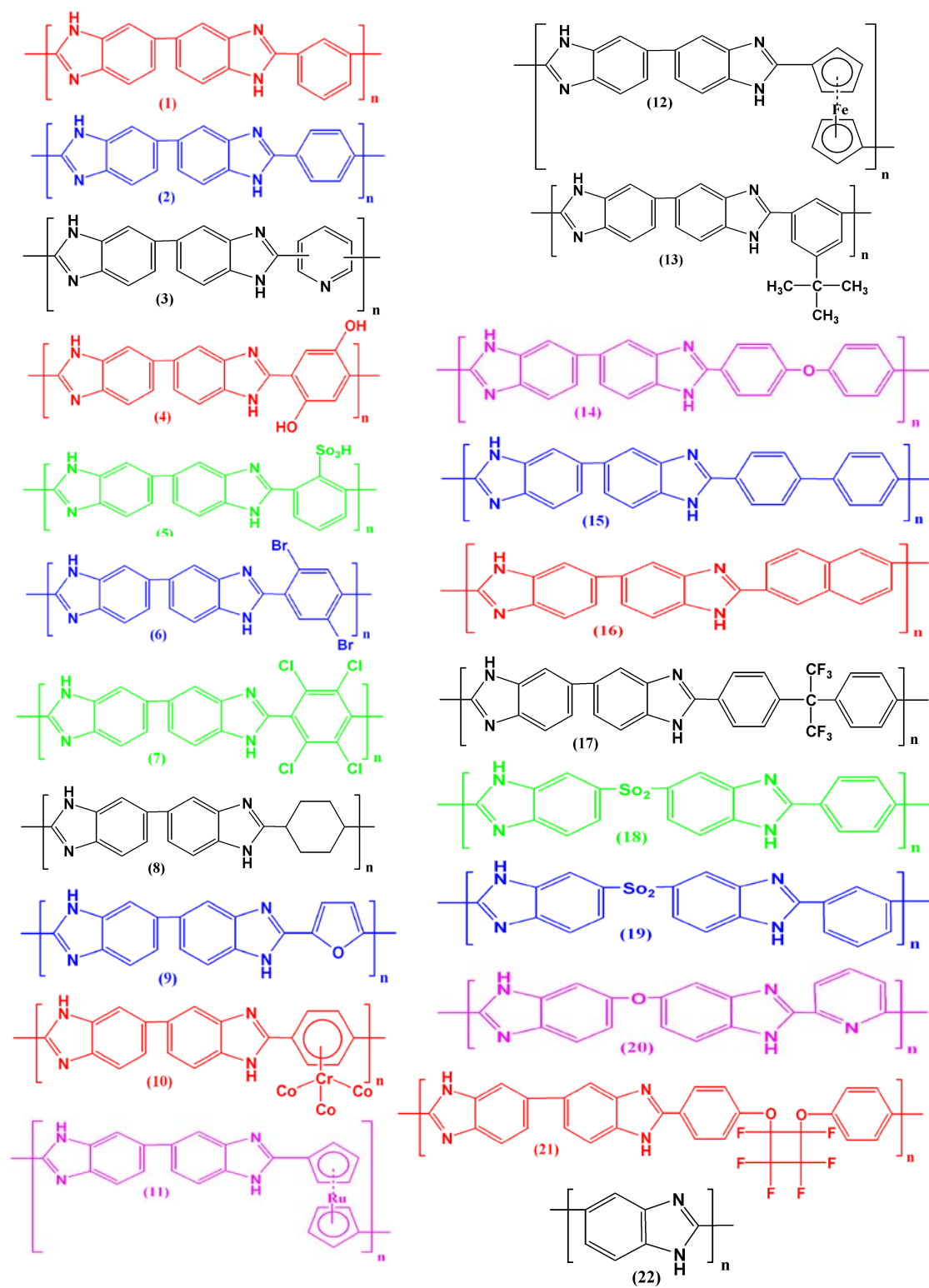
Scheme 1.11. *Representative polybenzimidazole homopolymers.*

(1)

(2)

(3)

(4)

(5)

(6)

(7)

(8)

(9)

(10)

(11)
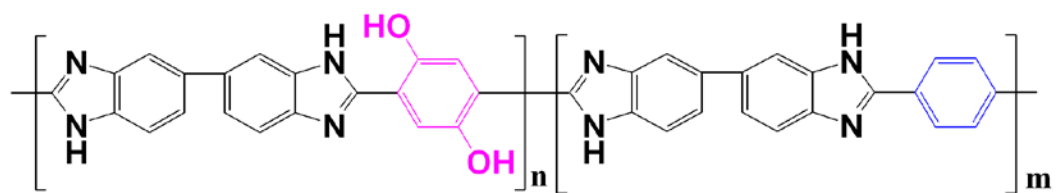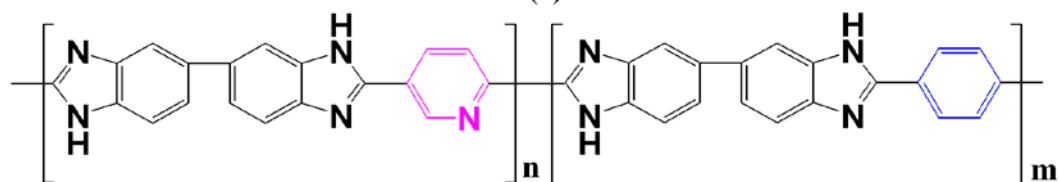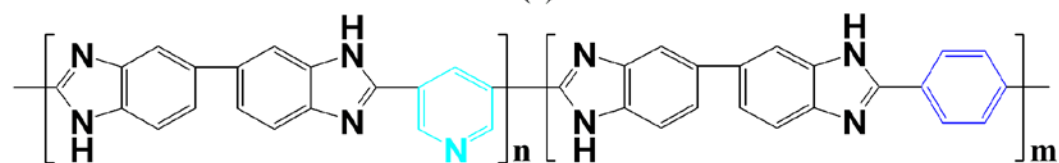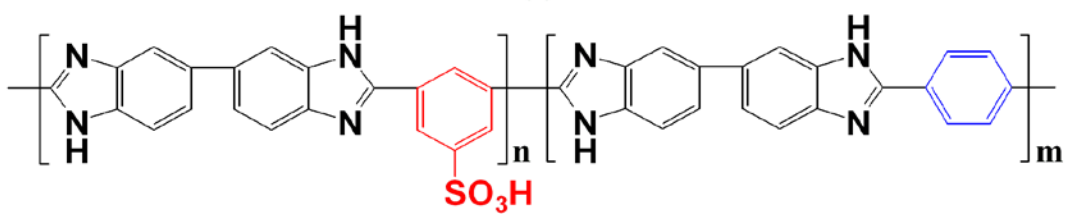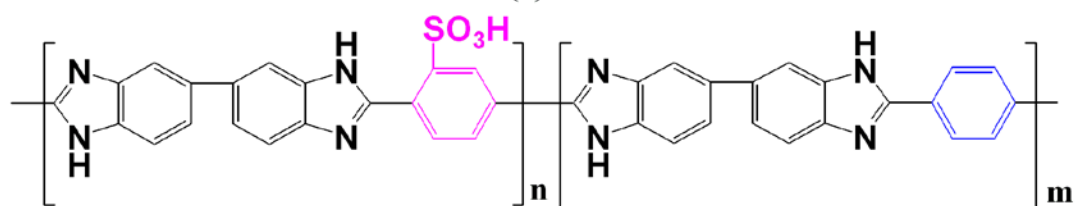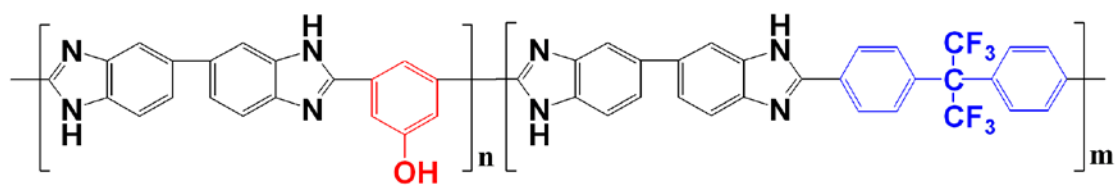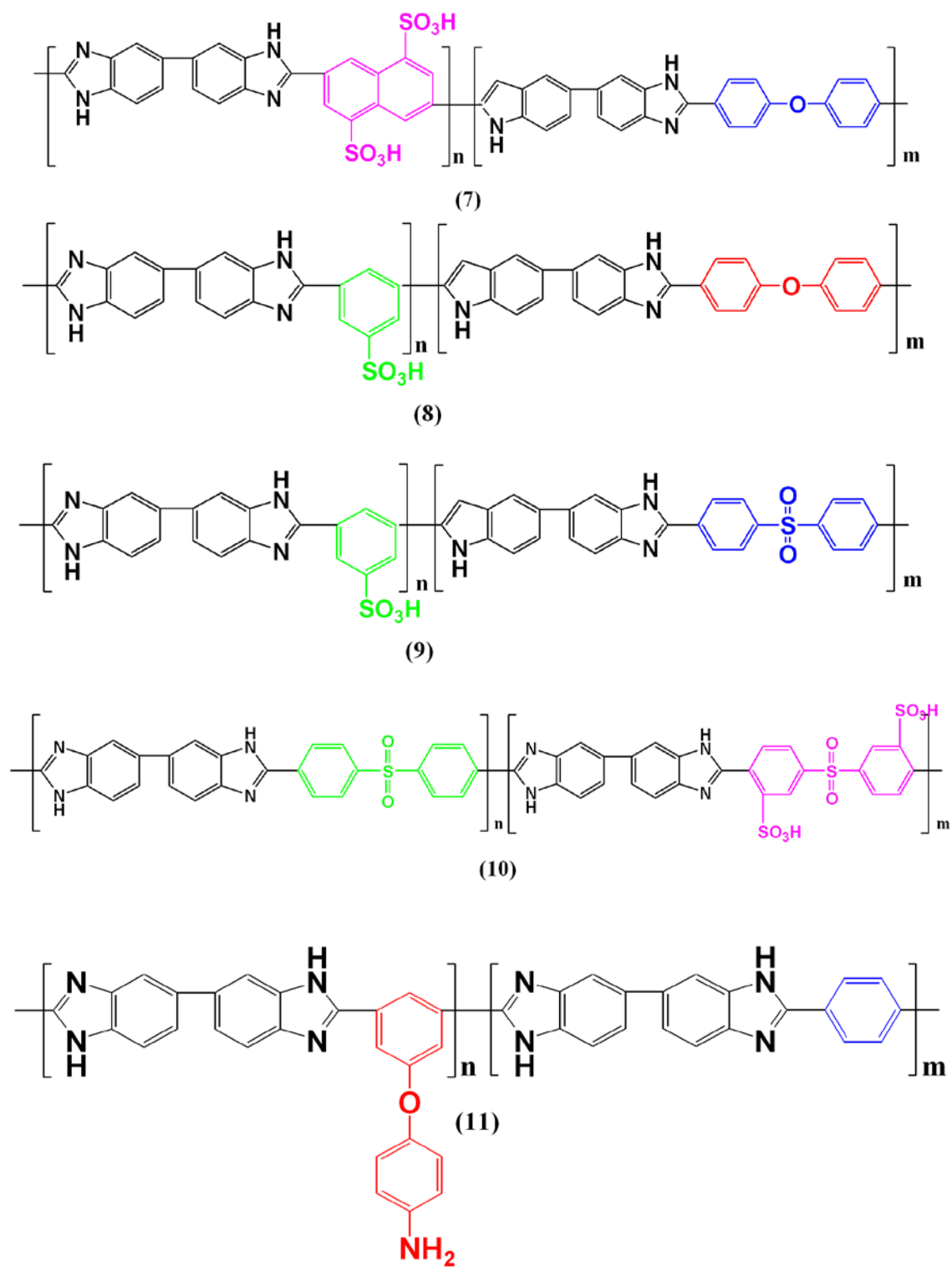
Scheme 1.12. *Representative polybenzimidazole copolymers.*

1.4.1. Solubility

Most of the aromatic PBIs are not soluble in most of the common laboratory organic solvents owing to their rigid backbone structure. However, most of the linear aromatic PBIs regardless of structure and origin dissolve partially and entirely soluble in strong protonic acids such as concentrated sulphuric acid (H_2SO_4), methane sulfonicacid (CH_3SO_3H), formic acid (HF) and in phosphoric acid (H_3PO_4) while heating and in polar aprotic solvent such as N,N-dimethyl acetamide(DMAc), N,N-dimethyl formamide (DMF) ,N,N-dimethyl sulfoxide (DMSO), N-methyl-2-pyrrolidone (NMP) [4,7,13,36,45]. Solubility of PBI is also depend on the microstructure, PBI having m-phenylene group showing better solubility than their structural isomer due to its highly order, closed packing and powerful conjugative p-phenylene ring.[13] The solubility increases by incorporating hetero atoms such as oxygen, sulfur, sulphone in between the aromatic units and thus has been attributed for the enhancement of chain flexibility.[13,46-47] N-alkylation also improves the solubility of the PBIs.[13] Heavily halogenated PBIs exhibit poorer solubility compare to halogen free counterpart. Dihydroxy-PBI (2OH-PBI) having two -OH group undergoes cross linking and due to strong intra and intermolecular hydrogen bonding interaction, this PBI has poor solubility even in concentrated sulfuric acid.[48] Gieselman et al. have prepared water soluble PBI by substituting the reactive benzimidazole N-H groups with alkylsulfonated or arylsulfonated halide.[49]

1.4.2. Viscosity and Molecular Weight

The solubility of aromatic PBIs is generally restricted to strong acids and polar aprotic solvents such as DMSO, DMAc, and NMP.[4, 7, 36, 51-55] The restricted solubility of these polymers complicates the determination of molecular weight using chromatographic characterization techniques. The molecular weight of polybenzimidazoles in the most of the literature been expressed in terms of inherent viscosity (I.V), determined from 96-98% sulphuric acid solution[53] or less frequently in formic acid [51-52] and methane sulfonicacid [50] or polar aprotic solvent such as DMSO,

DMAc. It is already reported by several workers that viscosities obtained for a given polybenzimidazole sample show considerable variation when measured in different solvents. PBI in formic acid gives higher I.V value compare to those measured in sulfuric acid solution.[13] Marvel reported that viscosity values are two to three times as high in formic acid compared to dimethyl sulfoxide.[4,5,7] PBI viscosities were strongly dependent on water content of the solvent when viscosities were measured in sulphuric acid and in dimethyl sulfoxide due to their hygroscopic nature.[13] Kojima et al[52] studied the dilute solution properties of poly(4,4′-diphenylether-5,5′-bibenzimidazole) (OPBI) in DMAc by light scattering and intrinsic viscometric study and determined the characteristic parameter like mean square radius of gyration from Zimm plots, the second varial coefficient (A_2) and weight average molecular weight ($\overline{M_w}$). Kojima et al. also determined the constant 'a' and K from Mark-Houwink relationship ($[\eta] = K \overline{M_w^a}$) for OPBI solution in formic acid. Recently, in 2006 Shogbon et al.[56] determined the molecular parameter and chain conformation for high molecular weight *m*-PBI in DMAc/LiCl using viscosity and light scattering measurements. Yuan et al.[57] very recently in 2009 found the correlation between the weight average molecular weight ($\overline{M_w}$) and intrinsic viscosity [η] for *m*-PBI and its phophonylated derivatives in H_2SO_4 and in DMF-LiCl solutions.

1.4.3. Solution Properties

Due to very limited and restricted solubility of aromatic PBIs, studies of solution properties of different polybenzimidazoles in various solvents have been gained interests in recent years. It was reported that 25% PBI- DMSO solution has a self life time of two weeks at room temperature and a month at 90°C. In general PBIs solubility increases with decreasing solid content and decreasing the molecular weight (I.V) of the polymer.[13] Earlier molecular aggregation of OPBI in DMAc solution was studied by Kojima et al.[51] and they found that due to the overlapping of polymer chains molecular aggregates are formed. PBI chain conformation was studied by Shogbon et al.[56] by

using viscosity measurements and static light scattering techniques by varying polymer or salt (LiCl) concentrations in the solution. They have measured the reduced viscosity as a function of varying polymer concentration and found that the polymer behaves like a polyelectrolyte in solution and the conformational changes occurred at higher concentrations. Using light scattering studies they have shown that variation of polymer or salt concentration lead to a conformational transition in the polymer chain from a random coil or wormlike chain to an "extended wormlike" chain. Furthermore, the presence of optical activity obtained from circular dichroism measurement was linked to this conformational transition, which occurred at higher polymer concentrations.[56] Recently, we have studied the aggregation of polybenzimidazole (*m*-PBI) in polar aprotic solvent like DMAc using viscosity, steady state and time dependent fluorescence techniques. It was found that with increase in concentration the conformational transition of PBI polymer chains occur from compact coil to an extended helical rod like structure.[58] The NMR and viscosity studies demonstrate that the intra- and intermolecular interactions (interchain hydrogen bonding) play an important role for the conformational transition and aggregation process. This topic is highlighted and addressed in Chapter 4 of this thesis.

Very recently we have reported the aggregation behavior of poly(4,4′-diphenylether-5,5′-bibenzimidazole) (OPBI) in polar aprotic (dimethyl acetamide, DMAc) and protic (formic acid, FA) solvents as a function of the polymer concentration and solution temperature (Figure 1.1).[59] We have observed that the aggregation of OPBI depends upon the protic character of the solvent molecules. In protic solvent aggregation takes place without swelling of the OPBI coils where as swelling is observed in case of aprotic solvent. Moreover we have found that in both the solvents the aggregations proceeds through intermolecular processes though their mechanisms are different owing to the polyelectrolytic nature of OPBI in FA medium.[59] Temperature dependent studies suggest that the aggregations in both the solvents destabilize with increasing temperature. The higher activation energy of aggregation (E_A) in DMAc (5.62 kJ/mol) compared to FA (3.07 kJ/mol) revealed that the aggregation formation pathways are different in two solvents and stronger aggregates are formed in the DMAc

solvent.[59] Schematic representations of the aggregation processes of OPBI in two different solvents were shown here in Figure 1.1.
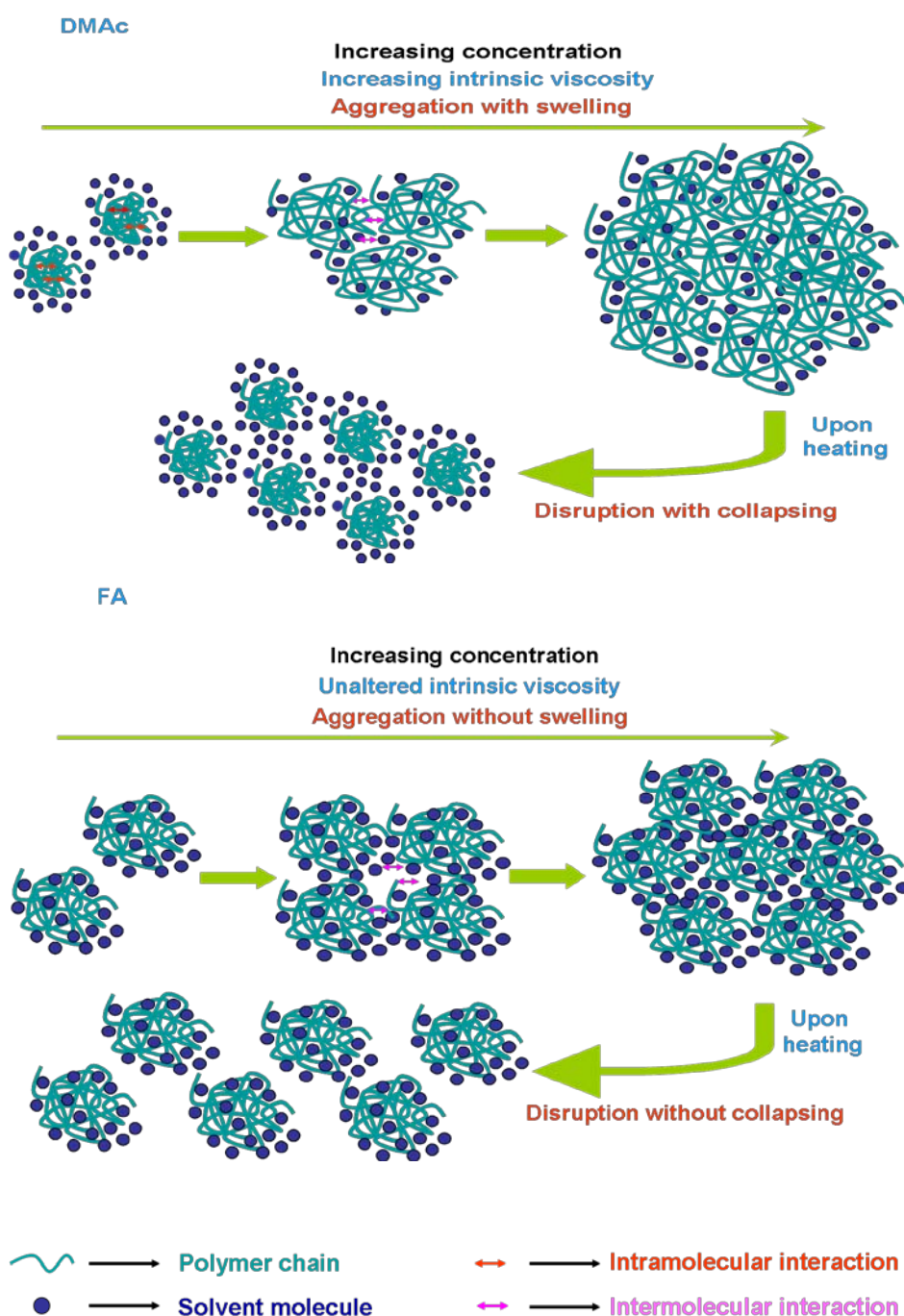
Figure 1.1. *Schematic representation of the aggregation behavior of OPBI in DMAc and FA solvent with increasing concentration and temperature .*[59]

1.4.4. Thermal Properties

There is an increasing demand in advance materials and technologies for high temperature resistance materials which can show stability up to elevated temperature. The first report of exceptionally high heat resistance of polymer containing benzimidazole unit was presented in Marvel's pioneer paper.[4] They demonstrated by thermogravimetric analysis (TGA) that most of the aromatic polybenzimidazoles show no change in properties on heating at 550°C and less than 5% weight loss after several hours at 600°C in nitrogen. Most of the aromatic PBIs show exceptionally thermal stability due to the following factors: [4, 7, 13, 18, 36]

(i)   Absence of weak bonds in the polymer backbone.

(ii)   High extent of conjugation and electronic delocalization along the polymer chain.

(iii)   High chain stiffness.

(iv)   "Bond healing" capabilities.

Thermal and oxidative stabilities of different PBIs have been reported by various research groups and they have found that PBI polymers have exceptional thermal stability up to 600°C, initial 5% wt loss at 100-120°C is due to loosely bound water molecules associated for hygroscopic nature of the polymer.[13, 43-44] Most of the cases, TGA and DTA have been employed to determine its thermal stability. Aromatic PBIs with flexible linkage such as –O-and -SO$_2$ – either in amine or acid moiety, are generally less thermally stable than all the ring systems.[13] Their decomposition temperatures in inert atmospheres or air range between 450 to 550°C. In oxidizing condition PBIs shows lower stability due to labile imidazole hydrogen. Introduction of N-Me produces very little increment in either thermal or oxidative stability. The thermal stability of *m*-PBI was slightly improved by substituting the imidazole hydrogen with phenyl under inert or oxidizing condition.[13] Marvel and other workers have not observed any significant thermal stability differences that exist between *m*-phenylene and *p*-phenylene substituted PBI. In our recent publication[60] (Chapter 2) we have observed that significant differences in the thermal stability exist owing to the *m*- and *p*-

phenylene groups in the chain and introduction of *p*-phenylene groups in the polymer backbone by copolymerization enhances the thermal stability of the polymer.[60] The thermal degradation mechanism or pyrolytic decomposition mechanism was proposed and the identification of pyrolysis products from the thermal degradation of poly [2,2'-(m-phenylene)-5,5'-bibenzimidazole] or *m*-PBI was demonstrated by several workers.[61-63] Major products identified were hydrogen, hydrogen cyanide, ammonia and water with less amounts of carbon monoxide and methane and a trace amounts of carbon dioxide, benzene, benzonitrile, aniline, phenol, aromatic diamines. Schulman and Lochte proposed a mechanism for thermal degradation of *m*-PBI which involved direct hemolytic cleavage of the imidazole ring to form benzyne and nitrene intermediates.[63] Later on Soviet workers studied the thermal degradation of *m*-PBI and N-phenylated analog using TG coupled with GC/TLC and IR/UV.[64] Tsur et al. demonstrated the thermal degradation of different PBIs in argon by TGA and mass spectrometry and showed that major pyrolytic decomposition begins at 600 °C.[61] The mechanistic pathway of thermo-oxidative degradation of *m*-PBI and related model compounds based on I.R and GC was carried out mainly by Conley and co-workers.[65-66]

PBI is a thermoplastic polymer. The polymer is almost completely amorphous in nature, crystallinity can be induced only under some specific conditions such as hydrogen bonding interaction with polar solvent,[58-59] blending with some crystalline polymer etc.[67-68] In most of the cases, it behaves as an amorphous polymer with very high glass transition temperature (T_g). It has the highest glass transition temperature (T_g) among the commercial available polymers: it is between 400 and 450°C depending on the method of measurement used.[13] Menczel estimated the glass transition temperature of *m*-PBI fiber using differential scanning calorimeter (DSC) and dynamical mechanical analysis (DMA) and calculated the T_g of the *m*-PBI fiber is 387°C.[69] He has shown that the T_g of the drawn fiber has a considerable dependence on the mode of the measurement; when fine fiber pieces was crimped in a standard aluminium DSC-pan, T_g of the drawn fiber is 401°C and if the fiber was wound around a steel plate before crimping in a DSC pan, the T_g was found considerably higher (435°C). He assigned the β-relaxation at 290°C associated with loss of water while the

γ-transition at 20°C was not identified clearly and assigned the δ-transition at 90°C correspond to rotation of the *m*-phenylene ring. Recently, we have calculated the glass transition temperatures (T_g) of PBI by DSC and shown the T_g the *m*-PBI and the *p*-PBI were 420°C and 361°C, respectively.[60] The T_g of the *p*-PBI is 59°C lower than that of the *m*-PBI which attributes that the *p*-PBI backbone is more flexible than the *m*-PBI chains. We have compared the glass transition temperature of OPBI and *p*-PBI and confirmed that T_g not only depends on the flexibility of the polymer chain but also the molecular weight of the corresponding polymer.[70]

1.4.5. Photophysical Property

All the PBIs have strong intense colour, reddish brown to yellow both in solid and solution states. Depending on the polymer chemical structure the color varies from strong reddish brown to light yellow. The presence of imidazole probes in the PBI backbone is the responsible for the intense colour of the PBI molecules. Despite of the availability of the color probes in the PBI backbone, the studies of photophysical properties of these polymers both in solution and solid states have not been carried out in details in the PBI literature except very few reports on UV-Vis spectra and their peak positions. The absence of photophysical studies of PBI is most probably due to their poor solubility in common organic solvents. However studies of photophysical properties, especially in dilute solution can address many complex phenomenons of these polymers in solution. Recently, our laboratory has made number of efforts to address the molecular aggregation of PBI in various solvents by studying their photophysical behavior both in solution and solid state.[58,60,70] U.V Visible spectrum of polybenzimidazoles was discussed earlier by several researchers.[13, 51, 58-60] The absorption spectra of the PBI polymers in DMAc shows distinct $\pi \rightarrow \pi^*$ transition at 340 nm due to imidazole moiety and longer wavelength peak at 440 nm is due to n→ π^* transition of the imidazole ring. The large bathochromic shift of the $\pi \rightarrow \pi^*$ absorption maxima for PBI is due to increased conjugation between phenylene groups and imidazole rings.[51, 60] PBI displays very long tail towards longer wavelength which

becomes prominent as concentration of the solution increases which indicates that aggregation of polymer chains through overlapping of polymer coils at higher concentration.[58-60] *p*-PBI polymer absorb at ~ 50 nm higher wavelength than the *m*-PBI polymer. The introduction of the para (1,4) phenylene linkage into the polymer backbone enhances the conjugation between the imidazole and the phenylene ring which results the above mentioned bathochromic shift of ~~the~~ $\pi\pi^{*}$ absorption maxima.[60] Polybenzimidazole is a highly fluorescent polymer with high quantum yield (>0.5). Most of the emission spectra in DMAc for PBI samples show two distinct fluorescence bands at 398 and 416 nm. These peaks are assigned by Kojima due to the 0 – 0 and 0 – 1 transitions from the excited $^{1}L_{b}$ state in the benzimidazole ring of PBI.[51] Concentration quenching and enormous increase of the above two peak intensity ratio with concentration are observed which was explained as an indication of that the polymer chains aggregation among themselves intermolecularlly at higher concentration.[58] Earlier Kojima calculated critical quenching volume for OPBI polymer and showed that intermolecular aggregation of polymer chains take place in DMAc. Recently the photophysical studied of OPBI suggest that the OPBI chains form aggregated structures in both DMAc and formic acid (FA) solutions when the OPBI concentration is increased.[59] The dependences of the emission spectra on the polymer concentrations in the two solvents are not similar in nature, indicating that in both the solvents the aggregations are intermolecular processes though their formation mechanisms are different owing to the polyelectrolytic nature of OPBI in FA medium. The temperature dependence emission spectra suggest that the aggregations in both the solvents destabilize with increasing temperature.[59]

1.5. PBI Derivatives, Blends and Composites

The extensive works were carried out and reviewed on synthetically modified PBI with varying the monomers structure, which primarily consist of bis-tetraaminodiphenyl containing ether, sulphone, ketone and aliphatic groups and various dicarboxylic acids or its derivatives.[13] Polybenzimidazoles are ideal candidates for

'nucleophilic substitution reaction', because they possess two potentially reactive N-H groups per repeating unit. The -NH groups in polybenzimidazole are generally chemically reactive and can be substituted by alkyl halide in presence of strong base. By introducing of methyl and ethyl groups in the imidazole moiety, the obtained N-substituted PBI showed high acid-doping levels and high proton conductivity. These variations in properties of the parent PBI is due to the elimination of hydrogen bonding interaction between the PBI chains and the added alkyl groups. Although PBI has good mechanical properties but it is very difficult to fabricate and process due to its high glass transition temperature ($T_g \sim 400\text{-}425°C$) and limited solubility in some restricted solvent.[4,7] Recently some high performance polyimide has been developed which has better thermooxidative stability at temperature above 260°C and easy to process but lack of thermal and mechanical properties. PBI was found miscible with a wide range of polyimide due to hydrogen bonding interactions with other polymers and by this way thermal and mechanical properties of PBIs were improved further.

1.5.1. N-substituted PBI

Polybenzimidazoles are ideal candidates for 'nucleophilic substitution reaction', because they possess two potentially reactive N-H groups per repeating unit. The NH groups in the imidazole rings are chemically reactive and can be substituted by replacing the hydrogen of the imidazole ring with less reactive substituents such as hydroxyethyl, sulphoalkyl, cyanoethyl, phenyl and alkyl, alkenyl or aryl groups. Generally N- substituted PBI was synthesized by first dissolving the unsubstituted PBI in DMAc or NMP and upon addition of alkali hydride (NaH), deprotonation occurred with formation of a polybenzimidazole poly-anion, which is then reacted with a substituted or unsubstituted alkyl, aryl or alkenyl methyl halide to produce an N-substituted PBI, as shown in Scheme 1.13. Earlier studies by Cassidy [2] provided the information that the substitution of the amino hydrogen by a methyl group lowers the softening temperature by 140°C, increases solubility by a factor of 5, and decreases thermal stability by 10°C where as methyl groups on the aromatic ring of the tetraamine

lower the softening temperature by only 10 to 40°C, indicates the importance of hydrogen bonding interaction between the chains in PBI polymer. Klaehn et al. recently prepared a series of N-substituted organosilane ($-CH_2SiMe_2R$ where R =methyl, vinyl, allyl, hexyl, phenyl, and decyl) PBI derivatives and shown on the basis of the NMR analysis that the substitution occurred almost fully and PBI derivatives possesed very much improved solubility in common organic solvents.[71] The modified polymers had comparable thermal properties to that of parent polymers, and the average molecular weights for the substituted polybenzimidazoles were higher than the parent PBI. Pu and Liu prepared poly(*N*-methylbenzimidazole) and poly(*N*-ethylbenzimidazole) and surprisingly when methyl and ethyl groups are introduced on the imidazole moiety, the obtained N-substituted PBI showed high acid-doping levels and high proton conductivity.[72-73] Kumbharkar et al. synthesized series of N-substituted polybenzimidazoles using selective alkyl groups with varying bulk and flexibility, viz., methyl, n-butyl, methylene trimethylsilane and 4-tert-butylbenzyl and showed that methyl group substituted PBI had highest T_g while the 4-tert-butyl benzyl substituted PBI was showing the lowest T_g.[74-75]
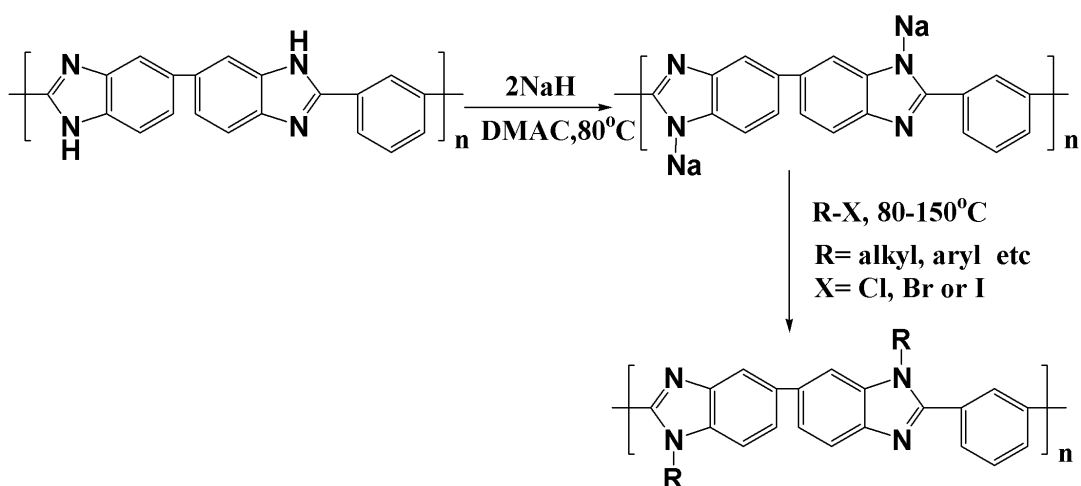
Scheme 1.13. *Synthesis of N-substituted PBI.*

1.5.2. PBI Blends

PBI is an amorphous polymer with very high glass transition temperature.[60] It possesses both proton donor (- NH -) and proton acceptor (- N =) hydrogen bonding sites which exhibit specific interaction upon blending with variety of polymers.[67] So far three types of PBI blends have been studied namely miscible blending, partially miscible blending, and blends of PBI fiber and other fibers.[76-77] The main objectives for PBI blending are to improve the properties, performance and reduction of price specifications through combinations of low-cost or high-performance materials. Various miscible or partially miscible blends based on PBI with several polymers such as polyimides (PI),[78] polyamideimide (PAI),[79] polyarylate (PAr),[79] high-modulus aramide (HMA),[80] Poly(ether imide),[81-82] poly(4-vinyl pyridine) (PVP),[76-77] sulfonated poly sulfone,[76-77] aromatic polyethers,[76-77] poly (vinylidene fluoride) (PVDF),[67] Nafion[84] have been discovered. The major driving force for the miscibility is mainly due to the hydrogen bonding effect and interaction between -NH groups of PBI and carbonyl or sulfonyl groups of the other polymers.[67, 76] Blend miscibility was evidenced in the form of IR spectra, Raman spectra, solid state NMR, single Tg's, and well-defined single tan delta relaxations from dynamical mechanical analyzer (DMA).[67, 81, 83, 85] It has been found that miscible phase is a metastable phase for the wider composition range. Blended polymers have showed better chemical resistance, thermal degradation properties, higher acid doping and higher conductivities due to the presence of PBI. The acid–base composite membranes were prepared using highly sulfonated poly (aryl ether ether ketone) (SPEEK) and polybenzimidazole (PBI) by Zhang et al.[86] We have reported the study of PBI/PVDF blend systems and their potential to use as a proton exchange membrane in PEMFC.[67] The hydrophobic PVDF component in the PBI/PVDF blend allows the blend membrane to absorb more phosphoric acid by pushing out the H_2O molecule from the membrane.

1.5.3. PBI Composites

Phosphoric acid (PA) doped polybenzimidazole (PBI) membranes are considered as one of the most attractive polymeric material in high temperature fuel cell application.[87-88] If the acid content of the membrane is too high it forms soft plastic type material which is very difficult to process where as pure solid inorganic proton conductors are generally brittle and mechanically poor when used directly as membranes.[35] PBI has been used as a binder to prepare composite membranes with improved mechanical strength, flexibility, and conductivity. Several PBI composites have been prepared containing inorganic fillers including zirconium phosphate (ZrP),[89] phosphotungstic acid (PWA),[90] silicotungstic acid (SiWA),[91] and boron phosphate (BPO_4)[92] and using carbon nano tubes[93]. These composites improve the properties like phosphoric acid (PA) doping, thermo-mechanical properties and display high conductivity upto 200°C. Jang et al.[94] prepared zirconium tricarboxybutylphosphonate $[Zr(O_3PC(CH_2)_3(COOH)_3)_2;$ Zr(PBTC)] membranes with PBI. 50% Zr(PBTC)-50% PBI composite membrane showed conductivity of $3.8x10^{-3}$ S cm^{-1} at 200°C and under an equilibrium water vapour pressure of 1.38MPa.[94] Heo et al. prepared composite membranes of $Sn_{0.95}Al_{0.05}P_2O_7$ with PBI and PTFE and obtained higher conductivity and stability compared to the system without PBI.[95] Chuang et al. prepared polybenzimidazole (PBI)/silica nanocomposite membranes via sol–gel process from an organosoluble fluorine-containing PBI copolymer with a silica precursor, tetraethoxysilane (TEOS), and a bonding agent.[96-97] The thermooxidative stability of the PBI membranes increased slightly with the increase of silica content and the coefficients of the thermal expansion (CTEs) of the nanocomposite membranes decreased slightly with increasing amounts of silica. The mechanical properties and the methanol barrier ability (permeability) of the PBI films were improved by the addition of silica. Jiang et al. recently prepared anhydrous proton conducting membrane based on fully organic components of PBI and tridecyl phosphate (TP) and compared the proton conductivity of PBI/TP and PBI/H_3PO_4 composite membranes and showed that the former having higher proton conductivity.[98] Pu et al. employed solvent-exchange method for the

preparation of organic/inorganic composite membranes based on polybenzimidazole (PBI) and nano-SiO$_2$.[99] A high conductive composite proton-exchange membrane of Cs$_{2.5}$H$_{0.5}$PMo$_{12}$O$_{40}$ (CsPOM)/ polybenzimidazole (PBI) for use in hydrogen proton-exchange fuel cells was prepared by Li et al.[100] Lu et al. improved the mechanical property of PBI by introduction of carbon fibers (CF) in to the polymer matrix.[101] Poly (4,4′-diphenylether-5,5′-bibenzimidazole) (OPBI) nanocomposites containing 0.1–1 wt% multiwall carbon nanotubes (MWNTs) were synthesized by Shao et.al via a ''one pot synthesis'' which combines the in situ modification of MWNTs and in situ polymerization of OPBI in one reaction pot.[93] Recently ABPBI/carbon nanotube (CNT) composites were prepared by Kang et al. via in situ polymerization of the AB-monomer in the presence of single-walled carbon nanotube (SWCNT) or multiwalled carbon nanotube (MWCNT) in a mildly acidic polyphosphoric acid medium.[102] Nafion–polybenzimidazole and PTFE-PBI composite membranes were prepared by Zhai et al.[103] and Lin et al.,[104-105] respectively and they have shown that the mechanical property of the composite membranes were improved.

1.6. PBI Applications

After the historical discovery by Marvel and Vogel in 1961, [4] uses of different types of polybenzimidazoles (PBIs) were started for various purposes. PBI has inherent high thermal stability, nonflammability due to the imidazole moiety and therefore finds enormous utility in a wide range of applications.[2, 3, 9, 11, 14] PBI was originally developed as a fiber-forming polymer for military applications. Due to intrinsic nonflammability and high moisture regain PBI application areas have expanded significantly very soon after it's discovery in 1960's. More recently, PBI flat hollow membranes were successfully tested as reverse osmosis membranes in brine and sea water desalination.[76, 77] Membranes based on PBI complexes with phosphoric acid (PA) have high proton conductivity at elevated temperature and low humidity, exhibiting good prospects for high temperature PEMFCs.[87, 88] The following section briefly highlights the use of PBI in different applications.

1.6.1. Traditional Applications

1.6.1.1. Structural Engineering Materials

Polybenzimidazole moldings have found use as structural components in automotive, aeronautical, and electrical engineering applications.[9]

1.6.1.2. Thermo-insulating Materials

Polybenzimidazoles are extremely useful materials for heat and sound-insulating applications in the form of foams or loosely mats. PBI-carbon fibers are generally high density, typically 0.5 g cm^{-3} but offer high compressive strength and excellent load-bearing characteristic, desirable for structural foam application at high temperature.[2, 9, 14] Low density PBI foams are excellent candidates for fire and thermal insulation in automotive, aircraft and aerospace vehicles, for ablative use, as well as for combined sound and high temperature insulation in jet engine nacelles.[13, 15]

1.6.1.3. Electro-insulating Materials

PBI can be used in electrical insulation and other dielectric application at very high temperature and aggressive chemical environments due to its retention of dielectric properties in a high temperature coupled with good corrosion resistance in contact with certain reactive chemicals. Typical applications were found in special cable and wire insulation, in the manufacture of circuit boards and insulating membrane for fuel cell application.[2, 3, 9, 14-16]

1.6.1.4. Adhesive Materials

Polybenzimidazole adhesive was originally developed in the early 1960s for the aerospace industry application as a supported film. It was thought to be an ideal adhesive for spacecraft application where temperatures could range from very high to very low depending on the craft's solar orientation.[13-14, 16] The polybenzimidazole (PBI) adhesive has shear strength on steel of 3,000 psi at room temperature and 2,500 psi at

550°C where as polyimide adhesives offer strength of approximately 3,000 psi at room temperature, but at 370–550°C polyimide adhesives do not have the excellent strength. For high temperature service, polybenzimidazoles are chosen when the maximum short term resistances to the temperatures are required. Polyimides are chosen when long term resistances to high temperatures are required. Polybenzimidazole adhesives retain their good mechanical properties at temperatures as low as -150°C. PBI represent one of only a few adhesives that exhibit good adhesion characteristics at high temperatures as well as in the cryogenic temperature range.[14-16]

1.6.1.5. PBI Fibers

Polybenzimidazole fiber is generally prepared by dissolving dry PBI powder and lithium chloride (LiCl) in DMAc under pressure at temperature above the boiling point of the solvent. LiCl is used to increase solution life time from days to several months. PBI fiber has impressive properties which were explored to its textile as well as non-textile applications.[9, 13-16] The thermal and fire-protective properties of PBI fibers and PBI blends with other high performance fibers and glass fibers were well reviewed.[76-77] PBI fiber / fabric has limiting oxygen index (LOI) of 40-46% where as Nomex® has 27%.[9] PBI does not burn in air, generates little or no smoke, shrinks only 3% in a 24 hr at 316°C and retains stability, integrity and flexibility after long exposure to flame.[9-16] PBI shows excellent flame resistance, comfort and wear resistance and are used for protective industrial application especially for firemen's suits and fire fighters' service gear. Few representative properties and applications of PBI fiber listed below. PBI fiber (i) does not burn and melt, (ii) contributes no fuel to flames, (iii) produce little or no smoke up to 550°C, (iv) begins to lose its strength above 300°C, (v) retains dimensional stability at high temperature, (vi) retains form at high temperature, (vii) provides comfort through high moisture region, (viii) resists to acids and bases and (ix) produces very comfortable fabrics etc.

The thermal stability and nonflammability of PBI fibers are attractive for many industrial and aerospace applications. Current PBI fibers applications include (i) aircraft

seat fire blocking, (ii) firefighters protective gear, (iii) high temperature gloves, (iv) race car driver uniform, (v) flight suits, (vi) filtration, (vii) insulation (Woven, Knits or Felts), (viii) expansion joints, (ix) gasketing and (x) glass handling belts etc.

1.6.1.6. Medical Application

PBI microporous resin beads, commonly known as Aurorez®, diameter from 50-500 µm and porous internal structure with 85% void have unique separation capacities. PBI Aurorez resin is used for the determination of urinary porphobilinogen concentration and used for separations gas and liquid chromatography.[9]

1.6.1.7. PBI Membrane

PBI membranes have been received considerable attention in late 1960s and U.S government initiated PBI membrane development because of its good chemical resistance and excellent fiber forming capacity.[9] PBI membrane used as semipermeable membrane for reverse osmosis membranes in high temperature, acidic or basic pH conditions and harsh environment. PBI is chosen mainly because of its unique nanofiltration characteristics, robust mechanical strength and excellent chemical stability.[9, 13, 76-77] Polybenzimidazole having basic imidazole group (pKa 5.25) with two nitrogen atoms, one is attached to the hydrogen atom being a hydrogen bond donor while the other nitrogen with the lone pair act as a proton acceptor. PBI films were extensively used for purification of water from sea. It was seen that at 20-50°C temperature range cellulose acetate film and PBI film showed same performance in term of provided flux.[9, 13] PBI films performed better as the temperature was raised up to 90°C. The salt (NaOH) rejection capacity of PBI membranes is quite high (95%). Extensive research works on polybenzimidazole (PBI) nanofiltration (NF) membrane has been carried out by several groups.[76-77, 106-112] The removal of both anions (phosphate, sulfate, chromate, arsenate, arsenite and borate ions) and cations (copper ions) were investigated by Chung research group by amphoteric polybenzimidazole (PBI) nanofiltration (NF) hollow fiber membrane.[107-112] It was reported that PBI NF

membranes have a mean effective pore size of 0.348 nm in radius and pure water permeability of 1.86×10^{-5} lm^{-2} h^{-1} Pa^{-1} (1.86 lm^{-2} h^{-1} bar^{-1}).[108] The amphoteric characteristics of PBI molecules are due to the imidazole group that makes PBI NF membrane to have an isoelectric point near pH 7.0 and show different charge signs based on the pH medium.[111] The PBI-NF membrane exhibits impressive rejection capability for various ions typical anions, e.g. phosphate, arsenate, arsenite, borate anions and typical heavy metal cations, e.g. copper ions. The rejection capacity are strongly dependent on the chemical nature of electrolytes, solution pHs and the feed concentrations. PBI NF was potentially used for the removal of sulfate from concentrated chlor-alkali brine.[110] Wang et al. fabricated polybenzimidazole (PBI) nanofiltration (NF) hollow fiber membranes by chemically cross- linking by *p*-xylene dichloride.[112]

1.6.2 Most Advanced Application

1.6.2.1 Fuel Cell

Fuel cells are electrochemical energy conversion devices that convert chemical energy directly to electrical energy via a chemical reaction.[113-117] Fuel Cells have emerged as one of the most promising candidates for the power generators for both stationary and transportation applications.[117] In principle, a fuel cell operates like a battery. Unlike a battery which is an energy storage device, a fuel cell does not run down or require recharging.[118] In 1839, Sir William Grove first introduced the concept of a hydrogen / oxygen fuel cell, it took 120 years for the real application until in1960s when it was used by NASA in the Gemini space program. Fuel cells are clean, efficient, reliable and eco–friendly silent power generator. Fuel cell differs from the internal combustion engine; due to its energy efficiency because they avoid the intermediate step of converting heat to mechanical energy and therefore overcome the efficiency limit imposed by the Carnot cycle.[117-119].A fuel cell produces electricity, water, and heat from fuel and oxygen. When pure hydrogen is used as fuel, fuel cells generates water as the

only by-product and produce zero emissions of carbon monoxide, oxides of nitrogen or other key pollutants that makes the fuel cell an environmentally friendly energy source.

The basic building block of a fuel cell usually consists of an electrolyte layer sandwiched between porous anode and a cathode.[114-116] The anode serves as an interface between the fuel (e.g. H_2) and the electrolyte, catalyses the oxidation reaction and provides a path through which free electrons can conduct to the load via the external circuit. The cathode provides an interface between the oxygen and the electrolyte, catalyses the oxygen reduction reaction, and provides a path through which free electrons are conducted from the load to the electrode via the external circuit. The electrolyte acts as a physical barrier between hydrogen and oxygen to prevent directly mixing but conducts ionic charge between the electrodes and thereby completes the cell electric circuit, as illustrated in Figure 1.2. The cell reaction is shown below.
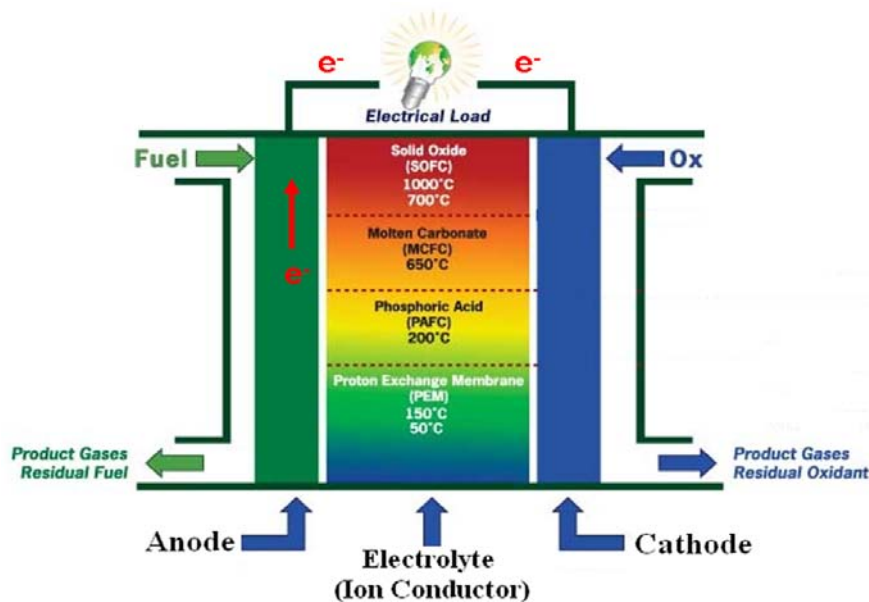
Figure 1.2. *Fuel Cell diagram.*

Cell reactions:

Anode: $H_2 \longrightarrow 2H^+ + 2e^-$

Cathode: $1/2\ O_2 + 2H^+ + 2e^- \longrightarrow H_2O$

Overall reaction: $H_2 + 1/2\ O_2 \longrightarrow H_2O + \text{Electrical Energy} + \text{Heat}$
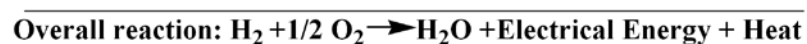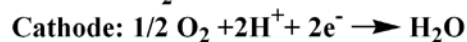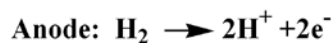
The classification of fuel cells is generally based on the type of electrolyte used in the cells and that includes (1) proton exchange membrane (polymer) electrolyte fuel cell (PEMFC), (2) alkaline fuel cell (AFC), (3) phosphoric acid fuel cell (PAFC), (4) molten carbonate fuel cell (MCFC), and (5) solid oxide fuel cell (SOFC). These fuel cells operate at different temperatures, and each is best suited to particular applications.[114-122] These fuel cells are listed in the order of approximate operating temperature, ranging from 50-150°C for PEMFC, ~100°C for AFC, ~200°C for PAFC, ~650°C for MCFC, and 800°C to 1000°C for SOFC (Table 1.3). Among the different types of fuel cells, polymer electrolyte membrane fuel cell (PEMFC) (i.e., proton exchange membranes, PEM) has attracted major recent research activities in recent years.

Table 1.3. *Different types of fuel cells*

Fuel Cells	Electrolyte	Operating Temperature (^{o}C)	Electric Power	Applications
PEMFC	Ion Exchange Membrane	50-150°C	Up to 250 kW	Vehicles, Stationary
AFC	Potassium Hydroxide	~100°C	Up to 20 kW	Submarines, Spacecraft
PAFC	Immobilized Liquid Phosphoric Acid	~200°C	> 50 kW	Power Stations
MCFC	Immobilized Liquid Molten Carbonate	~650°C	> 1 MW	Power Stations
SOFC	Ceramic	800–1000°C	> 200 kW	Power Stations

1.6.2.2. Proton Exchange Membrane Fuel Cell

Proton exchange membrane or polymer electrolyte membrane fuel cell (PEMFC) is the most promising candidates and attractive among all fuel cell systems due to its simplicity in uses in automobile and stationary applications.[117, 120, 123, 124] The PEMFC

is low cost and more compact than all other types of fuel cells. Depending upon the polymer electrolytes, PEMFCs can operate relatively low to high temperature (30-150°C) and generate relatively high power density than any other type of fuel cell.[120, 124-133] The heart of PEMFC consist of two electrodes (anode, cathode) separated by an ion-conducting polymer electrolyte membrane, commonly termed as membrane electrode assembly (MEA) unit (Figure 1.3). The working principle of PEMFC involves the oxidation of the fuel (e.g., hydrogen) at the anode and the reduction of oxygen at the cathode.[114-118] Both reactions are usually catalyzed by metal catalysts such as platinum. In presence of platinum, the hydrogen molecules split into protons and electrons at the anode. The resulting protons are transported in an aqueous environment across the electrolyte to the cathode compartment because the polymer membrane is only permeable for proton. Thus the electrons must travel through an external circuit and create the source of a direct electrical current. At the cathode the gaseous oxygen from the air is reduced and combines with proton which came across directly through the proton exchange membrane electrolytes and the returning electrons to form water.
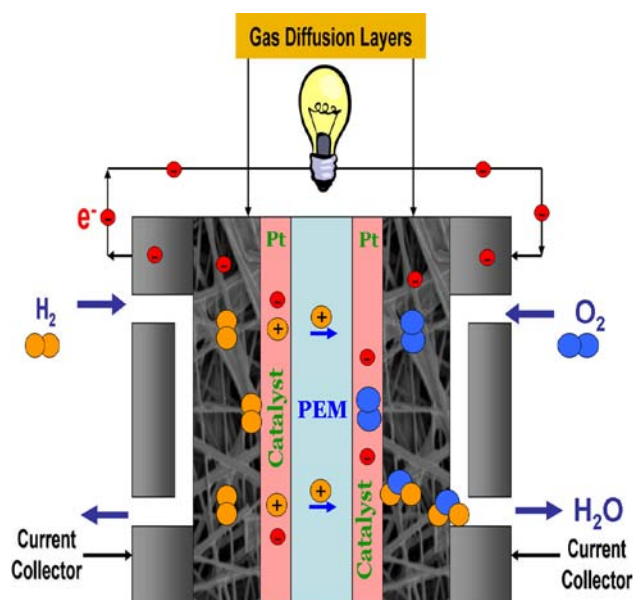
Figure 1.3. *Polymer Electrolyte Membrane Fuel Cell (PEMFC).*

1.6.2.3. Required Properties of Polymer Electrolyte or Proton Exchange Membrane

A polymer electrolyte membrane (PEM) not only serves as a proton carrier from anode to cathode and thereby completes the cell electrical circuit, but also provides a physical barrier to prevent the direct mixing of fuel (H_2) and oxygen gas. To obtain high performance polymer electrolyte membrane fuel cell (PEMFC), the polymer membrane should have the following characteristics.[117, 120, 123, 124, 131-133]

- High proton conductivity
- High mechanical stability
- High thermal and chemical stability
- Low gas permeability
- Good film-formation capacity
- Low cost
- Capable of fabrication into MEAs
- Mechanical durability at high temperature (80–140°C).

1.6.2.4. Commercially Available Polymer Electrolyte Membranes

Current polymer electrolyte membrane fuel cell (PEMFC) industry is ruled by perfluorosulfonic acid (PFSA) polymer membrane, known as Nafion$^®$ and it was introduced by DuPont in 1966. The perfluorosulfonic acid membranes are generally composed of the teflon-like, fluorocarbon backbone ($– CF_2 – CF – CF_2 –$) with the side chains, $–O– CF_2 – CF(CF_3) – O– CF_2 – CF_2 –$, which connect with sulfonic acid group (Scheme 1.14).[134-135] The teflon-like backbone provides Nafion with excellent long term stability in both oxidative and reductive environment. Nafion$^®$ is the most widely used PEM because of it's high proton conductivity, good mechanical strength, excellent

stability, and is commercially availability.[119-120, 124] It has been reported that the lifetime of commercialialy available Nafion type membrane under 80°C has been achieved more than 50,000 hours.[131-132, 136] In fully hydrated condition this type of membrane exhibit high protonic conductivity 10^{-2} S.cm^{-1} but dramatically decreases with temperatures above the boiling point of water (100°C) because of the loss of absorbed water in the membrane.[117, 124, 136-137] The membrane also will start loosing its mechanical and dimensional stability due to its low glass transition temperature (T_g) (80-120°C) above 100°C. Another major drawback of perflurosulfonic acid membranes is their very expensive cost (>$700/m^2) which is due to expensive fluorinated comonomer. [131-132, 136-137]

$$\left[CF_2\text{-}CF_2\right]_x\left[CF_2\text{-}CF\right]_y$$
$$O-CF_2\text{-}CF-O-CF_2\text{-}CF_2\text{-}SO_3H$$
$$Nafion^{TM} \quad CF_3$$

$$\left[CF_2\text{-}CF_2\right]_x\left[CF_2\text{-}CF\right]_y$$
$$Dow^{TM} \quad O-CF_2\text{-}CF_2\text{-}SO_3H$$
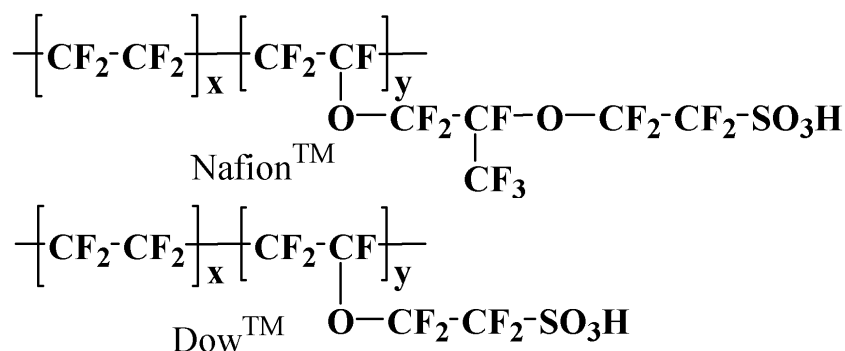
Scheme 1.14. *The chemical structures of PFSA-based PEM.*

Recently, large number of different verities polymers were used as proton-exchange membranes [117, 120, 124, 126-127] these include polystyrenesulfonic acids,[127] sulfonated polyimides,[139] sulfonated poly(ether ketone)s,[140, 141] sulfonated poly(arylene ether sulfone)s,[142] sulfonated poly(phenylene sulfide),[120] sulfonated polyphosphazenes,[143-144] polybenzimidazoles,[35, 129, 131, 133] etc Scheme 1.15 represents few of these polymer structures.
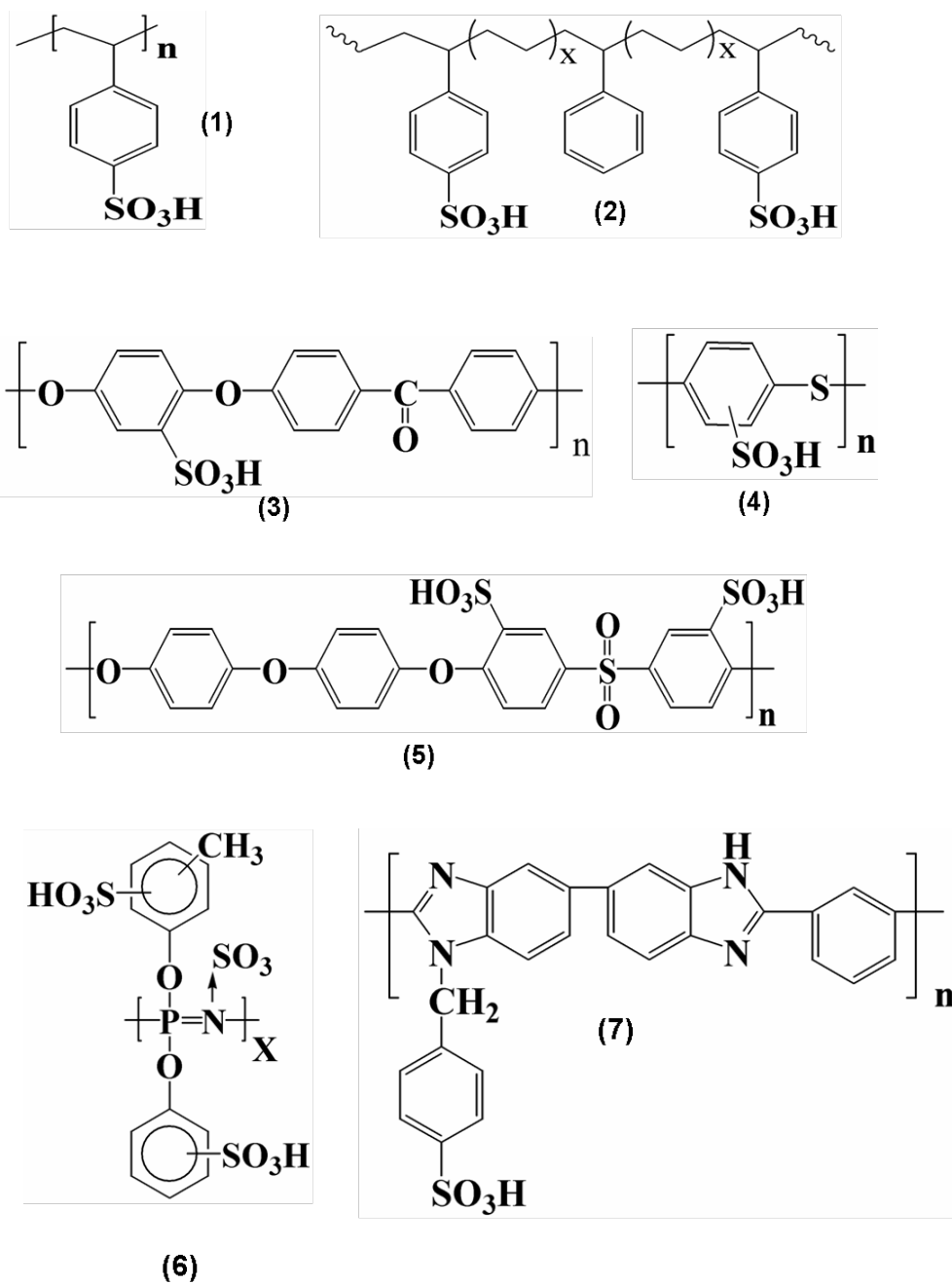
Scheme 1.15. *Polymers used as polymer electrolyte membrane (PEM). (1) Sulfonated polystyrene (2) Sulfonated styrene-ethylene copolymer (3) Sulfonated poly (etheretherketone) (4) Sulfonated polyphenylenesulfide (5) Sulfonated polysulfone (6) Sulfonated polyphosphazene (7) Sulfonated polybenzimidazole.*

1.6.2.5. High Temperature (>120°C) Polymer Electrolyte Membranes Fuel cell

The perfluorosulfonic acid (PFSA) membranes such as Nafion™ are most widely used polymer membrane material and commonly used in fuel cell stacks. This type of membrane although meets almost all the necessary requirements discussed above but still possesses several drawbacks.[117, 120, 124] At higher operating temperature, membrane dehydrated and subsequently decreased in protonic conductivity. Even these membrane made of with relatively robust materials but lose their mechanical attributes when dehydrated, resulting in shrinking and cracking. It has been observed that above the glass transition temperature (T_g) of the polymer, extensive morphological relaxation occurred. The glass transition temperature (T_g) of the membrane must be above the operating temperature of the fuel cell.[117, 137] The T_g of hydrated membrane not only depends on the chemical structure of polymer but also depends on the water content due to its plasticizing effect. Nafion$^{®}$ has glass transition temperature (T_g) between 130 -160 ^{o}C for dry membrane and between 80-100°C in hydrated condition.[134, 137] The presence of water limits the fuel cell operating condition typically around 80°C under atmospheric pressure. Fuel cells made up of low temperature membranes where the operation temperature is almost close to the boiling point of water involves a duel phase water system i.e., liquid water/water vapor when the humidification is too high, water condenses and the electrodes are flooded. Another decisive effect associated with a low temperature is the poor tolerance to fuel (H_2) impurities. The H_2 gas streams generally will contain trace amounts of carbon monoxide (CO) which poisons the platinum catalyst.[137, 145-147] This poisoning effect has been shown to be temperature dependent factor. Another major drawback of perflurosulfonic acid membranes is their high cost.[131, 137] Another approach towards high performance membrane relies on the sulfonation of polymers such as polystyrene, polyimides, poly (ether ketone)s, poly(arylene ether sulfone)s, poly(phenylene sulfide), polyphosphazenes etc. However these approaches have also some serious drawbacks.[120] The degree of sulfonation is generally a key parameter for these types of sulfonated aromatic polymers. The

excessive swelling and loss of mechanical integrity is observed at high sulfonation levels where as the low proton conductivity is observed at low degree of sulfonation.[120] Several attempts have been made to reduce the swelling problem without significantly lowering their sulfonation, one of them was incorporating cross-linker in the polymer backbone. Unfortunately, the cross linked membranes become very brittle upon drying out, which became a severe problem when these membranes were used in fuel cells. Most of the aromatic sulfonated polymer membranes start thermal degrading at 200-400 ^{o}C. A second approach investigated is the incorporation of inorganic fillers (SiO_2, ZrP, phosphotungstic acid (PWA), silicotungstic acid, carbon nano tubes) into the perfluorinated ionomer membranes to increase the binding energy of water.[117, 120, 124, 126] Also, composite membranes of these polymers are explored for the use as PEM. Among those all, acid-base complexation method represent most effective pathway for development of high temperature proton conducting membranes (Scheme 1.16). Basic polymers can be easily doped with strong acids which act as both proton donor and an acceptor in proton transfer mechanism and therefore facilitate the proton migration.

High temperature polymer electrolyte membrane (HTPEM) operating above 120°C overcomes above mentioned problems and offers many advantages which include elimination of humidification requirements, fast electrode kinetics, high tolerance to fuel impurity most notably carbon monoxide (CO), wide fuel choices, lower fuel reformation, and simplified water/thermal management etc.[35, 124, 137, 147] Normally at high temperature the CO tolerance will be enhanced from 10-20 ppm of CO at 80°C to 1000 ppm at 130°C and up to 30,000 ppm at 200°C due to the absorption of CO on Pt being weakened.[124, 137, 143] Above the boiling point of water, operation of PEMFC involved only a single phase of water i.e. water vapor and so transport of water in membrane, diffusion layers will be easier to balance.
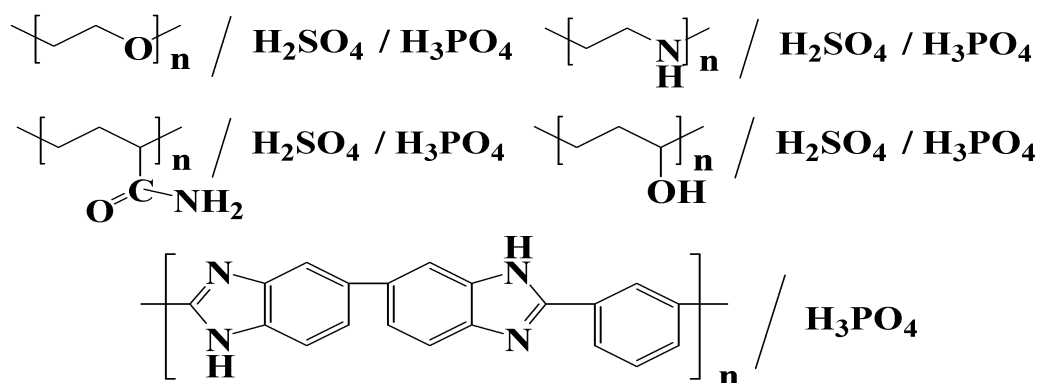
Scheme 1.16. *Polymer electrolyte membranes prepared by the method of acid base complexation.*

1.6.2.6. Phosphoric Acid (PA) Doped PBI Fuel Cell Membranes

Acid doped polybenzimidazole (PBI), proposed by Litt and Savinell has emerged as a promising candidate for a low-cost and high performance membrane material for the use in high temperature PEM fuel cells.[148] H_3PO_4 (PA)-doped PBI has received much attention in the last few years and it is suitable alternative of Nafion™ for high temperature operation. PA-doped PBI membrane exhibits high protonic conductivity at temperatures up to 200^oC, low gas permeability, excellent oxidative and thermal stability, good mechanical flexibility at elevated temperatures and nearly zero water drag coefficient.[35, 87-88, 129, 147-149] In phosphoric acid (PA) doped PBI, PA is the most interesting because they are more amphoteric, thermally stable and having low vapour pressure at elevated temperatures and having both proton donor and proton acceptor groups to form dynamic hydrogen bond networks, in which protons can readily transfer by hydrogen bond breaking and forming processes. Proton transfer in acid-base membrane is generally depends on the nature of the acid as well as the polymer, temperature and the humidity. Savadogo compared the protonic conductivity of acid doped PBI membrane in different acids and found that the conductivity changes are in the order of $H_2SO_4 > H_3PO_4 > HClO_4 > HNO_3 > HCl$ for high doping levels.[150] Phosphoric acid (PA) doped PBI membrane has been studied in the greatest details and

widely accepted that protonic conductivity is dependent on acid doping level, humidity, temperature and pressure, and widely reported in the literature that typically ranges between 0.04-0.08 Scm^{-1}.[35,129] Wasmus et al. used solid state NMR for characterization of H_3PO_4 doped PBI to show the PA sorbed by the PBI membrane is relatively immobile compared to free PA and revealed that there is an interaction between PBI and PA.[151] Gilpa et al. confirmed using IR spectroscopy that the proton transfer was happened from H_3PO_4 to the imino groups of PBI and the presence of undissoociated H_3PO_4 at higher doping level.[152] Kawahara et al. concluded from FTIR data that except H_3PO_4 others (H_2SO_4, CH_3SO_3H, $C_2H_5SO_3H$) protonate basic N moiety on the imidazole groups of PBI but in case of H_3PO_4 strong hydrogen bonding interaction exist between the OH group of acid and imino group of imidazole ring.[153] The presence of HPO_4^{2-} and $H_2PO_4^{-}$ anions, based on IR, implies that the proton conduction occurs through Grotthuss mechanism. They found that the *m*-PBI/PA complex was stable up to 500°C, with an anhydrous proton conductivity of 10^{-5} S.cm^{-1}. The thermal stability of *m*-PBI/strong acid complex was highest for phosphoric acid, and decreased in the order of sulfuric acid, methanesulfonic acid, and ethanesulfonic acid. The higher thermal stability of the PBI/PA suggests that the hydrogen bonding interaction imparts stability to the polymer/acid complex. Siebert developed a microscopic model based on IR spectroscopy study and suggesting that proton transfer from one imide site to another in which the anionic species participates by Grotthuss mechanism.[149] Generally the protonic conductivity is greatly influenced by the presence of water when H_3PO_4-blended PBI was allowed to absorb H_2O, the conductivity of the sample increased dramatically. These water molecules can act as additional proton solvents and contribute to the proton transport either by self-diffusion while carrying a proton (Vehicular type mechanism) or by the rapid exchange of protons via hydrogen bridges (Grotthuss type mechanism). Pu et al. proposed that proton transfer in PA doped PBI membrane was the consequences of the two contributions: one was based on rapid proton exchange (hopping) between phosphate and imidazole moieties via hydrogen bonds (Grotthuss type mechanism), and the other on self-diffusion of phosphate moieties (Vehicular type mechanism) (Scheme 1.17).[154]

(A) **(B)**
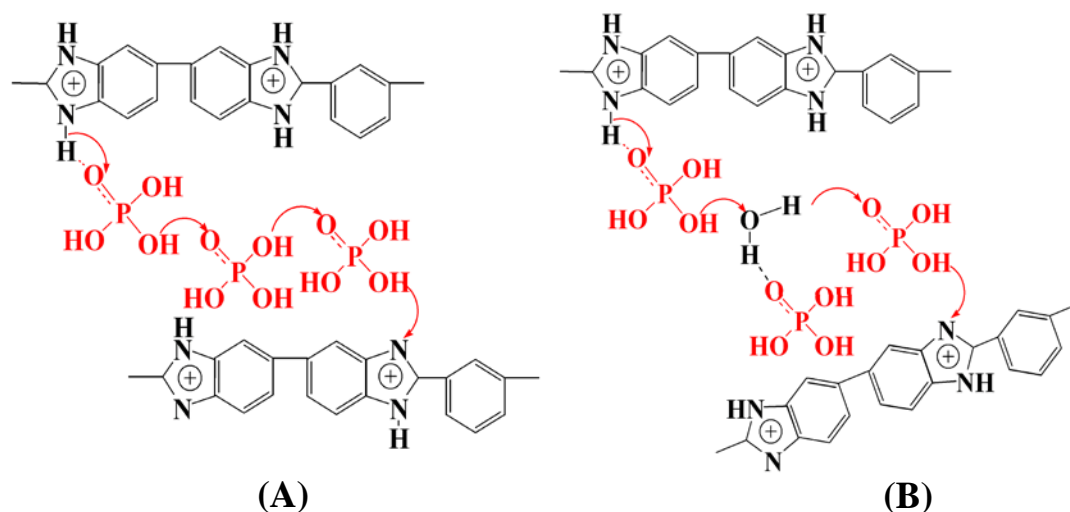
Scheme 1.17. *Proton transfer process (A) acid- PBI- acid (B) acid- water-acid PBI.*

Generally it is believed that the higher PA doping level leads to increased protonic conductivity and improved the fuel cell performance. Wainright reported [148, 155] that PA doped m-PBI (I.V=0.6 dl/g) with 5.0 moles PA per repeating unit (PRU) and conductivity of 2×10^{-2} Scm^{-1} at 130°C and 2.5×10^{-2} Scm^{-1} at 150°C. Pu et al. reported [154] m-PBI/PA doped membrane with 6.0 moles PA per repeating unit had conductivity 4.5×10^{-5} S.cm^{-1} at 25°C. Li et al.[156] reported m-PBI/PA complex with 16 moles PA/PRU and the conductivity of 0.13 S.cm^{-1} at 160°C. It has been observed that the conductivity of PA doped PBI membrane increased with higher PA doping but the mechanical strength decreased proportionally with the increase in doping level, leading to loss of mechanical properties at higher doping levels. He et al.[157-158] conducted a study on gas permeability, volume swelling, mechanical integrity, and conductivity of PA doped PBI membranes and found that an increased doping level led to an increase in volume swelling (0.3 mol PA/PRU had 22% swelling, while 5 mol PA/PRU corresponded to 118% swelling), seen mostly in the thickness of the polymer sample due to separation of the PBI backbone by acid molecules. They observed that PBI membranes with weight average molecular weight of 25,000 at 125°C with a doping

level of less than 2 mol PA/PRU, mechanical strength increased slightly due to hydrogen-bonding, then decreased sharply as acid loading increased. At 180°C, a linear decrease in mechanical integrity was found with increasing doping level, and values were overall lower than those at 125°C: for PBI acid doping level zero, stress at break was 150MPa at 125°C and 130MPa at 180°C whereas doping level of 2.3, stress at break was 160MPa at 125°C and 48 MPa at 180°C. They conclude that for pure PBI membranes, the hydrogen bonding between –N and –NH– groups is the dominating force that determines its mechanical strength but when phosphoric acid is introduced, the molecular cohesion of PBI is decreased but stronger hydrogen bonds between –N and phosphoric acid molecules are formed than that of between –N and –NH– groups as a result of the acidity of phosphoric acid. The elongation at break increases with higher doping levels, because the membrane become more plastic in nature at high acid doping levels and could more easily rearrange under load. Mechanical properties were found to improve with higher molecular weights, as shown by the 3.5 MPa stress at break for PBI with M_W of 17,800 and the 6 MPa stress at break for PBI with M_W of 25,000 and 12MPa for M_W 36,800. It is very essential that PBI has a molecular weight exceed a certain value for preparing superior quality membrane. According to Wainright et al.[148,155] for fuel cells applications, PBI acid doping level of about 5 is required for high enough conductivity and PBI molecular weight (M_W) should be above 11,000, corresponding to an inherent viscosity (I.V) of 0.3 dL g^{-1}.

1.6.2.7. PA doped PBI Membrane Fabrication

The discussion in the previous section clearly demonstrates that the PBI membrane with high PA loading and supub thermo-mechanical stability is required for the use in PEMFC. However, as it is mentioned in the previous section, the high PA loading PBI membrane display extremely poor mechanical stability. Hence there is need of compromise between these two. Therefore, in addition to the various synthetic attempts to prepare varities of PBI backbone structures, various approaches have been

adopted so far for fabrication of PA loaded PBI membrane. These are broadly classified as (1) Dimethyl acetamide (DMAc) casting method followed by soaking in phosphoric acid we call this as conventional imbibing process, (2) Trifluoroacetic acid (TFA) casting method, (3) Polyphosphoric acid (PPA) casting method (sol–gel process by direct casting of membrane from the high molecular weight PBI solution in polyphosphoric acid, PPA), (4) Porous PBI membrane method (porogens have been used to prepare porous PBI membrane, (5) Gel-casting method (preparation of thermoreversible gel of PBI in PA and followed by casting the PA doped membranes).[33-35,158-163]

The conventional imbibing method to prepare acid doped PBI membranes involved first dissolving the commercially available PBI in an appropriate solvent, such as dimethyl acetamide (DMAc) above the boiling point of the solvent under an oxygen-free atmosphere with minor amount of lithium chloride may optionally be added to the solution in order to prevent the polymer from separating from the solution during storage for an extended period of time. PBI membranes can be cast from solutions of different concentrations. After casting onto a glass plate, the majority of the solvent is evaporated at temperatures ranging from 60 to 120°C. The membranes are then washed with hot water in order to eliminate the stabilizer (LiCl) and trace amount of DMAC. The organic solvent, such as DMAc, are generally poisonous to the platinum fuel cell catalyst. So it is very important to remove. Finally DMAc cast membranes are dried under vacuum at of up to 190°C. Then the PBI membranes are subsequently immersed in desired phosphoric acid (PA) solution. The equilibrium generally reached after 50 h at room temperature for complete acid saturation. Typically an acid-doping level ranging between 5 to16 per repeat unit can be achieved by using 65–85 wt% acid solutions. The proton conductivity of the resulting membranes ranged from 0.01 to 0.04 S.cm^{-1} for temperature range of 130°C-190°C.[35, 129] The mechanical property is good enough for the fabrication of membrane electrode assembly (MEA).

It was known that the PBI is soluble in a mixture of trifluoroacetic acid (TFA) and phosphoric acid and the use of trifluoroacetic acid (TFA) as an acid solvent in combination with phosphoric acid not only facilitated the dissolution of PBI polymers

and the direct casting of acid-doped PBI membrane, but it also enhanced the proton conductivity of the resulting membranes. In this process PBI powder is first mixed with trifluoroacetic acid and after refluxing for a few hours, a certain amount of H_3PO_4, corresponding to the desired acid-doping level, is added for dissolution of the PBI. The obtained solution is then filtered and cast into membranes on a glass plate under nitrogen atmosphere. The membrane is then dried at room temperature under vacuum. PA doped PBI prepared from TFA/H_3PO_4 solution exhibited conductivities of 0.04-0.08 S.cm^{-1}, values higher than those for the PBI membrane cast from DMAc and the subsequently doped (imbibing process). The membranes cast from TFA solution gave poor mechanical properties even more rubbery and softer than the conventional imbibing process.[35, 159-160]

In the PPA casting procedure polyphosphoric acid (PPA) is used as an efficient condensation agent, polymerization solvent and membrane casting solvent. Xiao et al.[34] developed this new process where after the completion of polymerization in PPA medium, the hot (at 200°C) PBI solutions in PPA are cast directly without isolation of the polymer and the PPA hydrolyzed in-situ to phosphoric acid. After casting, the hydrolysis of PPA to phosphoric acid is allowed to take place by absorbing the moisture from the surrounding environment which induces a sol–gel transition, resulting in phosphoric acid-doped PBI membranes (Figure 1.4). These membranes have high PA doping levels, good mechanical properties, high conductivities, and excellent long term stabilities, even when operating at temperatures over 150°C. The acid doping levels as high as 20–40 mols PA per repeat unit of PBI can be achieved with high conductivity over 0.2 S.cm^{-1} with acceptable tensile strength of up to 3.5MPa. It is interesting that the sol–gel behaviors of the PPA membranes depend very much on the polymer structures and molecular weight. High molecular weight (I.V.) *para*-PBI seems to stabilize the gel state and produced membranes with better mechanical stability. This PPA method has been used to develop the PA doped PBI membrane with varity of PBI structure.[161]
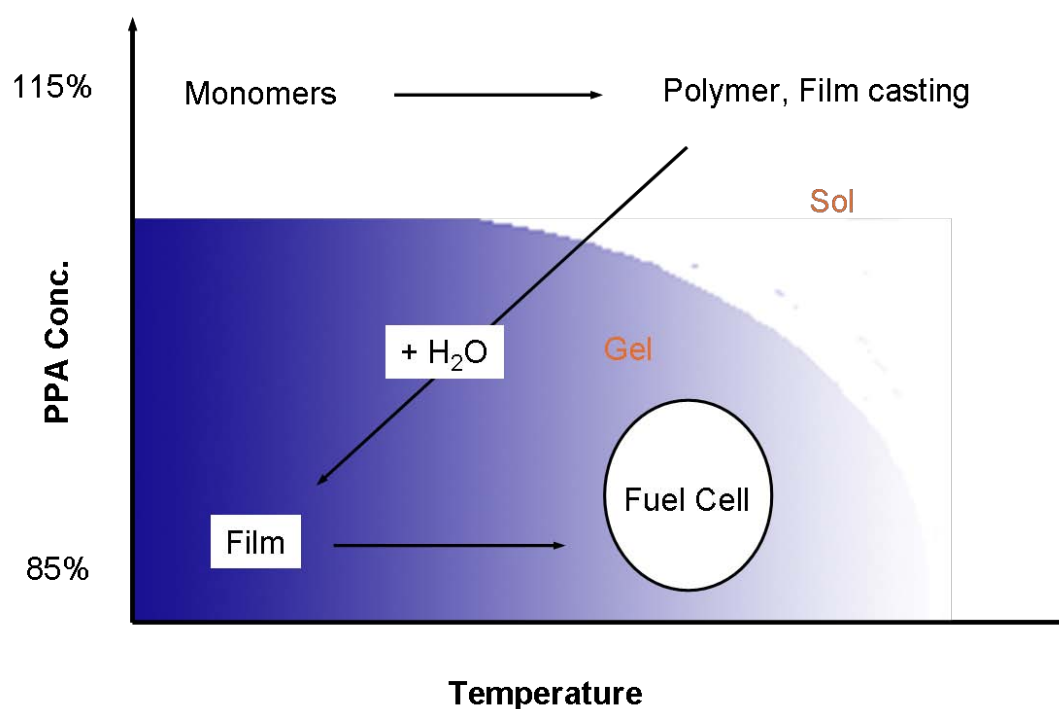
Figure 1.4. *Fabrication of PA doped PBI membrane by PPA process. Adapted from reference 34.*

In porous PBI method, the porous PBI films were prepared by leaching out a low molecular weight compound (porogen) using selective solvents of the porogen from polymer/porogen mixtures. Then the porous PBI membranes were soaked in phosphoric acid solution to obtain the PA doped PBI membrane (Figure 1.5)[162]. In this method different phthalates such as dimethyl, diethyl, dibutyl and diphenyl, as well as triphenyl phosphate were used as porogen. The pore size and morphology strongly depend upon the porogen/PBI ratio as observed from SEM (Figure 1.5). The PA doped porous PBI membranes obtained in this process are mechanically stable. The acid uptake and ionic conductivities of the PA doped PBI porous membrane increases with porosity.
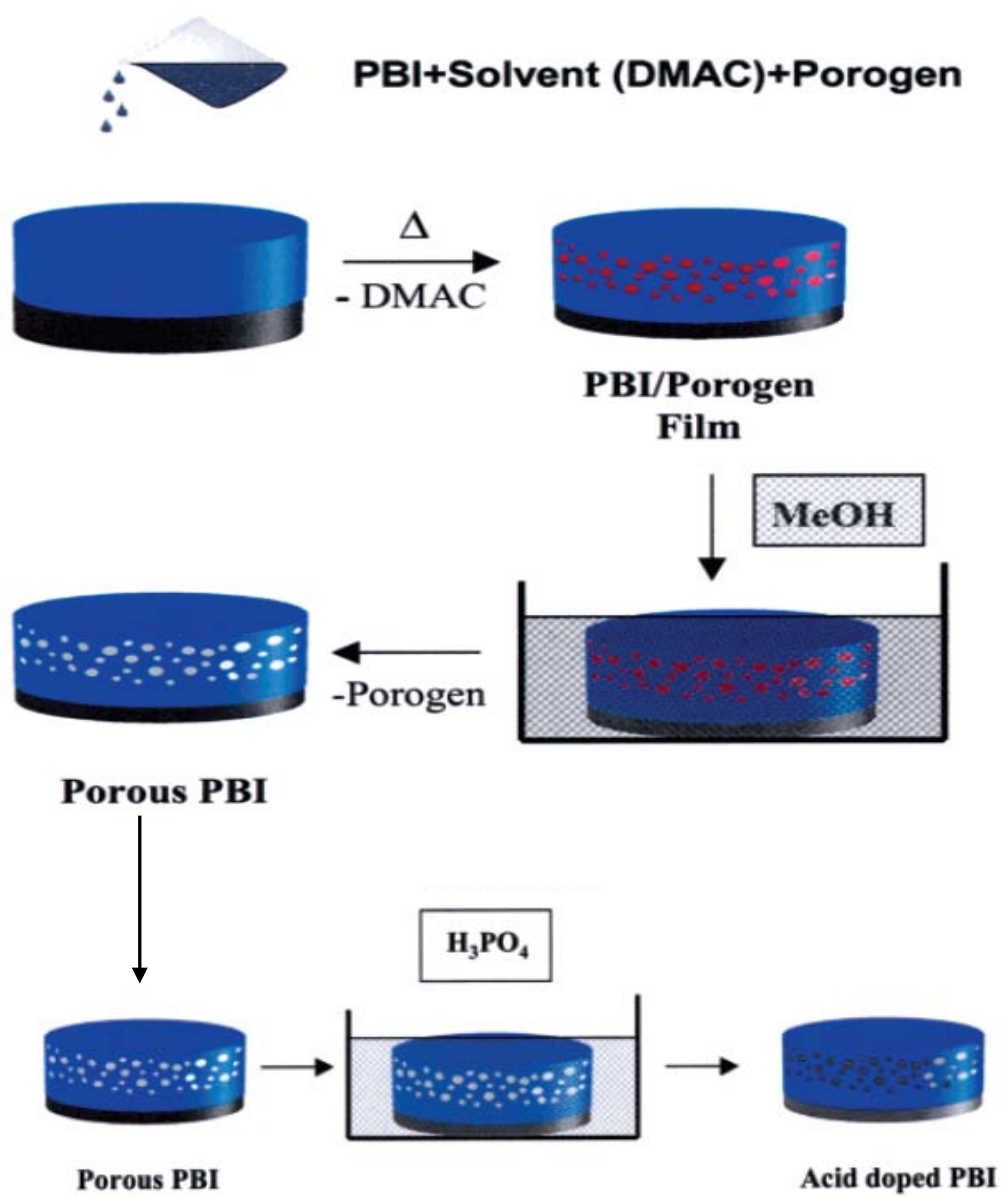
Figure 1.5. *Fabrication of PA doped PBI membrane by porous PBI process. Adapted from reference 162.*
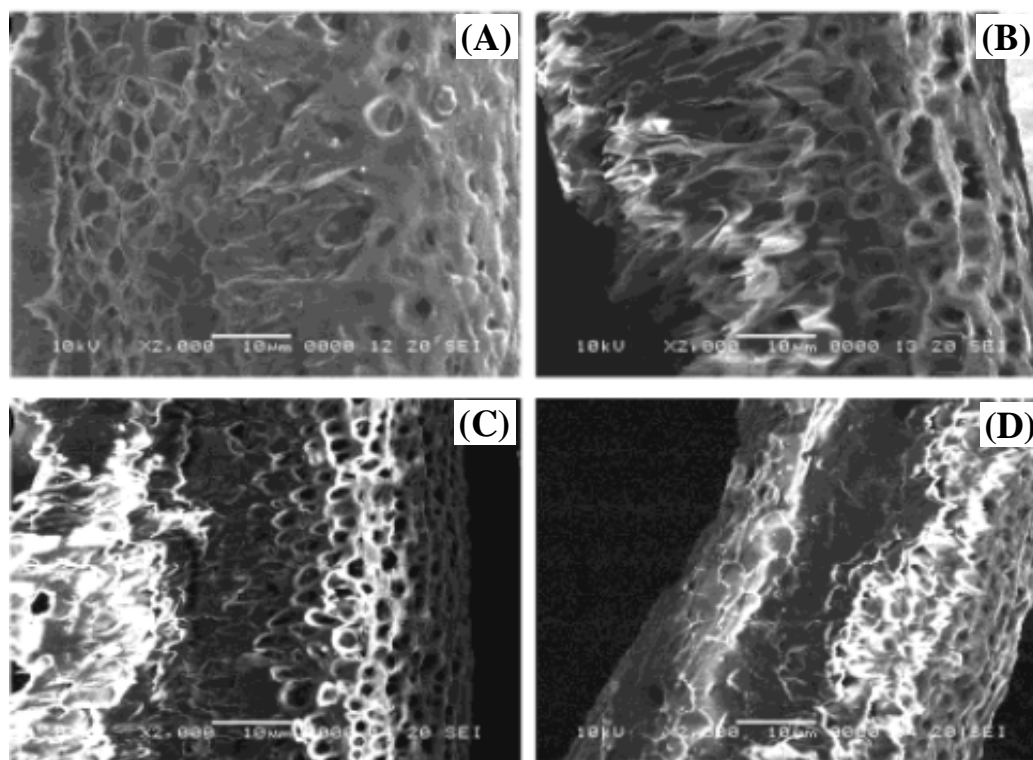
Figure 1.6. *SEM micrographs of cryogenic fractures of porous PBI membranes prepared from 25:75 wt % PBI/porogen films based on (a) dibutyl phthalate, (b) dimethyl phthalate, (c) diphenyl phthalate, and (d) triphenyl phosphate.*[162]

Very recently we have developed a method by which one can prepare mechanically strong and stable PA doped PBI membrane with very high PA doping level.[163] In this procedure *m*-PBI gel was prepared by taking require amount of solid *m*-PBI powder and in H_3PO_4. The mixture was then heated at 200$^{\text{o}}$C for 1 to 2 hour to get homogeneous reddish *m*-PBI solution in H_3PO_4. This hot solution was poured in petridish and within 2 minutes it forms the gel. This gel material can be easily pilled off from the glass surface as a strong free standing PA doped PBI film. We have found acid-doping levels as high as 40 mol PA per repeat unit of PBI depending upon the gel

concentration. We have observed for PA doped PBI membrane obtained from below the critical gelation concentration of m-PBI film are very weak in mechanically where as above the critical gelation m-PBI PA doped film are high mechanically stable. This process we named as gelation process or gel casting method. We will be describing this aspect in Chapter 5 and 6.

1.7. AIMS of the Thesis

The above discussion in this chapter about the PBI types polymers offers many opportunities to study the PBI chemistry. Despite the presence of huge literature on the PBI type materials, we found out that there are many issues which were not addressed and discussed in the literature appropriately. Large numbers of efforts have been made to synthesize variety of PBI backbone structure, however limited efforts were attempted to synthesize copolymers and moreover to established a correlation between their molecular properties and structure. Hence we have attempted to explore these aspects in Chapter 2 and 3. Surprisingly, the studies on solution properties of PBI is almost missing in the literature except only very few superficial reports. We have addressed this issue in Chapter 4. The gain of huge attention of PBI in recent years is due to their use in PEMFC. Despite the presence of large volume literature on the phosphoric acid doped PBI membrane for the use in PEMFC, till today the best suited membrane has not been achieved. We have aimed to resolve this and developed a new PBI-PA gel membrane. These topics are discussed in Chapter 4 and 5. The aims and objectives of each chapter of this thesis are elaborated at the end of the introductory part of the individual chapters.

References

(1)   Odian, G. *Principles of Polymerization*; John Wiley & sons, Inc.: **2004**.

(2)   Cassidy, P. E. *Thermally stable Polymers*; Dekker, New York, **1980**.

(3)   Sillion, B. *High Perform. Polym*. **1999**,*11*, 417.

(4)   Vogel, H. A.; Marvel, C. S. *J Polym Sci*. **1961**, *50*, 511.

(5)   Vogel, H.; Marvel, C. S. *J Polym Sci. A*. **1963**, *1*, 1531.

(6)   Plummer. L.; Marvel, C. S. *J Polym Sci. A*. **1964**, *2*, 2559.

(7)   Marvel, C. S.; Ariz, T.; Vogel, H. A. U. S. Patent 3 174 947,**1965**.

(8)   Brinker, K.C.; Robinson, I. M. U. S. Patent 2 895 948, **1959**.

(9)   Choe, E. W., Choe, D. D. In *Polymeric Materials Encyclopedia*; Salamone, J. C., Ed.; CRC Press: New York, **1996,** pp 5619-5638.

(10)   Lee, H.; Stoffey, D.; Neville, K. *New Linear Polymers;* McGraw-Hill, New York, **1967**, Chapter 9.

(11)   Frazerr, A. H. High *Temperature Resistant Polymers;* Interscience: New York, **1968**, pp 138.

(12)   Critchley, J. P. *Prog. Polym. Sci*. **1970**, *2*, 47.

(13)   Neuse, E. W. *Adv. Polym. Sci*. **1982**, *47*, 1.

(14)   Power, E. D.; Serad, G. A. *High Performance Polymer: Their origin and Development,* Elesevier, New York, **1986**, pp 355.

(15)   Buckley, A.; Stuetz, D.; Serad, G.A. *Encyclopedia of Polymer Science and Engineering,* Wiley, New York, **1987**, 572.

(16)   Critchley, J. P.; Knight, G. J.; Wright, W.W. *Heat-resistant Polymers, Plenum Press, New York,* **1983**, pp 259-322.

(17)   Prince A. E. U. S. Patent 3 509 108, **1970**.

(18)   Eguchi, T.; Ohfuji, Y. U. S. Patent 3 655 632, **1972**.

(19)   Choe, E W. *J Appl Polym Sci*. **1994**; *53*, 497.

(20)   Neuse, E.W.; Loonat, M. S. *Macromolecule*. **1983**,*16*,128.

(21)   Brand, R. A.; Bruma, M.; Kellman, R.; Marvel, C. S. *J. of Polym. Sci., Polym. Chem.Ed*.**1978**, *16*, 2275.

(22)   Higgins, J.; Marvel, C. S. *J. Polym. Sci.* **1970**, A-1, *8*, 171.

(23)   Wrasidlo, W. ; Levine, H. H. *J. Polym. Sci.; Part A*. **1964**, *2*, 4795.

(24)   Gray, D. N.; Schulman, G. P. *J. Macromol. Sci.A*. **1967**, *1*, 395.

(25)   Gray, D. N.; Rouch, L. L.; Strauss, E. L. *Macromolecule* **1968**, *1*, 473.

(26)   Pense, R.; Marvel, C. S. *J. Polymer Sci*. **1970**, A-18, 3189.

(27)   Brand, R.; Bruma, M.; Kellman.; Marvel, C. S. *J. Polymer Sci., Polym. Chem.Ed.* **1978**, *16*, 2275.

(28)   Sillion, B.; Gaudemaris, G, De. *Bull. Soc. Chim.(France).* **1970**, *12*, 4452.

(29)   Korshak, V.V.;Rusanov,A.L.;Tugushi,D.S.; Cherkasova, G.M. *Macromolecules*. **1972**, *5*, 807.

(30)   Tugushi, D.S.; Korshak, V.V.; Rusanov, A.L.;Danilov, V.G.;Cherkasova, G.M.; Tseitlin,G.M. *Polym. Sci. U.S.S.R*. **1973**,*15*, 1087.

(31)   Korshak V. V.; Rusanov, A. L.;. Gverdtsiteli, I. M. Tugushi D. S. Shubashvili A. S. *Dokl.Akad.nauk S.S.S.R.* **1978**, *240*, 346.

(32)   Korshak V. V.; Gverdtsiteli, I. M.; Kipiani, L.G.; Tugushi, D. S.; Shubashvili, A. S. *Polym. Sci. U.S.S.R.* **1979**, *21*,133.

(33)   Li, Q.;He, R.;Jensen, J. Q.; Bjerrum, N. J.; *Chem. Mater*. **2003**, *15*, 4896.

(34)   Xiao, L.; Zhang, H.; Scanlon, E.; Ramanathan, L. S.; Choe, E.-W.; Rogers, D.; Apple, T.; Benicewicz, B. C. *Chem. Mater.* **2005**, *17*, 5328.

(35)   Li ,Q.; Jensena, J. O.; Savinell, R. F.; Bjerrum, N. J. *Prog. Polym. Sci*. **2009**, *34*, 449.

(36)   Iwakura,Y.; Uno, K.; Imai, Y. *J. Polymer Sci.* **1964**, A2, 2605.

(37)   Choe, E. W.; Conciatori, A. B. U. S. Patent 4 452 972, **1984**.

(38)   Choe, E. W.; Conciatori, A. B.; Ward, B. C. U. S. Patent 4 463 167, **1984**.

(39)   Choe, E. W.; Conciatori, A. B. U. S. Patent 4 485 232, **1984**.

(40)   Choe, E. W.; Conciatori, A. B. ; Ward, B. C. U. S. Patent 4 506 068, **1985**.

(41)   Choe, E. W.; Conciatori, A. B. U. S. Patent 4 533 725, **1985**.

(42)   Choe, E. W.; Conciatori, A. B. U. S. Patent 4 535 144, **1985**.

(43)   Hedberg, F. L. ; Marvel, C. S. *J. Polymer Sci*., *Polym. Chem. Ed.* **1974**,*12*, 1823.

(44)   Brooks, N.W.; Duckett, R. A.; Rose, J.; Ward, I. M.; Clements, J. *Polymer* **1993**, *34*, 4038.

(45) Kulkarni, M.; Potrekar,R.; Kulkarni,R. A.; Vernekar, S. P. *Journal of Polymer Science: Part A: Polymer Chemistry*, **2008**,*46*, 5776.

(46) Varma, I. K.; Veena. *J. Polym. Sci., Polym. Chem.Ed.* **1976**, *14*, 973.

(47) Varma, I. K.; Veena. *J. Macromol.Sci., Chem.* **1977**, *11*, 845.

(48) Yu, S.; Benicewicz, B.C. *Macromolecules* **2009,** *42*, 8640.

(49) Gieselman, M.; Reynolds, J. R. *Macromolecules* **1992**, *25*, 4832.

(50) Chuang, S-W.; Hsu, S. L-C. *J . Polym. Sci.: Part A: Polym. Chem.* **2006**, *44*, 4508.

(51) Kojima, T. *J. Polym. Sci.: Polym. Phys. Ed.* **1980**, *18*, 1685.

(52) Kojima, T.; Yokota, R.; Kochi, M.; Kambe, H. *J. Polym. Sci.: Polym. Phys. Ed.* **1980**, *18*, 1673.

(53) Lobato, J.; Cañizares , P.; Rodrigo, M. A.; Linares, J. J.; Manjavacas , G. *J. Membr. Sci* **2006***, 280*, 351.

(54) Brock, T.; Sherrington, D. C.; Tang, H. G. *Polymer* **1991**, *32*, 353.

(55) Xu, H.; Chen, K.; Guo, X.; Fang, J.; Yin, J. *Polymer* **2007**, *48*, 5556.

(56) Shogbon, C. B.; Brousseau, J.-L.; Zhang, H.; Benicewicz, B. C.; Akpalu, Y. *Macromolecules* **2006,** *39*, 9409.

(57) Yuan, Y.; Johnson, F, Cabasso, I. *J. Appl. Polym. Sci.* **2009**, *112*, 3436.

(58) Sannigrahi, A.; Arunbabu, D.; Sankar, R. M.; Jana, T. *Macromolecules* **2007**, *40*, 2844.

(59) Ghosh, S.; Sannigrahi, A.; Maity, S. *J Phys Chem B* **2010**, *114*, 3122.

(60) Sannigrahi, A.; Arunbabu, D.; Sankar, R. M.; Jana, T. *J Phys Chem B* **2007**, *111*, 12124.

(61) Tsur, Y.; Freilich, Y. L.; Levy, M. *J. Polym. Sci.: Polym. Chem. Ed.***1974***, 12,* 1531.

(62) Ehlers, G.F. L.; Fisch, K. R.; Powell, W. R. *J. Polym. Sci. A* **1969**, *1*, 2931.

(63) Shulman, G. P.; Lochte, *J. Macromol. Sci. A* **1967**, *3*, 413.

(64) Rode, V. V.; Kotsoeva, N. M.; Cherkasova, G. M.; Tugushi, D. S.; Tseitlin, G. M.; Rusanov, A. L.; Korshak, V. V. *Polym. Sci. U.S.S.R.* **1970**, *12*, 2103.

(65) Gauchana, R. A.; Conley, R. T. *J. Macromol. Sci. Chem. A*. **1970**, 4, 441.

(66)   Conley, R. T.; Ghosh, S.; Kane. J. J. *Org. Coat and Plast. Chem. Pripents*, **1971**, *31*,151.

(67)   Arunbabu, D.; Sannigrahi, A.; Jana, T. *J Phys Chem B* **2008,** *112,* 5305.

(68)   Deimede, V.; Voyiatzis, G. A.; Kallitsis, J. K.; Qingfeng, L.; Bjerrum, N. J. *Macromolecules* **2000**, *33*, 7609.

(69)   Menczel, J. D. *J. Them. Analys. Calmetry,* **2000***,59,*1023.

(70)   Sannigrahi, A.; Ghosh, S.; Lalnuntluanga, J.; Jana, T. *J. Appl. Polym. Sci.* **2009**, *111*, 2194.

(71)   Klaehn, J. R.; Luther, T. A.; Orme, C. J.; Jones, M. G.; Wertsching, A. K.; Peterson, E. S. *Macromolecules* **2007**, *40*, 7487.

(72)   Pu, H. T.; Liu, Q. Z. ; Liu, G.H. *J. Membr Sci*. **2004**, *241*, 169.

(73)   Pu, H. T.; Liu, G.H. *Polym. Int.* **2005**, *54*,175.

(74)   Kumbharkar, S.C.; Islam, Md. Nazrul.; Potrekar, R.A.; Kharul, U. K. *Polymer* **2009**, *50*, 1403.

(75)   Kumbharkar, S.C.; Kharul, U. K. *J. Membr Sci*. **2010**, *357*,134.

(76)   Chang, T. S. *Handbook of Thermoplastics, Marcel Dekker. Inc,* **1997**, 703.

(77)   Chang, T. S. *Polymer Reviews.* **1997**, *37*, 277.

(78)   Guerra; G.; Cheo, S.; Williams, D. J.; Karasz, F. E.; Macknight, W. J. *Macromolecules* **1988**, *21*, 231.

(79)   Jaffe, M.; Chen, Paul.; Choe, E-W.; Chang, T. S.; Makhija, S. *Adv. Polym. Sci.* **1994**, *117*, 297.

(80)   Chang, T. S.; Herold, F. K.; *Polym. Eng. Sci.* **1991**, *31,*1950.

(81)   Musto, P.; Karasz, F. E., MacKnight, W. J. *Macromolecules* **1991**, *24*, 4762.

(82)   Chang, T. S.; Xu, Z. L. *J. Membr Sci*. **1998**, *147*, 35.

(83)   Deimede, V.; Voyiatzis, G. A.; Kallitsis, J. K.; Qingfeng, L.; Bjerrum N. J. *Macromolecules* **2000***,33*, 7609.

(84)   Wycisk, R.; Chisholm, J.; Lee, J.; Lin, J.; Pintauro, P. N. *J. Power. Sources.* **2006**, *163*, 9.

(85)   Li, Q. F.; Rudbeck, H.C.; Chromic, C.; Jensen, H, O.; Pan, C.; Steenberg, T.; Calverley, M.; Bjerrum N. J.; Kerres, J. *J. Membr Sci*. **2010**, *347*, 260.

(86) Zhang, H.; LI, X.; Zhao, C.; Fu, T.; Shi, Y.; Na, H. *J. Membr Sci.***2008**, *308*, 66.

(87) Savinell, R.; Yeager, E.; Tryk, D.; Landau, U.; Wainright, J.; Weng, D.; Lux, K.; Litt, M.; Rogers, C. *J. Electrochem. Soc.* **1994**, *141*, L46.

(88) Samms, S. R.; Wsmus, S.; Savinell, R. F. *J. Electrochem. Soc.* **1996,** *143,* 1225.

(89) He, R.; Li, Q.; Xiao, G.; Bjerrum, N. J. *J. Membr Sci.* **2003**, *226*, 169.

(90) Staiti, P.; Minutoli, M.; Hocevar, S.; *J. Power. Sources.* **2000**, *90*, 231.

(91) Staiti, P. *Mater. Lett.* **2001**, *47*, 241.

(92) Javaid Zaidi, S.M. *Electrochem. Acta.* **2005**, *50*, 4771.

(93) Shao, H.; Shi, Z.; Fang, J.; Yin, J.; *Polymer* **2009,** *50*, 5987.

(94) Jang, M.Y.; Yamazaki,Y. *J. Power. Sources.* **2005**, *139*, 2.

(95) Heo, P.; Kajiyama, N.; Kobayashi, K.; Nagao, M.; Sano, M.; Hibino, T. *Electrochem. Solid State Lett.* **2008**, *11*, B91.

(96) Chuang, S-W.; Hsu, S. L-C.; Yang, M-L. *Euro. Polym. J.* **2008**, *44,* 2202.

(97) Chuang, S-W.; Hsu, S. L-C.; Hsu, C-L. *J. Power. Sources.* **2007**, *168*, 172.

(98) Jiang, F.; Pua, H.; Meyer, W. H.; Guana, Y.; Wan, D. *Electrochem. Acta.* **2008,** *53*, 4495.

(99) Pua, H.; Liua, Lu.; Changa, Z,; Yuana, J. *Electrochem. Acta.* **2009**, *54*, 7536.

(100) Li , M-Q.; Shaob, Z-G.; Scott, K. *J. Power. Sources.* **2008**, *183*, 69.

(101) Lu, Y.; Chen, J.; Cui, H.; Zhou, H.; *Compo. Sci. Tech*, **2008**, *68*, 3278.

(102) Kang, J-Y.; Eo, S-M.; Jeon, I-Y.; Choi, Y. S.; Tan, L-S.; Baek, J-B. *J . Polym. Sci.: Part A: Polym. Chem.* **2010**, *48*, 1067.

(103) Zhai, Y.; Zhang, H.; Zhang, Yu, Xing, D. *J. Power. Sources.* **2007**, *169*, 259.

(104) Lin, H-L, Yu, T. L.; Chang, W-K.; Cheng, C-P.; Hua, C-R.; Jung, G-B. *J. Power. Sources.* **2007**, *164*, 481.

(105) Lin, H-L.; Chena, Y-C.; Li, C-C.; Chenga, C-P.; Yu, T. L. *J. Power. Sources.* **2008**, *181*, 228.

(106) Sawyer, L.C.; Jones, R .S. *J. Membr Sci.* **1984,** *20*, 147.

(107) Chung, T-S.; Xu, Z-L. *J. Membr Sci.* **1998**, *147*, 38.

(108) Wang, K. Y.; Chung, T-S. *J. Membr Sci.* **2006**, *281*, 307.

(109) Wang, K. Y.; Chung, T-S.; Qin, J-J. *J. Membr Sci.* **2007**, *300*, 6.

(110)   Wang, K. Y.; Chung, T-S.; Rajagopalan, R. *Ind. Eng. Chem. Res.* **2007,** *46,* 1572.

(111)   Lv, J.; Wang, K. Y.; Chung, T-S. *J. Membr Sci.* **2008**, *310*, 557.

(112)   Wang, K. Y.; Y, Q.; Chung, T-S.; Rajagopalan, R. *Chem. Eng. Sci.* **2009**, *64* 1577.

(113)   Yeager, E. *Science* **1961**, *134*, 1178.

(114)   Fuel Cell Handbook, 6 th. Edition, EG & G Technical Services, Inc. U.S. Department of Energy, November 2002.

(115)   Mench, M. M. *Fuel Cell Engines*, John Wiley & sons, Inc.: **2008**

(116)   Blomen, L. J. M. J. *Fuel Cell Systems*; Plenum Press, New York, **1993**.

(117)   Rikukawa, M.; Sanui, K. *Prog. Polym. Sci.* **2000**, *25*, 1463.

(118)   Winter, M.; Brodd, R.J. *Chem. Rev.* **2004**, *104*, 4245.

(119)   An article on *Fuel cells; Green Power*, down loaded from Los Alamos National Laboratory., U.S.

(120)   Hickner, M. A.; Ghassemi, H.; Kim, S. Y.; Einsla, B. R.; McGrath, J. E. *Chem. Rev.* **2004,** *104*, 4587.

(121)   Basu, S. *Recent Trends in Fuel Cell Science and Technology,* Springer, New York, **2007**.

(122)   Bruijn, F. de. *Green Chem.* **2005**, *7*, 132.

(123)   Kerres, J. A. *J. Membr Sci.* **2001**, *185*, 3.

(124)   Li, Q.;He, R.;Jensen, J. Q.; Bjerrum, N. J.; *Chem. Mater.* **2003**, *15*, 4896.

(125)   Rozi`ere, J.; Jones, D. J. *Annu. Rev. Mater. Res.* **2003**, *33*, 503.

(126)   Smitha, B.; Sridhar, S.; Khan, A.A. *J. Membr Sci.* **2005**, *259*, 10.

(127)   Gubler, L.; Scherer, G. G. *Adv Polym Sci.* **2008**, *215*, 1.

(128)   Maier, G.; Meier-Haack, J. *Adv Polym Sci.* **2008**, *216*, 1.

(129)   Mader, J.; Xiao, L.; Schmidt, T, J.; Benicewicz, B,C. *Adv Polym Sci.* **2008**, *216*, 63.

(130)   Marestin, C.; Gebel, G. ; Diat, O.; Mercier, R. *Adv Polym Sci.* **2008**, *216*, 185.

(131)   Xiao, L. Ph.D. Thesis, Rensselaer Polytechnic Institute, Troy, New York, **2003**.

(132)   Einsla, B. R. Ph.D.Thesis, Virginia Polytechnic, Blackburg, Virginia, **2005**.

(133)   Sukumar, P. R.; Ph.D.Thesis, Max-Planck-Institute for Polymer Science, Mainz, **2006**.

(134)   Mauritz, K. A.; Moore, R. B. *Chem. Rev*. **2004,** *104*, 4535.

(135)   Yoshitake, M.; Watakabe, A. *Adv Polym Sci*. **2008**, *215*, 127.

(136)   Mehta, V.; Cooper, J. S. *J. Power. Sources*. **2003**, *114*, 32.

(137)   Shao, Y.; Yin, G.; Wang, Z.; Gao,Y. *Journal of Power Sources* **2007**,*167*, 235.

(138)   Yang, Y.; Siu, A.; Peckham, T. J.; Holdcroft, S, *Adv Polym Sci*. **2008**, *215*, 55.

(139)   Marestin, C.; Gebel, G. ; Diat, O.; Mercie, R. *Adv Polym Sci*. **2008**, *216*, 185.

(140)   Gasa, J. V.; Weiss,R. A.; Shaw, M. T. *J. Polym. Sci.: Part B: Polym. Phys*, **2006**, *44*, 2253.

(141)   Zaidi, S.M.J.; Mikhailenko, S.D. ; Robertson, G.P. ; Guiver, M.D.; Kaliaguine, S. *J. Membr Sci*. **2000**, *173*, 7.

(142)   Wang, F.; Hickner, M.; Kim, Y. S.; Zawodzinski. T. A.; McGrath, J. E. *J. Membr Sci*. **2002**, *197*, 231.

(143)   Allcock, H. R.; Wood, R. M. *J. Polym. Sci.: Part B: Polym. Phys*, **2006**, *44*, 2358.

(144)   Wycisk, R.; Pintauro, P. N. *Adv Polym Sci*. **2008**, *216*, 157.

(145)   Santra, A. K.; Goodman, D.W. *Electrochim. Acta* , **2002**, 47 , 3595.

(146)   Li, Q. F.; He, R. H.; Gao, J. A.; Jensen, J. O.; Bjerrum, N. J. *J. Electrochem. Soc.* **2003**, *150*, A1599.

(147)   Zhang, J. et. al . *Journal of Power Sources*, **2006**, *160*, 872.

(148)   Wainright, J. S.; Wang, J-T.; Weng, D.; Savinell, R. F., Litt, M. *J. Electrochem. Soc.* **1995**, *142*, L121.

(149)   Bouchet, R.; Siebert, E. *Solid State Ionics*. **1999**, *118*, 287.

(150)   Xing, B.; Savadogo, O. *J. New. Mater. Electrochem. Syst.* **1999**, *2*, 95.

(151)   Wasmus, S.; Duch, B. A.; Moaddel, H.; Rinaldi, P. L.; Litt, M. H.; Rogers, C.; Valeriu, A.; Mateescu, G. D.; Tryk, D. A.; Savinell, R. F. *The Electrochem. Soc. Extended Abstracts*, **1995,** *95-1***,** 716.

(152) Glipa, X.; Bonnet, B.; Mula, B. ; Jones, D. J. ; RozieÁre, J. *J. Mater. Chem*, **1999**, *9*, 3045.

(153) Kawahara, M.; Morita, J.;Rikukawa, M.; Sanui, K.; Ogata, N. *Electrochimica Acta*, **2000**, *45*, 1395.

(154) Pu, H.; Meyer, W.; Wegner,G. *J. Polym. Sci.: Part B: Polym. Phys*, **2002**, *40*, 663.

(155) Ma, Y-L.; Wainright, J. S.; Litt, M.; Savinell R. F. *J Electrochem Soc*. **2004**, *151*, A8.

(156) Li, Q.; Hjuler, H. A.; Bjerrum, N. J. *J, Appl. Electrochem.* **2001**, *31*,773.

(157) He, R.; Li, Q.; Bach, A.; Jensen, J. O.; Bjerrum, N. J. *J. Membr Sci*. **2006**, *277*, 38.

(158) He, R.; Li, Q.; Bach, A.; Jensen, J. O.; Bjerrum, N. J. *J. Polym. Sci.: Part A: Polym. Chem*, **2007**, *45*, 2989.

(159) Wainright, J. S.; Litt, M. H; Savinell, R. F., *Hand Book of Fuel Cells*, John Wiley and Sons Ltd, **2003**, *3*, 436.

(160) Litt, M.; Ameri, R.; Wang, Y.; Savinell, R.; Wainright, J. *Mater. Res. Soc. Sym. Proc.* **1999**, *548*, 313.

(161) Xiao, L.; Zhang, H.; Jana, T.; Scanlon, E.; Chen, R.; Choe, E.-W.; Ramanathan, L. S.; Yu, S.; Benicewicz, B. C. *Fuel Cells* **2005**, *5*, 287.

(162) Mecerreyes, D.; Grande, H.; Miguel, O.; Ochoteco, E.; Marcilla, R.; Cantero, I. *Chem. Mater.* **2004**, *16,* 604.

(163) Sannigrahi, A.; Arunbabu, D.; Jana, T. *Macromol. Rapid Commun.* **2006**, *27*, 1962.

Chapter 2

Tuning the Molecular Properties of Polybenzimidazole by Copolymerization
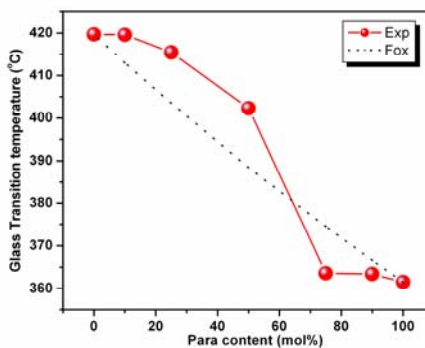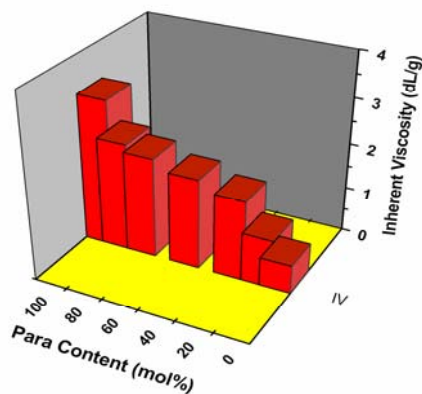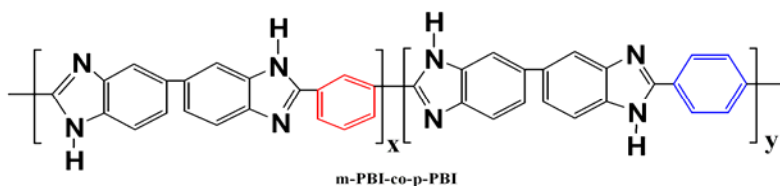
m-PBI-co-p-PBI

Novel random polybenzimidazole copolymers consisting of m- and p- phenylene linkages are synthesized and characterized. The architectural effects of dicarboxylic acid monomers on the copolymers properties are elucidated.

2.1. Introduction

The fuel cell is the most promising electrochemical device for the production of an efficient, environment-friendly, and economical power energy.[1] A polymer electrolyte membrane fuel cell (PEMFC) employing a solid polymer electrolyte to separate the fuel from the oxidant has received a great deal of attention due to its potential as a high energy density power generator.[2] The most widely used perflurosulfonic acid (PFSA) based polymer membrane such as Dupont's Nafion has severe limitations:[3] (1) proton conduction requires a water solvated membrane, (2) low operating temperature, and (3) high cost. However, a high-temperature polymer electrolyte membrane (HT-PEM) operating above 120°C overcomes the abovementioned problems and offers many advantages which include fast electrode kinetics, high tolerance to fuel impurity, etc.[4] Hence, proton conducting polymers with superior thermochemical and mechanical stability above 120°C have been strongly desired for PEMFC application.

Until now, a large number of various high-temperature polymer electrolyte membranes have been developed and reviewed.[5-8] Polybenzimidazole (PBI, Scheme 2.1) has excellent thermal and chemical resistance, fire retarding capacity, and insulating property and it forms a good textile fiber.[9] Phosphoric acid (PA) doped polybenzimidazole (PBI) has emerged as a promising candidate for a low-cost and high-performance fuel cell material.[10,11] PBI possesses both proton donor (-NH-) and proton acceptor (-N=) hydrogen-bonding sites which exhibit specific interaction with the polar solvents[12-14] and form miscible blends[15,16] with a variety of polymers. PBI is being used for various purposes especially for high-temperature application, fiber spinning, and as a reverse osmosis membrane, fluorescence sensor for halide ions, etc.[9,17] A variety of approaches have been explored to prepare the PA-doped PBI membrane such as (i) fabrication of the membrane from dimethylacetamide (DMAc) solution followed by soaking in phosphoric acid (PA),[10,11,18,19] (ii) via a sol-gel process by direct casting of the high molecular weight PBI solution in polyphosphoric acid (PPA),[20,21] and (iii) from a thermoreversible gel of PBI in PA.[22] The major challenges of these approaches are to

obtain a membrane that will show a very high acid doping level and moderately good mechanical stability. It has been shown that with increasing acid doping level, the mechanical stability becomes poor. Therefore, a trade-off between these two important parameters has to be maintained for preparing a superior quality membrane. Hence, there is an opportunity to prepare new PBIs having a variety of polymer backbone structures which could probably enhance the acid-doping level capacity without compromising the mechanical stability. Also, it would be a good addition to the PBI-type polymer system if polymers having different photophysical properties are synthesized, which may serve as potential applicants for the sensor materials.

Until now, a large variety of PBI polymers have been synthesized and studied. Among these, the commercially available PBI, poly[2,2$^/$ – (m – phenylene) – 5, 5$^/$ – benzimidazole] (known as *m*-PBI), is being widely used. Others include poly (2, 5 benzimidazole) (i. e. AB – PBI)[23], pyridine based PBI homopolymer[21], sulfonated PBI[24], hyperbranched polybenzimidazole (HPBI)[25], naphthalene based PBI[26], fluorinated PBI[27], PBI with sulfone group or sulfonic acid group in the backbone etc.[28] Although excellent thermo – chemical and mechanical stability make the PBI valuable for industrial application, however, the major draw back is their processibility arising due to the poor solubility and infusibility. A large number of efforts have been exercised in the literature to improve the processibility without sacrificing the brand PBI properties. For this purpose, several attempts have been made through the modification of the polymer backbone as well as side chain.[29] Many investigators have incorporated flexible spacers such as methylene and aryl methylenes, arylamide and ether linkages in the polymer backbone.[30] Recently, Persson et al. have synthesized ABA triblock copolymers having benzimidazole tethered end blocks with enhanced solubility.[31]

Earlier studies indicate that the molecular weight of the PBI polymers has great impact on their properties, in particular mechanical properties and acid-doping level capacity. Therefore, there is a demand for the preparation of high molecular weight PBI and obviously the best way to do that is to synthesize various polymer backbone structures. However, one should not heavily compromise the solubility issue aiming to increase the molecular weight. In a recent article (chapter 4) we have demonstrated the

aggregation behavior of the PBI chains in solution through spectroscopic studies.[14] Hence, the synthesis of new polymers with tunable spectroscopic characteristics is desired. Keeping these in mind, we hypothesize that incorporation of the *p*-phenylene linkage in the *m*-PBI backbone would probably be the right track to meet the above targets. Also, we would expect a more structurally symmetrical backbone resulting from the introduction of the para linkage, which in turn enhances the conjugation and flexibility of the polymers. Therefore, in the present study, we report the synthesis of a series of *m*-phenylene-*p*-phenylene based polybenzimidazole random copolymers. The synthesized polymers are characterized by determining inherent viscosity (IV) as a measurement of polymer molecular weight, thermogravimetric analysis (TGA) for the thermal stability, and differential scanning calorimetry (DSC) for the thermal transitions. Fourier transforms infrared (FT-IR) and proton NMR techniques are used to establish the polymer structure. Also, spectroscopic studies such as absorption and fluorescence are carried out to demonstrate the effect of copolymerization on the photophysical properties. We have studied the wide-angle X-ray scattering (WAXS) to look into the crystalline character of these polymers. Finally, we have determined and compare the PA doping level of direct cast PBI membranes from PPA and PA-doped DMAc membrane.

2.2. Experimental Section

2.2.1. Materials. 3, 3', 4, 4' – tetraaminobiphenyl (TAB) and polyphosphoric acid (115%) were received from Sigma-Aldrich. Isophthalic acid (IPA) and terephthalic acid (TPA) were purchased from SRL, India. Sulfuric acid (98%) and deuterated dimethyl sulfoxide (DMSO-d_6) were received from Merck, India. Dimethylacetamide (HPLC grade) was purchased from Qualigens (India). All chemicals were used as received without further purification.

2.2.2. PBI Synthesis. An equal number of moles of TAB and either IPA or TPA were taken into a three-necked flask with polyphosphoric acid (PPA) for homopolymers synthesis. IPA and TPA were used to prepare 100% *m*-PBI and 100% *p*-PBI,

respectively. For random copolymers (Scheme 2.1) synthesis the mole fraction of the diacids (IPA and TPA) in the reaction mixture was varied from 10% to 90% but maintaining the total moles of diacids equal to the moles of TAB taken in the reaction mixture along with PPA. The total monomer concentrations were gradually decreased with increasing TPA mole fraction in the mixtures. The reaction mixtures were stirred by an overhead stirrer continuously in nitrogen atmosphere at 190-210 °C for ~24 h. The PBI polymers were isolated, neutralized with sodium carbonate, washed thoroughly with water, and dried in a vacuum oven at 100°C for 24 h. The dried polymers were kept in a vacuum desiccator for further characterizations.

2.2.3. Viscosity. The viscosity measurements of the polymer solutions in H_2SO_4 (98%) were carried out at 30°C in a constant temperature water bath, using a Cannon Ubbelohde capillary dilution viscometer (model F725), and the inherent viscosity (IV) values were calculated from the flow time data. For all the flow time measurements 0.2 g/dL of polymer solution in H_2SO_4 (98%) was used.

2.2.4. IR and NMR Spectroscopy. The IR spectra of the samples were recorded on a (JASCO-5300) FT-IR spectrometer. The experiments were carried out at room temperature on PBI films having a thickness of 40 μm. All the NMR spectra of the PBI solutions in DMSO-d_6 were recorded with a Bruker AV 400 MHz NMR spectrometer at room temperature.

2.2.5. Thermal Study. Thermogravimetric and differential thermal analysis (TG-DTA) were carried out on a (Netzsch STA 409PC) TG-DTA instrument from 50 - 900°C with a scanning rate of 10°C / minute in presence of nitrogen flow. A differential Scanning Calorimeter (Pyris Diamond DSC, Perkin- Elmer) was used to find the glass transition temperature (T_g) of the PBI samples. Approximately 7-10 mg PBI samples were taken in an aluminum pan that was tightly crimped with the help of a DSC crimpier and then scanned from 50 to 500 °C at a heating rate of 10 deg/min in the presence of constant nitrogen gas purging. The DSC was calibrated with use of standard In and Zn before the PBI samples were scanned.

2.2.6. Absorption and Fluorescence Spectroscopy. Electronic absorption spectra were recorded on a Shimadzu model UV-3100 UV-visible spectrometer. Steady-state fluorescence emission spectra were recorded on a Jobin Yvon Horiba spectrofluorimeter (Model Fluoromax-3). PBI samples were dissolved in dimethylacetamide (DMAc) and the spectra were recorded. For determination of the fluorescence quantum yield (Φ_f) of the PBI samples, quinine sulfate (Φ_f = 0.546 in 1 N sulfuric acid) was used as a reference.

2.2.7. X-ray Diffraction. The X-ray diffraction (XRD) patterns of the dry PBI powders were collected in a Philips powder diffraction apparatus (model PW 1830). The powders were taken in a glass slide and the diffractograms were recorded with use of nickel-filtered Cu Kα radiation at a scanning rate of 0.6° 2θ /min.

2.2.8. Phosphoric Acid (PA) Doping. The PA doped PBI membranes were fabricated in two different methods: in the first method the dried polymers were dissolved in DMAc by refluxing the solution. The concentration of the solutions were 2% (w/v). Then the solutions were filtered through 0.5 μm PTFE membrane. These PBI solutions were poured in a glass petri-dish and the solvent was evaporated slowly inside an air circulating oven at 140°C. After the removal of the all the solvent, the membranes were pilled off from the petri-dish and boiled in water to remove the traces of DMAc. Then the membranes were dried in vaccum oven at 100°C for 24 hours. The dried membranes were immersed into 85% (w/v) H_3PO_4 for three days to obtain the PA doped PBI membrane. This method we called as imbibing process. In the second method PA doped PBI membranes were obtained by using PPA methods as described in the literature[20, 21] by Benicewicz et al. The PA doping level was determined by titrating of a preweighed piece of membrane sample against standardized 0.1 (N) sodium hydroxide (NaOH) solutions using an Autotitrator (Metrohm 702). The first H_3PO_4 acid equivalence point was used to determine the volume of sodium hydroxide necessary for the neutralization process. After the titration the membranes were washed with distilled water to remove if trace amount of acid is present in the membranes. This process was repeated three times. Finally the membranes were dried in the vacuum oven at 100°C for 24 hours. The

PA doping level was calculated as the number of PA mols present per PBI repeat unit using the following equation:

$$\text{PA doping level} = \frac{V_{NaOH} C_{NaOH}}{W_{dry}} M_w$$

Where V_{NaOH} and C_{NaOH} are the volume and the molar concentration of the sodium hydroxide, respectively. W_{dry} is the dry polymer membrane weight and M_w is the molecular weight of the polymer repeat unit.
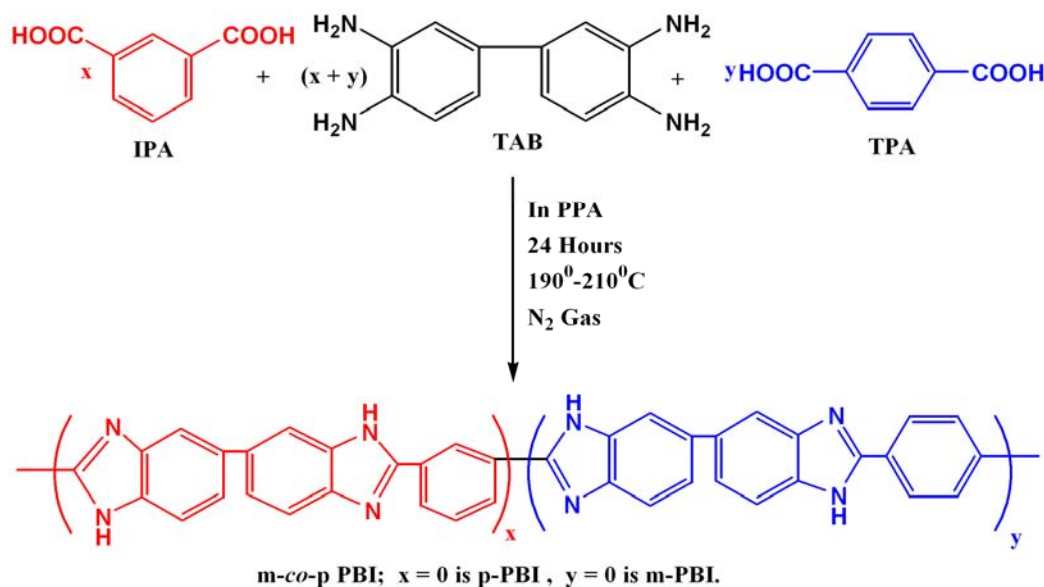
Scheme 2.1. *Synthesis of m-Polybenzimidazole-co-p-Polybenzimidazole (m-PBI-co-p-PBI)*

2.3. Results and Discussion

2.3.1. Synthesis and Molecular Weight Control. A series of *m*-polybenzimidazole-*p*-polybenzimidazole random copolymers (*m*-PBI-*co*-*p*-PBI) have been synthesized and the polymer backbone structure is shown in Scheme 2.1. We have varied the

composition of meta and para structures in the copolymer from 10% to 90% by changing the mole ratio of IPA and TPA, respectively, in the initial reaction mixture. Also, 100% meta homopolymer and 100% para homopolymer are prepared taking the respective diacid with the TAB. In all the polymerization processes the stoichiometric balance between the TAB and the diacids is well maintained. Also, the reaction conditions for all the reactions are similar except the initial monomer concentration in the reaction mixture. Inherent viscosity (I.V) is a measure of the molecular weight of the polymer; a higher I.V. value indicates a higher molecular weight.[32] The molecular weight of PBI has in the pertinent literature been expressed in terms of I.V, measured on sulfuric acid solution.[9,33] The monomer sensitivity to the polymerization conditions has a more significant influence on the viscosity behavior than that of the monomer structure.[33] Table 2.1 and Figure 2.1 show that low monomer concentration in the reaction mixture is required to prepare higher para content copolymer. We have also carried out the polymerizations with same monomer concentration (4.83 wt %) to prepare all the copolymers. But such reactions produce low inherent viscosity (I.V) polymers, in particular when the para content in the polymers keeps on increasing (Table 2.1). This observation proves the importance of the variation of the monomer concentration in the reaction mixture to achieve higher molecular weight PBI. We believe that the solubility of the TPA in PPA plays a major role for the polymerization. With the solubility of TPA in PPA being very low[34] when the monomer concentration is high (4.83 wt % in Table 2.1), more and more TPA is precipitating out from the reaction mixture as insoluble solid destroying the stoichiometric balance. This in turn disfavors the reaction equilibrium and yields low I.V. polymers.

Figure 2.1 is a plot of the inherent viscosity (I.V) against the para content of the copolymers. The inherent viscosity values of these copolymers could be compared to one another as a measure of their molecular weights since both the meta and para portions have identical weights and the only difference in the polymer structure is the isomeric phenyl moiety. Figure 2.1 clearly shows the effect of para content on the molecular weight of the polymer; with increasing para content the molecular weights increase. Hence, changing the carboxylic acid group position in the diacid from meta to

para enhances the molecular weight enormously and allows us to control the molecular weight by preparing the appropriate copolymer. The solubility of benzene dicarboxylic acids in polar acidic solvents depends upon the position of the carboxylic groups in the benzene ring. The poor solubility of dicarboxylic acid is observed with the carboxylic groups which are far apart in the benzene ring because acid groups are probably unable to form the internal dimmers through hydrogen bonding interaction between carboxylic groups of the same acids or coming from two different molecules of the acid.[35, 36] Thus TPA (1,4-) has lower solubility than IPA (1,3-) in acidic solvents. The reason behind the formation of higher molecular weight polymer with increasing para content can be explained by considering the extremely low solubility of TPA in PPA.[34] Because of the poor solubility of TPA in the reaction mixture, the growing polymer chain (oligomer) ends consist of the soluble monomer TAB (Scheme 2.2). This is clearly proved by the absence of any carboxylic phosphate ester or acid amide group in the oligomeric radicals isolated from the reaction mixture at different time intervals. The absence of carbonyl stretching at 1710 cm^{-1} in the IR spectra of the oligomer radical presented in Figure 2.2 to supports our argument. These oligomeric chain ends quickly react further with the dissolved TPA in the mixture and the reaction continues. As soon as the deficiency of TPA arises in the solution owing to its low solubility in PPA, more and more TPA dissolution takes place to maintain its saturation concentration and polymerization keeps on going producing bigger molecules. This type of polymerization mechanism is very unusual. In the polymerization medium the major path (Scheme 2.2) sets in equilibrium between the TPA monomers and the growing oligomeric chains. This equilibrium is a heterogeneous equilibrium and therefore we refer this unusual polymerization mechanism as heterogeneous polymerization. A similar type of observation was reported earlier in the case of polybenzoxazoles.[34,37] It is also interesting to note that the para structure of the diacid monomer introduces more symmetry in the polymer backbone. Hence, we hypothesize that molecular weight control and symmetry in the polymer backbone will help us to tune the molecular property, which is discussed in the following sections.
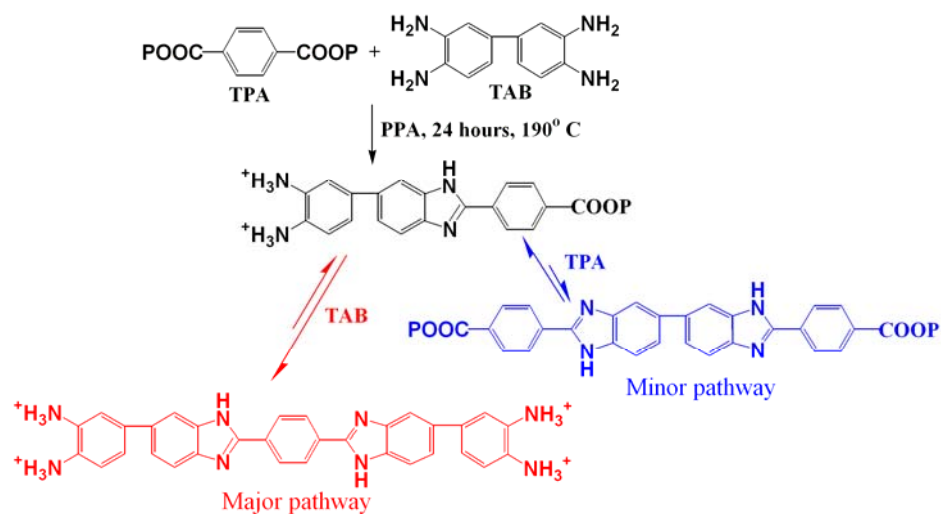
Scheme 2.2. *Heterogeneous polymerization mechanism of TPA in PPA medium.*
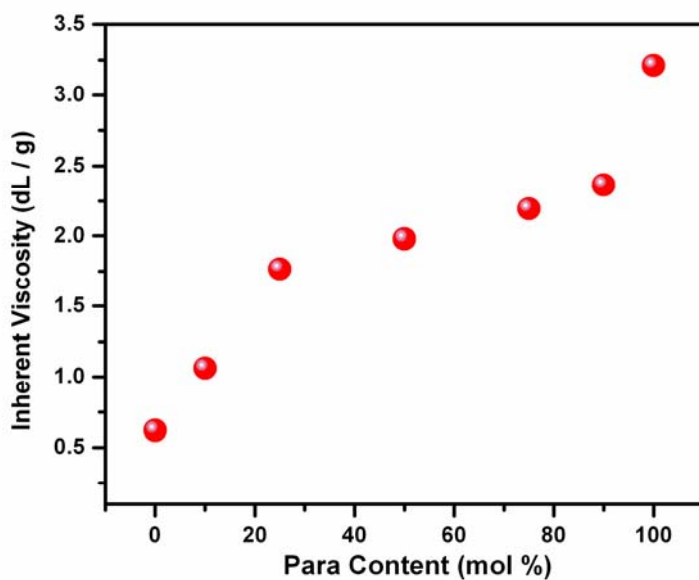
Figure 2.1. *Variation of molecular weight (inherent viscosity) with para content of the PBI copolymer.*

Table 2.1. *Various reaction parameters of PBI random copolymers.*

Para Content (mol %)	Monomer Concentration[a] (Wt. %)	Inherent viscosity[b] (dL / g)
0	4.83	0.621
10	4.75	1.151
25	3.85	1.111
50	3.7	1.699
75	3.6	1.527
90	3.4	1.621
100	3	1.772

[a]Figure 2.1 copolymers have been synthesized using the corresponding monomer concentrations.

[b]When the monomer concentrations for the synthesis of all the copolymers kept constant at 4.83 weight %
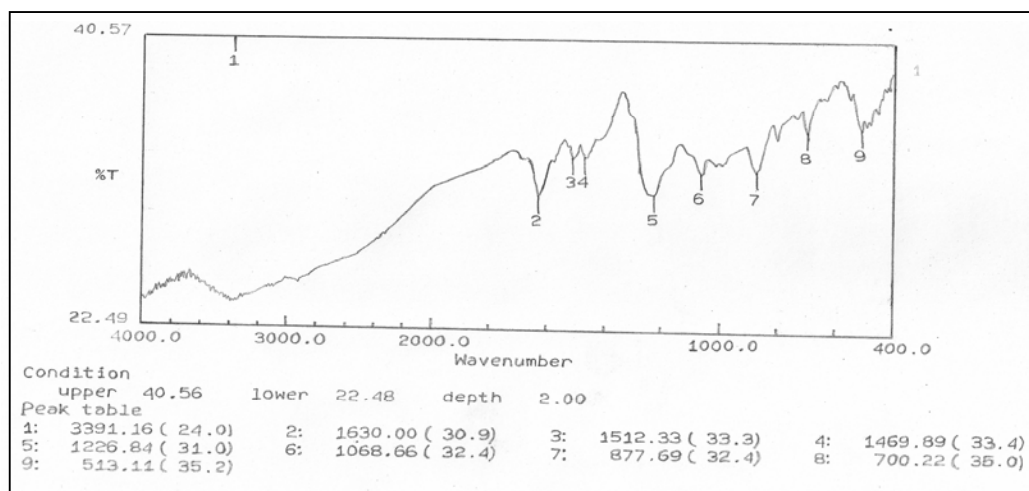
Figure 2.2. *FT - IR spectrum of oligomer isolated after 2 hours of 100% para PBI hompolymerization at 190°C.*

2.3.2. IR and NMR Spectroscopy. The IR spectra of all the PBI polymers are recorded on the thin film made from the dilute solution of the polymers in dimethylacetamide (DMAc) and are presented in the Figure 2.3. Before recording the IR spectra, the films

are boiled in hot water and dried in a vacuum oven at 100°C for 2 days to remove any traces of DMAc. In Figure 2.3 the absence of C-H stretching of CH_3 at 2940 cm^{-1} for DMAc indicates the efficiency of our drying process. PBI is slightly hygroscopic and it can absorb moisture up to 5% of its weight readily;[38] therefore O-H stretching at 3616 cm^{-1} is expected. The presence of O-H stretching of H_2O at 3616 cm^{-1} in all the spectra (Figure 2.3) indicates this fact. The IR spectra presented in Figure 2.3 for different PBI polymers are quite similar and the majority of the bands are for the characteristic stretching of PBI. These bands have been widely discussed earlier by several authors.[28,39,40] However, it is worth noting that the bands at 1536, 1444, and 1101 cm^{-1} indicated by the dotted line in the Figure 2.3 are not identical for all the samples. Previously, the bands at 1536 and 1444 cm^{-1} were assigned as in-plane ring vibration of 2-substituted benzimidazole and 2,6-disubstituted benzimidazole, respectively.[39] From Figure 2.3, it is evident that the band at 1536 cm^{-1} becomes less intense with increasing para content in the polymer chain and almost nonexistent for 100% *p*-PBI. On the other hand, the peak at 1444 cm^{-1} becomes more intense gradually with increasing para content. These deviations in the band intensities of the PBI polymers are obviously due to the substitution in the 2-position of the benzimidazole ring, which arises because of the different polymer backbone structure prepared by copolymerization. Another non-identical behavior of the different polymers is observed at the 1101 cm^{-1} band, which is shifted gradually to higher frequency with increasing para content. For 100% para, the band appears at 1120 cm^{-1}. This band is assigned as N-C stretching coupled with the stretching of adjacent bonds in the molecule and the position of the absorption depends on the pattern of the substitution on the R-carbon atom.[41] Upon copolymerization, the substitution pattern on the R-carbon atom varies, which results in the shifting of the band from 1101 to 1120 cm^{-1}. The introduction of para substitution in the polymer chain brings more flexibility and symmetry in the polymer backbone and it interferes with the vibration characteristics; therefore the N-C-C coupled vibration takes place at higher frequency. Hence, IR spectroscopy is found to be an efficient tool to demonstrate the effect of copolymerization and the polymer backbone structure.
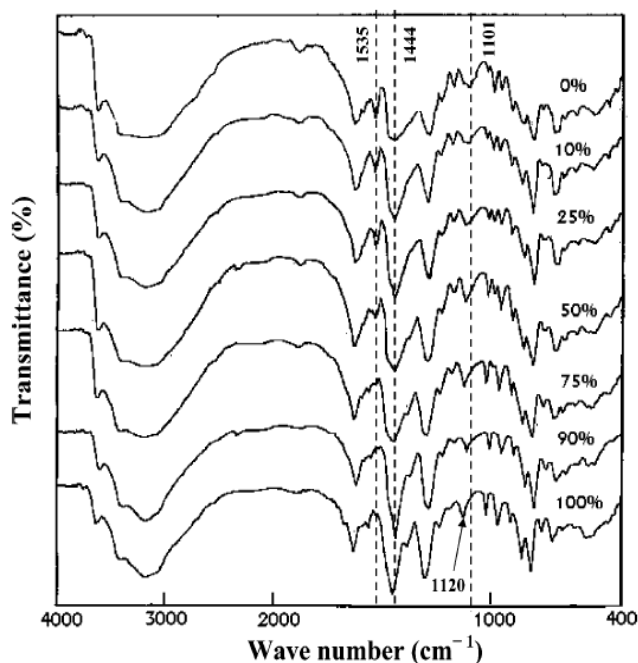
Figure 2.3. *FT-IR spectra of all the PBI polymers. Para content (mol%) of the polymers are indicated in the figure.*

Though IR study proves the structure of the copolymer qualitatively, it does not elucidate the copolymer backbone structure quantitatively. Rather the proton NMR study is more useful and it has been used extensively before in the literature to look into the copolymer structure and determine the copolymer composition more precisely.[24,28,42] Figure 2.4 shows the chemical structure of the copolymer, proton NMR spectra of all the copolymers, and the peak assignments of the NMR spectrum. The peak assignments presented in the Figure 2.4 are in good agreement with the anticipated chemical structure. The imidazole proton signals for the meta and para portions of the chain, denoted as H_a and H_b, are observed at around 13.26 and 13.15 ppm, respectively. Both signals are observed almost in the same region as expected; however, the slight downfield shift of the H_a proton is because of the different chemical environment of the meta structure compare to that of the para structure. In addition, three distinguishable

peaks are observed, denoted as H_f, H_g, and H_h at 9.15, 8.32, and 8.42 ppm. The H_f and H_g signals are purely due to the meta structure and the H_h signal is for the para structure.
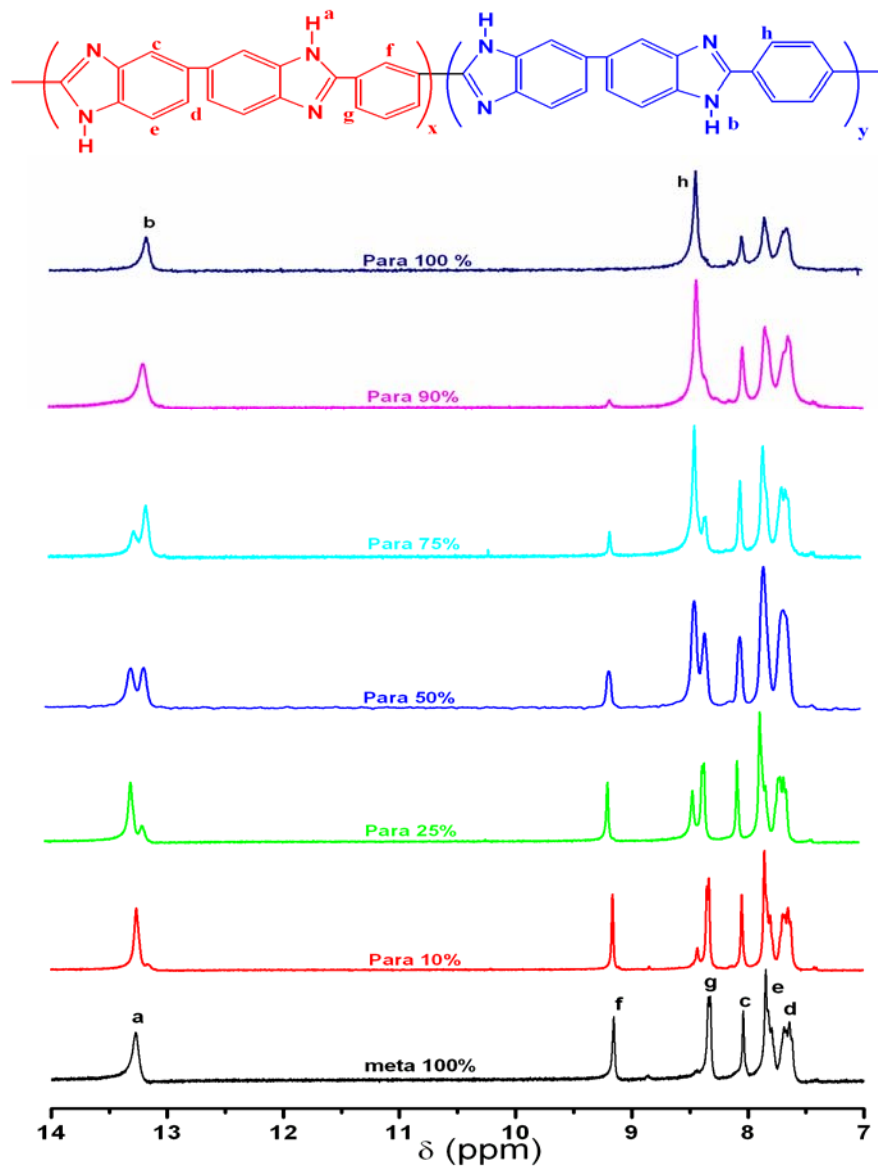
Figure 2.4. *The chemical structure, proton NMR spectra of all the co-polymers and the peak assignments of the NMR spectrum.*

From Figure 2.4, it is evident that the intensity of the characteristic meta signals (H_a, H_f and H_g) is decreasing and the para responsive signals (H_b and H_h) are increasing

with increasing para content in the polymer chain. For example, the intensity of the H_a and H_b signals for the 50% para sample is almost the same indicating the 50:50 compositions. This observation indicates that the copolymerization has taken place successfully and the ratio of the meta and the para mole fraction in the samples can be quantified. The percentages of the meta and the para mole fraction in the samples are calculated from the integral ratio of the proton peaks H_a, H_b, H_f, H_g, and H_h. We have calculated the percent of the para mole fraction in the samples from the proton NMR spectrum using equation 2.1 and these values are given in the Table 2.2.

$$\text{Para mol fraction (\%)} = \frac{H_b + H_h}{H_a + H_b + H_f + H_g + H_h} \times 100 \qquad (2.1)$$

Table 2.2 lists the contents of the para units in the series of copolymers. All the values are in good agreement with the monomer feed ratio taken in the initial reaction mixtures, which thus suggests that all the starting monomers are successfully incorporated into the copolymer chains. Also, it is evident that the meta and para composition in the copolymer chains can be readily controlled by changing the molar feed ratio (IPA:TPA) at the start of the polymerization.

Table 2.2. *Comparison of expected para content of the copolymers based on TPA feed in the reaction with measured para content calculated from proton NMR.*

Feed TPA (mol %)	Found Para content (mol %)
0	0
10	11.25
25	26.61
50	51.52
75	78.05
90	97.60
100	100

However, a critical observation of the Table 2.2 data brings our attention to a moderate deviation in the para composition from the monomer feed, in particular for the higher para content copolymer. We have presented in the Table 2.2 data graphically shown in Figure 2.5 to look at the type of deviation.
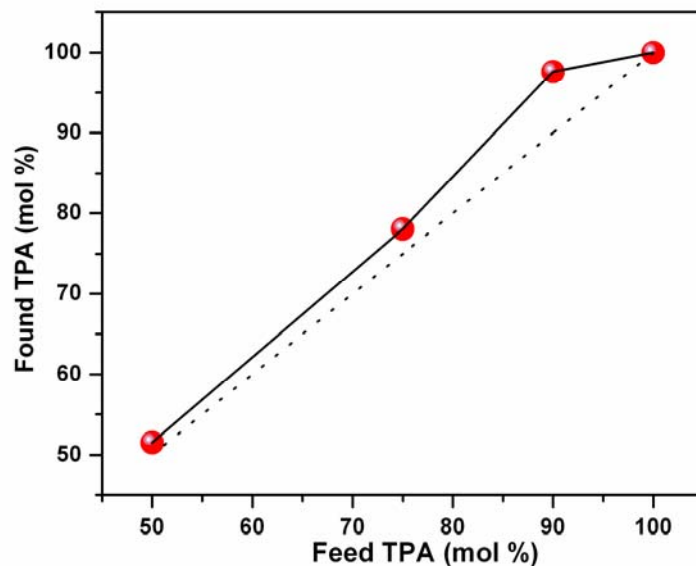
Figure 2.5. *Deviation of comonomer composition in PBI copolymers measured by proton NMR spectroscopy.*

Figure 2.5 shows a positive deviation (solid line) from the anticipated linearity (dotted line) based on the monomer feed in the polymerization mixture. This kind of behavior is unusual for the step growth polymerization since step reactions are carried out to close to 100% conversion for the synthesis of high molecular weight polymers and step polymerizations are equilibrium reactions. A few earlier studies on copolycondensation showed the deviation in composition.[43,44] In the present system because of the large difference in solubility of the IPA and TPA in PPA,[34,37] deviation in the copolymer composition from the monomer feed is expected. This observation gives a hint that probably the rates of the reactions of the monomers are not similar and hence the reactivity ratios of the monomers are different. On the basis of this argument, it was

thought necessary to obtain the reactivity ratios of the comonomers. A simple kinetic scheme for copolymerization is used to discuss the rates of the reactions of the monomers.[44] The M_1 and M_2 represent the IPA and TPA monomers, respectively. The asterisk in the prefix indicates the growing polymer chain. The four possible reaction sequences are the following:
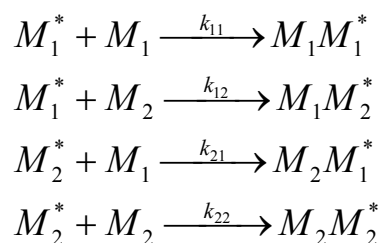
$$M_1^* + M_1 \xrightarrow{k_{11}} M_1 M_1^*$$
$$M_1^* + M_2 \xrightarrow{k_{12}} M_1 M_2^*$$
$$M_2^* + M_1 \xrightarrow{k_{21}} M_2 M_1^*$$
$$M_2^* + M_2 \xrightarrow{k_{22}} M_2 M_2^*$$

The rate constants of the respective reactions are denoted by "k" with appropriate sign in the suffix. We have calculated the reactivity ratio of IPA and TPA using the well-known Fineman and Ross[45] procedure (equation 2.2) from the proton NMR data. Fineman and Ross rearranged the Mayo and Lewis[46] equation as

$$\frac{f_1(F_1 - F_2)}{f_2 F_1} = \frac{F_2}{F_1}\left(\frac{f_1^2}{f_2^2}\right) r_1 - r_2 \qquad (2.2)$$

where f_1 and f_2 are the mole fraction of the monomer IPA and TPA respectively in the feed of the copolymerization, with F_1 and F_2 being their instantaneous compositions (mol fractions) in the copolymer. A plot (Figure 2.6) of the left-hand side (LHS) of equation 2.2 against F_2/F_1 $(f_1/f_2)^2$ results in a straight line with slope equal to r_1 and intercept equal to $-r_2$, where r_1 and r_2 are the reactivity ratios of the monomer IPA and TPA, respectively. The reactivity ratios are defined as $r_1 = k_{11} / k_{12}$ and $r_2 = k_{22} / k_{21}$. From Figure 2.6 the reactivity ratios obtained for IPA (r_1) and TPA (r_2) are equal to 1.014 and 2.251, respectively. The reactivity ratio of TPA being greater than unity and larger than that of IPA reveals that the TPA oligomers preferentially add TPA monomers instead of IPA monomers. Hence at higher para content copolymers the

actual para content is more than the feed, which explains the positive deviation in Figure 2.5. In comparison, the reactivity ratio of IPA (r_1) is equal to unity and less than that of TPA. This indicates that the IPA monomer is not biased toward IPA as that of TPA. Hence we do not observe any deviation in Figure 2.5 for the higher meta composition or the lower para composition of the copolymers. The r_2 is 2.22 times bigger than r_1 (r_2 / r_1 = 2.22), therefore TPA is 2.22 times more reactive than IPA toward TAB. Thus from the above results it is clear that during polymerization the TPA monomer is being consumed faster rate than the IPA monomer.
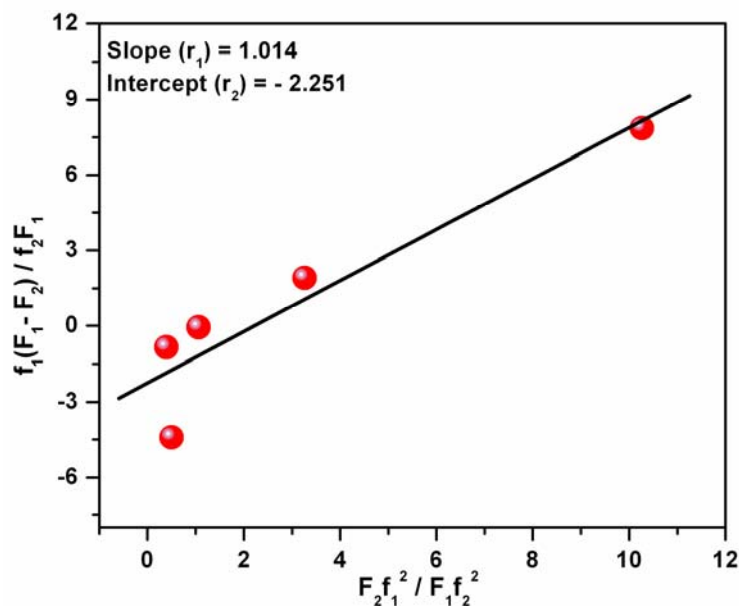
Figure 2.6. *Plot for calculating reactivity ratios of monomers (IPA and TPA) using equation 2.2.*

2.3.3. Thermal Study. The thermal stabilities of the synthesized PBI samples are performed under nitrogen atmosphere at a heating rate of 10 deg/min. The representative TGA curves for four different samples are shown in the Figure 2.7 and the thermal behavior data for all the samples are presented in Table 2.3. Two distinct different weight losses are observed from Figure 2.7. An initial weight loss at around 100-120°C and a second weight loss at around 570-600°C are observed. The first weight

loss is assigned to the loss of loosely bound absorbed water molecules.[24] All the samples used for studying the TGA and IR are subjected to exhaustive drying in a vacuum oven at 100 °C. Despite this drying process, we have observed the weight loss due to absorbed water in TGA (Figure 2.7) and O-H stretching for water molecules in the IR (Figure 2.3). These observations indicate that PBI absorbs moisture readily and it absorbs moisture even during the sample handling time, which also supports the earlier report that PBI can absorb ~5% (by weight) moisture very easily from the atmosphere.[39] The degradation of the polymer backbone is responsible for the second weight loss at ~570°C.[20,47] For all the PBI polymers heating to ~570°C results in only <10% weight loss (Table 2.3) indicating the remarkable thermal stability of the polymers. Though an earlier report[33] suggests identical thermal stability of both the meta and the para structure, we have observed that significant differences in the thermal stability exist owing to the *m-* and *p*-phenylene groups in the chain.
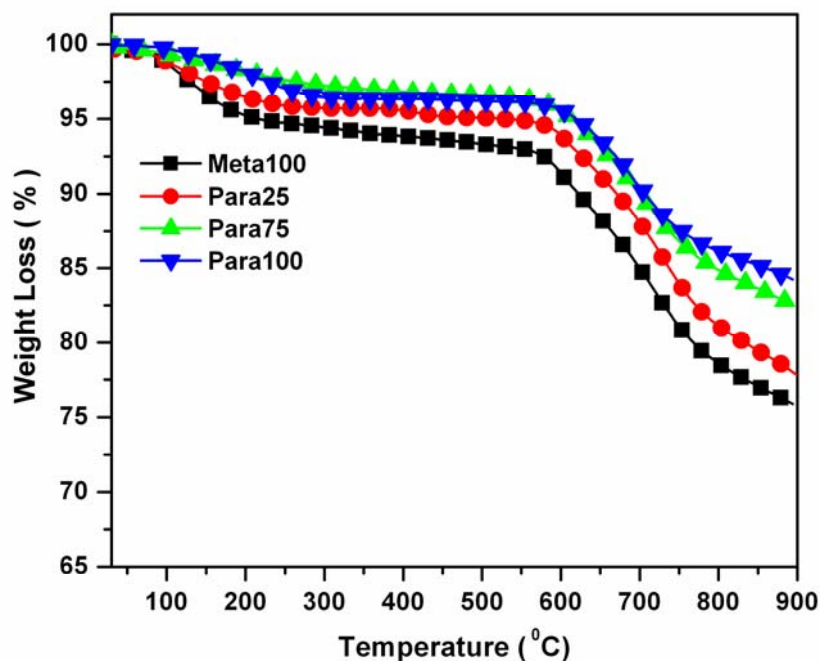
Figure 2.7. *TGA curves of the PBI polymers. Para content (mol %) of the polymers are indicated in the figure.*

Table 2.3 shows that the $T_{10\%}$ (temperature at which 10% weight loss is observed) increases as the para content increases in the polymer chain. Furthermore, the weight loss at the final temperature, viz., 890°C, becomes less for higher para content (Table 2.3). These observations clearly suggest that the introduction of *p*-phenylene groups in the polymer backbone enhances the thermal stability of the polymer.

Table 2.3. *Thermal stability data of all the PBI polymers.*

Para Content (mol %)	W_{570^oC} $(\%)^a$	$T_{10\%}$ $(^oC)^b$	W_{890^oC} $(\%)^c$
0	92.8	621	75.9
10	94.8	654	78.1
25	94.5	667	79
50	95.5	680	79.1
75	96.2	696	82.6
90	96.2	698	83.3
100	96.2	707	84.5

[a] Residual weight percent at 570°C. [b] Temperature at which the 10% weight loss is observed. [c] Residual weight percent at 890°C.

The glass transition temperatures of all the polymer samples are measured by using a differential scanning calorimeter (DSC). The DSC measurements show that the glass transition temperatures (T_g) of the *m*-PBI and the *p*-PBI are 420 and 361°C, respectively (Figure 2.8). In the literature, the T_g value of the *m*-PBI is reported by several authors. The reported values are between 400 and 450°C depending upon the measurement techniques followed and the molecular weight of the sample.[48,49] Therefore, our T_g value of the *m*-PBI is in agreement with the reported observations. To our knowledge until now no efforts have been made to measure the T_g of the *p*-PBI. The T_g of the *p*-PBI is 59°C lower than that of the *m*-PBI, which indicates that the *p*-PBI backbone is more flexible than the *m*-PBI chains. The flexibility in the *p*-PBI backbone arises because of the presence of better conjugation between the imidazole ring and the

p-phenylene linkage. From Figure 2.3, IR studies show that the coupled N-C-C linkage vibrates at a higher frequency for the *p*-PBI than the *m*-PBI indicating the presence of the double bond nature in the *p*-backbone. Moreover, para substitution in the polymer chain brings more symmetrical arrangement in the backbone. The flexibility and the symmetrical nature of the para backbone enhance the segmental mobility of the chains and hence show a lower glass transition temperature compare to the meta structure.[50] Figure 2.8 shows the representative DSC curves for various copolymers along with the two homopolymers. All the DSC curves for the homopolymers and the copolymers show a single T_g transition as observed in Figure 2.8. Also, we have measured the T_g of the copolymers from the tan δ vs temperature plot obtained from the dynamical mechanical analysis (DMA) as shown in Figure 2.9. The DMA and DSC results are tallying each other quite well. The glass transition temperatures of the copolymers first decrease slowly and then steadily with the increase in para content as presented in Figure 2.10. The expected T_g of the random copolymers are estimated by the Fox equation (equation 2.3) as follows:

$$\frac{1}{T_g} = \frac{w_1}{T_{g_1}} + \frac{w_2}{T_{g_2}} \qquad\qquad (2.3)$$

where w_1 and w_2 are the weight fractions and T_{g_1} and T_{g_2} are the glass transition temperatures of the two homopolymers. Figure 2.10 shows that the experimental T_g values obtained from the DSC measurements (solid line) deviate from the calculated values obtained from the Fox equation (dotted line). The positive deviation is observed for the higher meta content whereas the negative deviation is exhibited by the higher para content polymers. The positive deviation from the linear additive rule (eq 2.3) for the higher meta content region could be due to the intrachain steric hindrance arising from the less symmetrical meta structure. The negative deviation for the higher para content region can be explained in the light of the reactivity ratio of the TPA. Since the TPA reactivity ratio is bigger (2.251) and greater than unity, therefore higher para content copolymers contain more and more para segments and exhibit lower T_g than the anticipated T_g by the Fox equation.
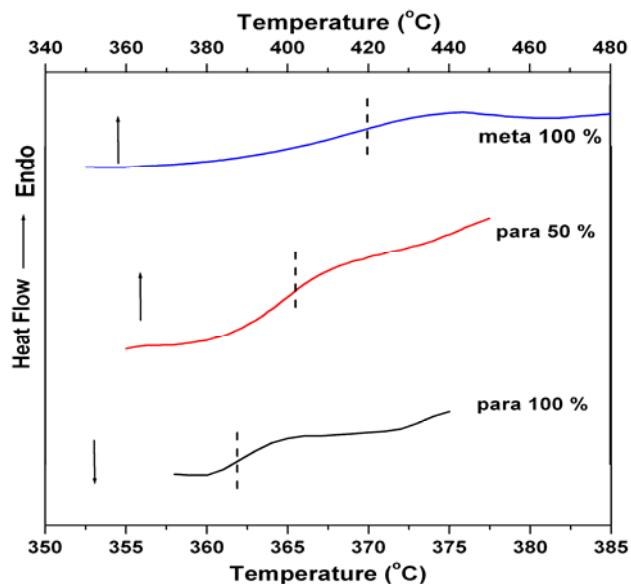
Figure 2.8. *DSC thermograms of PBI polymers. Arrows indicate the temperature axis and the vertical dotted lines represent the glass transition temperatures.*
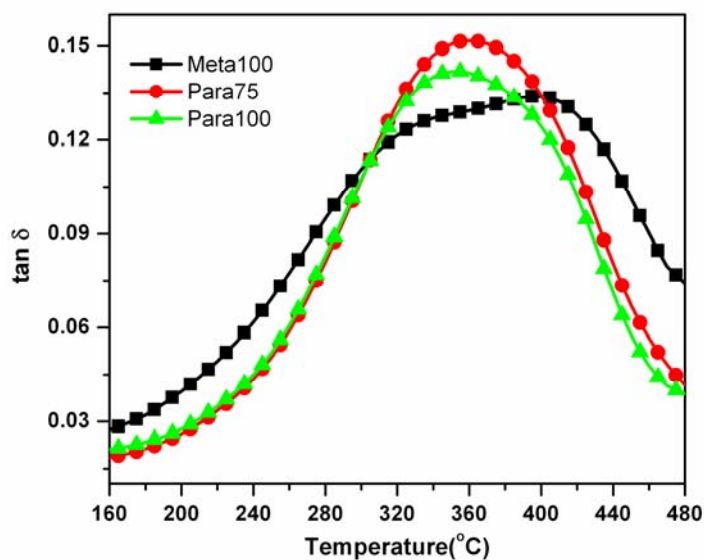
Figure 2.9. *Mechanical property (tan δ) vs. temperature plots of indicated copolymers as obtained from DMA analysis. Copolymer films of 25 × 5 × 0.04 mm (L × W × T) dimension was used for the mechanical study on the film tension clamp of a dynamical mechanical analyzer (model Q 800 of TA instruments).*
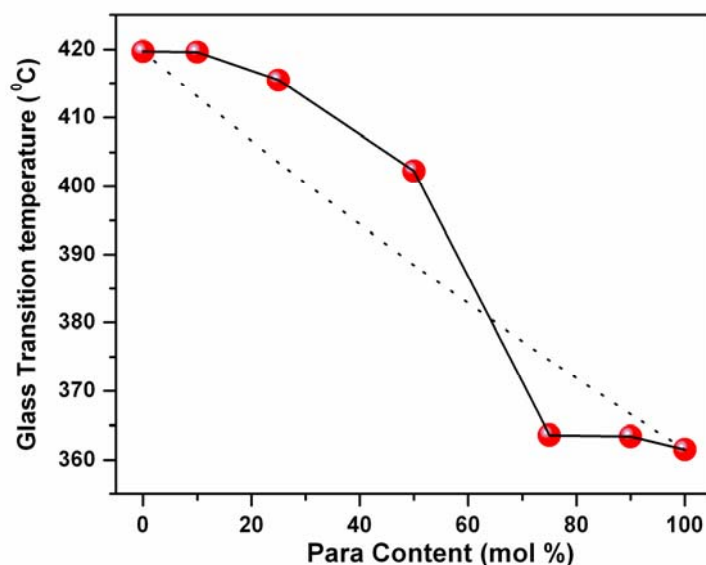
Figure 2.10. *Variation of glass transition temperature (T_g) with para content of the PBI copolymers. Solid line is experimentally obtained and dotted line is calculated from Fox equation.*

2.3.4. Spectroscopy. The absorption and the fluorescence emission spectra of all the PBI polymers are studied from their dilute solution (2×10^{-5} M) in dimethylacetamide (DMAc). The concentration is expressed by considering one repeat unit as 1 mol of PBI. The absorption spectra of the PBI polymers in DMAc are shown in Figure 2.11. Each spectrum shows distinct $\pi \rightarrow \pi^*$ transition peaks above 340 nm.[12,14] The peak positions are tabulated in Table 2.4. The gradual bathochromic shift of the $\pi \rightarrow \pi^*$ absorption maxima with increasing para content in the copolymer backbone is observed (Figure 2.11, Table 2.4). The 100% *p*-PBI homopolymer absorbs at ~50 nm higher wavelength than the 100% *m*-PBI homopolymer. The introduction of the *p*-(1,4)- phenylene linkage into the polymer backbone enhances the conjugation between the imidazole and the phenylene ring, which results in the above-mentioned bathochromic shift of the $\pi \rightarrow \pi^*$ absorption maxima.[26,33] Therefore, our argument about the increased conjugation in the backbone due to the para substitution using IR spectra and thermal studies discussed in the previous sections is in good agreement with the absorption studies.
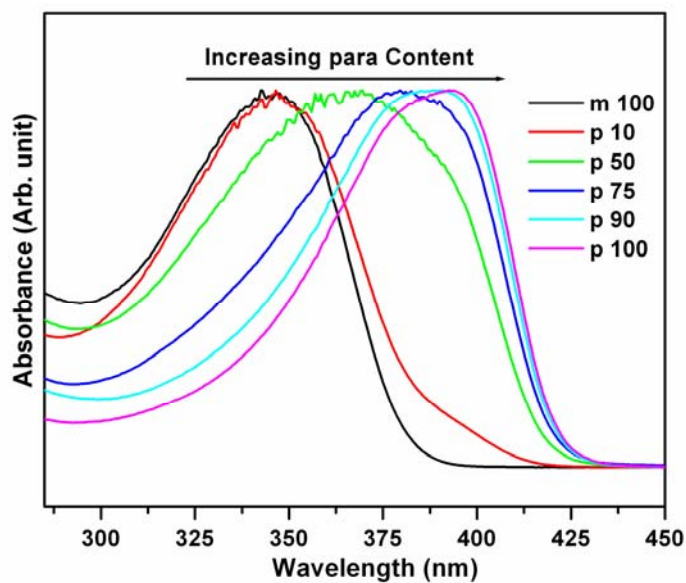
Figure 2.11 *Absorption spectra of the indicated PBI polymers in DMAc solution as recorded with a cuvette of 1 cm pathlength. Concentrations are 2 × 10^{-5} M.*

Table 2.4. *Electronic spectroscopy data of all the PBI polymers.*

Para content (mol%)	absorption peak (nm)	emission peaks (nm)	Φ_f
0	344	396	0.515
		416	
10	346	396	0.569
		416	
25	348	396	0.660
		416	
50	368	428	0.651
		450	
75	382	428	0.528
		450	
90	390	428	0.508
		450	
100	394	428	0.501
		450	

The emission spectra of the PBI polymers in DMAc are presented in the Figure 2.12. The excitation wavelengths (λ_{exc}) are chosen based on the $\pi \rightarrow \pi^*$ absorption maxima shown in Table 2.4. The concentration of the solution is 2×10^{-5} M, which is kept constant for all cases. The emission wavelengths and the measured fluorescence quantum yields (Φ_f) are presented in Table 2.4. All the emission spectra of the PBI samples show two fluorescence bands.[12,14] The lower wavelength and the longer wavelength peaks from the excited ^1L_b state in the benzimidazole ring of the PBI are assigned as 0-0 and 0-1 transitions, respectively. The spectral nature and shapes of the bands are similar to those of the earlier reports.[12,14] In a recent report, we have shown a longer wavelength peak at ~548 nm exists for the highly concentrated (5×10^{-3} M) *m*-PBI solution in DMAc due to the excimer/aggregation formation.[14] The concentration (2×10^{-5} M) that we have studied here is much lower than that concentration; hence the absence of the 548 nm band is expected. For the 100% meta homopolymer, 10% para copolymer, and 25% para copolymer the emission peak positions (398 and 416 nm) are the same (Figure 2.12. and Table 2.4). However, the emission bands are shifted gradually to the higher wavelength (428 and 450 nm) from the 50% para composition onward and resemble similar behavior of the other higher para content polymers. The shifting of the emission bands toward the longer wavelength also supports the conjugation along the polymer backbone due to the introduction of the *p*-phenylene linkage. This observation once again strengthens our previous argument about the better conjugation of the higher para content sample. The fluorescence quantum yields for all the samples are quite large (Table 2.4), which indicates that all the PBI samples studied here, are highly fluorescent. To our knowledge we are the first to report the fluorescence quantum yield of the PBI polymers. Table 2.4 shows that the quantum yields for all the PBI samples are almost identical, indicating similar fluorescent behavior. However, 25% and 50% para content samples show little higher quantum yield. This might be due to the existence of their less probable nonradiative pathways.
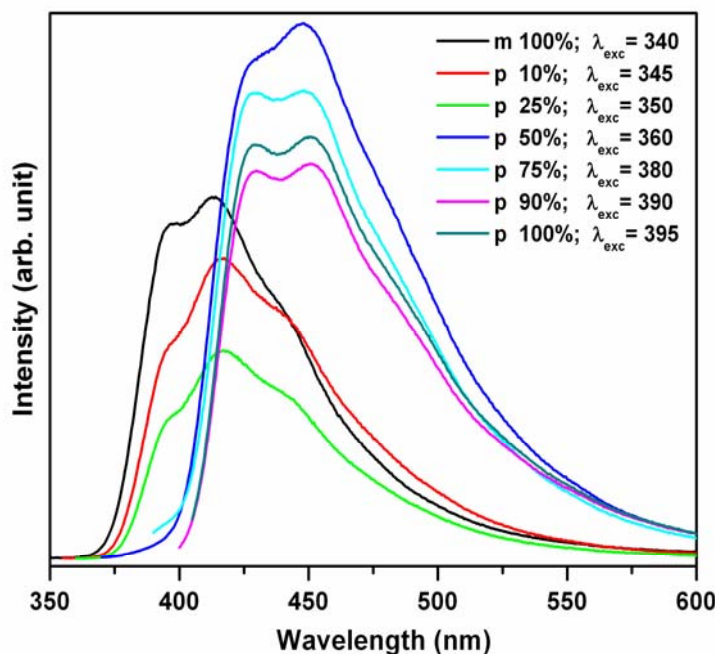
Figure 2.12. *Fluorescence emission spectra of the indicated PBI polymers in DMAc solution. Concentrations are identical to Fig 2.11. Excitation wavelengths (λ_{exc}) are indicated in the figure.*

2.3.5. X-ray Diffraction. The wide-angle X-ray diffraction (WAXS) patterns of all the PBI samples are presented in Figure 2.13. From the figure, it is evident that all the samples are amorphous in nature. In all cases two broad peaks at around 13 and 25 2θ (deg) are observed. But, no sharp peak is observed in any of the cases. The existence of the broad peaks results from a convolution of amorphous and crystalline scattering. Earlier several authors reported a similar observation for the PBI-type polymers.[22, 26, 30, 49] Therefore, we can conclude that the introduction of the *p*-phenylene linkage in the polymer backbone does not influence the packing capacity of the polymer chains though it brings more symmetry in the structure. All the polymers studied here are completely noncrystalline and hence we have not observed any crystalline melting peak in the DSC

study. We have obtained a single glass transition temperature (Figure 2.8) because of the amorphous nature of the polymers.
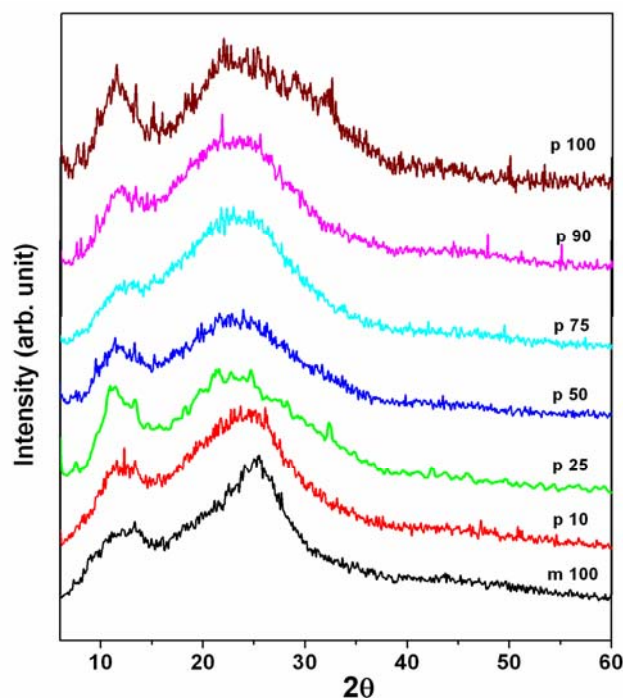
Figure 2.13. *WAXS diffractograms of all the PBI samples.*

2.3.6. Phosphoric Acid (PA) Loading. The PA loading capacity of the membrane has great influence on the performance of PEMFC. In general, higher acid loading is desirable to achieve the higher protonic conductivity. Higher acid content facilitates the transport of the protons easily, which significantly improves the fuel cell efficiency.[20-21] The PA doping level of the membrane is expressed as the number of PA mols per PBI repeat unit. We have prepared PA doped membranes for all the copolymer samples by imbibing and PPA processes and measured the acid (PA) doping level of the membranes by titrating against 0.1(N) NaOH. Copolymer membranes prepared from PPA process shows significant increment in acid loading (Figure 2.14) with increasing para mol% in the copolymer chain. However, the PA loading does not increases

significantly with para content in case of imbibing process. This is probably due to the poor solubility of higher para content PBI.
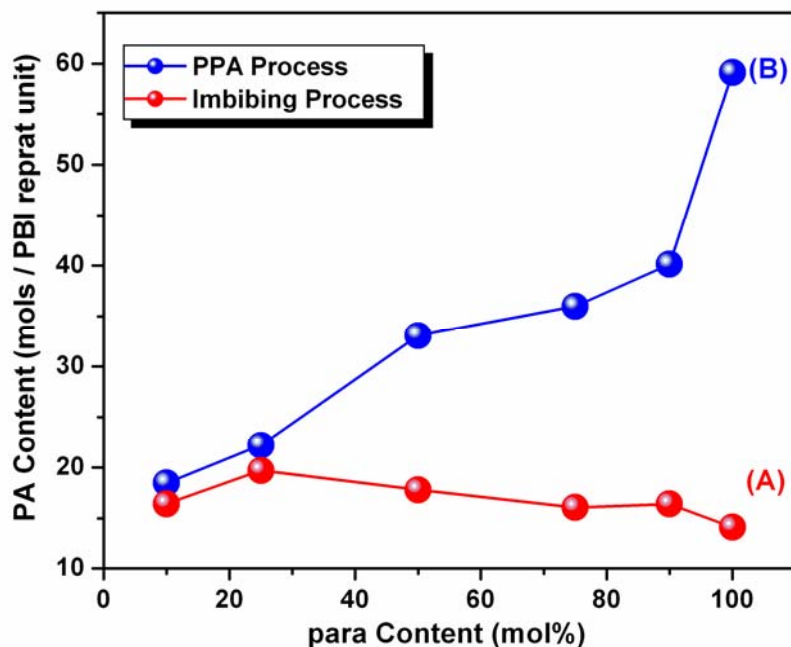
Figure 2.14. *PA loading of all the copolymers in two different methods (A) Imbibing process (B) PPA process.*

2.4. Conclusion

We have synthesized and characterized a series of random copolymers of polybenzimidazole consisting of *m-* and *p*-phenylene linkage in the backbone. Higher molecular weight polymers are obtained from higher para content copolymer due to the low solubility of the *p*-phenylene dicarboxylic acid (TPA) monomer. The higher reactivity ratio of TPA than isophthalic acid (IPA) obtained from the proton NMR studies provides the proof for the positive deviation of the copolymer composition from the monomer feed ratio. The thermal stability of the dry polymer powders is increased due to the copolymerization. The introduction of the *p*-phenylene linkage in the

backbone enhances the flexibility of the polymer chain and hence T_g decreases with increasing para content in the copolymer. The T_g of the copolymers shows deviation from the expected T_g calculated by the Fox equation. FT-IR study shows that the conjugation along the chain increases in the case of the para structure compare to the meta structure. The bathochromic shift in the absorption spectra and longer wavelength emission for higher para content PBI copolymer in DMAc solution are observed due to such increased conjugation along the chain. All the PBI polymers synthesized here are completely amorphous in nature. The PA loading increases with increasing para content in the PBI copolymer backbone. In summary we are able to demonstrate that the molecular properties (viz., molecular weight, thermal stability, T_g, and photophysical behaviors) and the PA loading of the PBI type polymers can be efficiently controlled by copolymerizing the isomers of the dicarboxylic acids with the tetraamine.

References

(1)   Fuel Cell Handbook, 6 th. Edition, EG & G Technical Services, Inc. U.S. Department of Energy, November 2002.

(2)   Blomen, L. J. M. J. *Fuel Cell Systems*; Plenum Press, New York, 1993

(3)   Gottesfeld, S.; Pafford, J. *J. Electrochem. Soc.* **1998**, *135*, 2651.

(4)   Yang, C.; Costamagna, P.; Srinivasan, S.; Benziger, J.; Bocarsly, A.B. *J. of Power Science* **2001**, *103*, 1.

(5)   Hickner, M. A.; Ghassemi, H.; Kim, S. Y.; Einsla, B. R.; McGrath, J. E. *Chem. Rev.* **2004,** *104*, 4587.

(6)   Savadogo, O. *J. New Mater. Electrochem. Syst.* **1998**, *1*, 47.

(7)   Roziere, J.; Jones, D. J. *Annu. Rev. Mater. Res.* **2003**, *33*, 503.

(8)   Kerres, J. *J. Membr. Sci.* **2001**, *185*, 3.

(9)   Choe, E. W.; Choe, D. D. In *Polymeric Materials Encyclopedia*; Salamone, J. C., Ed.; CRC Press, New York, 1996

(10)   Savinell, R.; Yeager, E.; Tryk, D.; Landau, U.; Wainright, J.; Weng, D.; Lux, K.; Litt, M.; Rogers, C. *J. Electrochem. Soc.* **1994**, *141*, L46.

(11)   Samms, S. R.; Wsmus, S.; Savinell, R. F. *J. Electrochem. Soc.* **1996,** *143,* 1225.

(12)   Kojima, T. *J. Polym. Sci.: Polym. Phys. Ed.* **1980**, *18*, 1685.

(13)   Shogbon, C. B.; Brousseau, J.-L.; Zhang, H.; Benicewicz, B. C.; Akpalu, Y. *Macromolecules* **2006,** *39*, 9409.

(14)   (a) Sannigrahi, A.; Arunbabu, D.; Sankar, R. M.; Jana, T. *Macromolecules* **2007**, *40*, 2844. (b) Ghosh, S.; Sannigrahi, A.; Maity, S. *J Phys Chem B* **2010**, *114*, 3122.

(15)   Musto, P.; Karasz, F. E., MacKnight, W. J. *Macromolecules* **1991**, *24*, 4762.

(16)   Deimede, V.; Voyiatzis, G. A.; Kallitsis, J. K.; Qingfeng, L.; Bjerrum, N. J. *Macromolecules* **2000**, *33*, 7609.

(17)   Yang, N. C.; Sang, M. L.; Suh, D. H. *Polymer Bulletin* **2003**, *49*, 371.

(18)   Weng, D.; Wainright, J.S.; Landau, U.; Savinell, R. F. *J. Electrochem. Soc.* **1996**, *143*, 1260.

(19)   Mecerreyes, D.; Grande, H.; Miguel, O.; Ochoteco, E.; Marcilla, R.; Cantero, I. *Chem. Mater.* **2004**, *16,* 604.

(20)   Xiao, L.; Zhang, H.; Jana, T.; Scanlon, E.; Chen, R.; Choe, E.-W.; Ramanathan, L. S.; Yu, S.; Benicewicz, B. C. *Fuel Cells* **2005**, *5*, 287.

(21)   Xiao, L.; Zhang, H.; Scanlon, E.; Ramanathan, L. S.; Choe, E.-W.; Rogers, D.; Apple, T.; Benicewicz, B. C. *Chem. Mater.* **2005**, *17*, 5328.

(22)   Sannigrahi, A.; Arunbabu, D.; Jana, T. *Macromol. Rapid Commun.* **2006**, *27*, 1962.

(23)   Asensio, J. N.; Borrós. S.; Gómez- Romero, P. *J. Electrochem. Soc.* **2004,** *151,* A304.

(24)   Jouanneau, J.; Mercier, R.; Gonon, L.; Gebel, G. *Macromolecules* **2007**, *40,* 983.

(25)   Li, Z. X.; Liu, J. H.; Yang, S. Y.; Huang, S. H.; Lu, J. D.; Pu, J. L.; *J . Polym. Sci.: Part A: Polym. Chem.* **2006**, *44*, 5729.

(26)   Chen, C. C.; Wang, L. F.; Wang, J. J.; Hsu, T. C.; Chen, C. F. *J. Mater. Sci* **2002**, *37*, 4109.

(27)   Chuang, S-W.; Hsu, S. L-C. *J . Polym. Sci.: Part A: Polym. Chem.* **2006**, *44*, 4508.

(28)   Qing, S.; Huang, W.; Yan, D. *Euro Poly J.* **2005,** *41*, 1589.

(29)   Pu, H.; Liu, Q.; Liu, G. *J. Membr. Sci.* **2004**, *241*, 169.

(30)   Scariah, K.J.; Krishnamurthy, V. N.; Rao, K. V. C.; Srinivasan, M. *J. Polym. Sci.: Part A: Polym. Chem.* **1987**, *25*, 2675.

(31)   Persson, J. C.; Jannasch, P. *Chem. Mater* **2006**, *18*, 3096.

(32)   Sun, S. F. *Physical Chemistry of Macromolecules: Basic Principles and Issues*; John Wiley & sons, Inc. : NY, 1994.

(33)   Neuse, E. W. *Adv.Polym. Sci.***1982**, *47*, 1.

(34)   So, Y – H. *Acc. Chem. Res.* **2001**, *34*, 753.

(35)   Apelblat, A.; Manzurola, E.; Balal, N. A. *J. Chem. Thermodynamics* **2006**, *38*, 565.

(36)   Long, B-W.; Wang, L-S.; Wu, J-S. *J. Chem. Eng. Data* **2005**, *50*, 136.

(37)   So, Y − H.; Heeschen, J. P.; Bell, B.; Bonk, P.; Briggs, M.; DeCarire, R. *Macromolecules* **1998**, *31*, 5229.

(38)   Brooks, N.W.; Duckett, R. A.; Rose, J.; Ward, I. M.; Clements, J. *Polymer* **1993**, *34*, 4038.

(39)   Musto, P.; Karasz, F.E.; MacKnight, W. J. *Polymer* **1993,** *34*, 2934.

(40)   Lobato, J.; Cañizares , P.; Rodrigo, M. A.; Linares, J. J.; Manjavacas , G. *J. Membr. Sci* **2006***, 280*, 351.

(41)   Silverstein, R. M.; Webster, F. X. *Spectroscopic Identification of Organic compounds*; John Wiley & Sons, Inc: NY, 2002.

(42)   Li, Y.; Wang, F.; Yang, J.; Liu, D.; Roy, A.; Case, S.; Lesko, J.; McGrath, J. E. *Polymer* **2006**, *47*, 4210.

(43)   Lyoo, W. S.; Kim, J. H.; Ha, W. S. *J. Appl. Poly. Sci.* **1996**, *62*, 473.

(44)   Sundarrajan, S.; Ganesh, K.; Srinivasan, K. S. V. *Polymer*, **2003**, *44*, 61.

(45)   Fineman, M.; Ross, S. D. *J. Polym. Sci.* **1950**, *2*, 259.

(46)   Mayo, F. R.; Lewis, F. M. *J. Am. Chem. Soc.* **1944**, *66*, 1594.

(47)   Asensio, J. A.; Borrós, S.; Gómez-Romero, P.   *J. Polym. Sci.: Part A: Polym.Chem.* **2002**, *40*, 3703.

(48)   Liang, K.; Bánhegyi, G.; Karasz, F, E.; MacKnight, W. J. *J. Polym. Sci.: Part B: Polym. Phys.***1991**, *29*, 649.

(49)   Kumbharkar, S.C.; Karadkar , P. B.; Kharul, U.K.; *J. Membr. Sci.* **2006**, *286*, 161.

(50)   Sperling, L. H. *Introduction to Physical Polymer Science*; John Wiley & Sons, Inc: NY, 1992.

Chapter 3

Monomer Structural Isomer Directed Copolymerization of Polybenzimidazoles and Their Properties
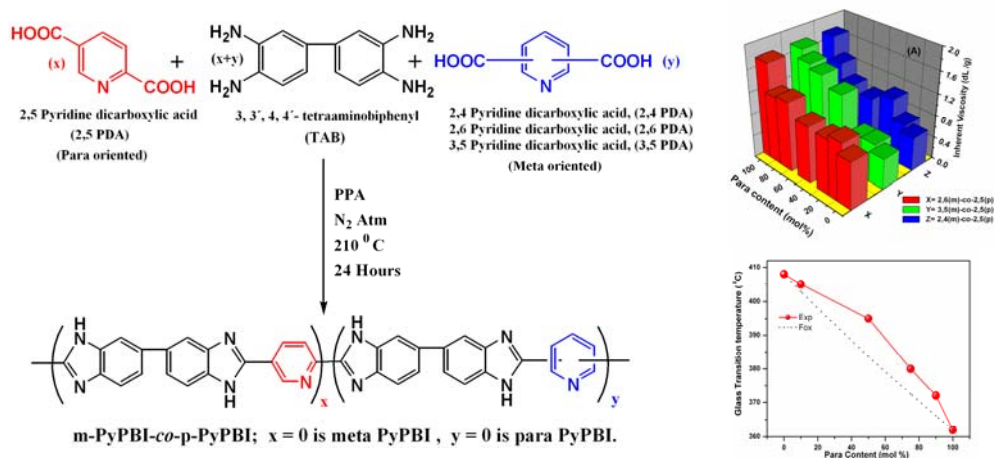
The structural isomeric effect of pyridine based dicarboxylic acid monomers on the copolymerizations of polybenzimidazoles and their properties are investigated.

3.1. Introduction

Recently, polymer electrolyte membrane fuel cell (PEMFC) operating at high temperature has attracted huge attention owing to its numerous advantages compared to PEMFC operating at lower than 100ºC.[1-3] Several efforts have been made to develop the variety of polymer membranes which can operate above 120ºC in their polyelectrolyte state.[4-6] Phosphoric acid (PA) doped polybenzimidazole (PBI) membrane is found to be the most attractive and promising for the use in high temperature PEMFC.[7-8] Till to date a large variety of PBI polymers have been synthesized and studied in the literature[9,10]. Therefore, synthesis of PBI polymers with variety of structure still remains an important area of investigation for the polybenzimidazole chemistry despite the fact that the first PBI was synthesized back in the year 1961 by Vogel and Marvel.[11]

The commercially available PBI, poly [2,2'–(1,3–phenylene)–5,5'–benzimidazole] (known as *m*- PBI)[12] is the most widely used among the all PBI. Others varieties include poly [2,2'–(1,4–phenylene)–5,5'–benzimidazole] (known as *p*-PBI),[13] poly(2,5 benzimidazole) (AB–PBI),[14] pyridine based PBI homopolymer,[15] sulfonated PBI,[16-17] hyperbranched polybenzimidazole (HPBI),[18] naphthalene based PBI,[19] fluorinated PBI,[20-22] meta and para PBI copolymer,[23] PBI with sulfone or sulfonic acid groups[24,25] in the backbone etc. PBI is a basic polymer (pK$_a$ ~5.25) and possesses both proton donor (- NH -) and proton acceptor (- N =) hydrogen bonding sites which exhibit specific interactions with the polar solvents[26-28] and forms miscible blends with variety of polymers.[29-31] Polybenzimidazole has excellent thermal and chemical resistance, fire retarding capacity, insulating property and it forms good textile fiber.[32] However, the poor solubility of PBIs resulting from the highly rigid polymer backbones and the strong intra-interchain hydrogen bonding interactions makes them hard to process.[26,27,33] Several attempts have been made through the modification of the polymer backbone as well as side chain to solve the solubility issues. Many investigators have incorporated flexible spacers such as methylene and aryl methylenes, arylamide and ether linkages in the polymer backbone.[34,38] Recently, Persson et. al. have synthesized ABA triblock copolymers having benzimidazole tethered end blocks which exhibits enhanced solubility.[39]

Phosphoric acid (PA) doped PBI is most interesting because of its amphoteric and strong thermal stability nature as well as it has low vapour pressure at elevated temperatures. It forms dynamic hydrogen bond networks in which protons can readily transfer by hydrogen bond breaking and forming processes.[9,40] Various approaches have been attempted so far for the fabrication of PA doped PBI membranes; these include casting PBI membrane by dissolving of PBI in dimethyl acetamide (DMAc) solvent followed by soaking of the membrane in phosphoric acid (PA),[9,41-44] via sol–gel process by direct casting of the high molecular weight PBI solution in polyphosphoric acid (PPA)[15,45] and from thermoreversible gel of *m*-PBI in PA.[46] The major challenge for the fabrication of PA doped PBI is to get a membrane with high acid doping level and moderately good mechanical stability. If the acid content of the membrane is too high it forms soft plastic type material which does not have enough mechanical strength to form a membrane.[9,46] To get a superior quality membrane, a compromise between these two important parameters (acid loading and mechanical stability) has to be maintained. Different methods have been explored to improve the acid loading without compromising on the mechanical strength or vice versa. These include synthesis of new PBI having variety of polymer backbone structure,[15-24] high molecular weight PBI polymer synthesis by copolymerization,[23] introduction of crosslinkage between the polymer chains,[47,48] incorporation of inorganic fillers in the PBI matrix.[49-51]

m-PBI was first synthesized by melt polycondensation method at high temperature in inert condition using 3, 3$'$, 4, 4$'$- tetraaminobiphenyl and biphenylisopthalate.[11] Choe et al developed a new method for preparation of high molecular weight PBI using isophthalic acid instead of biphenylisopthalate in the presence of organo phosphorus and organo silicon as a catalyst and they have successfully shown that P_2O_5 in phosphoric acid act as a solvent as well as condensing agent. Later on several groups have started using polyphosphoric acid (PPA) as a solvent as well as condensing agent.[32,52] Earlier studies indicated that the molecular weight of the PBI polymers has great impact on their properties, in particular mechanical properties and acid doping level capacity. Generally higher the molecular weight of a polymer better is the thermo mechanical property.[23, 32, 38, 45] Therefore, there

is a necessity for the preparation of high molecular weight PBI and obviously the best way to do that is to synthesize various polymer backbone structures. Synthesis of high molecular weight PBI depends upon various factors which include stoichiometry of starting monomers, purity of the monomers, temperature, inert atmosphere, time duration and monomer concentration. However, earlier (chapter 2) we have shown that the higher molecular weight PBI synthesis also depends upon the solubility of the monomers in PPA medium. In our previous report (chapter 2), we have demonstrated that the molecular weight of PBI polymer can be readily tuned by choosing the carboxylic acid architecture appropriately. The change in the molecular weight of PBI by changing the monomer structure also alters the molecular properties of the PBI copolymer. We have found that low solubility of para structure dicarboxylic acid (terephthalic acid) in PPA is the dominating factor for resulting the higher molecular weight polymer.[23]

In the present study (this chapter), we report synthesis and characterization and studies of series of pyridine based polybenzimidazole (PyPBI) random copolymers. We have chosen various isomers of pyridine di-carboxylic acid (PDA) monomers and synthesized variety of copolymers with meta-para oriented structures. The synthesized polymers are characterized by determining inherent viscosity (I.V) as a measurement of polymer molecular weight, thermo gravimetric analysis (TGA) for the thermal stability, dynamic mechanical analyzer (DMA) for the thermal transitions. Fourier transforms infrared (FT – IR) and Raman and proton NMR techniques are used to establish the polymer structure. Also, spectroscopic studies such as absorption and fluorescence are carried out to demonstrate the effect of copolymerization on the photophysical properties. Finally, we have studied the wide angle X–ray scattering (WAXS) to look into the crystalline characters of these polymers.

3.2. Experimental Section

3.2.1. Materials. 3, 3′, 4, 4′- tetraaminobiphenyl (TAB, polymer grade) and polyphosphoric acid (PPA, 115 %) were purchased from Sigma–Aldrich. 2,4 pyridine

dicarboxylic acid (98%), 2,5 pyridine dicarboxylic acid (98%), 2,6 pyridine dicarboxylic acid (99%) and 3,5 pyridine dicarboxylic acid (98%) purchased from Sigma-Aldrich and purified by recrystallization in water and dil HCL (9:1) mixture prior to use. Dimethyl acetamide (DMAc, HPLC grade) was purchased from Qualigens-India. Sulfuric acid (98%) was purchased from Merck, India. The NMR solvent dimethyl sulfoxide (DMSO-d_6) was obtained from Acros Organics. All the solvents were used without further purification.

3.2.2. Polymer Synthesis. Equal mols of pyridine dicarboxylic acids (2, 4 or 2, 5 or 2, 6 or 3, 5 PDAs) and TAB were taken into a three neck flask with polyphosphoric acid (PPA) for homopolymers synthesis. 2, 4; 2,6 and 3,5 pyridine dicarboxylic acids (PDA) were used to prepare meta oriented pyridine polybenzimidazole (PyPBI) and 2,5 was used to prepare para oriented pyridine polybenzimidazole (PyPBI) homo polymer, respectively. The two carboxylic acid groups position in the 2,5 PDA are opposite to each other so it is called para oriented and in other cases carboxylic acids groups positions are one carbon apart they are called meta oriented (scheme 3.1). Three sets of different random PyPBI copolymers (2,6 and 2,5) , (3,5 and 2,5) and (2,4 and 2,5) were synthesized by varying the mol fraction of the di-acids (meta and para) in the reaction mixture from 10 % to 90 % but maintaining the total mol of di-acids equal to the mol of TAB taken in the reaction mixture along with PPA. The polymerization reaction scheme is presented in Scheme 3.1. Total monomer concentrations were gradually decreased with increasing 2,5 PDA (para) mol fraction in the mixtures. The reaction mixture was placed in a digitally temperature controlled oil bath .The reaction mixtures were stirred by an overhead mechanical stirrer continuously in the nitrogen atmosphere at 190 - 210°C for ~ 24 hours. The viscosity of the reaction mixture increased as the polymerization proceeds and resulted in a dark brown colour at the end of the polymerization. The PBI polymers were isolated, neutralized with sodium carbonate, washed thoroughly with water and dried in a vacuum oven at 100°C for 24 hours. The dried polymers were kept in vacuum desiccators for further characterizations.
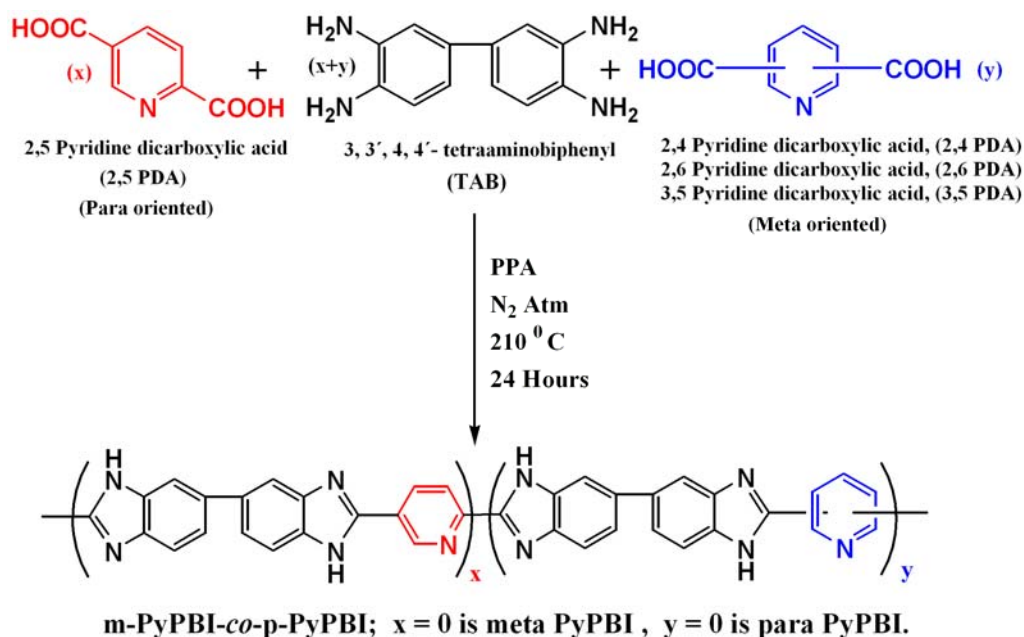
Scheme 3.1. *Synthesis of m-Pyridinepolybenzimidazole-co-p-Pyridinepolybenzimidazole (m-PyPBI-co-p-PyPBI).*

3.2.3. Viscosity. The viscosity measurements of the polymer solutions in H_2SO_4 (98 %) were carried out at 30°C in a constant temperature water bath using a Cannon Ubbelohde capillary dilution viscometer (model F725). The inherent viscosity (IV) values were calculated from the flow time data. For all the flow time measurements 0.2 g/dL polymer solution in H_2SO_4 (98 %) was used. The molecular weight of PBI in the related literature has been expressed in terms of I.V, measured from sulfuric acid solution.[13,32] The intrinsic viscosity ($[\eta]$) of the synthesized PyPBI was obtained by using Kuwahra single point method with the help of the following equation (3.1) [53]

$$[\eta] = \frac{\eta_{sp} + 3\ln\eta_{rel}}{4C} \qquad (3.1)$$

where η_{sp} and η_{rel} are the specific and relative viscosity of the polymer solution, respectively and C is the concentration of polymer in g/dL. The viscosity average

molecular weight ($\overline{M}_v$) was obtained by using Mark-Houwink equation, $[\eta] = K\overline{M}_v^a$ where K = 5.2×10^{-5} dL /g and a = 0.92 for H_2SO_4 (98%) solvent at 30ºC.[54]

3.2.4. IR Spectra. The IR spectra of the PyPBI homo and copolymers films were recorded on a (Nicolet 5700 FTIR) FT-IR spectrometer. The PyPBI films of thickness 30-40 μm were made from DMAc solutions (2 % w/v) of the polymers. The resolution of the IR spectrometer is about 4 cm^{-1}.

3.2.5. Raman Spectra. The Raman spectra were recorded using a Bruker Opus Raman spectrometer equipped with 1064 nm diode laser. The exposure time was 35 s. The resolution was about 4 cm^{-1}.

3.2.6. NMR Spectroscopy. All the NMR spectra were recorded using Bruker AV 400 MHz NMR spectrometer at room temperature using DMSO-d_6 as NMR solvent.

3.2.7. Thermal Study. Thermogravimetric and differential thermal analysis (TG-DTA) were carried out on a (Netzsch STA 409PC) TG-DTA instrument from 30 - 800°C with a scanning rate of 10°C / minute in presence of nitrogen gas flow.

3.2.8. Mechanical Property Study. The mechanical properties of the PyPBI films were measured using a dynamic mechanical analyzer (DMA) (TA Instruments, model Q-800). PyPBI films casted from DMAc (2% w/v) solution of the polymers were boiled repeatedly with distilled water for washing and finally dried in oven at 100ºC for 24 hours. Films of 25 mm × 5 mm × 0.05 mm (L × W × T) dimensions were cut and clamped on the films tension clamp of the pre-calibrated instrument. The samples were annealed at 150ºC for 30 minutes and then scanned from 150ºC to 500ºC at heating rate of 4ºC /minute. The storage modulus (E'), loss modulus (E'') and tan δ values were measured at a constant linear frequency of 5Hz with preload force of 0.01N.

3.2.9. Absorption and Fluorescence Spectroscopy. Electronic absorption spectra were recorded on a Cary-100 Bio (VARIAN) UV-visible spectrometer. Steady-state fluorescence emission spectra were recorded on a Jobin Yvon Horiba spectrofluorimeter (Model Fluoromax-4). PBI samples were dissolved in dimethyl acetamide (DMAc) and the spectra were recorded.

3.2.10. X – ray Diffraction. The wide angle X-ray diffraction (WAXRD) patterns of the dry PyPBI powders were collected in a Philips powder diffraction apparatus (model PW 1830). The powders were taken in a glass slide and the diffractogramms were recorded using nickel – filtered Cu Kα radiation at a scanning rate of $0.6^o \, 2\theta$/minute.

3.3. Results and Discussion

3.3.1. Synthesis and Molecular Weight Control. We have synthesized three series of m-Pyridinepolybenzimidazole-*co*-p-Pyridinepolybenzimidazole random copolymers (m-PyPBI-*co*-p-PyPBI) and the polymer backbone structures are shown in Scheme 3.1. Pyridine-dicarboxylic acid (PDA) has four different meta and para isomers (2,4; 2,5; 2,6 and 3,5) based on there positions in the pyridine ring. When two carboxylic groups lie anti or opposite to each other, called para orientation and one position apart called meta orientation. Three of these isomers (2,4; 2,6 and 3,5) are meta type and 2,5 is the para type isomer (Scheme 3.2). In this chapter our goal is to prepare meta-para PBI random copolymers based on PDA monomers. Since PDA has three meta and one para isomers, hence we have synthesized three different series of meta-para PyPBI random copolymers. These are 2,4(m)-PyPBI-*co*-2,5(p)-PyPBI; 2,6(m)-PyPBI-*co*-2,5(p)-PyPBI and 3,5(m)-PyPBI-*co*-2,5(p)-PyPBI. Polymer backbone structure of these three different sets of PDA based random copolymers and three different sets of PDAs are shown in Scheme 3.1 and Scheme 3.2, respectively. We have carried out the copolymerization by varying the meta and para contents (mol %) in the copolymers from 10% to 90% in the initial reaction mixture. Also, three different meta (2,4; 2,6 and 3,5) homopolymers and para (2,5) homopolymer were prepared by taking the respective di-acid with the TAB. In all the polymerization reactions the stoichiometry of TAB and the diacids (meta + para) were maintained as equal mols and the reaction conditions for all the polymerization were similar except the initial monomer concentrations in the reaction mixtures. In case of condensation polymerization higher monomer concentration yields the higher molecular weight polymers. However, the solubility of the monomer in the reaction mixture dictates the amount of monomers which can be taken in the reaction

mixture. In case of poor solubility of the monomer, a lower monomer concentration needs to be taken; otherwise the presence of insoluble monomers disfavors the polymerization reaction and resulting lower molecular weight polymer. We have carried out the polymerization reaction with gradually decrease in monomer concentration with increasing para content in the copolymer and higher monomer concentrations are used for meta PyPBI (Table 3.1). Earlier, it has been shown that the para structure PBI can be made with high molecular weight if the lower monomer concentration is employed owing to the lower solubility of para oriented dicarboxylic acid.[23, 38, 55]
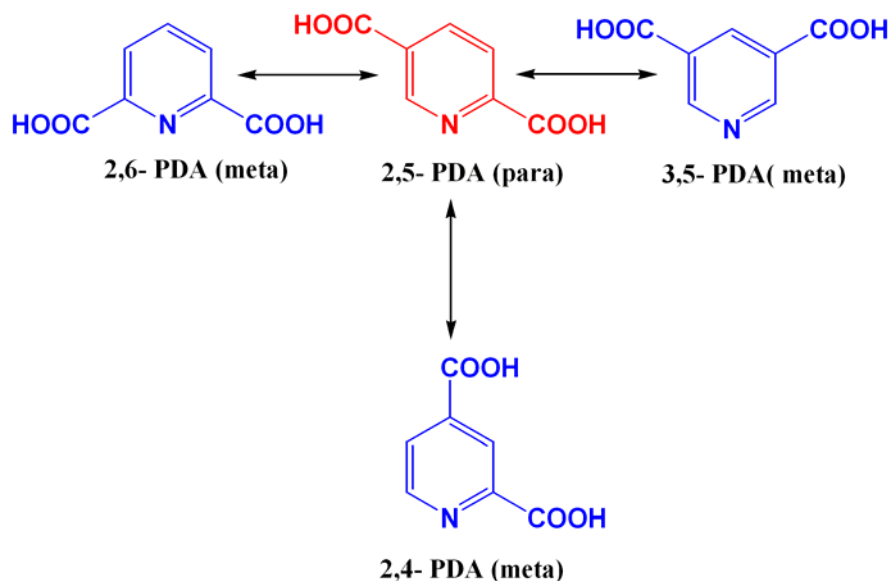
Scheme 3.2. *Three different sets of pyridine dicarboxylic acid (PDA) monomers.*

The molecular weight of the PBI family polymers are generally expressed in terms of their inherent viscosity (I.V).[13, 32] The higher I.V attributes higher molecular weight.[56] Recently viscosity average molecular weight ($\overline{M_v}$) is also calculated from the viscosity data as described in the experimental section.[54] Table 3.1 represent the I.V and $\overline{M_v}$ values of all the copolymer for all three series. Table 3.1 clearly demonstrates that lower monomer concentration is required for higher para content in all the cases to

obtain higher molecular weight polymer. In fact our attempts to prepare higher para content polymers with monomer concentration similar to meta polymer yield very low I.V polymers. These observations clearly prove the fact that low solubility of para oriented PDA demands the lower monomer concentration in the polymerization mixture. Hence the monomer concentration is an important parameter which needs to be adjusted to produce bigger PBI polymers.

Table 3.1. *Various reaction parameters and molecular weight of m-PyPBI-co-p-PyPBI random copolymers.*

Copolymer	Para Content (mol%)	Monomer Concentration (Wt. %)	Inherent viscosity (dL/ g)	$\overline{M_v} X 10^4$
	0	9.00	0.85	3.9
	10	8.75	1.07	5.1
	25	8.50	0.99	4.9
2,6(m)-PyPBI -*co*-2,5(p)- PyPBI	50	8.25	1.02	4.9
	75	8.00	1.25	6.1
	90	7.75	1.21	5.8
	100	6.00	1.75	8.9
	0	12.00	0.55	2.4
	10	11.75	0.72	3.2
	25	11.50	0.71	3.3
3,5(m)-PyPBI -*co*-2,5(p)- PyPBI	50	11.25	1.29	4.9
	75	11.00	1.47	7.3
	90	10.75	1.57	7.8
	100	6.00	1.75	8.9
	0	9.00	0.60	2.7
	10	8.75	0.75	3.4
	25	8.50	1.11	5.3
2,4(m)-PyPBI -*co*-2,5(p)- PyPBI	50	8.25	0.94	4.4
	75	8.00	1.02	4.8
	90	7.75	1.33	6.5
	100	6.00	1.75	8.9

Table 3.1 and Figure 3.1 exhibit that the molecular weight of all the three sets of m-PyPBI-*co*-p-PyPBI polymers increases with increasing para content in the polymer backbone. This observation is similar with our previous observation (chapter 2) in case of m-PBI-*co*-p-PBI, although in the previous case the increase is much more than the current one. Earlier, we have shown that the solubility of the monomers in PPA (polymerization medium) plays a vital role for the synthesis of high molecular weight PBI.[23] It has been found that para oriented dicarboxylic acid are less soluble in PPA medium because acid groups are probably unable to form the internal dimmers through hydrogen bonding interaction between carboxylic groups of the same acids or coming from two different molecules of the acid.[57, 58] Hence 2,5 PDA (para) is less soluble in PPA medium than all other PDAs. The less solubility of para dicarboxylic acid monomer forces the growing polymer chain oligomers to undergo an unusual heterogeneous reaction pathway in which the oligomer ends consist of soluble TAB monomer. This reaction pathway ensures the formation of bigger molecules. The similar observation we have made in our previous studies. The less distinct increase of molecular weight in the current copolymers compared to our previous report is due to the better solubility of 2,5 PDA monomer then the terephthalic acid (TPA) owing to the presence of pyridine nitrogen in 2,5 PDA.
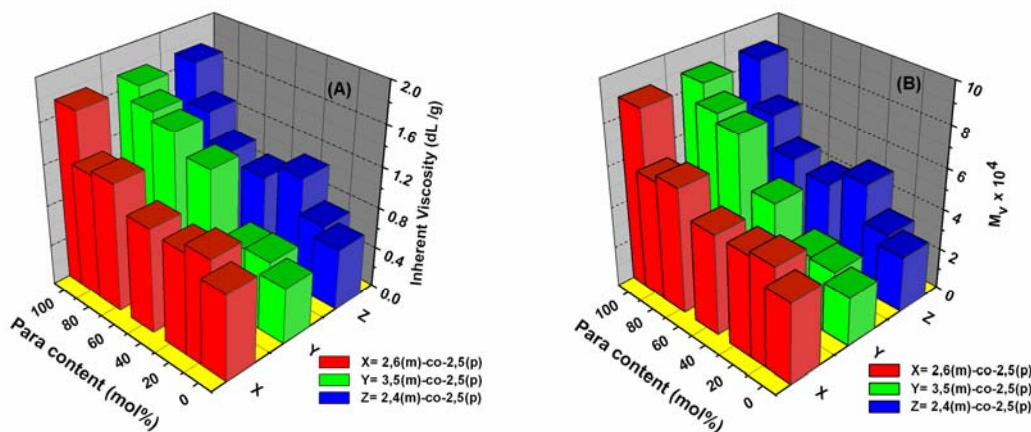
Figure 3.1. *Variation of molecular weight (A: inherent viscosity B: $\overline{M_v}$) with para content of the m-PyPBI-co-p-PyPBI random copolymers.*

3.3.2. IR and Raman Spectroscopy. FT-IR spectra of all the PyPBI homo and random copolymers are recorded from 30-40 μm thin polymer films made from the dilute solution (2% w/v) of the polymers in dimethyl acetamide (DMAc). Figure 3.2 shows the IR spectra of all four homopolymers. The IR spectra (2000-500 cm^{-1}) of all the three sets of copolymers with different para mol% are shown in Figure 3.3. All the films are boiled in hot water thoroughly and dried in vacuum oven at 100ºC for two days prior to recording of the IR spectra. The absence of C-H stretching of –CH$_3$ at 2940 cm^{-1} due to DMAc in the IR spectra proves the complete elimination of DMAc from the films by the above the drying process. The IR spectra of all the PyPBI homo and random copolymers are quite similar and the stretching bands are the characteristic bands of PBI. PBI polymers absorb moisture upto ~5% of their weight owing to their hygroscopic nature and therefore in all the IR spectra O-H stretching of H$_2$O at 3615-3620 cm^{-1} is observed (Figure 3.2).[59] The absorption at 3415 and 3175 cm^{-1} are because of free nonhydrogen bonded N-H stretching and self-associated N-H stretching, respectively. The low intense peak at 3063 cm^{-1} is due to the stretching modes of aromatic C-H groups (Figure 3.2). The similar kind of IR spectra of PBI polymers have been already discussed earlier by several authors. [29-31, 60] Our findings are very similar to our previous work (chapter 2) in case of all the three sets of copolymers. The in plane ring vibration of 2,6 disubstituted benzimidazole at ~1440 cm^{-1} becomes more sharp with increasing para content (Figure 3.3). It is evident from these spectra that the band at 1540 cm^{-1} (Figure 3.3A) and 1560 cm^{-1} (Figure 3.3B-C) gradually decreases with increasing para content in the polymer chain and becomes almost non existent for 100 % para PyPBI. The reason behind the deviation of these stretching bands intensities is because of the different substitution in the 2nd position of the benzimidazole owing to the different polymer backbone structure (meta and para) achieved by copolymerization. It is also worth noting that in all the cases (Figure 3.3) the peak at 1105 cm^{-1} for meta PyPBI slowly shifts towards the higher frequency with increasing para content in the copolymer and for 100% para the band appears at 1127 cm^{-1}. This band corresponds to the N-C stretching of benzimidazole group coupled with the substitution of the α carbon atom.[23, 61] The introduction of para substitution in the polymer chain brings more

flexibility and symmetry in the polymer backbone and it interferes the vibration characteristics, therefore the N – C --- C coupled vibration takes place at higher frequency.
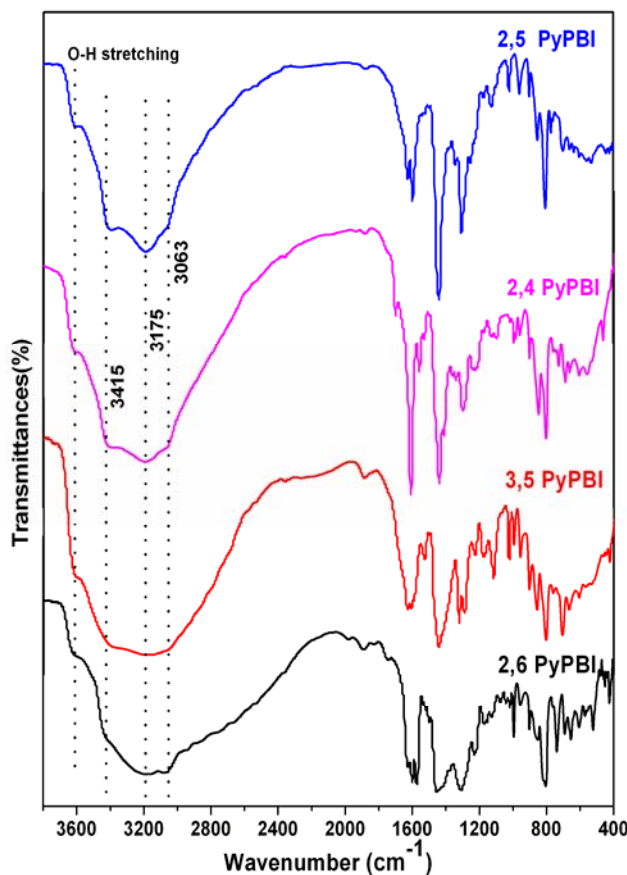
Figure 3.2. *FT- IR spectra of all the PyPBI homo polymers recorded from the thin (~30 μm) film obtained from 2% (w/v) DMAc solution.*

The IR studies described in the above section demonstrated the effect of copolymerization and the polymer backbone structure on the stretching of various groups. We have also studied FT-Raman spectra to understand the effect of copolymerization in a more deeper extent. The use of Raman spectroscopy as a tool to study the PBI type polymer is very rare. Recently meta PBI, 2,6-PyPBI and their

composites are characterized by Raman spectroscopy.[49, 62] Except these two reports, extensive use of Raman spectroscopy to characterization of the PBI is not known in the literature. Raman spectra of all the PyPBI homo and copolymers are recorded from solid powder sample and represented in the Figures 3.4-3.5.
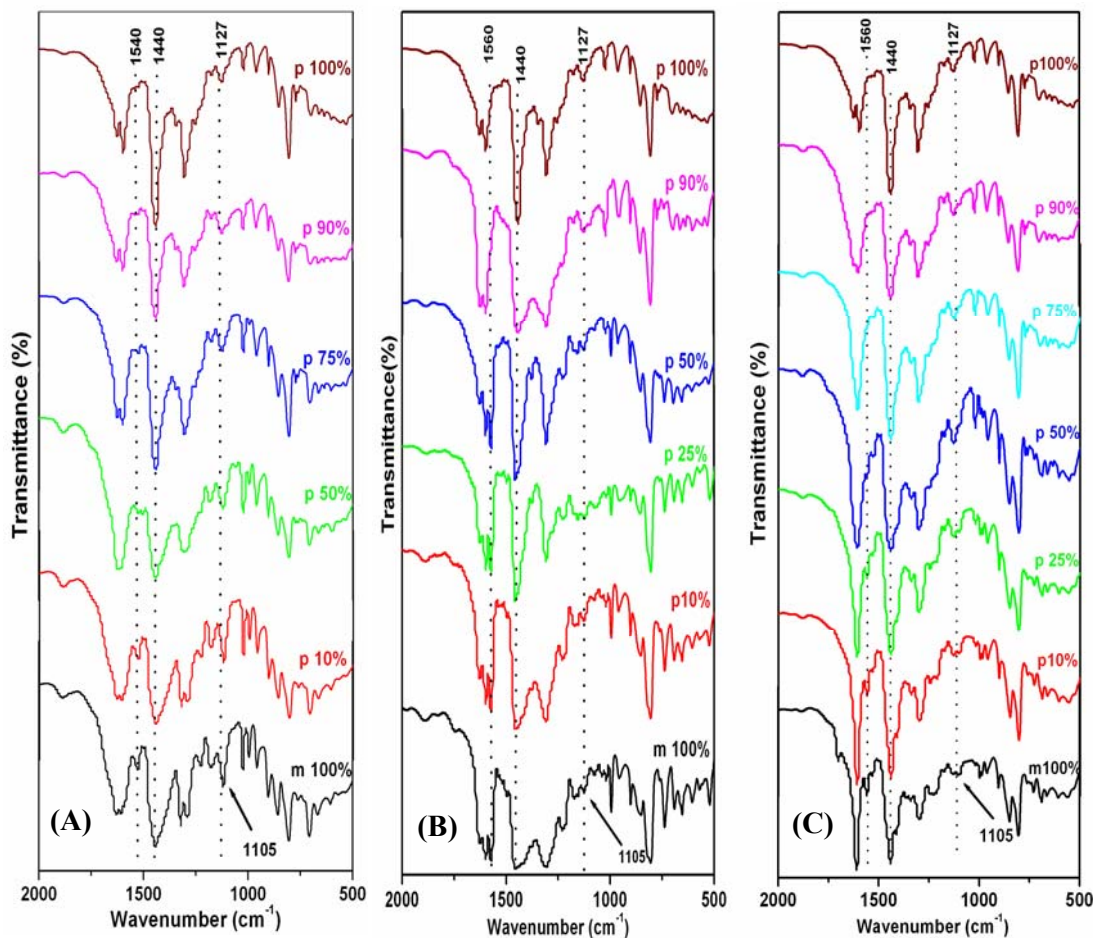
Figure 3.3. *FT-IR spectra of (A) 3,5(m)-PyPBI-co-2,5(p)-PyPBI (B) 2,6(m)-PyPBI-co-2,5(p)-PyPBI (C) 2,4(m)-PyPBI-co-2,5(p)-PyPBI random copolymers. The para content are shown in the figures. The dotted lines are shown to discuss the important IR bands. The films (30 μm) obtained from 2% (w/v) DMAc solution.*
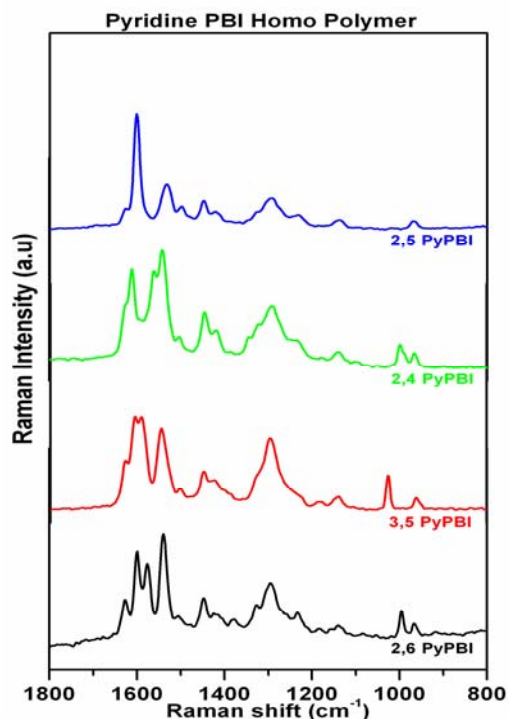
Figure 3.4. *FT-Raman spectra of pyridine PBI homo polymers.*

The various bands are previously assigned and our result matches well with the previous data.[49] The most prominent bands are located between 1630 to 1500 cm^{-1} and therefore we have analyzed the Raman data by plotting the spectra between 1650 to 1500 cm^{-1} as shown in Figure 3.6. All the bands in these regions are attributed to the benzimidazole ring stretching vibrations. These are the stretching of C=N and C=C bands of benzimidazole ring. The bands around 1600 cm^{-1} and 1500 cm^{-1} are due to C=N and C=C stretching of benzimidazole ring, respectively (Figure 3.6). In case of 2,6(m)-PyPBI-*co*-2,5(p)-PyPBI, the C=C stretching band at 1540 cm^{-1} (100% m) shifts towards lower wavenumber (1530 cm^{-1}) and becomes weaker with increasing para content (Figure 3.6). The other C=C stretching band at 1575 cm^{-1} (100% m) slowly disappear with increasing para content and become invisible for 100% para. These observations attribute the elongation or increased conjugation of the C=C with increasing para content. The C=N stretching at 1626 and 1600 cm^{-1}also exhibit significant change with increasing para content. The band at 1626 cm^{-1} almost

disappears and band at 1600 cm^{-1} becomes sharper with increasing para content (Figure 3.6). This finding once again hints the increased conjugation along the polymer backbone with increasing para content. The similar kind of displacements and changes of the C=N and C=C stretching vibrations are also observed for other two sets [2,4(m)-*co*-2,5(p) and 3,5(m)-*co*-2,5(p)] of PyPBI random copolymers. Therefore from the Raman study it is very much clear that the conjugation along the PyPBI copolymer backbone enhances with increasing para structure in the copolymer composition. In conclusion, both IR and Raman spectroscopy study demonstrate the effect of copolymerization on the better conjugation of PyPBI random copolymers with increasing para content in the copolymer chain.
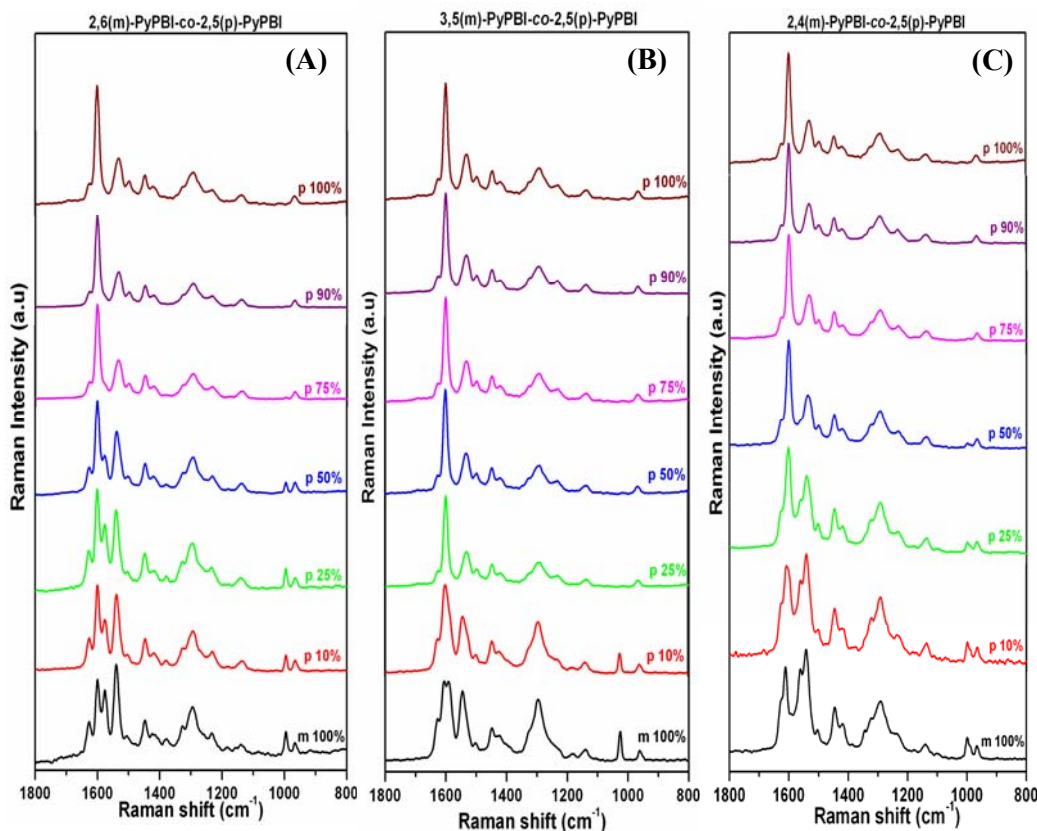
Figure 3.5. *Raman spectra of (A) 2,6(m)-PyPBI-co-2,5(p)-PyPBI (B) 3,5(m)-PyPBI-co-2,5(p)-PyPBI (C) 2,4(m)-PyPBI-co-2,5(p)-PyPBI random copolymers. Para contents are indicated in the figure.*
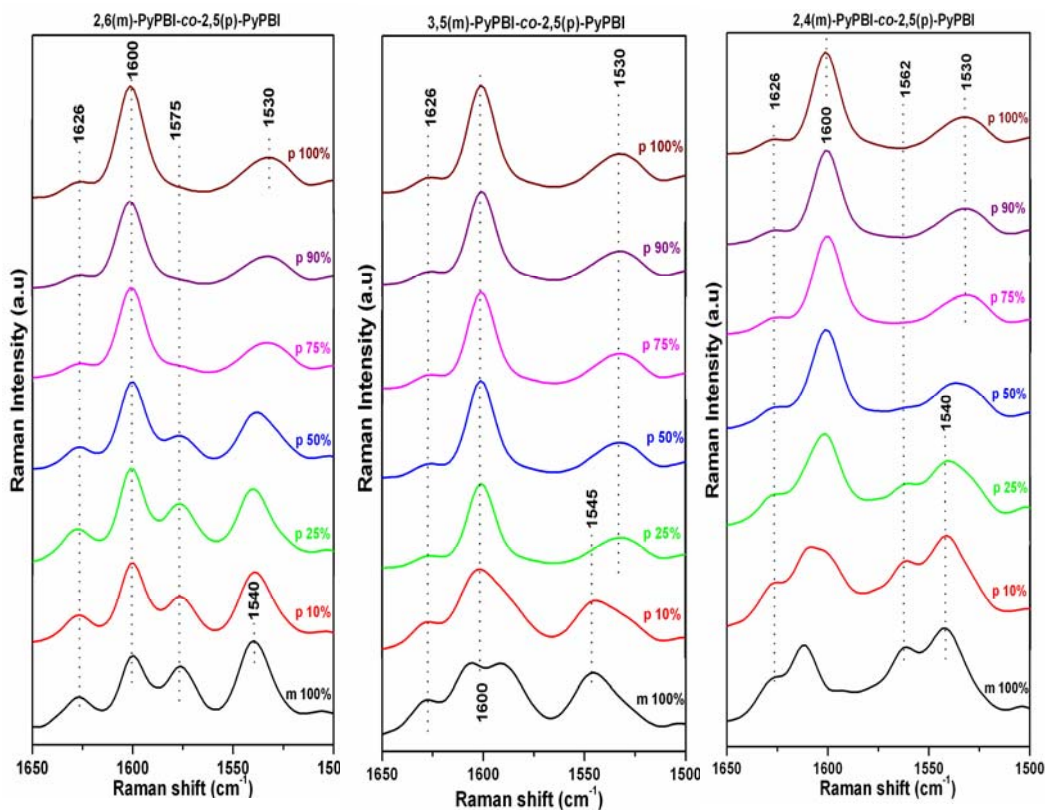
Figure 3.6. *Raman spectra (1650-1500 cm^{-1}) of all the three sets of random copolymers. The para content of the copolymers are shown in the figures. The important bands are indicated using dotted lines.*

3.3.3. NMR Studies and Monomer Reactivity Ratio. FT-IR and Raman spectroscopy studies described in the previous section, show the isomeric effect of PDA monomers on the copolymerization and used for the qualitative prediction of the structure of the copolymers.^{1}H NMR is very efficient and rapid method, and has been extensively used in the past to determine the micro structure of the copolymer and the copolymers compositions very precisely. ^{1}H NMR spectra of all the samples were recorded in Bruker AV 400 MHz NMR spectrometer in DMSO-d_6 solvent. The proton NMR spectra of all the PyPBI homopolymers are shown in Figure 3.7 along with their structure and the peak assignments. Figure 3.8 represents the NMR spectra of all the copolymer

samples of 3,5(m)-PyPBI-*co*-2,5(p)-PyPBI random copolymers. The NMR spectra of other two sets of copolymers [2,6(m)-PyPBI-*co*-2,5(p)-PyPBI and 2,4(m)-PyPBI-*co*-2,5(p)-PyPBI] are presented in Figure 3.9 and 3.10 respectively. The peak assignments as shown in the figures are in good agreement with the anticipated chemical structure. The ^{1}H NMR spectra of PyPBI homopolymers are quite different owing to their different chemical environment (Figure 3.7). Especially the imidazole and pyridine protons chemical shifts display significant differences among the PyPBI homopolymers (Figure 3.7). The imidazole protons signals for 3,5(m)-PyPBI-*co*-2,5(p)-PyPBI denoted as H_g and H_n for the meta and para positions of the chain, are observed at around 13.60 and 13.30 ppm respectively (Figure 3.8). The downfield shift of the H_g imidazole proton from the H_n proton is because of the different chemical environment of the 3,5 meta structure compare to the 2,5 para structure. The peaks denoted by H_h (9.45) and H_i at (9.36) are for the 3,5 meta structure (3,5 PDA). The para (2,5 PDA) structure has distinguishable peak at 9.59 , 8.75 and 8.35 ppm, denoted by H_q, H_p and H_o, respectively. The intensity of the characteristic meta signals (H_g, H_h and H_i) are decreasing and para responsive signals (H_n, H_q, H_p and H_o) are increasing with increasing para content in the polymer chain (Figure 3.8). Similar kinds of observations are noted from the figures 3.9 and 3.10 for other two sets of PyPBI random copolymers. 2,6(m)-PyPBI-*co*-2,5(p)-PyPBI copolymers do not show any splitting of imidazole protons, instead we observed a broad imidazole signals because both –NH signal appear almost in the same region (13.28 and 13.30 ppm; Figure 3.7 and Figure 3.9). The other proton signals (H_q, H_p and H_o) for the para structure of this pair decreases with increasing meta content in the polymer chain. The imidazole protons signals in case of 2,4(m)-PyPBI-*co*-2,5(p)-PyPBI copolymers are splitted, denoted by Hj and Hn (Figure 3.10). Similar to previous two sets of copolymers in this case also proton signals (H_k, H_l, H_m) for meta decreases with increasing para content in the polymer chain as shown in Figure 3.10. These above observations from the ^{1}H NMR results demonstrated that in all the cases successful copolymerization have taken place and these NMR data can be utilized to determine the ratio of meta and para mol fraction in the copolymer samples.
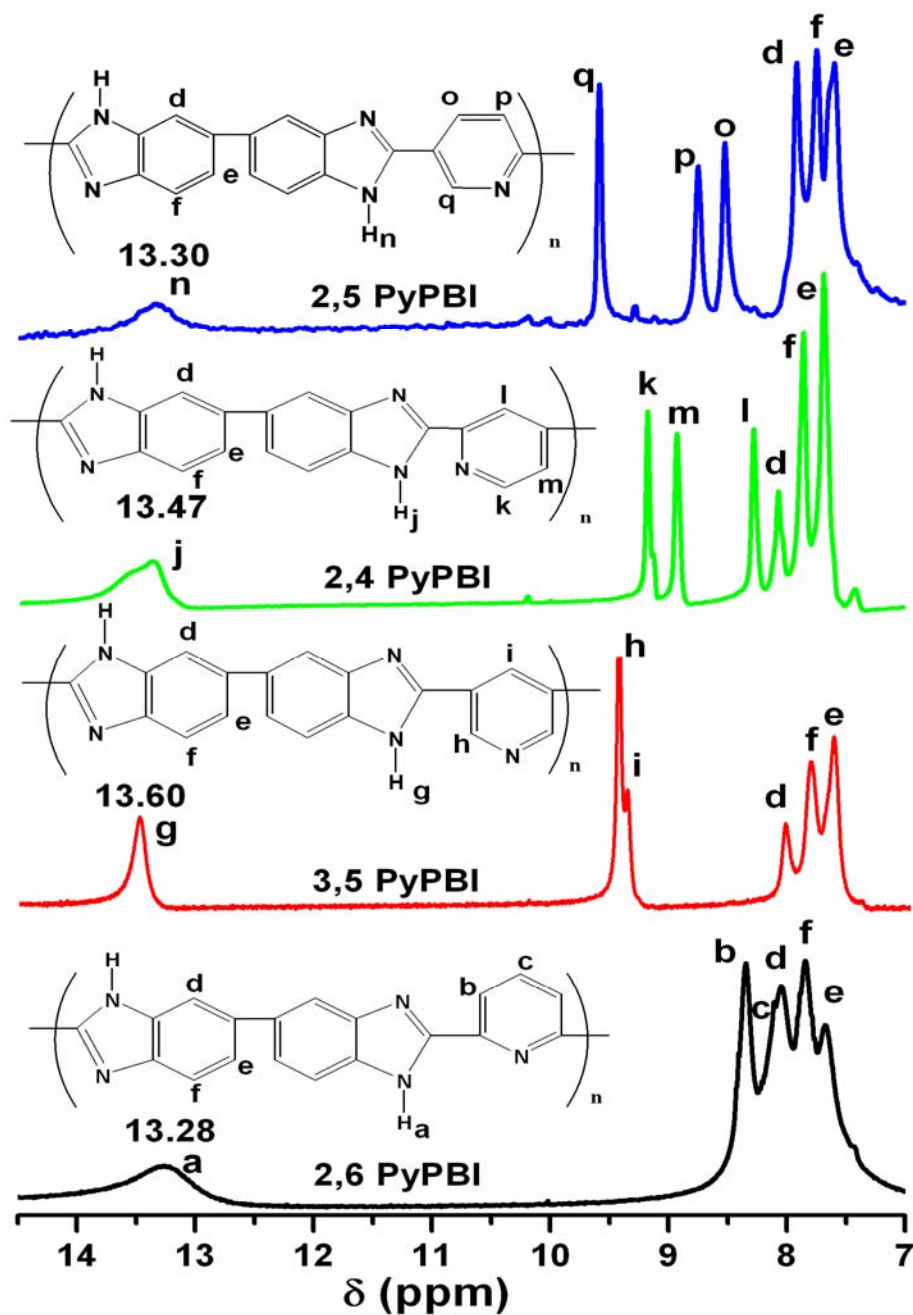
Figure 3.7. *Proton NMR spectra of all PyPBI homo polymers recorded in DMSO-d$_6$ solvent. The chemical structure and the peak assignments are also shown in the picture.*
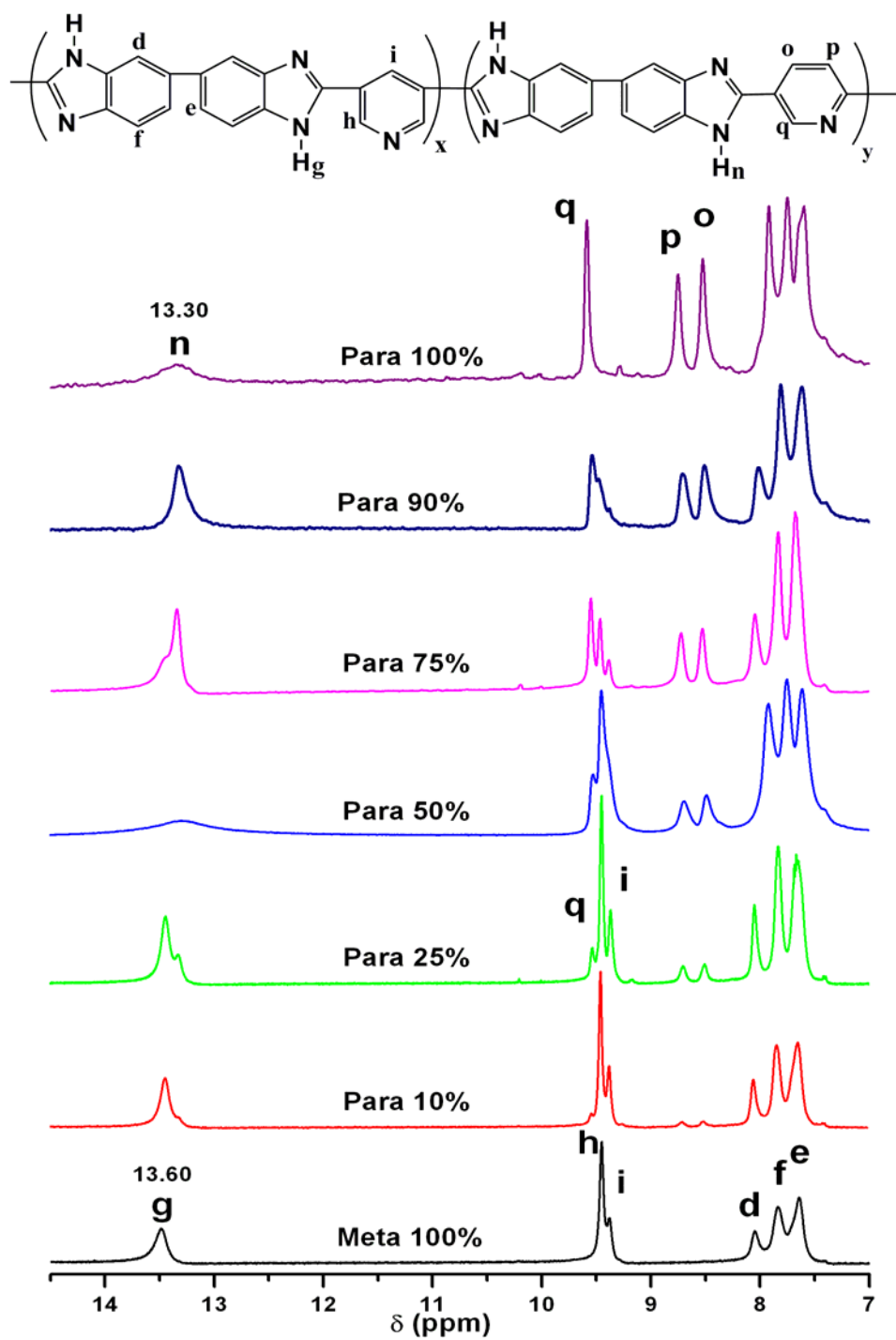
Figure 3.8. *The chemical structure, proton NMR spectra of all the 3,5(m)-PyPBI-co-2,5(p)-PyPBI copolymer and their peak assignments.*
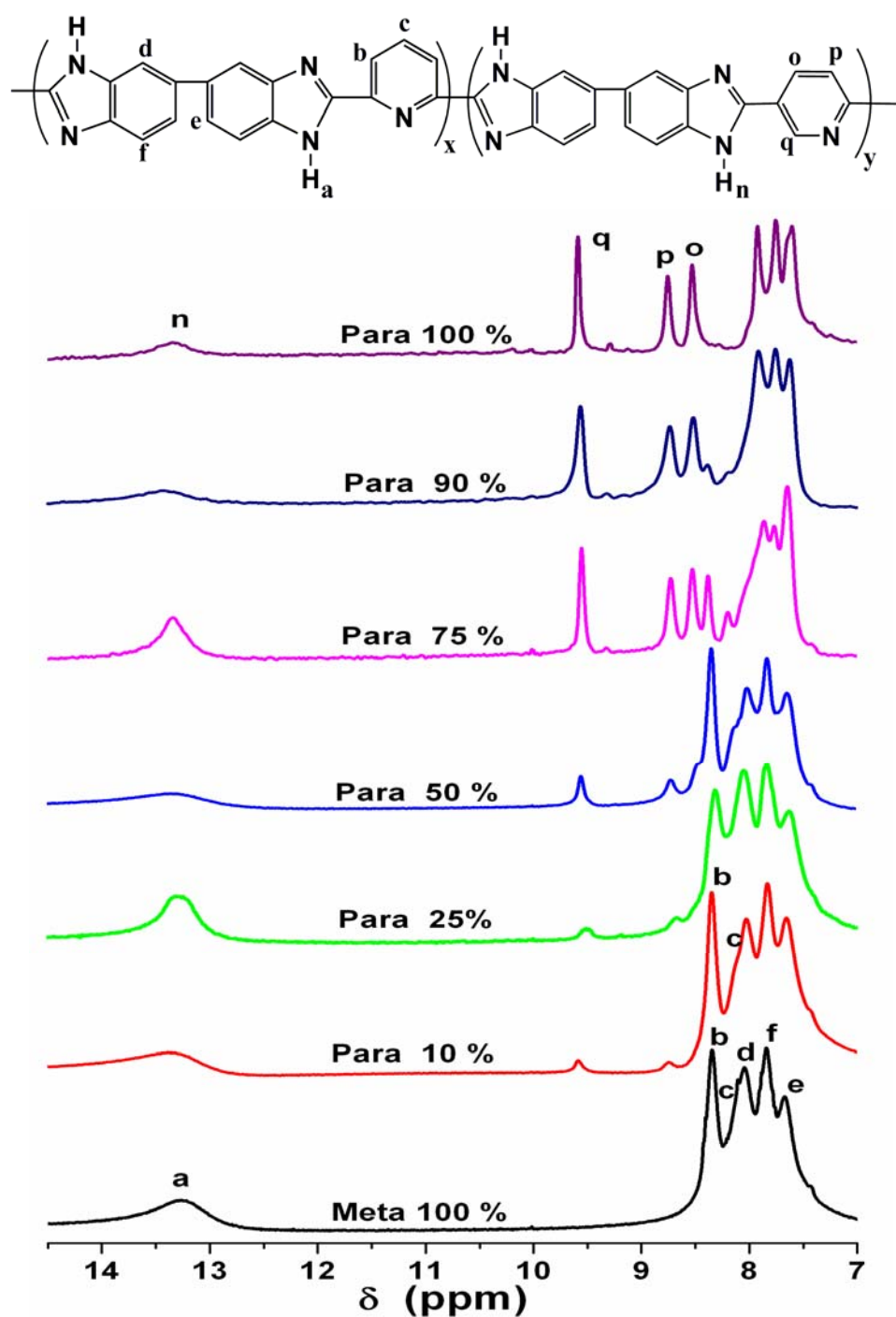
Figure 3.9. *The chemical structure, proton NMR spectra of all the 2,6(m)-PyPBI-co-2,5(p)-PyPBI random copolymers and their peak assignments.*
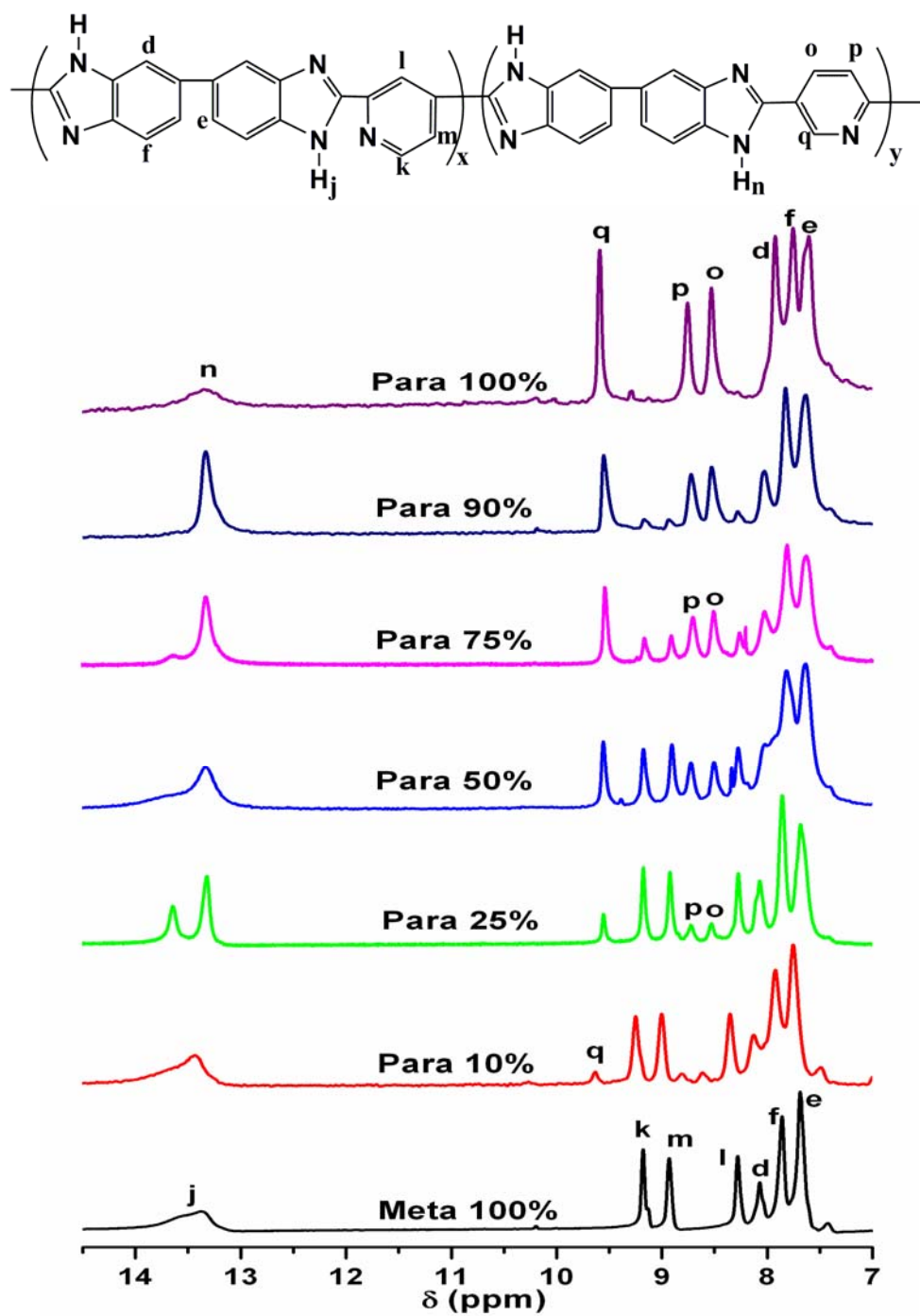
Figure 3.10. *The chemical structure, proton NMR spectra of all the 2,4(m)-PyPBI-co-2,5(p)-PyPBI random copolymers and their peak assignments.*

We have calculated the % of para mol fraction in the copolymers from the integral ratio of the distinguishable proton peaks from the NMR spectrum using equation 3.2 to 3.4 for the three sets of copolymer and the results are shown in the Table 3.2.

Para mol fraction (%) for 2,6(m)-PyPBI -*co*-2,5(p)-PyPBI

$$= \frac{H_q + H_p + H_o}{H_b + H_c + H_q + H_p + H_o} \times 100 \qquad (3.2)$$

Para mol fraction (%) for 3,5(m)-PyPBI -*co*-2,5(p)-PyPBI

$$= \frac{H_n + H_q + H_p + H_o}{H_g + H_n + H_q + H_p + H_o + H_h + H_i} \times 100 \qquad (3.3)$$

Para mol fraction (%) for 2,4(m)-PyPBI -*co*-2,5(p)-PyPBI

$$= \frac{H_n + H_q + H_p + H_o}{H_j + H_n + H_q + H_p + H_o + H_k + H_m + H_l} \times 100 \qquad (3.4)$$

The para content in all the three sets of PyPBI random copolymers shown in the Table 3.2 suggests the successful incorporation of meta and para components in the copolymer chains and the values are in good aggrement with the monomer feed ratio taken in the initial reaction mixtures. Hence, it is apparent that the meta and para composition in the copolymer chains can be readily tuned by changing the molar feed ratio of meta and para monomers in the starting of the polymerization. However, a critical observation of the Table 3.2 data brings our attention to a moderate deviation in the para composition from the monomer feed, in particular for lower para content copolymer. In addition it is worth noting that the deviation in the para composition from the monomer feed (or anticipated composition) is not similar in all the three sets of copolymer despite the fact that in all the cases 2,5 PDA has been used as a para structure. These observations are quite unusual since in case of step polymerization, reactions are carried out close to 100

% conversion for the synthesis of high molecular weight polymers. Also, step polymerizations are equilibrium reactions and in which reactivity of the functional groups are independent of chain length to which it is attached. Earlier few studies on copolycondensation showed the deviation in composition.[23, 63, 64] In our previous studies we have observed the similar behavior in case of meta-PBI-*co*-para-PBI. This deviation may be noticed due to the differences in monomer reactivates which in turn depend upon various structural factors like proximities of the functional groups and the solubility of the corresponding monomer. This suggests that probably the rates of the reactions of the monomers are not alike and hence the reactivity ratios of the monomers are different. Therefore, the deviation from the feed depends upon the structures of the monomers and this argument made it necessary for us to determine the reactivity ratios of the comonomers.

Table 3.2. *Comparison of expected para content of the copolymers based on 2,5 PDA feed in the reaction with measured para content calculated from proton NMR.*

Feed 2,5PDA (Para)(mol %)	Found Para content (mol %)		
	2,6(m)-PyPBI -co- 2,5(p)-PyPBI	3,5(m)-PyPBI -co-2,5(p)-PyPBI	2,4(m)-PyPBI -co-2,5(p)-PyPBI
0	0	0	0
10	23.07	15.38	12.90
25	33.30	29.03	31.42
50	47.36	53.84	50.84
75	79.41	73.80	74.35
90	93.10	87.87	88.57
100	100	100	100

A simple kinetic scheme for co-polymerization is used to discuss the rates of the reactions of the monomers.[23] The M_1 and M_2 represent the para (2,5 PDA) and meta (2,6; 3,5; 2,4 PDAs) dibasic acid monomers, respectively. The asterisk in the prefix indicates the growing polymer chain. The four possible reaction sequences are following:
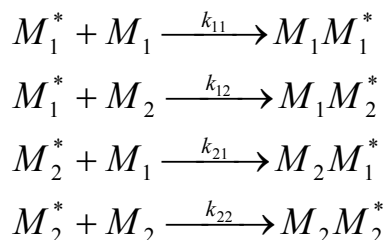
$$M_1^* + M_1 \xrightarrow{k_{11}} M_1 M_1^*$$

$$M_1^* + M_2 \xrightarrow{k_{12}} M_1 M_2^*$$

$$M_2^* + M_1 \xrightarrow{k_{21}} M_2 M_1^*$$

$$M_2^* + M_2 \xrightarrow{k_{22}} M_2 M_2^*$$

The rate constants of the respective reactions are denoted by 'k' with appropriate sign in the suffix. We have calculated the reactivity ratio of three sets of PyPBI copolymers by applying Fineman-Ross[65] using the proton NMR data.

$$\frac{f_1(F_1 - F_2)}{f_2 F_1} = \frac{F_2}{F_1}\left(\frac{f_1^2}{f_2^2}\right)r_1 - r_2 \qquad\qquad (3.5)$$

where f_1 and f_2 are the para and meta monomer mol fraction in the feed of the copolymerization, respectively. F_1 and F_2 are the instantaneous monomer mol fraction in the copolymer. A plot (Figure 3.11) of equation (3.5) results a straight line with slope equal to r_1 and intercept equal to $- r_2$, where r_1 (k_{11}/k_{12}) and r_2 (k_{22}/k_{21}) are the reactivity ratios of the monomer para (2,5 PDA) and, meta (2,4 ; 2,6 and 3,5 PDA), respectively. Table 3.3 lists reactivity ratios values calculated by using equation (3.5) for all the three sets of PyPBI copolymer. Figure 3.11 represents the Fineman-Ross plot

for all the three sets of copolymers [2,6(m)-PyPBI-*co*-2,5(p)-PyPBI; 3,5(m)-PyPBI-*co*-2,5(p)-PyPBI; 2,4(m)-PyPBI-*co*-2,5(p)-PyPBI]. Table 3.3 data clearly indicates that in all the three cases the reactivity ratio (r_1) of para monomer (2,5 PDA) is higher than the reactivity ratio (r_2) of its meta counter parts. This attributes that the reactivity of para monomer is higher than the meta monomers. The higher reactivity is due to lower solubility of para in the PPA medium and hence we obtained higher molecular weight polymers (Figure 3.1) with increasing para content in the polymer backbone. The higher reactivity of para explains the positive deviation from the feed of the monomer (Table 3.2). It is also interesting to note that the vales of the reactivity ratios (r_1 / r_2) for three sets are not similar. In Table 3.2, also we have observed the similar behavior, where the deviations of the copolymer composition from the feed are not similar; instead it depends on the monomer pairs. Therefore, these results attributes to the fact that the reactivity of para monomer (2,5 PDA) depends upon not only by its low solubility in the polymerization medium (PPA medium) but it also can be tuned by choosing appropriate counter part.

Table 3.3. *Reactivity ratio values calculated from Fineman-Ross method. r_1 and r_2 are the reactivity ratio for para (2,5 PDA) and meta (2,6; 3,5; 2,4 PDAs), respectively.*

	r_1	r_2	r_1/r_2
2,6(m)-PyPBI- *co*-2,5(p)-PyPBI	1.084	0.626	1.73
3,5(m)-PyPBI- *co*-2,5(p)-PyPBI	0.779	0.593	1.31
2,4(m)-PyPBI- *co*-2,5(p)-PyPBI	2.02	1.13	1.79
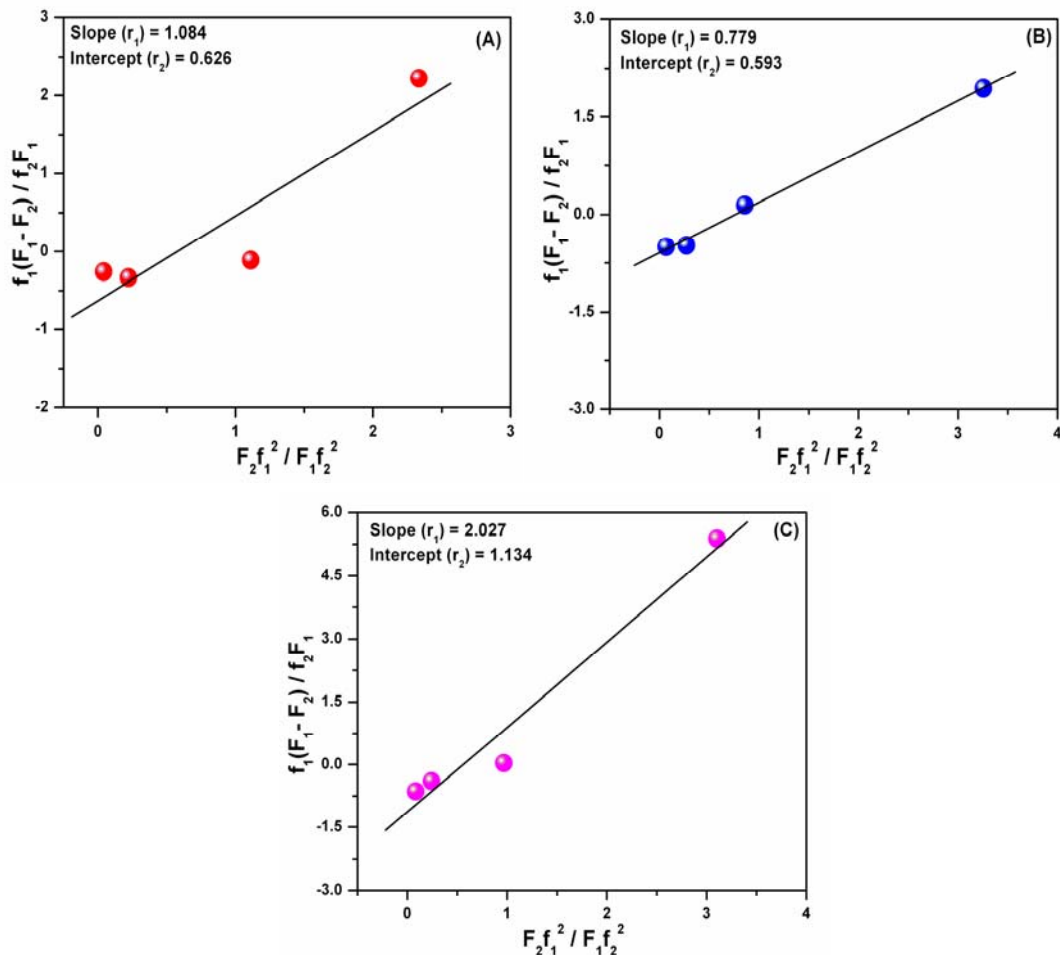
Figure 3.11. *Fineman-Ross plot for calculating reactivity ratios of monomers of (A) (2,5 PDA and 2,6 PDA) in case of 2,6(m)-PyPBI-co-2,5(p)-PyPBI copolymer (B) (2,5 PDA and 3,5 PDA) in case of 3,5(m)-PyPBI-co-2,5(p)-PyPBI copolymer (C) (2,5 PDA and 2,4 PDA) in case of 2,4(m)-PyPBI-co-2,5(p)-PyPBI copolymer.*

3.3.4. Thermal Stability Study. The remarkably high thermal stability owing to the rigidity of PBI types polymers are well known and have been addressed by many authors in the literature.[11, 13, 23, 32, 38] In chapter 2, we have shown that the thermal

stability of m-PBI-*co*-p-PBI enhances significantly with increasing para content in the copolymer. The TGA studies of all the PyPBI copolymer samples are performed under nitrogen atmosphere at a heating rate of 10°C / minute. TGA curves of all homo PyPBI copolymers are shown in the Figure 3.12 and the thermal stability data obtained from the Figure 3.12 for all the homopolymers are presented in the Table 3.4. Two distinct weight losses are observed: initial weight loss at around $100 - 120^{o}$C and the second weight loss at around $520 - 540^{o}$C. The initial weight loss is due to the loss of loosely bound absorbed water molecule. Despite of exhaustive drying in vacuum oven at 100°C, PBI types of polymers can absorb ~ 5 % (by weight) moisture very easily from the atmosphere during the sample handling time due to hygroscopic in nature. The presence of absorbed moisture also confirmed from O-H frequency seen in the IR spectra (Figure 3.2).[59] The degradation of the polymer backbone is seen at ~520-540°C. Figure 3.12 and Table 3.4 data suggest that <10% weight loss is observed at 520°C, indicating the very high thermal stability of these polymers. TGA curves and Table 3.4 data clearly suggest that the thermal stability of these homopolymers depends upon the isomeric structure of PDA. It must be noted that 2,5 PDA (the para structure) shows the highest thermal stability among the four. TGA curves of few representative samples of 2,6(m)-PyPBI-*co*-2,5(p)-PyPBI copolymer are shown in Figure 3.13. The TGA curves for other two sets of copolymers, 2,4(m)-PyPBI-*co*-2,5(p)-PyPBI and 3,5(m)-PyPBI-*co*-2,5(p)-PyPBI are presented in Figure 3.14 and 3.15, respectively. Table 3.5 and 3.6 represent thermal stability data of PyPBI copolymers. From all these TGA curves, Table 3.5 and 3.6 data, it is very much clear that the thermal stability of the copolymer increases with increasing para content. Hence, we can conclude that the introduction of para pyridine linkage in the polymer backbone significantly influences and enhances the thermal stability of the PyPBI random copolymers. Another important observation must be noted that the thermal stability behavior of these copolymers depends on the monomer pairs, for example the temperature at which the 10% weight loss is observed for the 50% para content sample in case of 2,6(m)-PyPBI-*co*-2,5(p)-PyPBI copolymer is 650°C (Table 3.5) where as the same is 595°C (Table 3.6) in case of 2,4(m)-PyPBI-*co*-2,5(p)-

PyPBI copolymer. Hence the isomeric structure of PDA monomers influences the thermal stabilities of PyPBI copolymers.
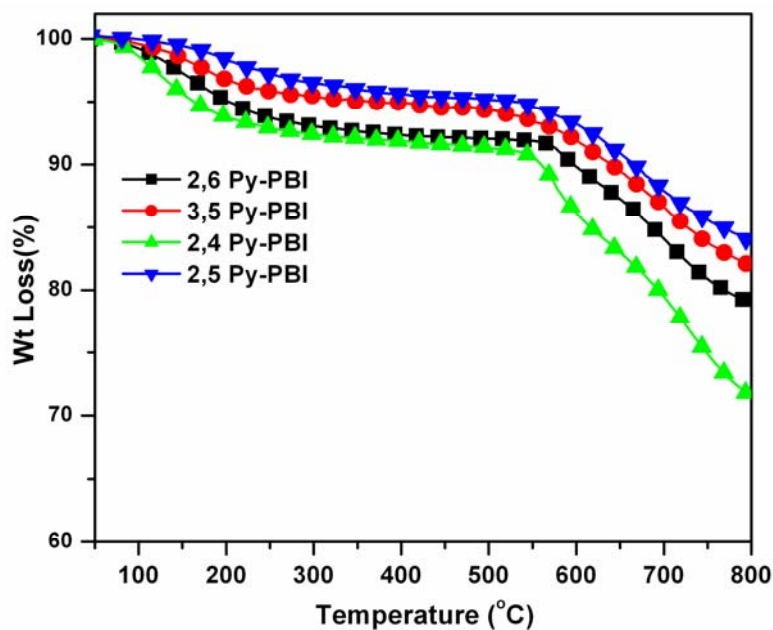
Figure 3.12. *TGA curves of the PyPBI homopolymers.*

Table 3.4. *Thermal stability data of all PyPBI homo polymers.*

Homopolymer	W_{520} (%) [a]	T_{10} % (°C) [b]	W_{750} (%) [c]
2,5 PyPBI	95.25	668	85.62
3,5 PyPBI	94.16	641	83.75
2,6 PyPBI	92.16	596	80.96
2,4 PyPBI	91.25	560	75.06

[a] Residual weight percent at 520°C, [b] Temperature at which the 10 % weight loss is observed and [c] Residual weight percent at 750°C.
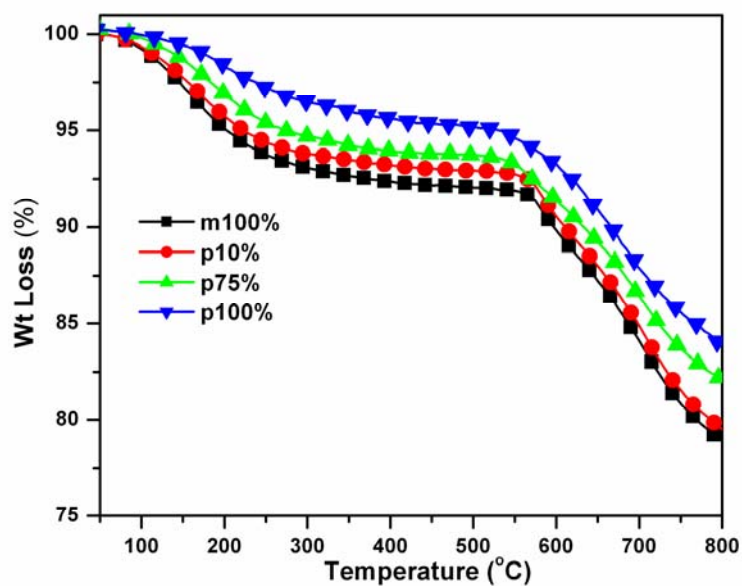
Figure 3.13. *TGA curves of the 2,6(m)-PyPBI-co-2,5(p)-PyPBI random copolymers. Para content (mol %) of the polymer is indicated in the figure.*

Table 3.5. *Thermal stability data of 2,6(m)-co-2,5(p) PyPBI polymers.*

Para Content (mol %)	W_{520^oC} $(\%)^a$	$T_{10\%}$ $(^oC)^b$	W_{750^oC} $(\%)^c$
m 100%	92. 09	596	80.96
p 10%	92.87	609	81.59
p 25%	91.21	608	76.93
p 50%	95.02	650	83.14
p 75%	93.65	632	83.81
p 90%	92.98	632	84.03
p 100%	95.25	668	85.62

[a] Residual weight percent at 520°C, [b] Temperature at which the 10 % weight loss is observed and [c] Residual weight percent at 750°C.
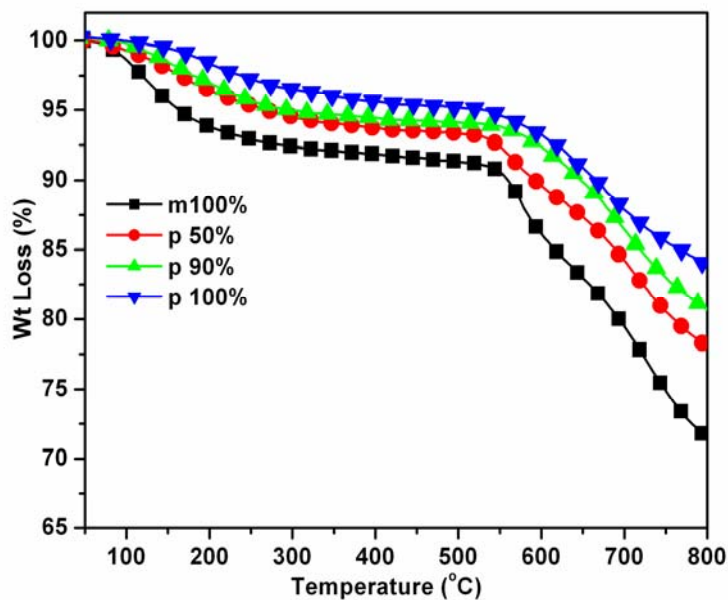
Figure 3.14. *TGA curves of the 2,4(m)-PyPBI-co-2,5(p)-PyPBI random copolymers. Para content (mol %) of the polymer is indicated in the figure.*

Table 3.6. *Thermal stability data of 2,4(m)-co-2,5(p) PyPBI polymers.*

Para Content (mol %)	$W_{520}^{o}C$ $(\%)^{a}$	$T_{10\%}$ $(^{o}C)^{b}$	$W_{750}^{o}C$ $(\%)^{c}$
m 100%	91.25	560	75.06
p 10%	92.73	581	77.63
p 25%	93.25	596	79.70
p 50%	93.25	595	80.48
p 75%	95.19	654	83.94
p 90%	94.15	645	83.07
p 100%	95.25	668	85.62

[a] Residual weight percent at 520°C, [b] Temperature at which the 10 % weight loss is observed and [c] Residual weight percent at 750°C.
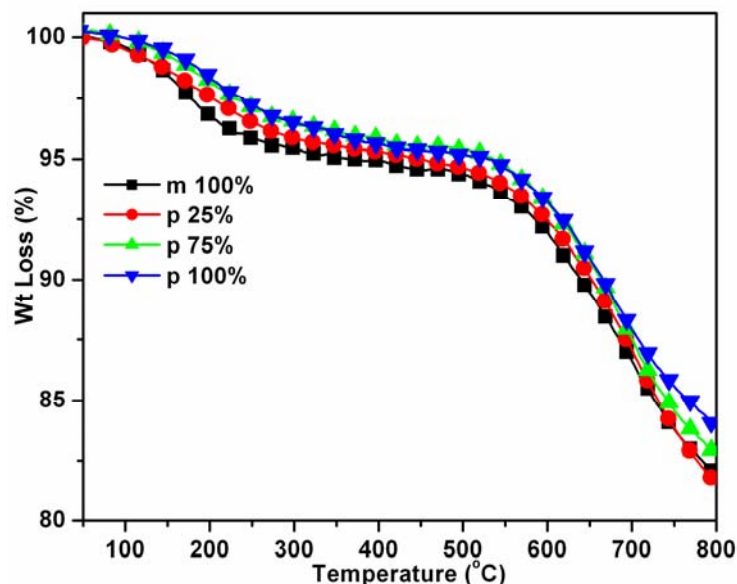
Figure 3.15. *TGA curves of the 3,5(m)-PyPBI-co-2,5(p)-PyPBI random copolymers. Para content (mol %) of the polymer is indicated in the figure.*

3.3.5. Glass Transition Temperatures (T_g) of Copolymers. The thermomechanical properties of all the pyridine homo and copolymers are studied by using a dynamical mechanical analyzer (DMA). The glass transition temperatures (T_g) of all the PyPBI homo and copolymers are obtained from the DMA study. The temperature at which the maximum in loss modulus and tan δ plot is observed that corresponds to the glass transition temperature (T_g). All the samples films are scanned in DMA from 150ºC to 500ºC at a heating rate of 5ºC /min. The storage modulus (E'), loss modulus (E") and tan δ values are measured at a constant frequency of 5 Hz with a preload force of 0.01N. We have carried out the DMA heating scan after the annealing the samples (films) at 150ºC for 30 minutes. Earlier studies on PBI blend system showed that the first DMA heating run results a complicated structure because of the involvement of various processes such as removal of residual solvent, the glass transitions and the phase separation.[66] Also, it is proved from the I.R and TGA studies that the PBI is very hygroscopic in nature and can easily absorb ~ 5 % (by weight) moisture from the atmosphere. The absorbed moisture may affect the mechanical properties and hence the

glass transition temperature. Therefore, we have annealed the samples at 150°C prior to the heating scan and we obtained reproducible T_g from the DMA study for all the samples. The temperature dependent plot of tanδ and loss modulus (E″) for PyPBI homopolymers, 2,6(m)-PyPBI-co-2,5(p)-PyPBI, 3,5(m)-PyPBI-co-2,5(p)-PyPBI and 2,4(m)-PyPBI-co-2,5(p)-PyPBI copolymers are presented in Figures 3.16, 3.17, 3.18 and 3.19 respectively. In all the cases, the T_g obtained from loss modulus plot is somewhat lower than tan δ plot. Earlier several author reported similar type difference in T_g from the two plots for various polymer system. In our discussion we will be dealing with the T_g s obtained from tan δ plots. However, it must be noted that the nature of variation of T_g from sample to sample in the copolymers are identical for both tan δ and E″ plots. The tan δ plots of PyPBI homopolymers (Figure 3.16) show that the glass transition temperature (T_g) of the 2,6(m)PyPBI, 2,4(m)PyPBI, 3,5(m)PyPBI, and 2,5(p)PyPBI homopolymers are 408, 401, 387 and 360°C, respectively. Typically PBI polymer shows very high T_g (>350°C).[13, 31, 38] So our values are in agreement with the reported values. To our knowledge until now no efforts have been made to measure the T_g of the PyPBI homopolymers. The above T_g values have two important implications: the T_g of the para structure PyPBI (2,5 Py-PBI) is significantly lower (~ 40°C) than all meta structure PyPBI (2,6; 3,5 and 2,4 PyPBI) and the T_g of PyPBI not only depends upon the meta-para structure but it also varies depending upon the position of carboxylic acid in the pyridine ring (isomeric effect). The lower T_g value attributes that the para structure PyPBI backbone is more flexible than the meta structure PyPBI. Our IR and Raman studies (described in the previous section) suggest the presence of better conjugation between the imidazole rings and para pyridine linkage in case of para PyPBI. Also, para structure PBI has symmetrical backbone. The flexibility and symmetrical nature of the 2,5 PyPBI (para) homopolymer increases the segmental mobility of the chain and hence para structure shows lower T_g compare to the meta structure.[67] Among the meta structure PyPBI homopolymer, the T_g of 3,5 PyPBI is lower (387°C) compare to 2,6 and 2,4 PyPBI (408 and 401°C). This is due to the position of carboxylic acid group in the pyridine moiety. The better symmetrical nature

of 3,5 PyPBI than other two meta PyPBI is responsible for lower T_g of former compare to other two meta PyPBIs.
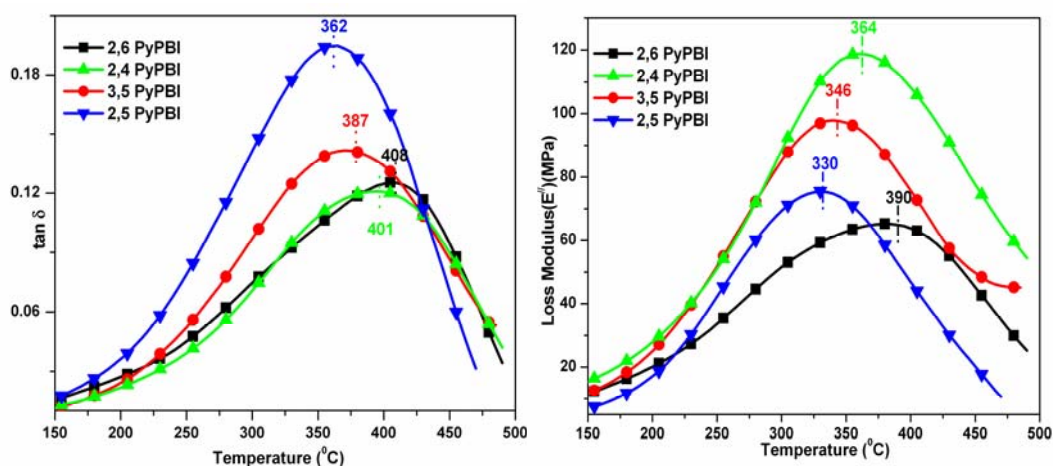
Figure 3.16. *DMA plots (tan δ and E″ against temperature) of PyPBI homopolymers. The vertical dotted lines shown in the plots represent the glass transition temperatures.*
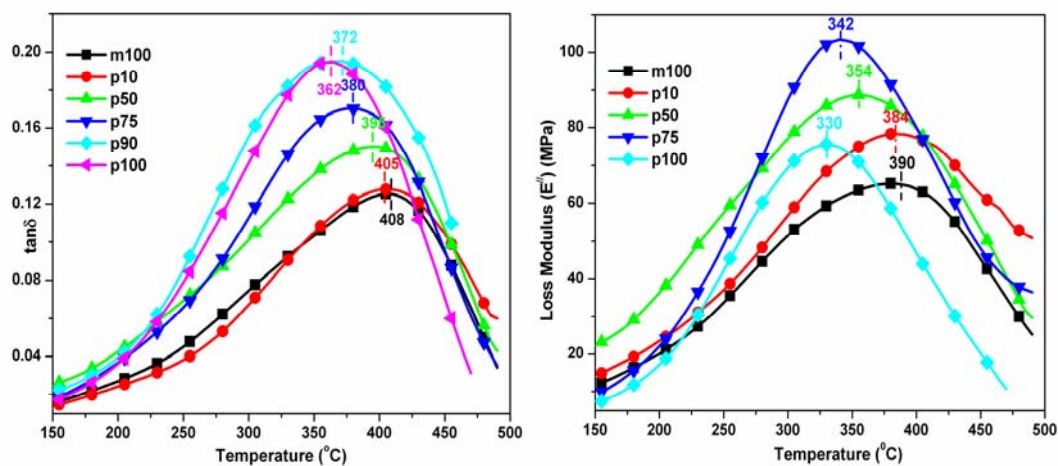
Figure 3.17. *DMA plots (tan δ and E″ against temperature) of 2,6(m)-PyPBI-co-2,5(p)-PyPBI copolymers. The T_gs are shown in the figure by vertical dotted lines.*
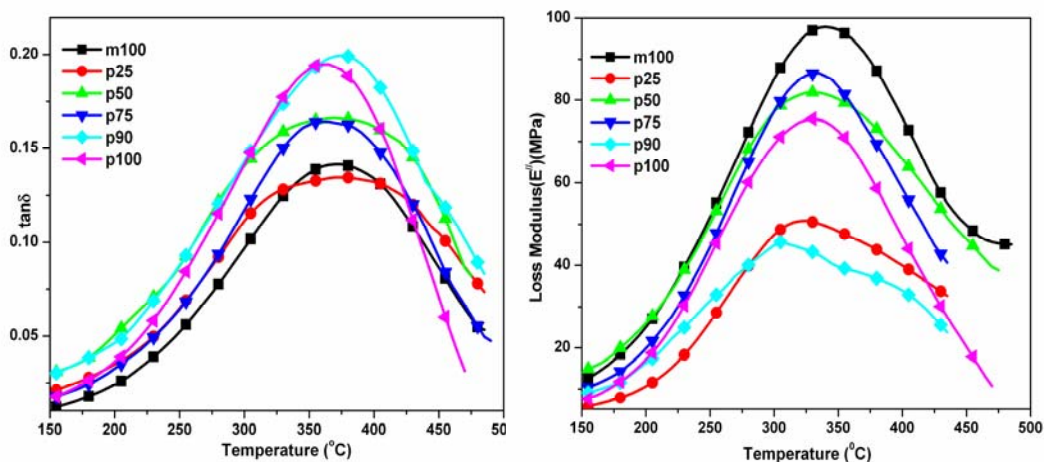
Figure 3.18. *DMA plots (tan δ and E'' against temperature) of 3,5(m)-PyPBI-co-2,5(p)-PyPBI copolymers.*
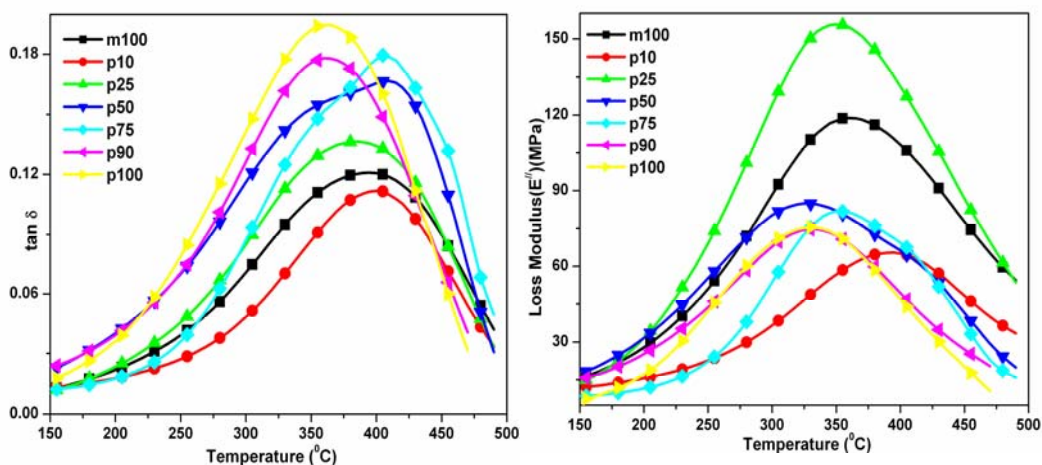
Figure 3.19. *DMA plots (tan δ and E'' against temperature) of 2,4(m)-PyPBI-co-2,5(p)-PyPBI copolymers.*

All the DMA plots of PyPBI copolymers (Figures 3.17, 3.18 and 3.19) exhibit a single T_g, indicating the randomness of the copolymer backbone. In all the three sets of copolymer, the T_g decreases with increasing para content as expected from their representative values for homopolymers. It is interesting to note that the T_g values of copolymers are highly dependent on the structure of the monomer pairs. Figure 3.20

shows a comparison of T_g value for 50% para content copolymer of three different sets. Hence the T_g is controlled not only by the meta –para combination structure but also tuned by the different isomeric structure of meta PDAs.
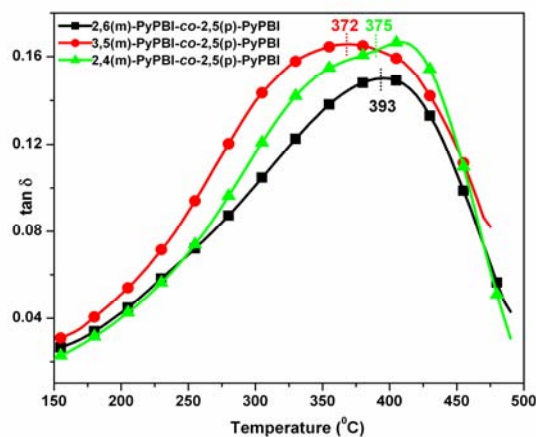
Figure 3.20. *Comparison of T_g s of 50% para content sample of three different copolymers obtained from the tan δ vs temperature plot.*

The variations of copolymers T_g s with para content (mol %) for three sets of copolymers are presented in Figure 3.21. The expected T_g of the random copolymers are estimated by the Fox equation (Equation 3.6) as follows:

$$\frac{1}{T_g} = \frac{w_1}{T_{g_1}} + \frac{w_2}{T_{g_2}} \qquad (3.6)$$

where w_1 and w_2 are the weight fractions and T_{g_1} and T_{g_2} are the glass transition temperatures of the two homopolymers. Figure 3.21 shows that the experimental T_g values obtained from the DMA measurements (solid line) are deviated from the calculated values obtained from the Fox equation (dotted line). Positive deviation obtained from the linear additive rule in case of 2,6(m)-PyPBI-*co*-2,5(p)-PyPBI whereas other two sets copolymers exhibit the negative deviation from the Fox equation (Figure 3.21). The positive deviation in case of 2,6(m)-PyPBI-*co*-2,5(p) PyPBI from linear additive rule could be due to the less symmetrical structure of polymer backbone arising because of 2,6 PDA which pushes two polymer chains away from each other owing to

the interchain steric hindrance. Infact the higher T_g is shown by the 2,6 PyPBI homopolymer also supports this arguments. In other two sets of copolymers the negative deviation are observed due to the fact that in these two cases, the meta component PDAs (2,4 and 3,5) are more symmetrical and has some similarities with 2,5 PDA. The most important observation from the above study is that the dependence of T_g with para content depends upon with whom 2,5 PDA is being partnered. Hence the effect of isomeric structure of PDA on the flexibility of the PyPBI random copolymer is demonstrated.
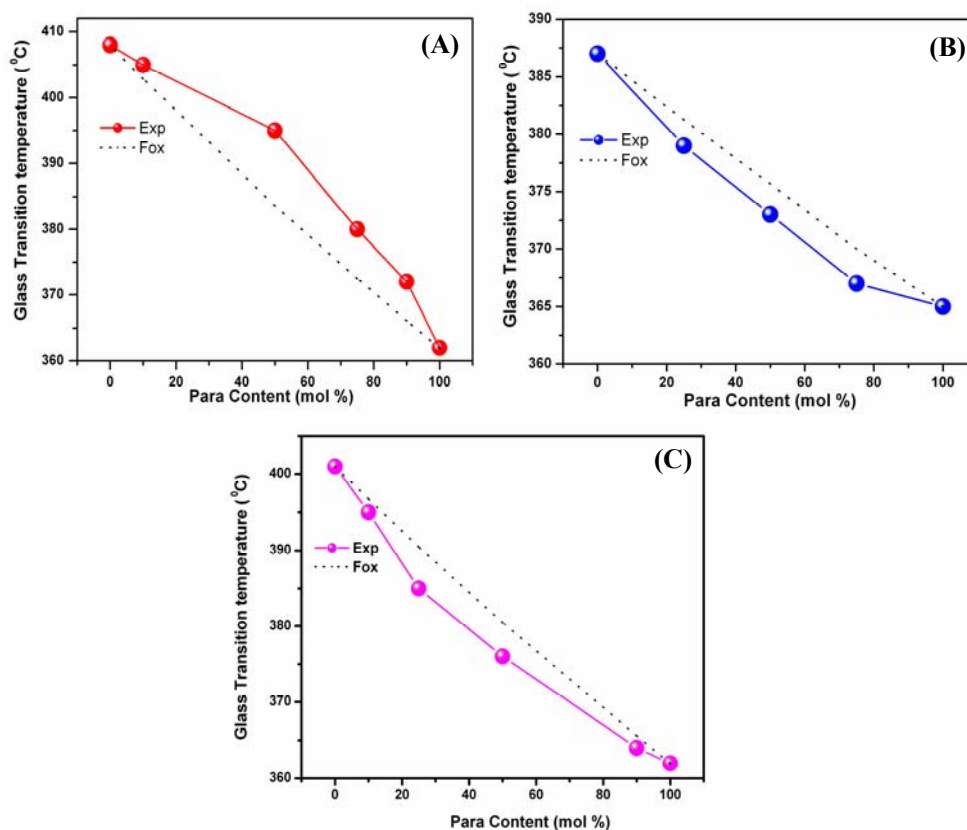
Figure 3.21. *Variation of glass transition temperature (T_g) with para content (mol %) of the PyPBI copolymers. Solid line is experimentally obtained from the tanδ vs temperature plots and dotted line is calculated from the Fox equation. (A) 2,6(m)-PyPBI-co-2,5(p)-PyPBI (B) 3,5(m)-PyPBI-co-2,5(p)-PyPBI (C) 2,4(m)-PyPBI-co-2,5(p)-PyPBI.*

3.3.6. Spectroscopy. The absorption and the fluorescence emission spectra of all the PyPBI homo and copolymers are studied from their dilute solution (2×10^{-5} M) in dimethyl acetamide (DMAc). The concentration is expressed by considering one repeat unit as one mol PyPBI. The absorption spectra of PyPBI homo and three sets of PyPBI copolymers in DMAc are shown in the Figure 3.22. All the polymers exhibit very distinct $\pi \rightarrow \pi^*$ transition peak above 350 nm. The absorbance maximum (λ_{max}) peak positions are presented in the Table 3.7. Figure 3.22 and Table 3.7 exhibit that the λ_{max} for $\pi \rightarrow \pi^*$ transition varies depending on the positions of carboxylic acids in the pyridine ring. Hence the isomeric effect of PDA on the conjugation of the PBI backbone is demonstrated. Table 3.7 data suggests the increasing conjugation order as follows: 2,5 > 2,4 > 2,6 > 3,5 and the λ_{max} of para structure (2,5) is ~ 50 nm higher than the others. This indicates that para is much more conjugated and all others have similar type conjugation. The observation is in good agreement with our other studies. A gradual bathochromic shifts of the $\pi \rightarrow \pi^*$ absorbance maximum observed in all the copolymers (Figure 3.22) with increasing para content in the copolymers. We have noticed a similar observation to our previous work on m-PBI-*co*-p-PBI where the 100% para homopolymer absorbs at ~50nm higher wavelengths than the 100% meta homopolymer (Chapter 2). The introduction of the para linkage into the polymer backbone enhances the conjugation between the imidazole and the pyridine ring which results the above mentioned bathochromic shift of the $\pi \rightarrow \pi^*$ absorption maxima. So our argument about the increased conjugation in the backbone due to the para substitution using IR spectra and Raman studies discussed in the previous sections are in good agreement with the absorption studies.
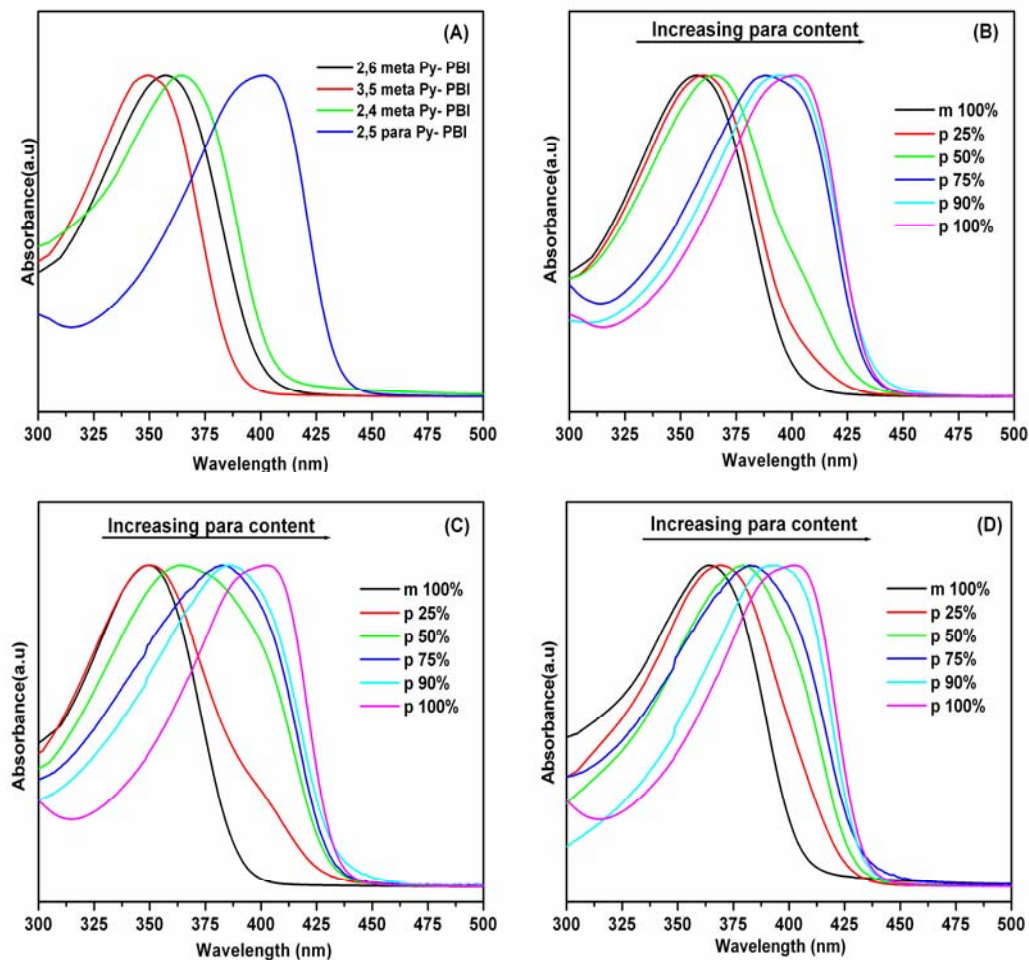
Figure 3.22. *Absorption spectra of the PyPBI homo and copolymers polymers in DMAc solution as recorded with a cuvette of 1 cm path length. Concentrations are 2 × 10^{-5} M. (A) PyPBI homo polymers (B) 2,6(m)-PyPBI-co-2,5(p)-PyPBI (C) 3,5(m)-PyPBI-co-2,5(p)-PyPBI (D) 2,4(m)-PyPBI-co-2,5(p)- PyPBI.*

Table 3.7. *Electronic spectroscopy data of all the Py -PBI copolymers.*

Copolymer	Para Content (mol %)	Absorption (λ_{max}) peak (nm)	Emission peak (nm)
2,6(m)-PyPBI-*co*-2,5(p)-PyPBI	0	355	411,430
	10	360	460
	25	362	460
	50	365	465
	75	390	448,466
	90	395	448,468
	100	400	448,468
3,5(m)-PyPBI-*co*-2,5(p)-PyPBI	0	350	424
	10	348	437
	25	352	464
	50	365	468
	75	382	468
	90	385	469
	100	400	448,468
2,4(m)-PyPBI-*co*-2,5(p)-PyPBI	0	365	450
	10	365	460
	25	370	463
	50	380	465
	75	383	467
	90	395	468
	100	400	448,468

Earlier, it has been shown that all PBI types of heterocyclic polymers exhibit fluorescence emission and various phenomenon of PBI such as aggregation, gelation, conformational transition and sensing of halide ions have been explained by the help of fluorescence spectroscopy.[26-28,33] Therefore, it is very important to understand the photophysical behavior of the PyPBI polymer as we introduced pyridine moiety in the polymer backbone which has potential to act as cationic sensor material. To our knowledge until now no such efforts have been made to study the photo-physical behavior of the PyPBI type polymers. The emission spectra of the PyPBI homo and copolymers recorded in DMAc and are presented in the Figure 3.23. The excitation wavelengths (λ_{exc}) are chosen based on the $\pi \rightarrow \pi^{*}$ absorption maxima shown in the Table 3.7. The concentrations of the solutions are 2×10^{-5} M and kept constant for all the cases. 2,6 PyPBI and 2,5 PyPBI exhibit two fluorescence bands, however other two homopolymers (3,5 and 2,4 PyPBI) show only one fluorescence band with a very broad shoulder at the lower wavelength side which is almost undetectable (Figure 3.23). Earlier, it was shown that PBI has two emission bands in which the lower and longer wavelength bands from the excited $^{1}L_{b}$ state in the benzimidazole ring of PBI are assigned as 0 – 0 and 0 – 1 transition respectively. Table 3.7 and Figure 3.23 indicate that the para structure PyPBI emits at higher wavelength than the meta structure PyPBI. Among the meta structure PyPBI, the 2,4 PyPBI emits towards higher wavelength, indicating that the position of carboxylic acid in the pyridine ring (isomeric effect) control the conjugation in the polymer backbone. All the three types of copolymer pairs the emission bands are shifted gradually to the higher wavelength with increasing para content (Figure 3.23 and Table 3.7). The shifting of the emission bands towards the longer wavelength also supports the conjugation along the polymer backbone due to the introduction of the para pyridine linkages. This observation once again strengthens our previous argument about the better conjugation of higher para content copolymers.
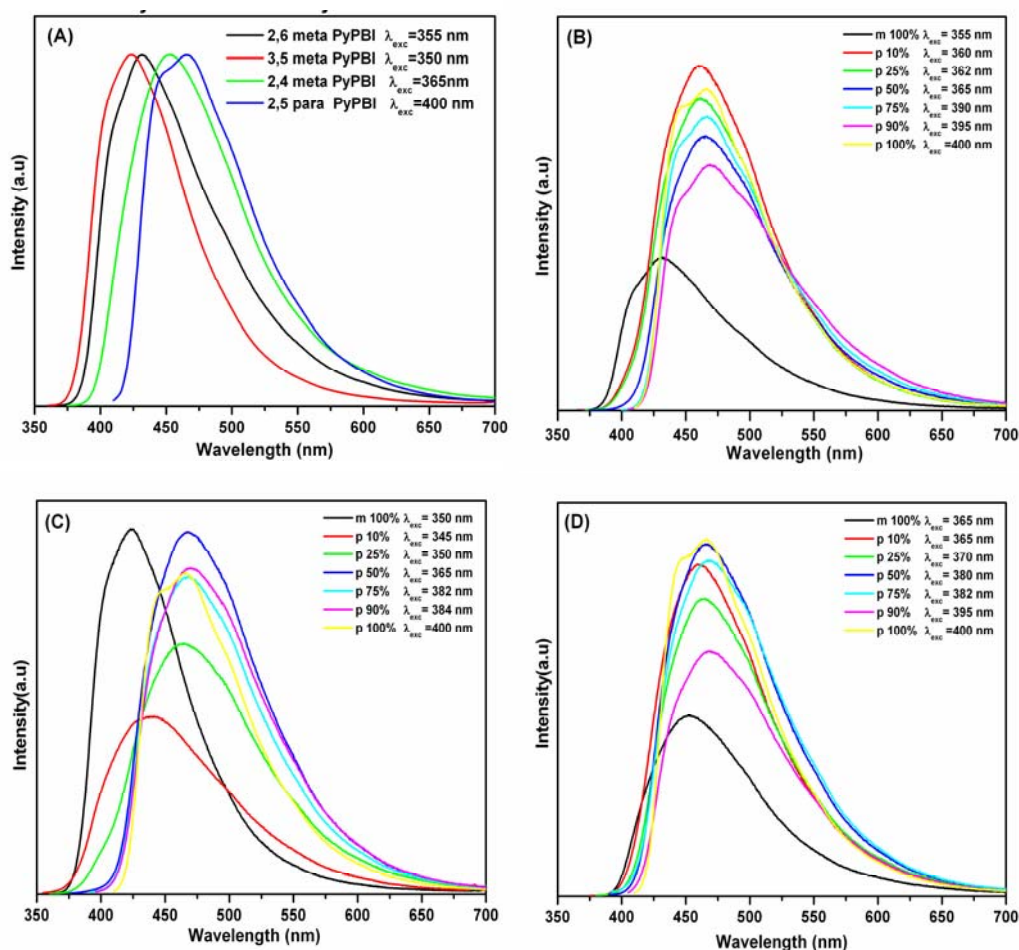
Figure 3.23. *Fluorescence emission spectra of the PyPBI homo and copolymers in DMAc solution. Concentrations are identical to Figure 3.22. Excitation wavelengths (λ_exc) are indicated in the figure. (A) PyPBI homo polymers (B) 2,6(m)-PyPBI-co-2,5(p)-PyPBI (C) 3,5(m)-PyPBI-co-2,5(p)-PyPBI (D) 2,4(m)-PyPBI-co-2,5 (p) PyPBI.*

3.3.7. X – Ray Diffraction. The wide angle X-ray diffraction (WAXS) patterns of all the PyPBI samples homo and copolymer are presented in the Figure 3.24. From the figures, it is evident that all the samples are amorphous in nature. In all the cases two broad peaks at around 13 and 25 2θ (degree) are observed. But, no sharp peak is

observed in any of the cases. The existence of the broad peaks results from a convolution of amorphous and crystalline scattering. Earlier several authors reported similar observation for the PBI type polymers.[23, 37, 38, 46] Therefore; we can conclude that the introduction of the pyridine moiety and para linkage in the polymer backbone does not influence the packing capacity of the polymer chains though it brings more symmetry in the structure. All the polymers studied here are completely non – crystalline.
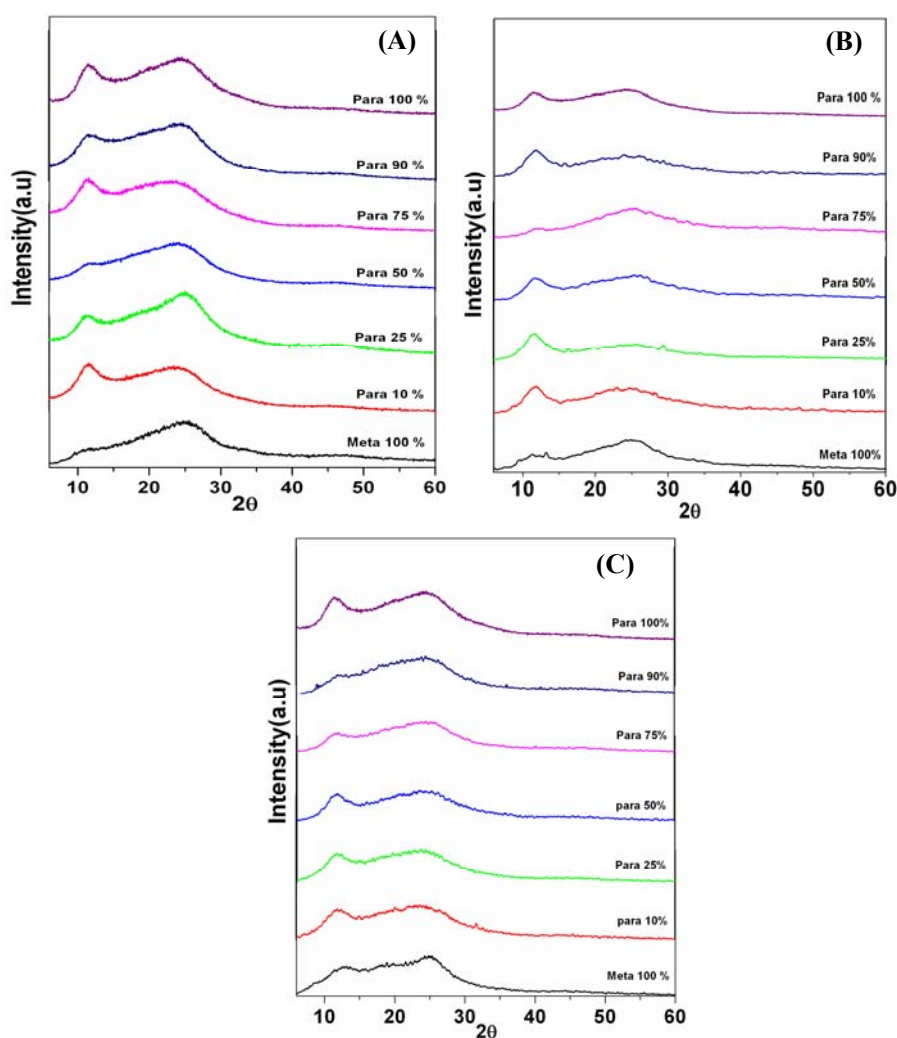
Figure 3.24. *WAXS diffractograms of (A) 2,6(m)-PyPBI-co-2,5(p)-PyPBI (B) 3,5(m)-PyPBI-co-2,5(p) PyPBI (C) 2,4(m)-PyPBI-co-2,5(p)-PyPBI.*

3.4. Conclusion

We have synthesized and studied various molecular properties of three different sets of polybenzimidazole random copolymers consist of meta and para pyridine linkages in the backbone. We have used four different isomers of pyridine dicarboxylic acid (PDA); among which 2,4; 2,6 and 3,5 are meta structure and 2,5 is para structure, with tetraamine (TAB) to obtained the three sets of random PyPBI copolymers. In all the cases the higher para content copolymer yielded higher molecular weight polymers owing to low solubility of para structure 2,5 pyridine dicarboxylic acid (2,5 PDA) in the polymerization medium. FT-IR and Raman spectroscopy studies demonstrate the increase of conjugation along the polymer chain for higher para content polymers. The monomer reactivity ratios of all the PDAs are determined by analyzing the ^{1}H NMR data of the copolymers. The para structure 2,5 PDA has the higher reactivity than all other meta structure PDAs and most importantly the reactivity of 2,5 PDA varies depending upon with which meta PDA it forms the copolymer pair. In all the three sets of copolymers the thermal stabilities are increased with increasing para content in the copolymers. The position of the carboxylic acid groups in the pyridine ring of PDA monomers influences the T_g of the PyPBI homo and copolymers. The T_g of the copolymers decrease with increasing para content in all the cases due to the incorporation of conjugated, symmetrical and flexible para structure in the copolymers. The nature of deviations of T_g of copolymers from the expected T_g (as per the Fox equation) are not similar in three cases, attributing the influence of isotopic structures of monomers. The absorption maxima and the emission wavelength are shifted towards the higher wavelength with increasing para content in the polymer provide the proof for increased conjugation. In summary, we have demonstrated the effect of structural isomers of PDA monomers on the copolymerization and the various molecular properties of PyPBI random copolymers.

References

(1)   Fuel Cell Handbook, 6 th. Edition, EG & G Technical Services, Inc. U.S. Department of Energy, November **2002**.

 (2)   Blomen, L. J. M. J. *Fuel Cell Systems*; Plenum Press, New York, **1993**.

(3)   Rikukawa, M.; Sanui, K. *Prog. Polym. Sci*. **2000**, *25*, 1463.

(4)   Hickner, M. A.; Ghassemi, H.; Kim, S. Y.; Einsla, B. R.; McGrath, J. E. *Chem. Rev.* **2004,** *104*, 4587.

 (5)   Roziere, J.; Jones, D. J. *Annu. Rev. Mater. Res.* **2003**, *33*, 503.

(6)   Higashihara, T., Matsumoto, K.; Ueda, M. *Polymer*, **2009**, *50*, 5341.

(7)   Bouchet, R.; Siebert, E. *Solid State Ionics,* **1999**, *118*, 287.

(8)   Ma, Y. L.; Wainright, J. S.; Litt, M. H.; Savinell, R. F. *J Electrochem Soc,* **2004**,*151*, A8.

(9)   Li ,Q.; Jensena, J. O.; Savinell, R. F.; Bjerrum, N. J. *Prog. Polym. Sci.* **2009**, *34*, 449.

(10)   Mader, J.; Xiao, L.; Schmidt, T, J.; Benicewicz, B, C; *Adv Polym Sci.* **2008**, *216*, 63.

 (11)   Vogel, H.; Marvel, C. S. *J Polym Sci.* **1961**; *50*, 511.

 (12)   Lobato, J.; Ca˜nizares, P., Rodrigo, M.A.; Linares, J.J.; Manjavacas G. *J. Membr Sci*. **2006**, *280*,351.

(13)   Neuse, E. W. *Adv.Polym. Sci.***1982**, *47*, 1.

 (14)   Asensio, J. N.; Borrós. S.; Gómez- Romero, P. *J. Electrochem. Soc.* **2004,** *151,* A304.

(15)   Xiao, L.; Zhang, H.; Jana, T.; Scanlon, E.; Chen, R.; Choe, E.-W.; Ramanathan, L. S.; Yu, S.; Benicewicz, B. C. *Fuel Cells* **2005**, *5*, 287.

 (16)   Jouanneau, J.; Mercier, R.; Gonon, L.; Gebel, G. *Macromolecules* **2007**, *40*, 983.

(17)   Jouanneau, J. ; Gonon, L. ; Gebel, G., Martin, V., Mercier, R. *J. Polym. Sci.: Part A: Polym.Chem*. **2010**, *48*, 1732.

(18)   Li, Z. X.; Liu, J. H.; Yang, S. Y.; Huang, S. H.; Lu, J. D.; Pu, J. L.; *J . Polym. Sci.: Part A: Polym. Chem.* **2006**, *44*, 5729.

(19)   Chen, C. C.; Wang, L. F.; Wang, J. J.; Hsu, T. C.; Chen, C. F. *J. Mater. Sci* **2002**, *37*, 4109.

(20)   Chuang, S-W.; Hsu, S. L-C. *J . Polym. Sci.: Part A: Polym. Chem.* **2006**, *44*, 4508.

(21)   Qian, G.; Benicewicz, B. C. *J. Polym. Sci.: Part A: Polym.Chem.* **2009**, *47*, 4064.

(22)   Pu, H.; Wang, L., pan, H.; Wan, D. *J. Polym. Sci.: Part A: Polym.Chem.* **2010**. *48*, 2115.

(23)   Sannigrahi, A.; Arunbabu, D.; Sankar, R. M.; Jana, T. *J Phys Chem B* **2007**, *111*, 12124.

(24)   Qing, S.; Huang, W.; Yan, D. *Euro Poly J.* **2005,** *41*, 1589.

(25)   Qing, S.; Huang, W.; Yan, D. *React and Func Polym* **2006**, *66*, 219.

(26)   Kojima, T. *J. Polym. Sci.: Polym. Phys. Ed.* **1980**, *18*, 1685.

(27)   Shogbon, C. B.; Brousseau, J.-L.; Zhang, H.; Benicewicz, B. C.; Akpalu, Y. *Macromolecules* **2006,** *39*, 9409.

(28)   Sannigrahi, A.; Arunbabu, D.; Sankar, R. M.; Jana, T. *Macromolecules* **2007**, *40*, 2844.

(29)   Musto, P.; Karasz, F. E., MacKnight, W. J. *Macromolecules* **1991**, *24*, 4762.

(30)   Deimede, V.; Voyiatzis, G. A.; Kallitsis, J. K.; Qingfeng, L.; Bjerrum, N. J. *Macromolecules* **2000**, *33*, 7609.

(31)   Arunbabu, D.; Sannigrahi, A.; Jana, T. *J Phys Chem B* **2008,** *112,* 5305.

(32)   Choe, E. W.; Choe, D. D. In *Polymeric Materials Encyclopedia*; Salamone, J. C., Ed.; CRC Press, New York, **1996**.

(33)   Ghosh, S.; Sannigrahi, A.; Maity, S. *J Phys Chem B* **2010**, *114*, 3122.

(34)   Pu, H.T.; Liu, Q. Z.; Liu, G. H. *J Membr Sci* **2004**; *24,* 169.

(35)   Sansone M. J.; Kwiatek M. S. US patent 4,933,397.;**1990**.

(36)   Klaehn, J. R.; Luther, T. A.; Orme, C. J.; Jones, M. G.; Wertsching A. K. Peterson E. S. *Macromolecules* **2007**;*40,* 7487.

(37)   Scariah, K. J.; Krishnamurthy, V. N.; Rao, K. V. C.; Srinivasan, M. *J. Polym. Sci.: Part A: Polym. Chem.* **1987**, *25*, 2675.

(38)   Sannigrahi, A.; Ghosh, S.; Lalnuntluanga, J.; Jana, T. *J. Appl. Polym. Sci.* **2009**, *111*, 2194.

(39)   Persson, J. C.; Jannasch, P. *Chem. Mater* **2006**, *18*, 3096.

(40)   Li, Q.;He, R.;Jensen, J. Q.; Bjerrum, N. J.; *Chem. Mater*. **2003**, 15, 4896.

(41)   Savinell, R.; Yeager, E.; Tryk, D.; Landau, U.; Wainright, J.; Weng, D.; Lux, K.; Litt, M.; Rogers, C. *J. Electrochem. Soc.* **1994**, *141*, L46.

(42)   Samms, S. R.; Wsmus, S.; Savinell, R. F. *J. Electrochem. Soc.* **1996,** *143,* 1225.

(43)   Weng, D.; Wainright, J.S.; Landau, U.; Savinell, R. F. *J. Electrochem. Soc.* **1996**, *143*, 1260.

(44)   Mecerreyes, D.; Grande, H.; Miguel, O.; Ochoteco, E.; Marcilla, R.; Cantero, I. *Chem. Mater.* **2004**, *16,* 604

(45)   Xiao, L.; Zhang, H.; Scanlon, E.; Ramanathan, L. S.; Choe, E.-W.; Rogers, D.; Apple, T.; Benicewicz, B. C. *Chem. Mater.* **2005**, *17*, 5328.

(46)   Sannigrahi, A.; Arunbabu, D.; Jana, T. *Macromol. Rapid Commun.* **2006**, *27*, 1962.

(47)   Li, Q.; Pan, C.; Jensen, J. O.; Noye´, P.; Bjerrum, N. J. *Chem. Mater.* **2007,** *19,* 350.

(48)   Yu, S.; Benicewicz, B.C. *Macromolecules.* **2009,** *42*, 8640.

(49)   Quartarone, E.; Magistris, A.; Mustarelli, P.; Grandi, S.; Carollo, A.;. Zukowska, G.Z.; Garbarczyk, J. E.; Nowinski, J. L.; Gerbaldi, C.; Bodoardo. S.; *Fuel Cells* **2009**, *4*, 349.

(50)   Chaung, S. W.; Hsu, S. L-C.; Hsu, C-L. *J. Power Sources* **2007**, *168*, 172.

(51)   Shao, H.; Shi, Z.; Fang, J.; Yin, J.; *Polymer* **2009,** *50,* 5987.

(52)   Choe, E -W. *J Appl Polym Sci.* **1994**; 53, 497.

(53)   Kuwahara, N. *J. Polym. Sci.* **1963**, *A1*, 2395.

(54)   Yuan, Y.; Johnson, F, Cabasso, I. *J. Appl. Polym. Sci.* **2009**, *112*, 3436.

(55)   Yu, S.; Zhang, H.; Xiao, L.; Choe, E.-W.; Benicewicz, B. C. *Fuel Cells* **2009**, 4, 318.

(56)   Sun, S. F. *Physical Chemistry of Macromolecules: Basic Principles and Issues*; John Wiley & sons, Inc. : NY, 1994.

(57)   Apelblat, A.; Manzurola, E.; Balal, N. A. *J. Chem. Thermodynamics* **2006**, *38*, 565.

(58)   Long, B-W.; Wang, L-S.; Wu, J-S. *J. Chem. Eng. Data* **2005**, *50*, 136.

(59)   Brooks, N.W.; Duckett, R. A.; Rose, J.; Ward, I. M.; Clements, J. *Polymer* **1993**, *34*, 4038.

(60)   Musto, P.; Karasz, F.E.; MacKnight, W. J. *Polymer* **1993,** *34*, 2934.

(61)   Silverstein, R. M.; Webster, F. X. *Spectroscopic Identification of Organic compounds*; John Wiley & Sons, Inc: NY, 2002.

(62)   Li, Q.;He, R.; Berg, R.W.; Hjuler, H.A.; Bjerrum, N. J.; *Solid State Ionics* **2004**,168,177.

(63)   Lyoo, W. S.; Kim, J. H.; Ha, W. S. *J. Appl. Poly. Sci.* **1996**, *62*, 473.

(64)   Sundarrajan, S.; Ganesh, K.; Srinivasan, K. S. V. *Polymer*, **2003**, *44*, 61.

(65)   Fineman, M.; Ross, S. D. *J. Polym. Sci.* **1950**, *2*, 259.

(66)   Liang, K.; Bánhegyi, G.; Karasz, F. E.; MacKnight, W. J. *J. Polym. Sci.: Part B Polym. Phys.* **1991**, *29*, 649.

(67)   Sperling, L. H. *Introduction to Physical Polymer Science*; John Wiley & Sons, Inc: NY, 1992.

Chapter 4

Aggregation Behavior of meta-Polybenzimidazole in Aprotic Polar Solvent

Increasing concentration of polymer in solution
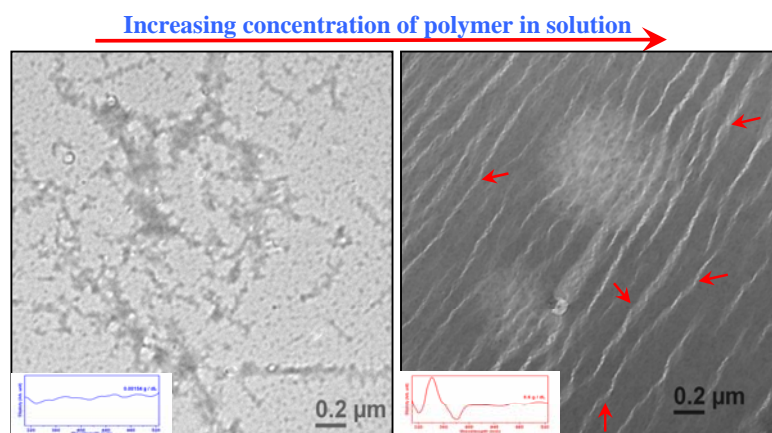
Aggregation behavior of meta-polybenzimidazole (m-PBI) in aprotic polar solvent with increasing concentration is studied. A conformational transition (compact coil to extended helical rod) of m-PBI chains associated with aggregation is observed and monitored.

4.1. Introduction

Polymers and biopolymers are known to form variety of aggregated structures in solution. These macromolecules in solution often interact with each other through the intermolecular interaction resulting in ordered structures. Intramolecular interactions are also possible when different parts of single chain interact with each other. The major driving forces for both inter and intramolecular interactions are mainly hydrogen bonding, electrostatic interactions, and hydrophobic interactions etc.[1,2] The outcomes of these interactions are very fascinating; it is possible to tune various molecular properties of the macromolecules by controlling the nature and extent of these interactions. It has been shown that for biopolymers such as peptides, proteins etc. both intra- and intermolecular interactions play an important role in many biological functions.[3-5] A thorough investigation of the mechanism and the factors influencing these interactions on synthetic polymers is very much desirable since these synthetic polymers serve as model systems for biopolymers. A large number of efforts have been already put forward to address these issues in the literature.[3,4,6-8] The effect of intra- and intermolecular interactions on the polymer chain conformation, conformational transition have been demonstrated extensively for polyelectrolyte-surfactant complexes in solutions.[9] The majority of the research reports have been focused mainly on vinyl polymers, polypeptides and simple structure polymers.[3-9] There are few reports available in the literature addressing these interactions for polymers with highly complex molecular structures.[10-12] For example, polymers having aromatic structure in the main chain and heteroatoms in the chain and also many condensation polymers have not been studied thoroughly to look at their aggregation behavior in different solvents manifested by intra- and intermolecular interactions.

meta-Polybenzimidazole (*m*-PBI, Scheme 4.1) is an aromatic heterocyclic thermally stable polymer that possesses both proton donor (-NH-) and proton acceptor (-N=) hydrogen-bonding sites, which exhibit specific interactions with protic and aprotic polar solvents.[12,13] The availability of hydrogen-bonding sites in the polymer chain made it a suitable candidate for miscible blending with various polymers possessing carbonyl and sulfonyl functionality. [14,15] For example PBI forms a miscible blend in a

wider composition range with polyimide, poly(ether imide), and sulfonated poly sulfone through the specific interaction of its proton donating (-NH-) site with the proton accepting site of the other polymers.[14,15] PBI is being used for various applications, in particular, for high temperature applications, fiber spinning, and reverse osmosis membranes, because of its excellent thermal-chemical tolerance and film forming capability.[16] Recently, phosphoric acid (PA) doped PBI membrane was found to be the most promising material to use as polymer electrolyte in high-temperature proton exchange membrane fuel cell (PEMFC).[17] It has been shown that the PA-doped PBI exhibits high proton conduction at high temperature up to 200°C, excellent oxidative and thermal stability, low gas permeability, and nearly zero water drag coefficient.[17-19] A variety of approaches have been explored to prepare PA doped PBI membrane. Most of these approaches deal with the dissolution of the solid polymer in polar aprotic solvent such as dimethylacetamide (DMAc) and then fabrication of membrane followed by soaking in polar protic solvent such as phosphoric acid (PA).[17-20] Recently, Xiao et. al made PA-doped PBI membrane via sol-gel process by direct casting of high molecular weight PBI polymerization solution in polyphosphoric acid (PPA), and subsequently, PPA is hydrolyzed to PA.[21,22] It was also shown that the imidazole nitrogens present in the polymer backbone play a crucial role for the doping process through a specific interaction with the solvent molecule. We have observed that the fairly concentrate solution of *m*-PBI in PA produces a thermoreversible polymer gel.[23] We have discussed this topic in Chapter 5 and 6.The driving force for the gel formation is the hydrogen bonding of the PA molecules with the nitrogen atoms of imidazole ring, producing the *m*-PBI crystallites.[23] We are able to show that a conformational transition of *m*-PBI chain takes place when a hot *m*-PBI solution in PA cools down to gelation temperature.[23] In the present chapter, we demonstrate the possible aggregation behavior of a very dilute *m*-PBI solution in polar aprotic solvent such as DMAc, which may reveal a better understanding of the polymer chain conformation in dilute solution and help us to get an idea of preparing membrane of superior quality from both polar protic and polar aprotic solvents.
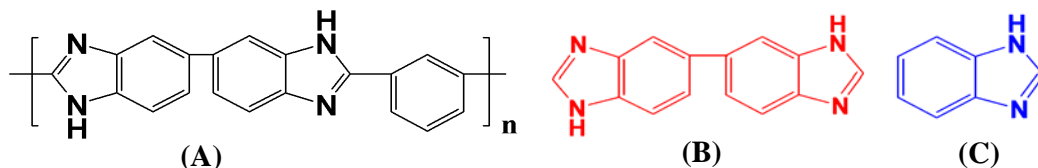
Scheme 4.1. *(A) Poly (2, 2$'$-(m-phenylene)-5, 5$'$ – bibenzimidazole) (m-PBI), (B) 3, 3$'$ Bibenzimidazole (BBI) and (C) Benzimidazole (BI)*

Fluorescence spectroscopy has been utilized as a prime tool for the investigation of intra- and intermolecular interactions of polymer chains and their aggregations.[7,10-12,24-27] The photophysical studies of polymer solution have been limited almost entirely to olifinic polymers with aromatic[24] and heterocyclic pendent groups such as polystyrene,[25] poly(*N*-vinyl carbazole),[26] poly(vinyl anthracene)[27] etc., and their copolymers.[28] All these polymers show either intra- or intermolecular[28] excimer formation in solution. Exciplex formation in polymers was also studied as a measure of molecular interactions.[10] The fluorescence studies of condensation polymers[10,29] especially aromatic heterocyclic polymers such as polybenzimidazole,[11,30] polyquinoline,[12] etc. were attempted to elucidate intra- and intermolecular aggregations. However these studies are not as extensive as olifinic polymers; perhaps the poor solubility of these aromatic heterocyclic polymers in most common organic solvents is the major restriction for photophysical studies in solution. Huang et al. reported that polyquinolines form excimers in acidic solution resulting in concentration quenching and showed that excimer formation is controlled by intermolecular repulsion between the polymer chains.[12] Kojima showed that the molecular aggregation in the ground state of PBI in DMAc solution is due to the overlapping of polymer coils.[11] It is to be noted that the PBI used by Kojima[11] which has 4, 4$'$ -oxybibenzyl linkage with imidazole group is not exactly similar to Scheme 4.1 where *m*-phenylene linkage is present. However, in the literature there is no thorough investigation of various photophysical processes of *m*-PBI (Scheme 4.1) using both steady state and time-resolved fluorescence study at various concentration. This could probably give us a better understanding of intra and intermolecular interaction of the polymers in solution, which leads to

aggregation/excimer formation. In this present chapter, we study intra- and intermolecular interaction of dilute PBI in DMAc solution studying steady state and time resolved fluorescence, viscosity at different temperatures, nuclear magnetic resonance at different temperatures and different concentrations, and morphology obtained from transmission electron microscopy.

4.2. Experimental Section

4.2.1 Materials. 3, 3', 4, 4' –Tetraaminobiphenyl (TAB) and polyphosphoric acid (115%) were purchased from Sigma-Aldrich. Isophthalic acid (IPA) was received from SRL, India. Benzimidazole (BI) and sulfuric acid (98%) were received from Merck, India. Dimethylacetamide (HPLC grade) and deuterated dimethyl sulfoxide (DMSO-d_6) were received from Qualigens (India) and Merck (India), respectively. All chemicals were used as received.

4.2.2. *m*-PBI Synthesis. Equal mols of TAB and IPA were taken into a three neck flask with PPA and the reaction mixture was stirred continuously in nitrogen atmosphere at 190-210°C for ~24 h. The *m*-PBI polymer was isolated, neutralized with sodium carbonate, washed thoroughly with water, and dried in a vacuum oven at 100°C for 24 h. The dried polymer was characterized by viscosity measurements in H_2SO_4 (98%) and has an inherent viscosity (IV) value of 0.62 dL/g at 30°C.

4.2.3. 3, 3' -Bibenzimidazole (BBI) Synthesis. BBI (Scheme 4.1) synthesis was carried out according to the previously reported method[31] and characterized using NMR, IR, and LC-MS.

4.2.4. Viscosity. The viscosity measurements of *m*-PBI solutions in DMAc were carried out at various temperatures (308 K–343 K) using a Cannon Ubbelohde capillary dilution viscometer (model F725). The viscosity data were analyzed according to the Huggins equation (4.1):

$$\frac{(t - t_0)}{C} = \frac{\eta_{sp}}{C} = \eta_{red} = [\eta] + k_H [\eta]^2 C \qquad (4.1)$$

where t and t_0 are the flow time of the polymer solution and solvent, respectively, C is the concentration of polymer in g/dL, η_{sp} , η_{red}, [η] are the specific, reduced and intrinsic viscosity of the polymer solution, respectively and k_H is the Huggins constant.

4.2.5. Spectroscopy. Electronic absorption spectra were recorded on a Shimadzu model UV-3100 UV-visible spectrometer. Steadystate fluorescence emission spectra were recorded on a Jobin Yvon Horiba spectrofluorimeter (model Fluoromax-3). Time-resolved fluorescence measurements were carried out using a time-correlated single-photon counting (TCSPC) spectrophotometer (IBH Nano LED). A diode laser (λ_{exc} = 374 nm) was used as the excitation source and the instrument response time was 75 ps (fwhm). The emission was detected at right angle to the excitation beam using a Hamamatsu 323P MCP photomultiplier. A dilute solution of Ludox in water was used to record the lamp profile. The decay curves were analyzed by nonlinear least-squares iteration using IBH DAS6 (Version 2.2) decay analysis software. All NMR spectra of PBI solutions in DMSO-d_6 at various dilution and temperatures were recorded using a Bruker AV 400 MHz NMR spectrometer. Circular dichroism (CD) spectra of polymer solutions were recorded on a spectro polarimeter (Jasco-810) at 30°C using a 2 mm quartz cuvette.

4.2.6. Microscopy. The morphological features of the *m*-PBI samples obtained from various solution concentrations were examined using a Jeol (JEM 2000) transmission electron microscope (TEM) operating at 120 kV. For TEM experiments, appropriate concentrated polymer solutions were dropped in carbon coated copper mesh and imaged.

4.3. Results and Discussion

4.3.1. Spectroscopy. The absorption spectra of *m*-PBI and nonpolymeric model compounds such as BBI and benzimidazole (BI) (Scheme 4.1) in DMAc are presented in Figure 4.1. The *m*-PBI concentration is expressed by considering one repeat unit as 1 mol *m*-PBI. The lower wavelength peaks; 344 nm for *m*-PBI,[32] 295 nm for BBI, and 270 nm for BI are due to π → π* transition of the imidazole moiety and longer wavelength

peaks; 440 nm for *m*-PBI (Figure 4.2), 350 nm for BBI and 345 nm for BI are due to n → π* transition of the imidazole ring. The large bathochromic shift of the π → π* absorption maxima for *m*-PBI and BBI is due to increased conjugation between phenylene groups and imidazole rings. A more distinct red shift of the polymer peaks compared to those nonpolymeric model compounds is attributed due to the large extent of conjugation along the polymer chain. Figure 4.2 show that *m*-PBI has a very long tail toward longer wavelength which becomes prominent as the concentration of the solution increases (Figure 4.3). In contrast to *m*-PBI, we have not observed any such long tail for nonpolymeric model compounds. This observation indicates the possibility of aggregation of polymer chains through overlapping of polymer coils at higher concentration.
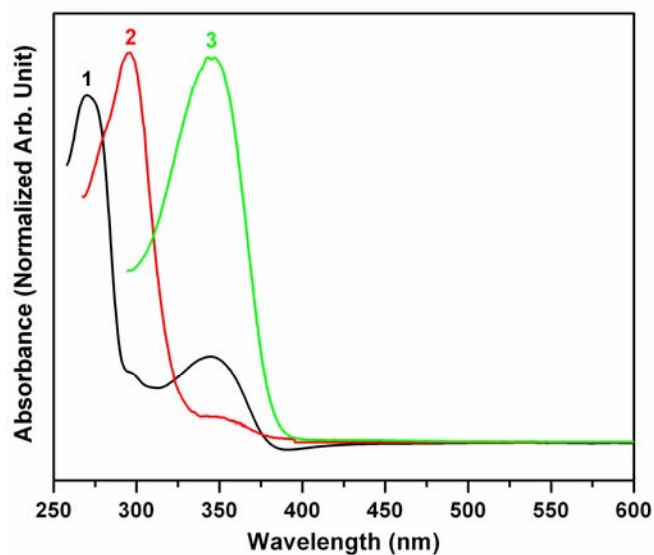
Figure 4.1. *Absorption spectra of (1) BI, (2) BBI and (3) m-PBI in DMAc solution as recorded with a cuvette of 1 cm path length. Concentrations are (1) 5.9 × 10^{-4}, (2) 1.17 × 10^{-3} and (3) 1.54 × 10^{-3} g/dL (all are 5 × 10^{-5} molar concentration).*
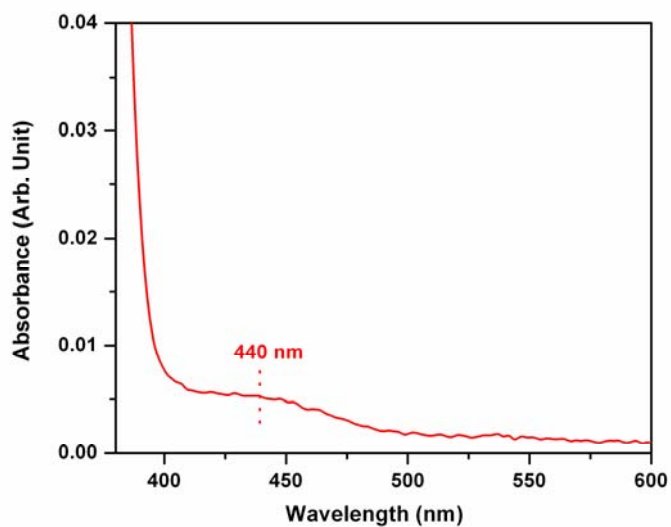
Figure 4.2. *A magnified spectrum of m-PBI in DMAc solution (spectrum of Figure 4.1) to show the 440 nm peak position.*
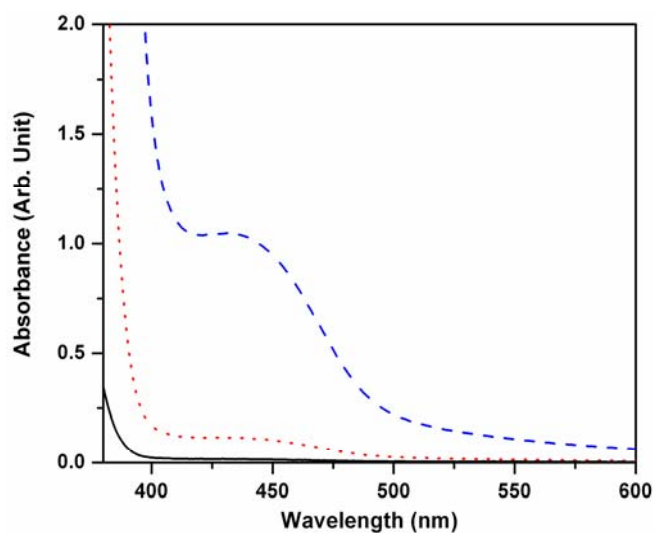
Figure 4.3. *Absorption spectra of m-PBI in DMAc solution at various concentrations; (- - -) 1.54 × 10^{-1}, (-----) 1.54 × 10^{-2} and (—) 1.54 × 10^{-3} g/dL.*

The major fluorescence emission of polybenzimidazole and molecules with imidazole moiety has been assigned previously by several authors as the emission from the excited ^1L_b state.[11, 33] The emission spectra of *m*-PBI, BBI, and BI in DMAc of similar concentrations are shown in Figure 4.4. The emission spectrum of *m*-PBI shows two fluorescence bands at 398 and 416 nm. These peaks are assigned to the 0-0 and 0-1 transitions from the excited ^1L_b state in the benzimidazole ring of *m*-PBI.[11] The spectral nature and shapes presented in Figure 4.4 are consistent with the earlier report of very similar molecules by Kojima.[11] The emission bands for *m*-PBI are observed at longer wavelength relative to those nonpolymeric molecules is the result of existence of higher conjugation in the polymer.[11] Figure 4.5 and 4.6 show the emission spectra of *m*-PBI and BBI, respectively, at various concentrations in DMAc. In all the cases emission intensity is decreased with increasing solution concentration indicating the presence of concentration quenching. The peak at 398 nm of *m*-PBI gradually diminishes with increasing *m*-PBI concentration and finally at higher concentration (0.154 g/dL) 416 nm peak exists along with another broad peak at ~548 nm. The concentration dependence of emission intensity for *m*-PBI is almost similar to nonpolymeric molecules; though it is more distinctly visible for *m*-PBI. The ratio of the peak intensities (longer wavelength peak to lower wavelength peak) in the emission spectra increases with concentration. The presence of concentration quenching and enormous increase of peak intensity ratio with concentration indicate that the polymer chains are aggregated among themselves intermolecularlly at higher concentration. Earlier Kojima calculated the critical quenching volume for a similar type of PBI polymer and showed that intermolecular aggregation of polymer chains takes place in DMAc.[11]
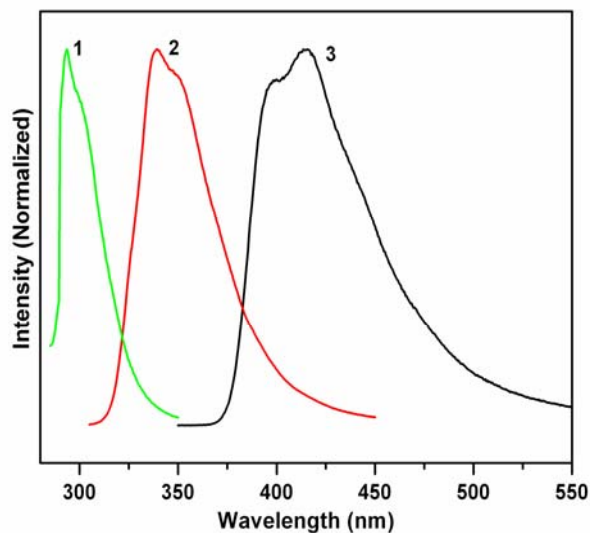
Figure 4.4. *Fluorescence emission spectra of (1) BI, (2) BBI and (3) m-PBI in DMAc solution. Concentrations are identical to Figure4.1. Excitation wavelength (λ_{exc}): (1) 275, (2) 295 and (3) 340 nm.*
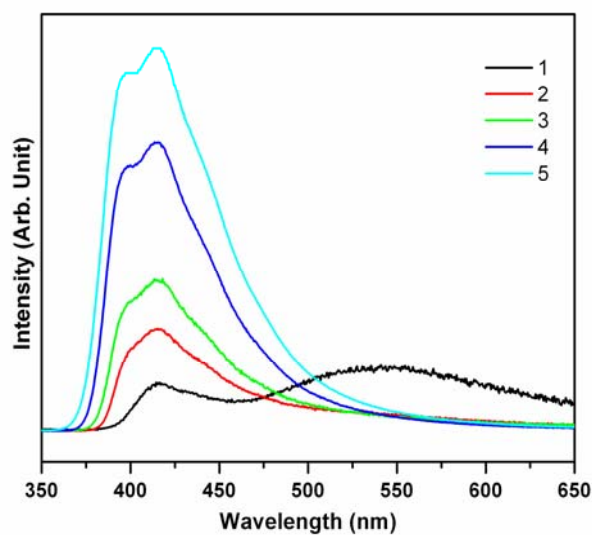
Figure 4.5. *Fluorescence emission spectra of m-PBI in DMAc solution at various concentrations; (1) 1.54×10^{-1} (2) 1.54×10^{-2} (3) 5.0×10^{-3} (4) 1.54×10^{-3} and (5) 1.54×10^{-4} g/dL. Excitation wavelength (λ_{exc}) is 340 nm.*
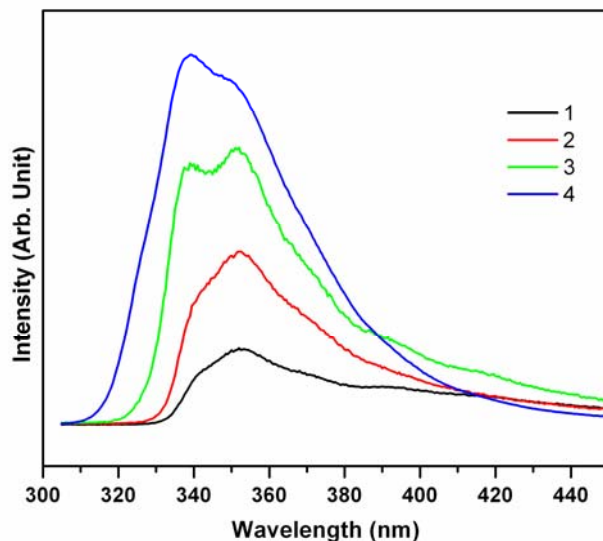
Figure 4.6. *Fluorescence emission spectra of BBI in DMAc solution at various concentrations; (1) 1.5×10^{-1} (2) 1.17×10^{-1} (3) 1.17×10^{-2} and (4) 1.17×10^{-3} g/dL. Excitation wavelength (λ_{exc}) is 295 nm.*

Moreover, Figure 4.5 shows a broad emission band at longer wavelength (~548 nm) for the highly concentrated (0.154 g/dL) solution. For similar solution concentrations, Kojima[11] have not observed this broad fluorescence band. We have not observed this broad emission peak for nonpolymeric molecules at similar concentration. To understand the role of this broad peak, we have recorded the emission spectra of a series of *m*-PBI solutions where the concentration gradually increases, and this is presented in Figure 4.7. From Figure 4.7, it is clearly visible that as concentration increases the broad 548 nm peak becomes prominent and the intensity of 416 nm band decreases. It is worth noting that Figure 4.7 shows an isoemissive point at ~460 nm. The presence of a broad emission at a higher wavelength and isoemissive point attributes the formation of a complex between excited-state and ground state molecules, known as the excimer complex.[34] Olifinic polymers with pendent aromatic groups very often form an excimer both in solution and in the solid state.[24,25,28] Though it is very rare for a polymeric system such as the present one, our steady-state fluorescence study on *m*-PBI

at various concentrations (Figure 4.7) clearly satisfies the required criteria for excimer formation. It is also important to note that the nonpolymeric molecules such as BBI and BI do not show a similar photophysical behavior at similar concentrations. Hence the spectral behavior presented in Figure 4.7 is exclusively for a polymeric system in DMAc at higher concentration. Hence, we can argue that *m*-PBI in DMAc forms an excimer; the broad 548 nm peak is for excimer emission and the 416 nm peak is for monomer emission. The excimer and monomer emission intensities are denoted as I_E and I_M, respectively. However, the question arises that the broad 548 nm peak is really the emission from an excited-state species (excimer) or an aggregated species which forms in the ground state itself and emits separately at longer wavelength. To clarify this, we have adopted two methods; first we have recorded emission spectra of a concentrated (0.154 g/dL) solution by varying the excitation wavelength, and second, we have carried out a time-resolved fluorescence life time measurement of *m*-PBI in DMAc solution at very dilute (0.00154 g/dL) and high (0.154 g/dL) concentrations. If emission spectra depend on excitation wavelength, then aggregation in the ground state occurs,[11,35] and if a growth is observed (a negative pre-exponential factor) in the decay profile, then excimer formation is attributed.[36] Figure 4.8 shows excitation wavelength (λ_{exc}) dependence emission spectra for a concentrated solution. As the λ_{exc} increases, the 548 nm peak shifts toward the longer wavelength side. Similar observations were reported for *m*-PBI and imidazolium based room-temperature ionic liquids; this is explained as molecular aggregation in the ground state.[11,35] The dependence of the emission band on λ_{exc} can be explained with the help of absorption spectra presented in Figure 4.2 and Figure 4.3. A long tail in the absorption band indicates the presence of a large number of aggregated species in the ground state that are energetically different. Each aggregated species is characterized by its own absorption and fluorescence maxima. When the λ_{exc} is shifted, a different species is excited and emission characteristic of that species is observed. Therefore, we can conclude that molecular aggregation is present in the *m*-PBI in DMAc solution. The extent of emission peak position shift is shown in the Figure 4.9.
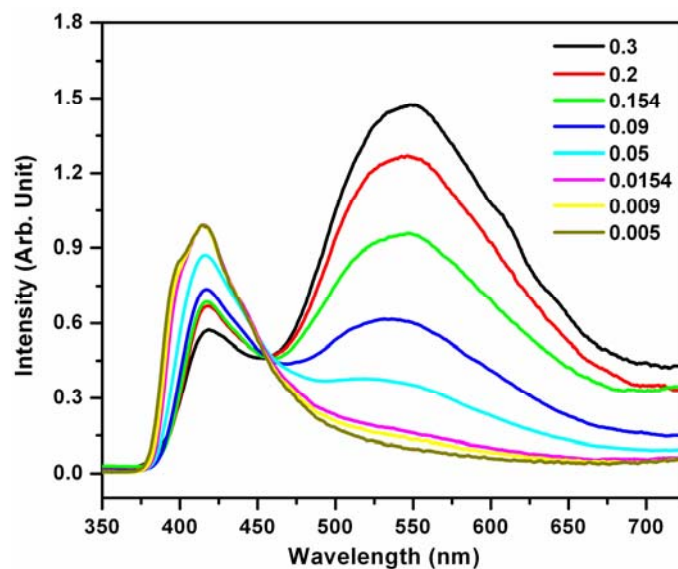
Figure 4.7. *Fluorescence emission spectra of m-PBI in DMAc solution at indicated concentrations (in g/dL); Excitation wavelength (λ_exc) is 340 nm.*
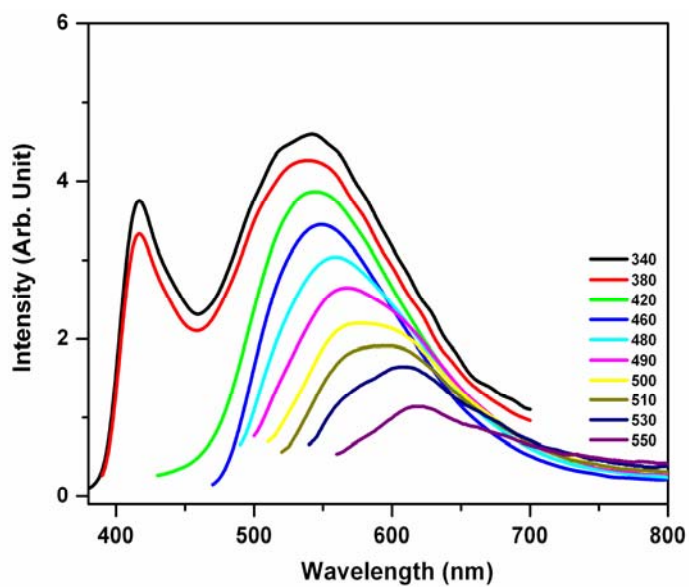
Figure 4.8. *Dependence of fluorescence emission spectra on excitation wavelength (indicated in the figure) for m-PBI in DMAc solution (Concentration is 0.2 g/dL).*
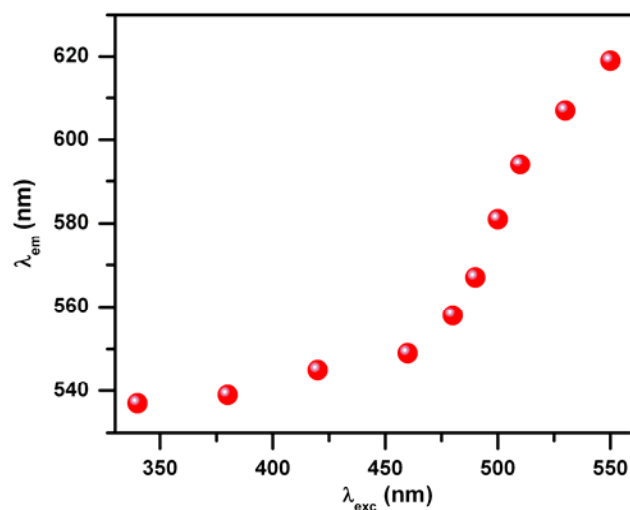
Figure 4.9. *Plot of λ_{em} against λ_{exc} obtained from the Figure 4.8.*

The decay profiles of dilute (0.00154 g/dL) and concentrate (0.154 g/dL) *m*-PBI in DMAc solution are obtained by exciting the samples at 374 nm and monitoring the fluorescence at 417 nm. The decay profiles are shown in Figure 4.10, and the best fit and fluorescence decay parameters are presented in Table 4.1. The decay profiles for both the cases are found to follow a triexponential decay function as observed from Table 4.1. The nature of the decay profiles are not the same in both the cases. From Figure 4.10(B), it is visible that for concentrate solution the decay profile shows a growth (a negative pre-exponential factor) which is not observed for dilute solution (Figure 4.10A). This observation is more understandable from Table 4.1; a negative fraction contribution (α_3) is obtained from concentrate solution. The growth in the decay profile and the negative pre-exponential are concrete proof for excimer formation.[36] Therefore, we can conclude that at higher concentration of *m*-PBI in DMAc excimer is formed and the broad peak at 548 nm is due to the excimer formation. Hence, from the above analysis it can be concluded that *m*-PBI forms aggregated species as well as exited state dimmer (excimer) in the DMAc solution when the concentration of the solution is reasonably large. The broad 548 nm peak is the contribution from both

aggregation and excimer. The excited state life time for the concentrate solution is found to be 4.14 ns, longer than that for the dilute solution, for which the life time is 502 ps (Table 4.1). Previously, Liu et al.[37] showed that the excited-state life time depends upon the polymer chain conformations. Theoretically, they demonstrated that excited state life time of polymer molecule becomes shorter as their root-mean square end-to-end distance decreases. Our results fit well with this reported argument. In the following sections, we have shown that as concentration of *m*-PBI in DMAc decreases the *m*-PBI chains form a compact coil structure and produce an extended conformation at higher concentration. Therefore, the excited-state life times of concentrate solution is longer (4.14 ns) than the dilute solution (502 ps). It is interesting to note that the ratio of aggregation or excimer intensity with monomer intensity (I_E / I_M or I_{548} / I_{416}) increases linearly with concentration (Figure 4.11). This indicates that the aggregation or excimer formation is an intermolecular process.[28,38] The large value of I_E / I_M for higher concentration attributes the presence of a strong intermolecular association in the aggregated species.
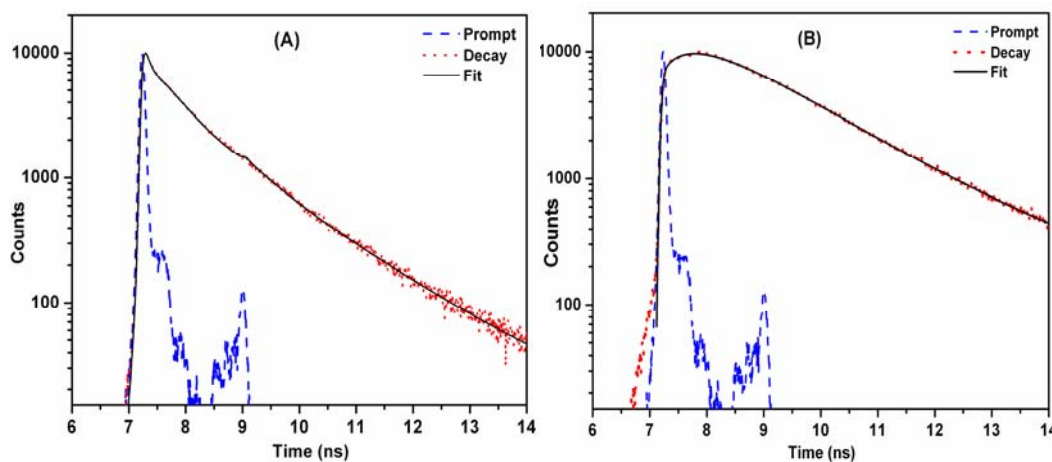
Figure 4.10. *Time resolved fluorescence decay profile of m-PBI in DMAc solution of two different concentrations: (A) 0.00154 and (B) 0.154 g/dL; λ_{exc} = 375 nm.*

Table 4.1. *Fluorescence decay parameters for m-PBI in DMAc solutions at different concentrations[a]*

PBI Concentration (g / dL)	$\tau_1(ns)$	α_1	τ_2 (ns)	α_2	τ_3 (ns)	α_3	τ_{avg} (ns)	χ^2
0.00154	0.59	0.35	1.5	0.17	0.07	0.48	0.502	1.27
0.154	1.56	3.13	6.31	0.07	0.55	-2.20	4.14	1.26

[a]The three lifetimes (τ_1, τ_2 and τ_3) and the respective fractional contributions (α_1, α_2 and α_3), the weighted average lifetime (τ_{avg}) and the quality of fitting (χ^2) for the data in Figure 4.10 are shown.
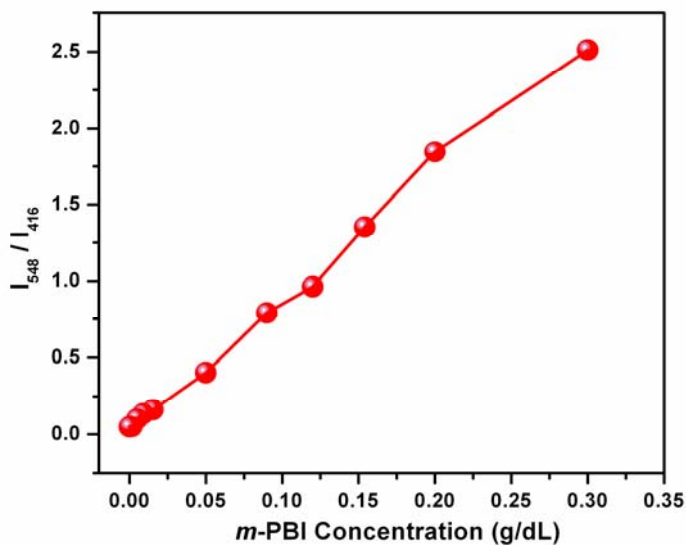
Figure 4.11. *Dependence of excimer to monomer intensity ratio with concentration of m-PBI in DMAc solution.*

4.3.2. Viscosity. The interactions between polymer molecules and solvent have been studied previously by viscosity measurement method. The Huggins constant (k_H) and intrinsic viscosity ([η]) can be obtained for a dilute solution of a simple binary system

using this method. It is well-known that the value of the Huggins constant (k_H) is used to predict the degree of the polymer-solvent interaction and can determine the polymer chain conformation in solution. The bigger value of k_H indicates that the polymer chains collapse and the intramolecular aggregation occurs easily. On the other hand, the smaller k_H value attributes extended conformations and the intermolecular interactions.[39,40] The viscosity of *m*-PBI at various dilutions was measured and a plot of reduced viscosity vs. concentration is presented in Figure 4.12. The Huggins constants (k_H) are estimated from the slopes of the viscosity vs concentration line. At the lower concentration region (0.075-0.009 g/dL) (Figure 4.12, curve b), the k_H value is 1.634; at the higher concentration region (0.6-0.1 g/dL) (Figure 4.12, curve a), it is 0.723. The higher k_H value (1.634) indicates the intramolecular interaction between different parts of the polymer chain, which results in a collapsed compact coil conformation of the polymer chain. At these concentrations, the excluded volume of polymer chain gets smaller and it does not allow the solvent molecules to go inside the polymer coil for swelling. As a result, polymer chains produce a compact coil structure. When concentration increases, more and more polymer molecules come into the solution and polymer chains start interacting with each other intermolecularly. Because of this intermolecular interaction, polymer chains swell by allowing solvent molecules to go inside the polymer coil, and the excluded volume of the polymer chain becomes larger. Therefore, it is reasonable to argue that the low k_H value (0.723) for the higher concentration range is in agreement with the above justification (intermolecular interactions), which results an extended conformation. Hence, at this concentration range, we would expect an extended rodlike aggregated structure. The above observations clearly exhibit a conformational transition of the *m*-PBI chains in DMAc solution when the solution concentration varies.[13] Figure 4.13 is the plot of reduced viscosity vs concentration for both the concentration region (similar to Figure 4.12) including the intermediate concentrations. The plot shows a clear transition of reduced viscosity and reveals that a conformational transition (compact coil to extended rodlike) in the polymer chain takes place.[9] Here, we can argue that in the smaller concentration range DMAc acts as a poor solvent (large k_H value and compact conformation) for *m*-

PBI whereas it acts as a good solvent (small k_H value and extended conformation) in the higher concentration range. Therefore, from spectroscopic and viscometric studies, it is proven that upon increasing the *m*-PBI concentration in DMAc solution intramolecular interactions diminish but intermolecular interactions are enhanced, which triggers a conformation transition of polymer chain and produces an aggregated rodlike structure at higher concentration. A more detail understandings of the aggregation process with proofs are obtained from NMR and microscopic studies described in the preceding sections.
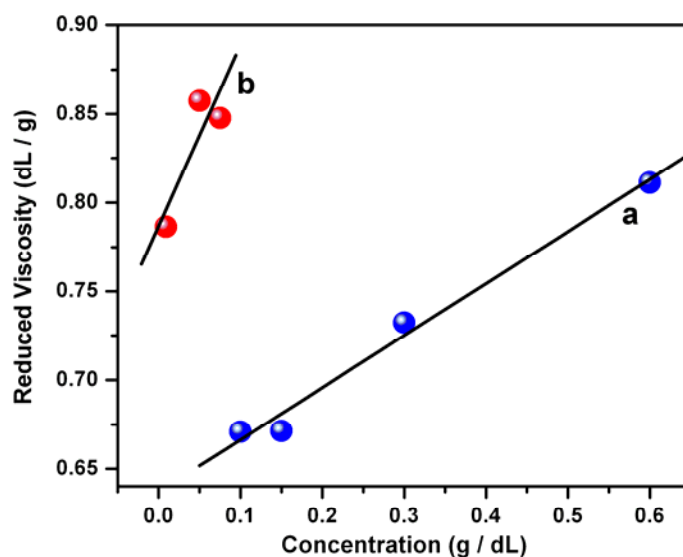
Figure 4.12. *Concentration dependence of the reduced viscosity of m-PBI in DMAc solutions measured at 35°C for two different concentrations regions: (a) 0.6 – 0.1 and (b) 0.075 – 0.009 g/dL.*
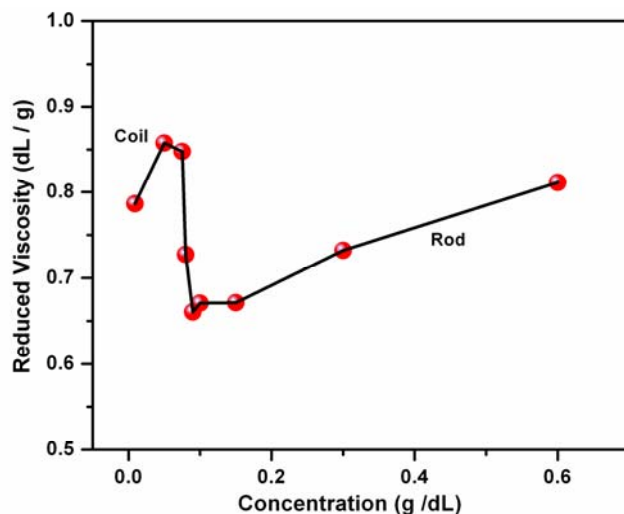
Figure 4.13. *Plot of reduced viscosity against concentration of m-PBI in DMAc solutions measured at 35°C.*

4.3.3. NMR Study. The concentration dependence proton NMR study can be utilized effectively to monitor the intermolecular interactions (interchain hydrogen bonding) between the polymer chains in solution. It has been shown that proton NMR spectroscopy is an effective tool for studying the conformational transition which arises by the disruption of interchain hydrogen bonding of polyelectrolyte-surfactant complexes in solution.[9] Unlike all other studies, NMR studies were carried out in DMSO-d_6 solvent, since it is less expensive compared to DMAc-d_9. *m*-PBI exhibits similar behavior in both the solvents. A representative proton NMR spectrum of *m*-PBI in DMSO-d_6 is presented in Figure 4.14. The spectrum is consistent with the earlier reports. The peak at 13.3 ppm is due to the imino proton signal of imidazole rings and other peaks (7.65- 9.15 ppm) are due to aromatic protons signals.[32, 41] The imino proton signal of *m*-PBI in DMSO-d_6 is gradually shifted upfield with decreasing concentration of the solution (Figure 4.15), which proves the disruption of intermolecular interactions such as hydrogen bonding [9] and formation of a more compact conformation of the polymer chain. This observation clearly indicates a conformational transition of the polymer chain from extended conformer to compact coil conformer. Hence,

concentration dependence NMR spectroscopy is also consistent with our results discussed in the previous section. A more interesting result is obtained when we added 1% (w/v) urea in the *m*-PBI solutions, measured their viscosity and recorded NMR spectra. Urea is capable of breaking the hydrogen bonding. After addition of 1% urea in the 0.6 g/dL *m*-PBI solution, the 13.3 ppm peak is shifted (upfield) and peak intensity is diminished (Figure 4.16) which indicates the breaking of interchain hydrogen bonding. Similar observations were reported before for PBI in DMAc/LiCl solution.[41,42] The intrinsic viscosity and Huggins constant obtained for the concentration range 0.6-0.1 g/dL at 35°C in the presence of 1% urea are 0.3649 dL/g and 3.277, respectively. These values are remarkably different from the values obtained in the same concentration range at 35°C in absence of urea (intrinsic viscosity 0.6369 dL/g and k_H = 0.7233). A decrease of the intrinsic viscosity and increase of the Huggins constant supports the decrease of intermolecular interactions or increase of intramolecular interactions [8, 39].
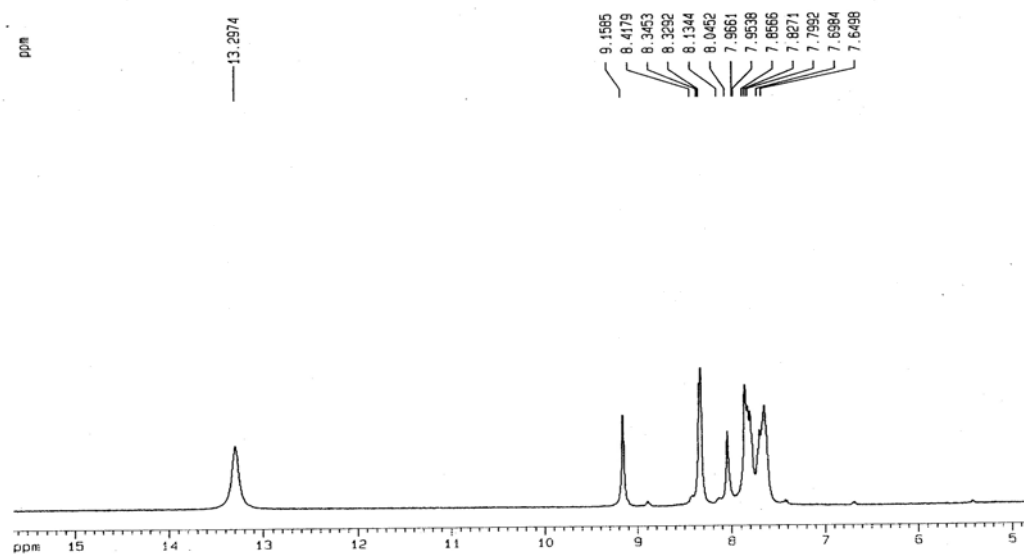
Figure 4.14. *Proton NMR spectrum of m-PBI in DMSO – d₆.*
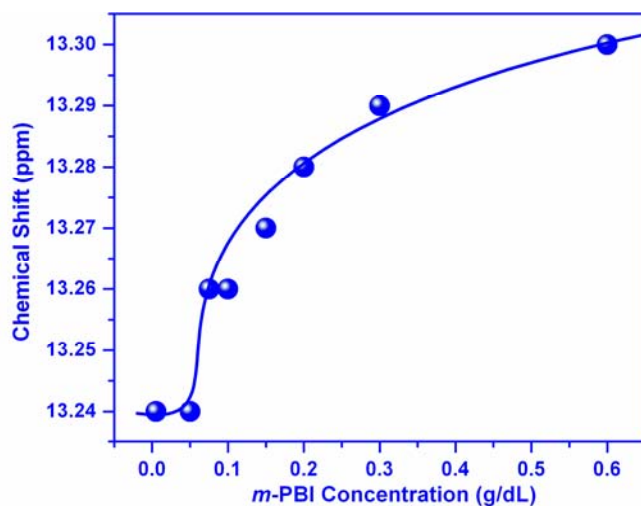
Figure 4.15. *Dependence of imino proton signal with m-PBI concentration in DMSO–d₆ solution.*
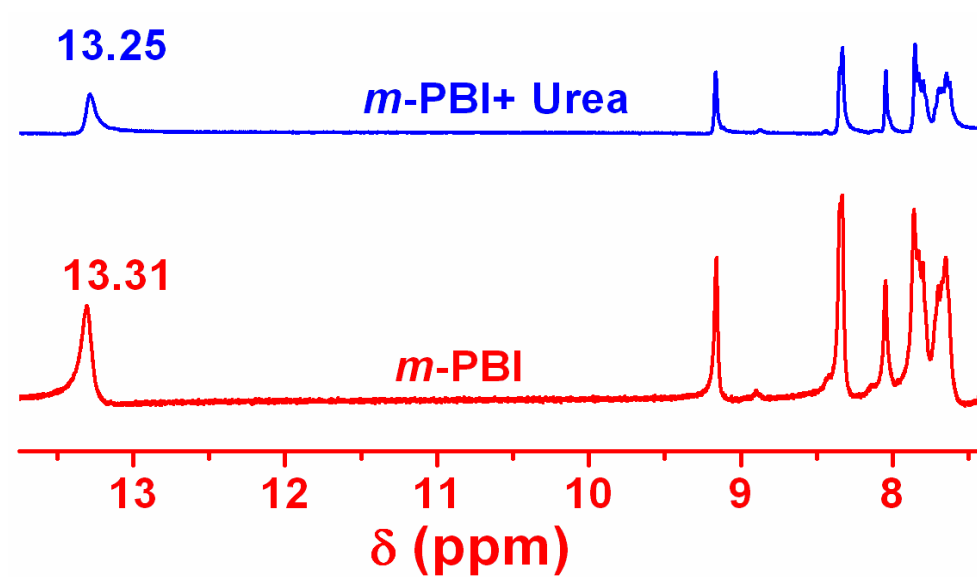
Figure 4.16. *Upfield shift and reduced intensity of imino proton signal of m-PBI in presence of urea. Note that other signals have not changed.*

4.3.4. Microscopy. It has been shown above that, at very low concentrations, the intramolecular interaction is prominent, which results in a compact coil type structure. Therefore, we do not expect any characteristic morphology at this concentration. Figure 4.17A represents the microscopic image obtained from *m*-PBI solution in DMAc of concentration 0.00154 g/dL. The micrograph is almost featureless, except for a few polymer particles, consistent with our arguments from spectroscopic, viscometric and NMR data. We have demonstrated that with increasing concentration of *m*-PBI in DMAc, intermolecular interaction increases and produce an aggregated structure. Because of this aggregation process, the *m*-PBI chain in DMAc at higher concentration (0.6 g/dL) shows an extended rod conformation. Figure 4.17B represents the TEM image for *m*-PBI in DMAc solution of concentration 0.6 g/dL. The morphology of Figure 4.17B is entirely different compared to that of Figure 4.17A, which exhibits the effect of *m*-PBI concentration on morphology. From Figure 4.17B, it is seen that *m*-PBI forms extended rod-type morphology. It is important to note that all the rods in the image show helical turns (indicated by arrows). The circular dichroism (CD) studies show the presence of optical activity of 0.6 g/dL solution at 342 nm and absence of any optical activity of dilute PBI solution (Figure 4.18). This observation exhibits the presence of ordered structure for *m*-PBI at higher concentration whereas no such defined structure for *m*-PBI is evident at low concentration. Similar CD results were observed for PBI in DMAc/LiCl solution.[13] Hence these results prove that a helical rod like structure formation takes place when the solution concentration is high. Therefore, we can conclude that the microscopic and CD data also support a conformational transition (compact coil to extended helical rod like) of *m*-PBI chains when the concentration of the polymer in solution increases.

A schematic presentation for the conformational transition (compact coil to extended helical rod like) due to the aggregation of *m*-PBI chains in DMAc solutions with increasing concentration is shown in Figure 4.19. The scheme is proposed based on our results discussed above.
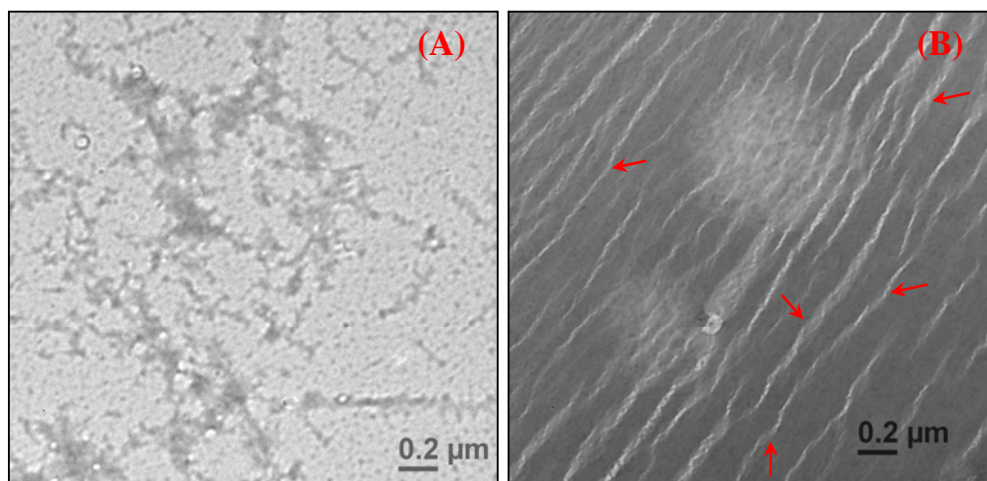
Figure 4.17. *TEM micrographs of (A) 0.00154 and (B) 0.6 g/dL m-PBI in DMAc solution Arrows in the (B) image indicate the helical turns.*
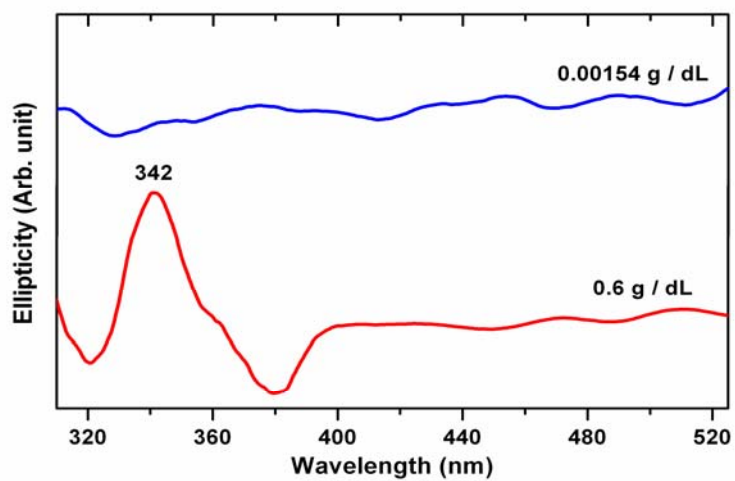
Figure 4.16. *Circular dichroism spectra of m-PBI in DMAc solution at indicated concentrations.*
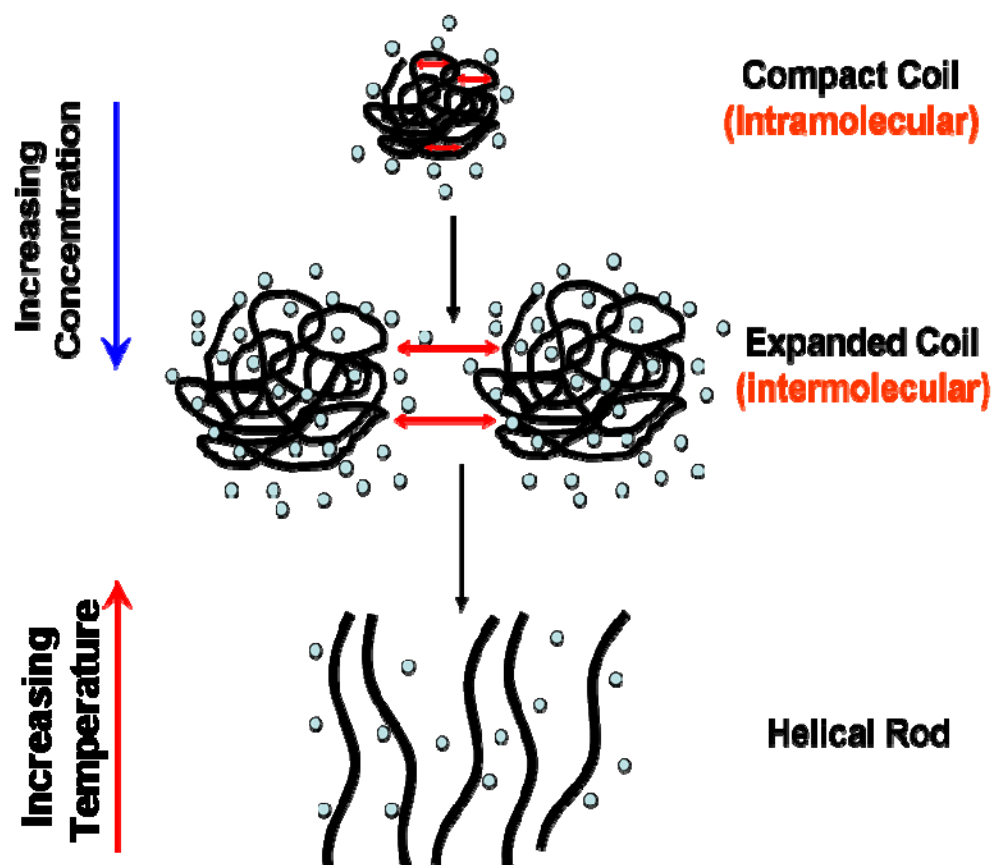
Figure 4.19. *Schematic presentation for the conformational transition of m-PBI in DMAc solution. Tiny circles represent the solvent molecules.*

4.3.4. Temperature Effect. We have observed from the above discussion that at the higher concentration (0.6-0.1 g/dL) of *m*-PBI in DMAc at room temperature, the polymer chains form an aggregated structure and exist as an extended helical conformation because of the intermolecular interaction (interchain hydrogen bonding) between themselves (Figure 4.19). This conclusion immediately brings up a question: How stable is this aggregated structure in response to the environmental stimuli such as temperature change? And answer to this question is of utmost importance to know since it could provide a valuable piece of data which may help us to prepare a good quality

membrane for PEMFC applications. We have carried out temperature dependent studies such as viscosity and NMR to answer the above question. Figure 4.20 shows the variation of viscosity parameters with temperature (308-343°K). The intrinsic viscosity of *m*-PBI in DMAc decreases and Huggins constant increases as temperature increases (Figure 4.20). Kojima et al.[43] have also observed the decrease of intrinsic viscosity with increase in temperature. It is well-known that for a polymer of fixed molecular weight, intrinsic viscosity is directly proportional to the end to end distance of the polymer chain. The *m*-PBI used in this work has a fixed molecular weight (inherent viscosity 0.62 dL/g). So, the decrease of intrinsic viscosity with increase in temperature indicates the shrinkage of polymer chains; i.e., chains are collapsed at higher temperatures. Similarly, the increase of Huggins constant with increase in temperature attributes that at higher temperatures the solvent behaves as a poorer solvent for the polymer chains, producing a compact coil type conformation. The above results clearly demonstrate that at higher temperature, aggregated structure with extended helical polymer chain conformation does not exist. The probable reason behind this is that intermolecular interaction such as interchain hydrogen bonding breaks at higher temperature. A better understanding of the disruption of interchain hydrogen bonding is obtained from the temperature-dependent NMR studies of *m*-PBI solution. The imino proton signal of *m*-PBI (concentration is 0.3 g/dL) at various temperatures are presented in Figure 4.21. An upfield shift of the imino proton signal is observed with increase in temperature. The upfield shift of the imino proton, a strong hydrogen-bonding proton, is due to the disruption of interchain hydrogen bonding. Earlier we have shown the conformational transition of *m*-PBI chains in phosphoric acid solution with temperature.[23] Therefore, it can be argued that at higher temperature the aggregated structure of concentrated PBI solution breaks and a conformational transition occurs from extended helical conformer to collapsed compact coil conformer. Hence, the effect of temperature is just reverse of concentration effect. We have indicated temperature effect in the schematic presentation shown in Figure 4.19. Similar type of observation and conclusion was made by MacKnight et. al. for polyelectrolyte – surfactant complexes in solution with an increase of trifluoroacetic acid (TFA) content in the solution [9].
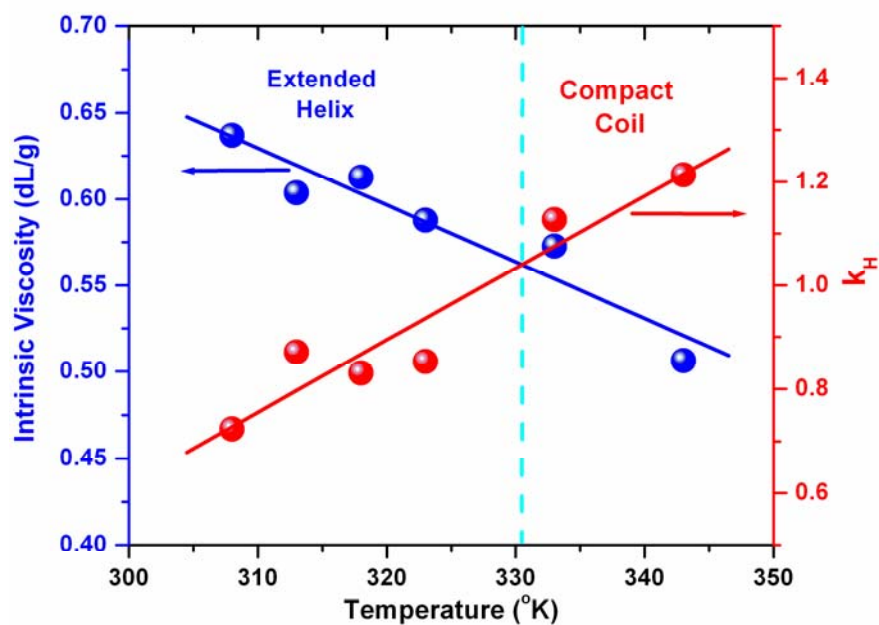
Figure 4.20. *Effect of temperature on Huggins constant and intrinsic viscosity of m-PBI in DMAc solutions for the concentrations regions 0.6 – 0.1 g/dL.*
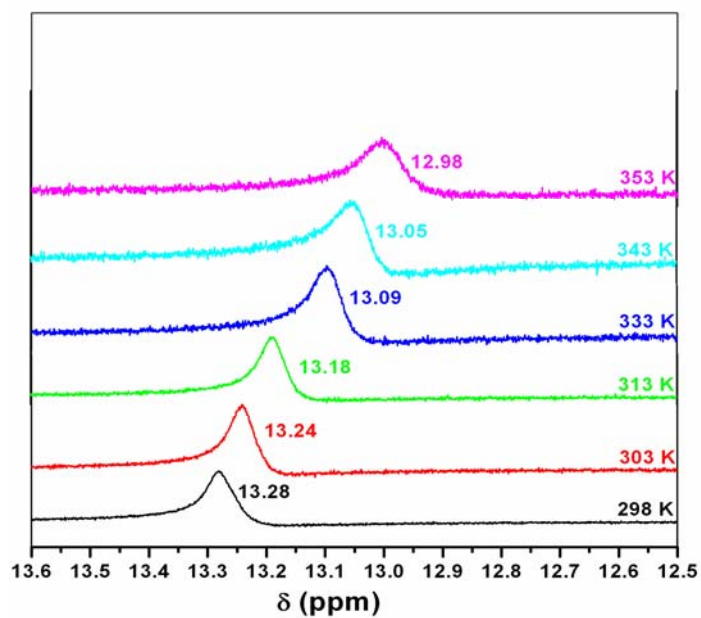
Figure 4.21. *Temperature dependent imino proton signals of m-PBI in DMSO-d_6 Concentration is 0.3 g/dL.*

4.4. Conclusion

We have studied the aggregation behavior of *m*-PBI in polar aprotic solvent such as dimethylacetamide (DMAc) by varying the polymer concentration in the solution. Various methods such as photophysical, viscometric, microscopic, and NMR have been used to study the aggregation behavior and associated conformational transition of the polymer chains. Steady state and time resolved fluorescence spectroscopy studies demonstrated the formation of an aggregated structure at higher concentration of *m*-PBI in solution. These photophysical studies also proved excited state complex, i.e., excimer formation at higher concentrations. It has been also shown that both aggregation and excimer formation is an intermolecular process. Viscometric studies indicated that a conformational transition from a compact coil to an extended helical rod like structure takes place in *m*-PBI solution when polymer concentration is high. A sharp decrease of Huggins constant and abrupt decrease of reduced viscosity with increase in polymer concentration validated the conformational transition argument. The intramolecular interaction within the various parts of polymer chain at lower concentrations and intermolecular interactions between the polymers chains at higher concentrations could be the probable reason behind the conformational transition. An additional evidence for conformational transition is obtained from the NMR studies. An upfield shift of the imino proton signal indicated the disruption of interchain hydrogen bonding. Microscopic images and CD spectra obtained from various polymer concentrations also supported the conformational change behavior of *m*-PBI in DMAc and helical rod shaped morphology for a 0.6 g/dL solution. Finally, temperature-dependent studies (viscosity and NMR) showed that the aggregated structure is not stable at higher temperature. Therefore, in summary, we can conclude that polymer chains of *m*-PBI in DMAc solution form a coil structure at lower concentration due to intramolecular interaction and produce an aggregated extended helical rodlike structure at higher concentration because of intermolecular interaction, although the aggregated structure is not stable at higher temperature.

References

(1)   Lehn, J. *Angew. Chem., Int. ed. Engl.* **1988,** *27*, 90.

(2)   Lehn, J. *Angew. Chem., Int. ed. Engl.* **1990,** *29*, 1304.

(3)   Bekturov, E. V.; Bimendina, L. A. *Adv. Polym. Sci.* **1981**, *41*, 99.

(4)   Tschuchida, E.; Abe, K. *Adv. Polym. Sci.* **1982**, *45*, 1.

(5)   Whitesides, G.; Mathias, J.; Seto, C. *Science* **1991**, *254*, 1312.

(6)   Minato, K, I.; Ohkawa, K.; Yamamoto, H. *Macromol. Biosci* **2006,** *6,* 487.

(7)   Sivadasan, K.; Somasundaran, P.; Turro, N, J. *Colloid. Polym. Sci* **1991**, *269*, 131.

(8)   Simon, S.; Dugast, J.Y.; Le Cerf, D.; Picton, L.; Muller, G. *Polymer* **2003**, *44*, 7917.

(9)   MacKnight, W. J.; Ponomarenko, E. A.; Tirrell, D. A. *Acc. Chem. Res.***1998**, *31*, 781.

(10)   Tazuke, S.; Matsuyama, Y. *Macromolecules* **1975,** *8*, 280.

(11)   Kojima, T. *J. Polym. Sci.: Polym. Phys. Ed.* **1980**, *18*, 1685.

(12)   Huang, H.Y.; Yun, H.; Lin, H. S.; Kwei, T. K.; Okamoto, Y. *Macromolecules* **1999**, *32*, 8089.

(13)   Shogbon, C, B.; Brousseau, J.-L.; Zhang, H.; Benicewicz, B. C.; Akpalu, Y. *Macromolecules* **2006,** *39*, 9409.

(14)   Musto, P.; Karasz, F. E., MacKnight, W. J. *Macromolecules* **1991**, *24*, 4762.

(15)   Deimede, V.; Voyiatzis, G. A.; Kallitsis, J. K.; Qingfeng, L.; Bjerrum, N. J. *Macromolecules* **2000**, *33*, 7609.

(16)   Choe, E. W., Choe, D. D. In *Polymeric Materials Encyclopedia*; Salamone, J. C., Ed.; CRC Press: New York, 1996.

(17)   Savinell, R.; Yeager, E.; Tryk, D.; Landau, U.; Wainright, J.; Weng, D.; Lux, K.; Litt, M.; Rogers, C. *J. Electrochem. Soc.* **1994**, *141*, L46.

(18)   Samms, S. R.; Savinell, R. F. *J. Electrochem. Soc.* **1996,** *143,* 1225.

(19)   Weng, D.; Wainright, J.S.; Landau, U.; Savinell, R. F. *J. Electrochem. Soc.* **1996**, *143*, 1260.

(20) Mecerreyes, D.; Grande, H.; Miguel, O.; Ochoteco, E.; Marcilla, R.; Cantero, I. *Chem. Mater.* **2004**, *16,* 604.

(21) Xiao, L.; Zhang, H.; Jana, T.; Scanlon, E.; Chen, R.; Choe, E.-W.; Ramanathan, L. S.; Yu, S.; Benicewicz, B. C. *Fuel Cells* **2005**, *5*, 287.

(22) Xiao, L.; Zhang, H.; Scanlon, E.; Ramanathan, L. S.; Choe, E.-W.; Rogers, D.; Apple, T.; Benicewicz, B. C. *Chem. Mater.* **2005**, *17*, 5328.

(23) Sannigrahi, A.; Arunbabu, D.; Jana, T. *Macromol. Rapid Commun.* **2006**, *27*, 1962.

(24) Aspler, J. S.; Guillet, J. E.; *Macromolecules* **1979**, *12*, 1082.

(25) Gupta, M. C.; Gupta, A.; Horwitz, J.; Kliger, D.; *Macromolecules* **1982**, *15*, 1372.

(26) Gatica, N.; Marcelo, G.; Mendicuti, F.; *Polymer* **2006,** *47*, 7397.

(27) Cuniberti, C.; Perico, A.; *European Polymer Journal* **1980**, *16*, 887.

(28) Fox, R.B.; Price, T. R.; Cozzens, R. F.; Mcdonald, J. R. *J. Chem. Phys* **1972,** *57***,** 534.

(29) Ravindranath, R.; Vijilaa, C.; Ajikumar, P. K.; Hussain, F. S. J.; Ng, K. L.; Wang, H.; Jin, C. S.; Knoll, W.; Valiyaveettil, S. *J. Phys. Chem. B* **2006**, *110*, 25958.

(30) Fujimura, T.; Tsuchiya, M.; Koizumi, T.; Ishimaru, K.; Kojima, T. *J. Appl. Polym. Sci* **2003,** *89*, 1412.

(31) Boydston, A. J.; Williams, K. A.; Bielawski, C, W. *J. Am. Chem. Soc.* **2005**, *127*, 12496.

(32) Neuse, E. W. *Adv.Polym. Sci.***1982**, *47*, 1.

(33) Zimmermann, H.; Joop, N. *Ber. Bunsenges. Phys. Chem.* **1962**, *66*, 342

(34) Turro, N. J. *Modern Molecular Photochemistry*; The Benjamin / Cummings Pub. Com. Inc.: California, 1978.

(35) Samanta, A. *J. Phys. Chem. B* **2006**, *110*, 13704.

(36) Gilbert, A.; Baggott, J. *Essentials of Molecular Photochemistry*; Blackwell Sci. pubs.: Oxford, 1991.

(37) Liu, G.; Guillet, J. E. *Macromolecules* **1990**, *23*, 4292.

(38) Birks, J. B. *Photophysics of Aromatic Molecules*; Wiley Interscience: NY, 1970.

(39) Hong, P. D.; Chou. C.M.; He, C. H. *Polymer* **2001,** *42*, 6105.

(40) Sun, S. F. *Physical Chemistry of Macromolecules: Basic Principles and Issues*; John Wiley & sons, Inc. : NY, 1994.

(41) Kojima, T. *J. Polym. Sci: Polym. Phys. Ed.* **1980**, *18*, 1791.

(42) Ryan, M. T. and Helminiak T. E. *Polym. Prepr. Am. Chem. Soc. Div. Polym. Chem.* **1973**, *14*, 1317.

(43) Kojima, T., Yokota, R.; Kochi, M.; Kambe, H. *J. Polym. Sci.: Polym. Phys. Ed.* **1980**, *18*, 1673.

Chapter 5

Thermoreversible Gelation of meta-Polybenzimidazole in Phosphoric Acid
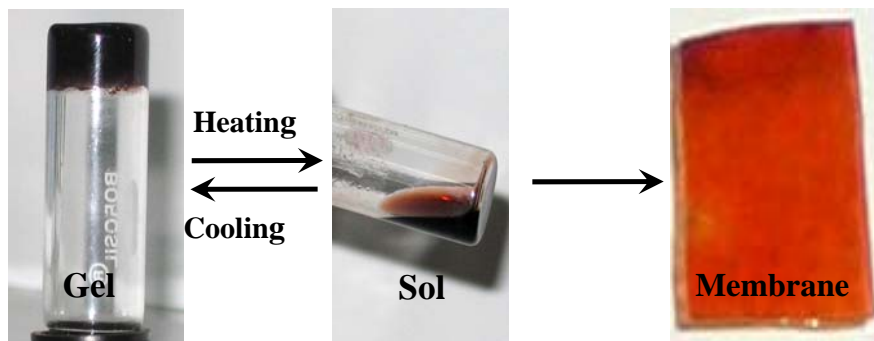
Thermoreversible gelation of meta-polybenzimidazole (m-PBI) in phosphoric acid (PA) is investigated. The PA doped PBI membrane with significantly high loading is obtained from the gel.

5.1. Introduction

In recent years, thermoreversible polymer gels have been studied extensively because of their potential application in various fields.[1,2] The preparation of thermoreversible gel often offers many advantages such as easy processing of infusible intractable polymers,[3,4] fabrication of mechanically strong film etc. Various synthetic and biopolymer systems are studied, and the driving force of gelation is different in different cases. The gelation mechanism depends upon both polymer and solvent. Usually, it occurs due to various types of physical processes like crystallization, conformational ordering, mesomorphic phase transition and liquid- liquid phase separation etc.[1,2,5]

meta-Polybenzimidazole (*m*-PBI, Scheme 4.1) is an aromatic heterocyclic thermally stable macromolecule that possesses both proton donor (- NH -) and proton acceptor (- N =) hydrogen bonding sites, which exhibit specific interaction with protic, aprotic polar solvents and upon blending with other polymers.[6,7] Recently, phosphoric acid (PA) doped *m*-PBI membrane was found to be the most promising material for use as polymer electrolyte in high temperature proton exchange membrane fuel cell (PEMFC).[8] It has been shown that the PA doped *m*-PBI exhibits high proton conduction at high temperature up to 200°C, excellent oxidative and thermal stability, low gas permeability, and nearly zero water drag coefficient.[8-10] A variety of approaches have been explored to prepare PA doped *m*-PBI membrane. A large body of literature is centered on PBI membrane prepared by conventional process, where it casts either from *m*-PBI solution in dimethyl acetamide (DMAc) followed by soaking it with PA or from *m*-PBI solution in a mixed acid solvent such as trifluoroacetic acid (TFA) and PA.[8-10] Recently, in another approach porous *m*-PBI membrane was made by leaching out low molecular weight compound (porogen) from polymer / porogen mixture and then soaking it in PA solution.[11] Very recently, Xiao et. al made PA doped *m*-PBI membrane via sol – gel process by direct casting of high molecular weight *m*-PBI polymerization solution in polyphosphoric acid (PPA) and subsequently PPA is hydrolyzed to PA.[12,13] The quantity of PA present in the membrane depends upon the method of membrane

preparation techniques described above. Also, mechanical strength of the membrane is varying with the amount of PA present in it. Apart from the above methods, membrane can be prepared from the gel hypothesizing that the gel may able to trap more PA and provide better mechanical strength because of its highly dense interconnected network structure. Xiao et al.[13] reported PA doped *m*-PBI gel membrane, though in our knowledge there is no report on thermoreversible *m*-PBI gel. In this chapter we discuss morphology, thermal, WAXS, gelation kinetics and UV-Vis study of thermoreversible *m*-PBI gel in PA.

5.2. Experimental Section

5.2.1. Materials. 3, 3′, 4, 4′- tetraaminobiphenyl (TAB, polymer grade) and polyphosphoric acid (PPA, 115 %) were purchased from Sigma–Aldrich. Isopthalic acid (IPA) (99%), purchased from SRL, India and purified by recrystallization in water and ethanol (2:8) mixture prior to use. Sulfuric acid (98%) and phosphoric acid (85%) was purchased from Merck, India.

5.2.2. PBI Synthesis and Preparation of Gel. Equal amounts (mols) of TAB and IPA were taken into a three necked flask with PPA and the reaction mixture was stirred continuously in nitrogen atmosphere at 190 - 210°C for ~ 24 h. The *m*-PBI polymer was isolated, neutralized with sodium carbonate, washed thoroughly with water, dried in a vacuum oven at 100°C for 24 h. The dried polymer was characterized by viscosity measurement in H$_2$SO$_4$ and showed an inherent viscosity (IV) of 0.92 dL / g at 30°C. The reported number average molecular weight ($\overline{M_n}$) was 26,300 Da and the weight-average molecular weight ($\overline{M_w}$) was 50,300 Da for a similar *m*-PBI structure with an IV of 0.97 dL/g [14]. The gels were prepared by taking the required amount of *m*-PBI polymer and PA in a sealed glass vial. Homogeneous red color solutions were made at 180°C and reddish brown color gels obtained by quenching at 30°C. These gels were transformed into solution and vice versa upon repeated heating and cooling cycle.

5.2.3. Characterization of Gel. The morphology of the gel was studied in Scanning Electron Microscope (SEM). For SEM study entrapped PA was substituted with water gradually from the gel samples by washing and vacuum dried at 60°C for 3 days. Since PA is a viscous, high boiling and non – volatile solvent therefore solvent removal by both freeze drying and simple evaporation techniques were unsuccessful. Instead, substitution of PA from the gel network with relatively low boiling solvent water was found to be the best suitable method. A differential Scanning Calorimeter (DSC) was used to find out the gel melting (T_{gm}) and gelation (T_{gel}) temperature. Gels were taken in Large Volume Capsule (LVC) pan and tightly sealed in a quick press. The DSC was scanned from 30°C to 160°C at a heating rate of 10°C / min. and from 160°C to 30°C at a cooling rate of 5°C / min. The Wide Angle X-ray Scattering (WAXS) patterns were collected by taking the gels were taken in a glass slide and the diffractograms were recorded using nickel – filtered Cu Kα radiation at the scanning rate of 1.5° 2θ / min. The gelation kinetics was followed by test tube tilting method.[15-17] A series of gels of different concentration were prepared in a sealed glass vial (1.3 mm inner diameter) by dissolving required amount of *m*-PBI in 0.5 mL of PA at 180°C and quickly transferred to a thermostatic bath preset at a gelation temperature. The gelation rate (t_{gel}^{-1}) is the inverse of gelation time (t_{gel}), which was obtained by measuring the time required for complete cease of fluidity of the solutions even after inverting the vial upside down. The UV-Vis. spectroscopic study was carried out in a UV-Vis-NIR spectrophotometer by dissolving 0.1 % (w/v) *m*-PBI solution in PA was made at 180°C and immediately transferred to the spectrophotometric cell, which was kept at gelation temperature.

5.3. Result and Discussion

5.3.1. Morphology. The morphology of the dried *m*-PBI – PA gel obtained form SEM study is presented in Figure 5.1. From the SEM micrograph it is evident that the network morphology consisting of fibrils is present in the gel sample. A magnified SEM photograph (Figure 5.1b) shows well – defined interconnected fibrillar network. This fibrillar network type morphology is a characteristic feature of thermoreversible

polymer gel.[2, 4, 15-18] Though fibrillar network morphology is present in the gel, the solid powder *m*-PBI which is not treated with any solvent has no distinct domains or domain boundaries on the scale probed by SEM, rather it is almost featureless. Also the *m*-PBI dissolved in PA much below the critical gelation concentration (discussed later) is not showing any fibrillar network morphology. It must note that the substitution drying method adopted here retains the characteristic fibrillar morphology as seen in Figure 5.1. So, from this morphological analysis we ensure that the *m*-PBI – PA gel is a physical polymer gel. An in-depth study of morphological behavior with gelation concentration and molecular weight of the sample is addressed in chapter 6.
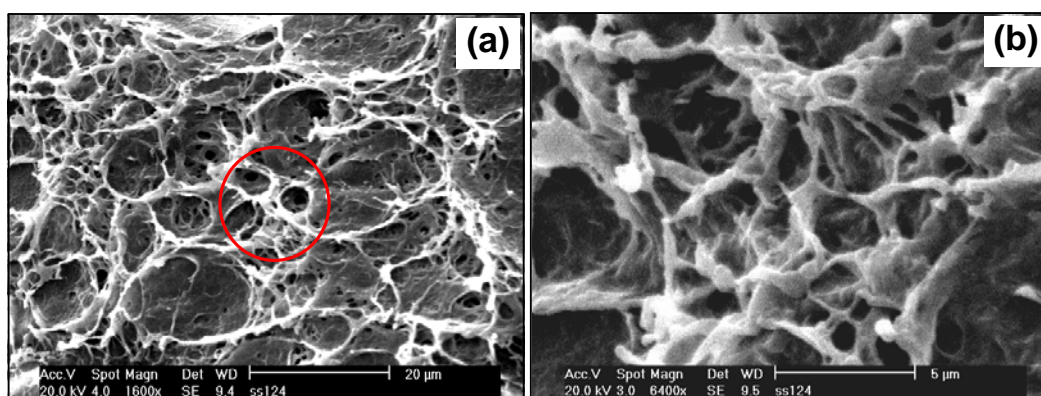
Figure 5.1. *(a) SEM micrographs of m-PBI – PA gel; (b) a magnified view of selected area (shown with a red circle) of 'a' micrograph.*

5.3.2. Thermal Study. The most important criterion for a polymer gel to be thermoreversible is that it must exhibit reversible first order phase transition in DSC during heating and cooling scan.[2, 4, 15-18] The thermogramms of *m*-PBI – PA gel presented in Figure 5.2 clearly show the endothermic peak at 125.75°C while heating (Figure 5.2 A) and exothermic peak at 84.5°C (Figure 5.2 B) while cooling scan in DSC. The difference between the two peak positions is due to hysteresis effect of the first order phase transition process.[15,18] The broad nature of heating endoderm is due to poor crystallinity of *m*-PBI in PA and the presence of large amount of solvent in the gel sample. Also, WAXS (following section) study shows that the *m*-PBI is not a highly

crystalline polymer rather it is an amorphous polymer and gains crystallinity to a certain extent when treated with PA. Therefore, it is evident from morphological and DSC study that *m*-PBI produces thermoreversible gel in PA
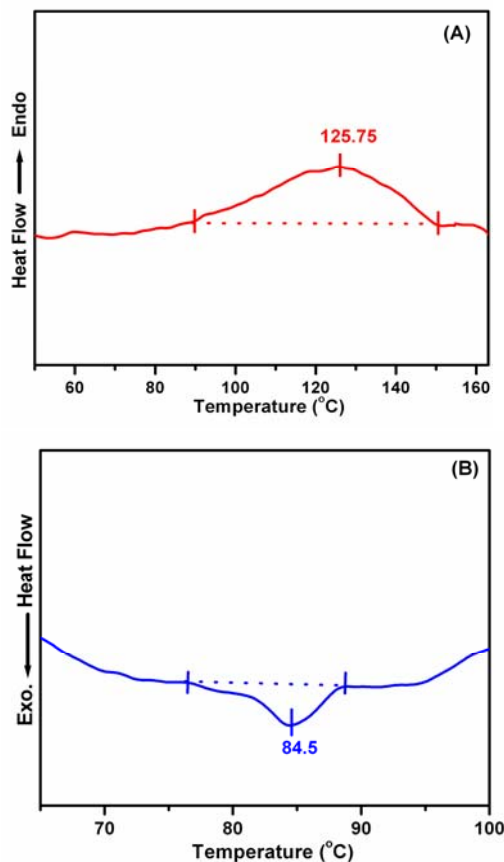
Figure 5.2. *DSC thermogramms of m-PBI – PA gel (A) Heating and (B) Cooling.*

5.3.3. WAXS Study. The X – ray diffraction patterns of dry *m*-PBI powder and *m*-PBI – PA gel are presented in Figure 5.3. The diffraction pattern of the gel is different from the dry polymer powder. The powder has no distinct diffraction peak, whereas the gel sample shows a very sharp highly intense distinct crystalline peak at $2\theta = 12.5$ along with other peaks at 21.5, 24.5, 26.5, 29.3 and 34.2. The *m*-PBI polymer (Scheme 4.1) used here is a predominantly amorphous polymer which is evident from X-ray study (Figure 5.3) and also reported by several authors earlier.[19 – 21] It is possible to prepare

semi-crystalline *m*-PBI polymer and fiber by treating the amorphous PBI with certain reagents under appropriate conditions of temperature and concentration.[19] Among those reagents formic acid can induce the crystalline character in *m*-PBI at room temperature.[22] *m*-PBI exhibits polyelectrolyte behavior both in formic acid [6] and PA as evident from their viscosity data. The measured reduced viscosity (η_{red}) of *m*-PBI solution in PA displays an anomalous behavior. η_{red} increases with decreasing concentration (Figure 5.4). This observation violates the dilute solution properties of the polymer solution and the Huggins equation ($\eta_{red} = [\eta] + k_H[\eta]^2C$) where η_{red} decreases with decreasing concentration. Such upswings in the viscosity curves might be attributed either to polyelectrolyte effect or capillary wall effect. We have analyzed the viscosity data in the following manner. The data from figure 5.4 are replotted in Figure 5.5 and 5.6 as the reciprocal of the reduced viscosity against the square root of concentration, and reduced viscosity minus the inherent viscosity ($\eta_{inh} = \ln\eta_{rel}/C$) against concentration, respectively. A plot of the reciprocal of the reduced viscosity of *m*-PBI in PA against the square root of the concentration shows linearity, which implies the polyelectrolyte behavior.[23,24] The nonlinearity of curves shown in Figure 5.6 eliminates the possibility of capillart wall effect.[25] Similar observation was reported in the literature for *m*-PBI in formic acid [6].
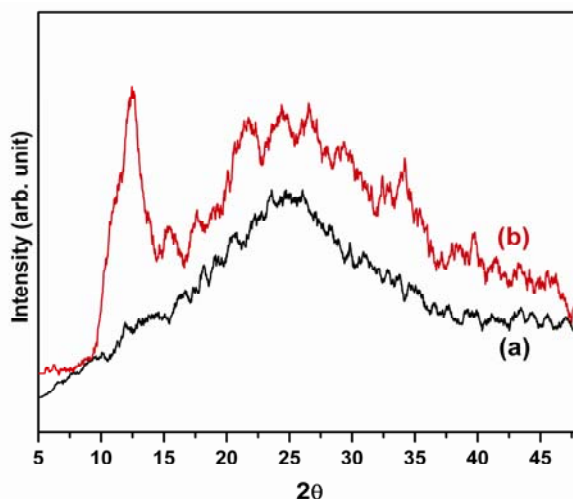
Figure 5.3. *WAXS diffractograms (a) dry m- PBI powder and (b) m-PBI – PA gel.*
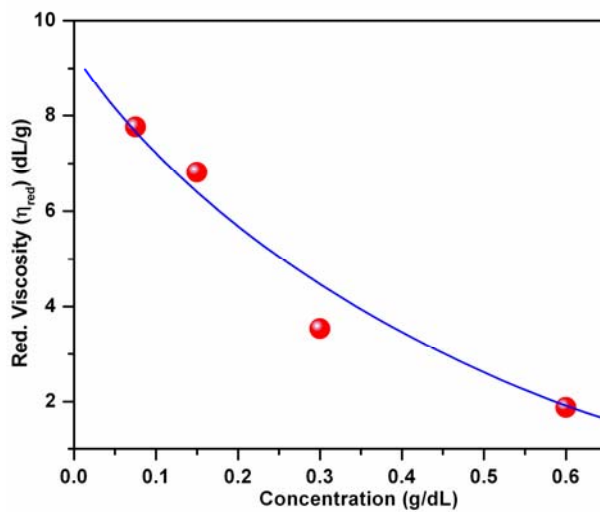
Figure 5.4. *Reduced viscosity vs concentration curve of m-PBI in phosphoric acid solution.*
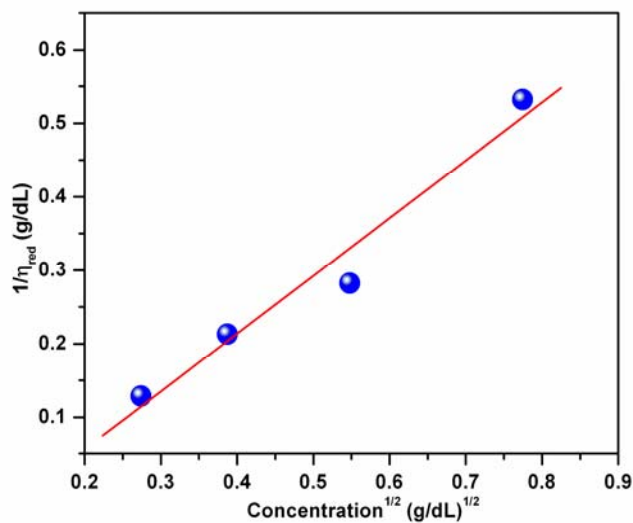
Figure 5.5. *Reciprocal of reduced viscosity vs square root of concentration curve of m-PBI in phosphoric acid solution.*

Hence, we can consider that *m*-PBI will also produce crystallites in PA and this is observed in the X-ray diffractogram (Figure 5.3). These *m*-PBI crystallites act as a cross- linking junction of the fibrils in the *m*-PBI – PA gel. Therefore, we can conclude that *m*-PBI gel in PA is produced from fibrillar crystallites. The reason behind the

formation of semi - crystalline *m*-PBI in PA is due to the hydrogen bonding between *m*-PBI and PA. *m*-PBI possesses both hydrogen donor (- NH -) and hydrogen acceptor functionality into its imidazole ring which can easily take part in hydrogen bonding. The presence of hydrogen bonding in the gel sample is clearly observed from frequency shifts and peaks broadening in the IR spectra. The N – H stretching band of powder *m*-PBI at about 3422 cm^{-1} (sharp) displays a substantial displacement to lower frequency at about 3402 cm^{-1} (broad) in the *m*-PBI – PA gel sample. Detail IR and Raman studies are carried out to proof the hydrogen bonding and discussed in Chapter 6. Also PA molecules can form a chain by intermolecular hydrogen bonding. The two end of the PA chain can form hydrogen bond with two different *m*-PBI chains and help them to produce *m*-PBI crystallites. Since in the gelation condition PBI concentration is high, it is possible to align more *m*-PBI chains through hydrogen bonding and produce sufficient number of crystallites for gel formation.
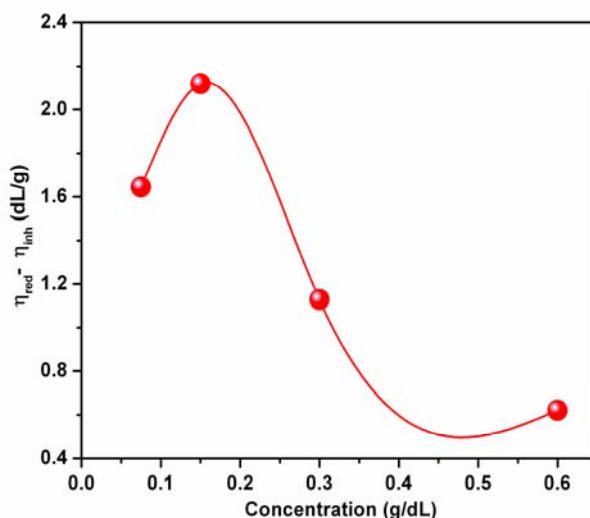
Figure 5.6. *Capillary wall effect test of m-PBI in phosphoric acid solution.*

5.3.4. Gelation Kinetics. The reciprocal of gelation time (t_{gel}) of the *m*-PBI solution is referred to as the gelation rate (t_{gel}^{-1}).[15-17] The tube tilting method for measuring gelation kinetics can only be used if the kinetics is reasonably fast. In case of *m*-PBI – PA gel the gelation time is very short, for example it is only 3 minutes for 7 % (w/v) solution at

30°C. Also, UV- Vis study (discussed in the following section) of very dilute solution such as 0.1 % (w/v) shows that the first step of the gelation process requires ~ 10 minutes in the leveling up of the absorbance value (Figure 5.9). Moreover, we have not observed gel formation below critical gelation concentration even after seven days at 30°C. Therefore, above observations suggest that the *m*-PBI – PA gelation kinetics is reasonably fast and can be measured by tube tilting method. A plot of gelation rate (t_{gel}^{-1}) against the *m*-PBI concentration at different gelation temperature (T_{gel}) is presented here in Figure 5.7. The t_{gel}^{-1} is varying non-linearly with gelation concentration at different temperature. Therefore, the t_{gel}^{-1} can be written as $t_{gel}^{-1} \propto f(C)f(T)$, where *f* (*C*) and *f*(*T*) are the concentration and temperature function of the gelation process respectively.[15-17] The critical gelation concentrations ($C^{*}_{t\ =\ \infty}$) are obtained by extrapolating each curve to zero gelation rate and presented in Table 5.1. The extrapolation is carried out by non-linear fit of the kinetic data using Origin 6.1 software. Figure 5.7 and Table 5.1 clearly indicate that both t_{gel}^{-1} and $C^{*}_{t\ =\ \infty}$ are highly dependent on the gelation temperature.[26] The effect of molecular weight of the *m*-PBI on the gelation rate are discussed in the Chapter 6.
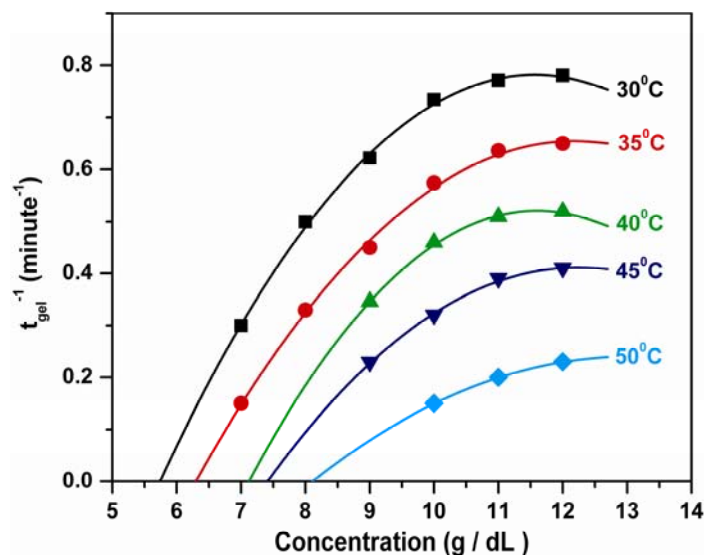
Figure 5.7. *Gelation rate vs. concentration plot at different temperature.*

Table 5.1: $C^{*}_{t=\infty}$ *obtained from Figure 5.4 at different temperature.*

Temperature (°C)	$C^{*}_{t=\infty}$ (g /dL)
30	5.73
35	6.29
40	7.11
45	7.41
50	8.11

5.3.5. UV – VIS Spectroscopic Study. We have monitored the change in absorbance value with time of the dilute *m*-PBI solution spectrophotometrically. Unfortunately, we are unable to follow this absorbance change above critical gelation concentration because of very high absorbance value of the *m*-PBI – PA solution. The hot homogeneous 0.1 % (w/v) solution was transferred into the quartz cell and immediately UV- Vis. spectra from 800 – 400 nm were recorded in every 1 minute time interval for 1 hour at 30°C and presented in Figure 5.8. Two peaks at around 440 nm and 480 nm are observed due to n → π* transitions of bibenzimidazole groups In addition, a new shoulder at around 615 nm is developed and red shift is observed gradually with time. In contrast, we have not observed any growing shoulder at ~ 615 nm in case of control experiments with benzimidazole and bibenzimidazole molecules (Scheme 4.1) in the similar condition. Therefore, it can be argued that a conformational transformation takes place of the polymer chains at the gelation temperature. The Figure 5.9 shows that the absorbance at 615 nm increases with time indicating that the conformational transition is a kinetically controlled process. We would expect an increase of the transformed conformer's concentration with increasing *m*-PBI concentration in the solution. Finally, when the *m*-PBI concentration exceeds the critical gelation concentration, transformed conformers are aggregated themselves and produce the *m*-PBI crystallites which results the gel. Therefore, the gelation occurs in two steps: first, a conformational transition and then aggregation.
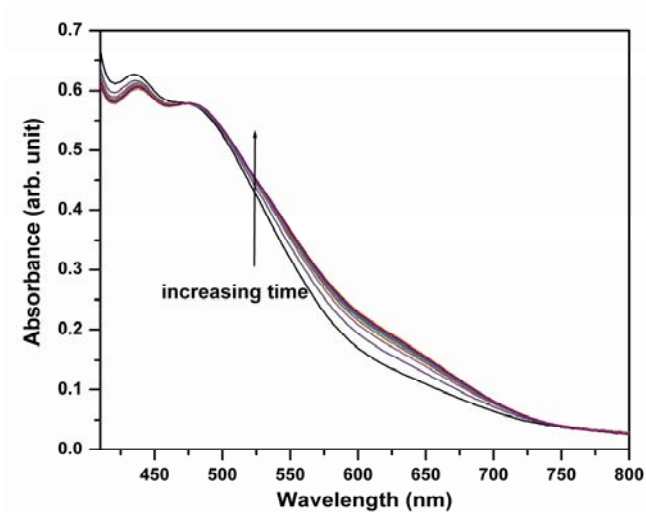
Figure 5.8. *UV – Vis. spectra of 0.1 % (w/v) m-PBI – PA solution at 30^oC recorded for 1 hour duration.*
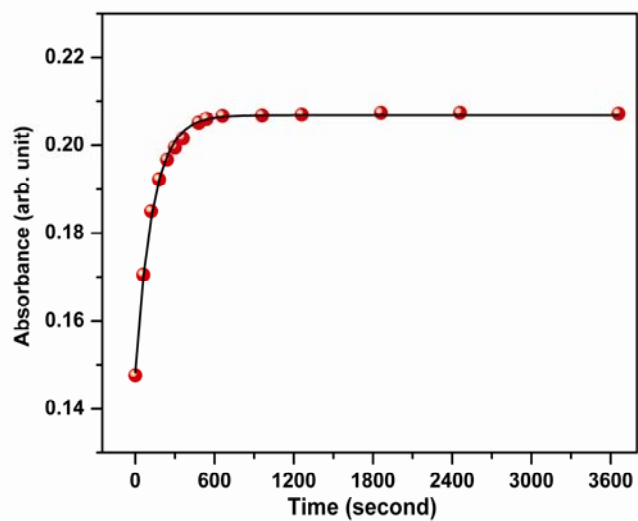
Figure 5.9. *Absorbance at 615 nm vs. time plot obtained from Figure 5.8.*

5.3.6. PA doping level. An effort has been made to prepare the PA doped *m*-PBI membrane from the gel. The PA doping level was measured by titrating a piece of membrane against NaOH and calculated as the number of PA mols per *m*-PBI repeat

unit. In our study, the doping level of the membrane is $\sim 35 - 40$ moles per PBI repeat unit when made from a solution above $C^{*}_{t=\infty}$ such as 8 % (w/v), considerably higher than the previously reported value for *m*-PBI (Scheme 4.1). The typical values of highest PA doping level reported in the literature are $\sim 15 - 20$ mols per repeat unit [11, 13, 27]. It seems obvious that gelation enhances the PA doping level enormously.

5.4. Conclusion

Thermoreversible gelation of *m*-PBI in PA has been developed and studied thoroughly. SEM and DSC experiments indicate the presence of fibrillar morphology and reversible phase transition respectively. WAXS study proves the presence of crystallites in the gel. The gelation occurs in a two step process of conformational transformation followed by aggregation. The membrane produced from the gel solution shows very high PA doping level.

References

(1)   Russo, P. S, *"Reversible Polymeric Gels and Related Systems"*, Ed, ACS Symposium Series, American Chemical Society, New York, **1986**.

(2)   Guenet, J. M. *"Thermoreversible Gelation of Polymers and Biopolymers"*, Academic Press: London, **1992**.

(3)   Vikki, T.; Ruokolainen, J.; Ikkala, O. T.; Passiniemi, P.; Isotalo, H.; Torkkeli, M.; Serimaa, R.; *Macromolecules* **1997**, *30*, 4064.

(4)   Jana, T.; Nandi, A. K. *Langmuir* **2000**, *16,* 3141.

(5)   Berghmans, H. *"Integration of Fundamental Polymer Science and Technology"*, *P. J.* Lemstra, L. A. Kleintjens, Eds, Elsevier Applied Science: London, 1988, Vol. 2, p 195.

(6)   (a) Kojima, T. *J. Polym. Sci. Polym. Phys. Ed.* **1980**, *18*, 1685. (b) Ghosh, S.; Sannigrahi, A.; Maity, S. *J Phys Chem B* **2010**, *114*, 3122.

(7)   Musto, P.; Karasz, F. E.; Macknight, W. J. *Macromolecules* **1991**, *24*, 4762.

(8)   Savinell, R.; Yeager, E.; Tryk, D.; Landau, U.; Wainright, J.; Weng, D.; Lux, K.; Litt, M.; Rogers, C. *J. Electrochem. Soc.* **1994**, *141*, L46.

(9)   Samms, S. R.; Savinell, R. F. *J. Electrochem. Soc.* **1996,** *143,* 1225.

(10)   Weng, D.; Wainright, J. S.; Landau, U.; Savinell, R. F. *J. Electrochem. Soc.* **1996**, *143*, 1260.

(11)   Mecerreyes, D.; Grande, H.; Miguel, O.; Ochoteco, E.; Marcilla, R.; Cantero, I. *Chem. Mater.* **2004**, *16,* 604.

(12)   Xiao, L.; Zhang, H.; Jana, T.; Scanlon E.; Chen, R.; Choe, E.-W.; Ramanathan, L. S.; Yu, S.; Benicewicz, B.C. *Fuel Cells* **2005**, *5*, 287.

(13)   Xiao, L.; Zhang, H., Scanlon, E., Ramanathan, L. S.; Choe, E.-W.; Rogers, D.; Apple, T.; Benicewicz, B. C.; *Chem. Mater.* **2005**, *17*, 5328.

(14)   Buckley, A.; Stuetz, D.; Serad, G. A. *Encyclopedia of Polymer Science and Engineering,* Ed. J. I. Kroschwitz, Wiley, New York, **1987,** Vol 11, p – 577.

(15)   Dikshit, A. K. ; Nandi, A. K. *Macromolecules* **1998**, *31*, 8886.

(16)   Malik, S.; Jana, T.; Nandi, A. K.; *Macromolecules* **2001**, *34*, 275.

(17) Dikshit, A. K.; Nandi, A. K.; *Langmuir* **2001**, *17*, 3607.

(18) Daniel, C.; Dammer, C.; Guenet, J. M.; *Polymer* **1994**, *35*, 4243.

(19) Conclatori, A. B.; Chenevey, E. C.; Noether, H. D.; Dunay, M. U.S. Patent 3495931, (1970).

(20) Iwakura, Y.; Uno, K.; Imai, Y. *J. Polym. Sci. Part A* **1964**, *2*, 2605.

(21) Qingfeng, L.; Hjuler, H. A.; Bjerrum, N. J. *J. of Applied Electrochemistry* **2001**, *31*, 773-779.

(22) *Symposium on Fibrous Materials* compiled by Ross, J. H. **1963**, p 57, ASD –TDR 62-964.

(23) Fuoss, R.M.; Strauss, U.P. *J. Polym. Sci.* **1948**, *3*, 246.

(24) Johnston, N. J.; Epps, L. B. *J. Polym. Sci.* **1972**, *10*, 275.

(25) Oene Van, H. ; Cragg, L. H. *Nature*, **1962**, *196*, 1197.

(26) Guenet, J. M. *J. Rheol.* **2000**, *44*, 947.

(27) Li, Q.; Hjuler, H. A.; Bjerrum, N. J. *J. Appl. Electrochem* **2001**, *31*, 773.

Chapter 6

Detailed Insights of meta-Polybenzimidazole Thermoreversible Gelation in Phosphoric Acid

---
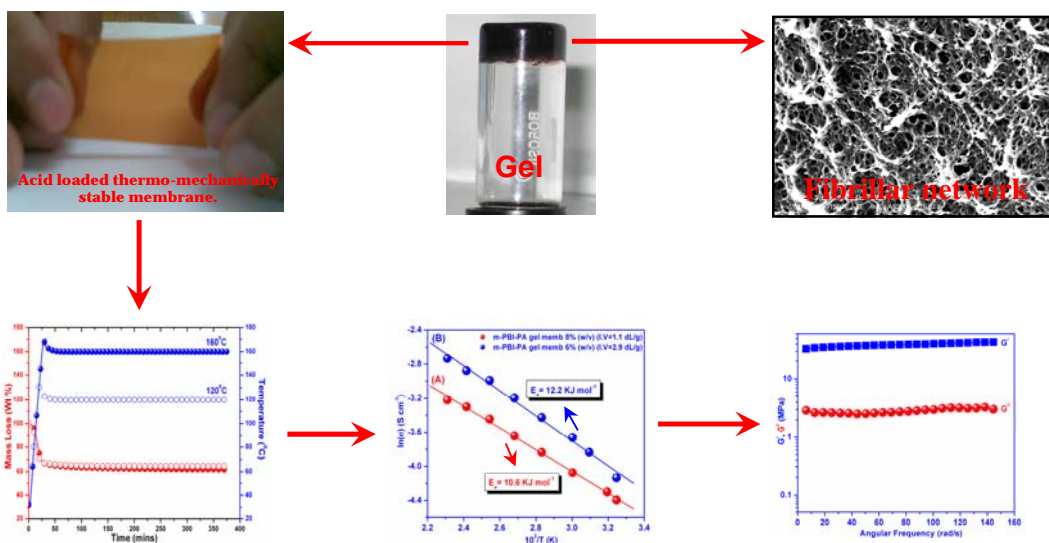
Thermoreversible gelation of meta-polybenzimidazole (m-PBI) in phosphoric acid (PA) is studied by varying the gel concentration and the polymer molecular weight. The PA doped m-PBI obtained from the m-PBI-PA gel has remarkably high loading, excellent thermo-mechanical stability and high durability. This membrane displays high and faster proton conduction behavior.

6.1. Introduction

Polymer gels are most interesting materials for their versatility in application in different areas of materials science[1-2]. The intrinsic stiffness of polymer chains or enhancements of the persistence chain length of the polymers are the major ingredients for the formation of thermoreversible fibrillar gel[3]. Thermoreversible gels most often called physical gels because of the interactions involved in the formation of fibrillar gels are hydrophobic, hydrogen bonding and electrostatic interactions between certain segments of the polymer chains. These interactions are in the order of kT and therefore they can be easily destructed and reformed reversibly by heating and cooling. In contrary chemical gels are thermo irreversible and form due to the covalent bond formation. The physical gelation mechanism depends on the polymer and solvent pairs interaction that brings in crystallization, conformation ordering, liquid-liquid phase separation, mesomorphic phase transition[1, 2, 4] etc.

Meta-Polybenzimidazole (*m*-PBI) (Scheme 4.1) is an aromatic heterocyclic thermally stable basic polymer (pK$_a$ ~5.25), acts as a proton acceptor like in a normal acid–base reaction. It possesses both proton donor (- NH -) and proton acceptor (- N =) hydrogen bonding sites which exhibit specific interaction with the polar solvents[5-7] and forms miscible blends with variety of polymers[8-10]. meta-Polybenzimidazole has excellent thermal and chemical resistance, fire retarding capacity, insulating property and it forms good textile fiber[11]. However, the poor solubility of *m*-PBIs resulting from the highly rigid polymer backbones and the strong interchain hydrogen bonding interaction makes them hard to process[12]. Phosphoric acid (PA) doped meta-polybenzimidazole (*m*-PBI) membranes are considered as one of the most attractive alternatives to Nafion in high temperature polymer electrolyte membrane fuel cells (HTPEMFCs) application[13-17]. It has been shown that the PA doped *m*-PBI exhibits high proton conduction at high temperature up to 200°C, excellent oxidative and thermal stability, low gas permeability, and nearly zero water drag coefficient[18-20]. Various attempts have been made so far for the fabrication of the PA doped *m*-PBI membranes, these include casting of *m*-PBI membrane from dimethyl acetamide (DMAc) solution followed by soaking in phosphoric acid (PA) [21-24], via sol–gel process by direct casting

of the high molecular weight *m*-PBI solution in polyphosphoric acid (PPA) [25-28] and leaching out low molecular weight compound (porogen) from polymer / porogen mixture and then soaking it in PA solution[29]. Recently, (Chapter 5) we have fabricated membrane from a novel thermoreversible *m*-PBI gels in PA[30].

A large number of synthetic approaches have been attempted through the modification of the polymer backbone[31-36] as well as the side chain[37-39] to obtain the new PBI and hence the PA doped PBI membranes. The major obstacle is to get a membrane with high acid doping level and as well as moderately good mechanical stability. Often, if the acid content of the membrane is too high it forms soft plastic type material which is very difficult to process and possess very poor mechanical stability.[40] In addition, if the PA doped membrane does not have good thermal stability then above 160ºC leaching of the free phosphoric acid from the membrane is observed, which causes a drop in conductivity of many orders of magnitude during fuel cell operation.[41] Hence to get a superior quality membrane, a compromise between these two important parameters (acid loading and mechanical strength) has to be maintained. We have reported the thermoreversible gelation of *m*-PBI in phosphoric acid (PA) earlier.[30] We proposed that gelation of *m*-PBI in PA are two step processes; where coil-to-rod transformation takes place followed by the aggregation of the rods which yields the gel.

In this chapter, we report detailed insights of thermoreversible gelation of *m*-PBI in PA solution by elucidating the gelation kinetics, thermodynamics, gel morphology and structures. We have looked into the gelation behavior and mechanism by varying the *m*-PBI molecular weight and the concentration of the polymer in the gel (gelation concentration). We have utilized infrared spectroscopy (FT-IR), Raman spectroscopy (FT-Raman), differential scanning calorimetry (DSC), thermogravimetric analysis (TGA), dynamic mechanical analysis (DMA), UV-visible spectroscopy, test tube tilting for gelation kinetics, scanning electron microscope (SEM), transmission electron microscope (TEM) techniques. Finally, we have prepared PA doped *m*-PBI membrane from various molecular weight *m*-PBI and by varying the gelation concentration. Also, we have studies the proton conduction behavior of these membranes with temperature and tested their durability at high temperature.

6.2. Experimental Section

6.2.1. Materials. 3, 3', 4, 4' – tetraaminobiphenyl (TAB) and polyphosphoric acid (115%) were purchased from Sigma – Aldrich. Isophthalic acid (IPA) was purchased from SRL, India and purified by recrystallization in water and ethanol (2:8) mixture prior to use.. Phosphoric acid (85%) and sulfuric acid (98%) were received from Merck, India. All chemicals were used as received.

6.2.2. Polymer Synthesis. The m-PBI synthesis procedure is same as described elsewhere.[30,31] Briefly it is as follows: equal moles amount of TAB and IPA were taken into a three-neck round bottom flask along with polyphosphoric acid (PPA). The reaction mixture was stirred by using a mechanical overhead stirrer and a slow stream of purged moisture free nitrogen gas was maintained throughout the reaction. The reaction mixture was placed in a digitally controlled temperature oil bath and the temperature was controlled step wise throughout the reaction. Typically polymerization was carried out at 190-210°C for approximately 26 hours. The reaction mixture became more viscous and developed a dark brown colour at the end of the polymerization. The reaction mixture was poured into double distilled water and isolated as brown mass. The mass was pulverized, neutralized with sodium bicarbonate, washed thoroughly with water and finally dried in a vacuum oven for 24 hours at 100°C to obtain the dry meta-PBI for further characterization. The various molecular weights m-PBI was obtained by varying the polymerization conditions especially by altering the monomer concentrations at the beginning of the polymerization.

6.2.3. Viscosity. The viscosity of the polymer was measured in H_2SO_4 (98%) solutions at 30°C in a constant temperature water bath using a Cannon Ubbelohde capillary dilution viscometer (model F725) and the inherent viscosity (I.V.) values were calculated from the flow time data. The concentration of the polymer solution in H_2SO_4 was 0.2 g/dL for the viscosity measurements.

6.2.4. Gelation Kinetics. The gels were prepared by taking required amount of m-PBI polymer and PA in a sealed glass vial. Homogeneous red color solutions were made at 180°C, then it was quickly transferred in a preset water bath at a fixed temperature,

watched until the solution freezes upon tilting and becomes reddish brown color. These gels were transformed into solution and vice versa upon repeated heating and cooling cycle. The time at which no flow of the sample was observed by tilting the test tube was known as gelation time (t_{gel}).The reciprocal of gelation time (t_{gel}) of the PBI solution is referred to as the gelation rate (t_{gel}^{-1}). The tube tilting method for measuring gelation kinetics can only be used if the kinetics is reasonably faster and in the present case gelation occurs within 2-3 minutes. The gelation does not occur below a certain concentration even after waiting for 3 days.

6.2.5. IR and Raman Spectra. The IR spectra of the m-PBI and m-PBI gel were recorded on a (Nicolet 5700 FT-IR) FT-IR spectrometer. The FT-IR spectra of the gel sample were performed from the KBr pellet of the sample where as the FT-IR of m-PBI sample was taken from DMAc-film of thickness 30-40 µm. The Raman spectra recorded using a (Nicolet 6700 FT-RAMAN) Raman spectrometer equipped with 1064 nm diode laser. The exposure time was 35 s. The resolution was about 4 cm^{-1}.

6.2.6. Morphological Investigation. The morphology of the gel samples were studied using a Scanning Electron Microscope (SEM). For SEM study entrapped phosphoric acid (PA) was removed with water gradually from the gel samples by washing five to six time with Millipore water and vacuum dried at room temperature for 3 days. Then they were gold-coated and their micrographs were taken in a SEM apparatus (Philips – XL30ESEM). The Transmission Electron Microscope (TEM, FEI Tecnai Model No. 2083) working at 120kV used to study the gel morphology. The TEM samples were prepared by putting a drop of dilute solutions of gel sample on a carbon coated copper grid of 200 mesh size. Then the grid was dried in vacuum oven at 120ºC for 24 hours.

6.2.7. Fabrication of PA doped *m*-PBI gel membrane. The *m*-PBI gel in PA was heated at 180ºC to make the homogeneous solution and then this solution was poured in a glass petri dish immediately. The solution formed gel within 2-3 minutes and we obtained PA doped PBI gel membrane.

6.2.8. Thermal Measurement. Differential scanning calorimetry (DSC) experiments were performed in a Pyris Diamond DSC (Perkin-Elmer) instrument under nitrogen atmosphere. The gel samples were taken in a large volume capsule (LVC) pan. The

samples were scanned from 30°C to 160°C at the heating rate of 10°C/min and from 160°C to 30°C at the cooling rate of 5°C/min. The heating and cooling scans were performed repeatedly to check the reproducibility. The DSC instrument was calibrated with indium and zinc before each set of experiments. The thermogravimetric analysis (TGA) of PA doped *m*-PBI gel membranes samples were carried out on a (Netzsch STA 409PC) TG-DTA instrument from 30 to 800°C with a scanning rate of 10° C/min. Isothermal heating scan of the PA doped *m*-PBI gel membrane samples were also performed at different temperature such as 120°, 160° C in the presence of nitrogen flow for six hours.

6.2.9. Absorption Spectroscopy. The UV-Visible spectroscopic study was carried out in a UV-Vis-NIR spectrophotometer (Shimadzu 3101PC) using a 1 mm. path length quartz cuvette. 0.1 % (w/v) PBI solutions in PA were made at 180°C and immediately transferred to the spectrophotometric cell, which was kept at the gelation temperature.

6.2.10. PA Doping Level. The PA doping level of PBI gel membranes were determined by titrating of a membrane samples with standardized 0.1(N) sodium hydroxide solutions using a Metrohm Titrino Titrator (702). The dry weight of the polymer was obtained by washing the samples with water and then drying in vaccum oven at 100^oC for 24 hours. The acid doping levels are expressed as mols of phosphoric acid per mole of PBI repeat unit. The acid doping level was calculated as follows:

$$\text{Acid (PA) doping level} \quad = \frac{V_{NaOH} C_{NaOH}}{W_{dry}} M_w$$

Where V_{NaOH} and C_{NaOH} are the volume and the molar concentration of the sodium hydroxide, respectively. W_{dry} is the dry polymer membrane weight and M_w is the molecular weight of the polymer repeat unit. For each sample, at least three similar size pieces of samples were titrated and the acid doping level reported is the average of these three.

6.2.11. Mechanical Property Study. The mechanical properties of the PA doped m-PBI gel films were measured using a dynamic mechanical analyzer (DMA) (TA

Instruments, model Q-800). PA doped *m*-PBI gel films of 25 mm × 5 mm × 0.05 mm (L × W × T) dimensions were cut and clamped on the film tension clamp of the pre-calibrated instrument. The storage modulus (G'), loss modulus (G") were measured by frequency swept process with a preload force at 0.01N.

6.2.12. Stress-Strain Study. The stress-strain relationship of the PA doped *m*-PBI gel membranes were measured utilizing a Zwick/Roell Universal Tesing Machine (Z005) with 0.3(N) load cell. Dumb-bell specimens were cut following the ASTM standard D653 (Type V specimens). Tensile properties of all films were measured in an air atmosphere at room temperature with a cross head speed of 1 mm min^{-1}.

6.2.13. Conductivity Study. The proton conductivity is generally obtained by measuring the resistance of the proton-conducting membrane against the flow of either alternating current (ac) or direct current (dc). We have measured the protonic conductivities by using a four-probe impedance method by using a Zahner Impedance spectrometer (ZENNIUM PP211) over a frequency range from 1 Hz to 100 kHz. A rectangular size PBI membrane (1.5 cm × 4.0 cm) and four platinum wire current collectors were set in a home made Teflon cell (picture is shown in the results section). Two outer electrodes (1.5 cm apart) supply current to the cell, while the two inner electrodes 0.5 cm apart on opposite sides of the membrane measure the potential drop. The four-probe technique offers many advantages over the two-probe technique which includes (1) measures the bulk property of the membrane instead of the surface property and (2) minimizing the error stemming from contact resistance and electrode resistance. For the temperature dependence proton conductivity measurement the cell was placed in an oven. The membranes were dried at 100°C by heating and holding at 100°C isothermally for 2 hours. The membrane samples were then cooled in a vacuum oven and taken out just before conductivity measurement in an effort to keep the samples dry. The conductivities of the membranes were measured from room temperature to 160°C at 20°C intervals. Before the measuring the conductivity, the samples were held in the oven at each temperature for 30 minutes. Reproducible results were obtained using the above temperature profile and testing procedure. A two-component model with an

ohmic resistance in parallel with a capacitor was employed to fit the experimental curve of the membrane resistance across the frequency range (the Nyquist plot). The conductivities of the membrane at different temperatures were calculated from the membrane resistance obtained from the ohmic resistance of the model simulation. Proton conductivity was then calculated from the following equation:

$$\sigma = \frac{D}{LBR}$$

where *D* is the distance between the two current electrodes 0.5 cm apart, *L* and *B* are the thickness and width, respectively, and *R* is the measured resistance value.

6.3. Result and Discussion.

6.3.1. Gelation Kinetics. The test tube tilting method is used to study the gelation kinetics of *m*-PBI in PA. We have measured the gelation kinetics for various molecular weight (inherent viscosity; this point onwards we refer it as I.V.) samples. The test tube tilting method for measuring gelation kinetics can only be used if the kinetics is reasonably fast. As mentioned in the experimental section, the current gelation is fast enough to apply this test tube tilting method. The reciprocal of gelation time (t_{gel}) is referred to as the gelation rate (t_{gel}^{-1})[42-45] which is measured for the PBI-PA solution as function of temperature and concentration for different I.V. samples and presented in the Figure 6.1. The critical concentration of *m*-PBI in PA below which gelation is not observed, is called as the critical gelation concentration ($C^*_{t=\infty}$) and this is an important parameter to study the gelation rate. Figure 6.1 represents the plot of t_{gel}^{-1} against the *m*-PBI concentration (wt %) at different gelation temperatures for various I.V. samples. In all the cases the gelation rates exhibit a non-linear relation with gelation concentration in all the gel temperatures. The critical gelation concentrations ($C^*_{t=\infty}$) are obtained from t_{gel}^{-1} vs. concentration plots by extrapolating each curve (Figure 6.1) to zero gelation rate and presented in Table 6.1 for various I.V. samples in all the gelation temperatures.
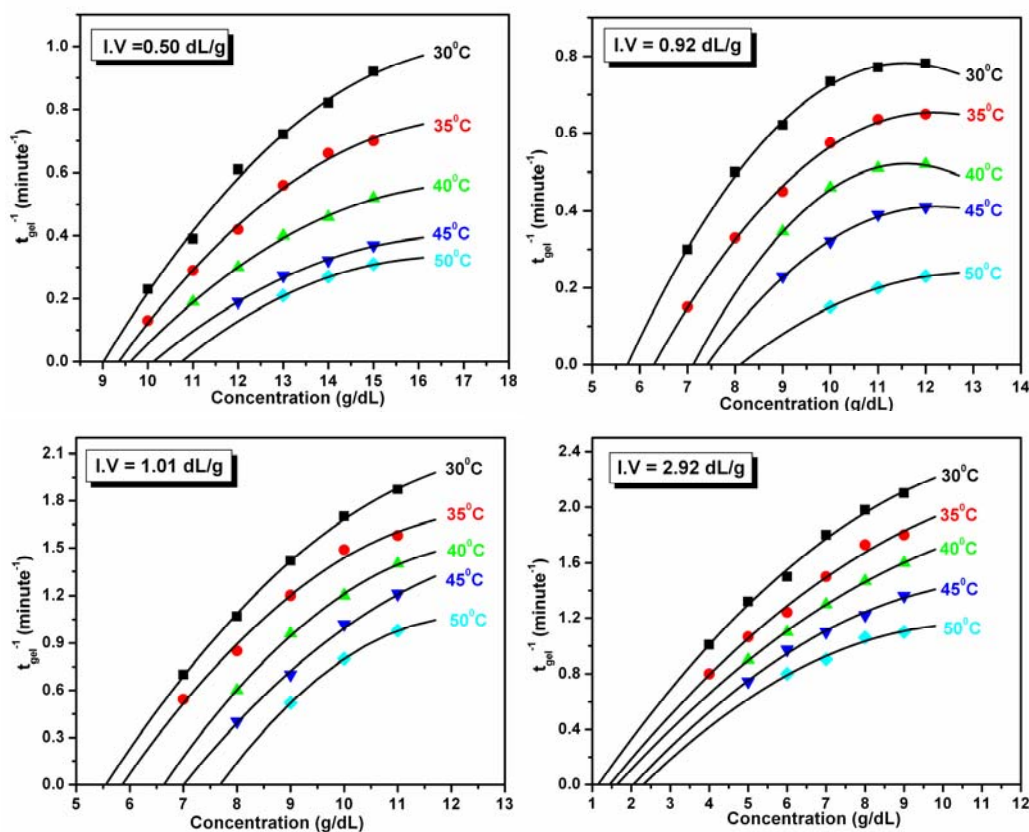
Figure 6.1. *Gelation rate (t_{gel}^{-1}) vs. concentration (g/dL) plot of different I.V m-PBI at different gelation temperatures.*

Figure 6.1 clearly demonstrates the t_{gel}^{-1} is dependent on both the gelation concentration and the gelation temperature. A careful observation of Figure 6.1 also indicates that t_{gel}^{-1} depends upon the molecular weight of the sample. To understand this dependency we have plotted the Figure 6.1 gelation kinetics data at a fixed temperature for different I.V. samples (Figure 6.2). The five plots are obtained for five different temperatures. The rate of gelation increases or other words time required for the gelation decreases with increasing the molecular weight (I.V.) of the *m*-PBI in all the gelation temperature (Figure 6.2). Also, it must be noted from Figure 6.2 that, much lower polymer concentration is required to obtain the gel in case of higher I.V. sample for all the gelation temperature. Therefore, it is expected that the $C^{*}_{t=\infty}$ should displays

the dependency on both the I.V. of the sample and the gelation temperature.[46] Table 6.1 data clearly proofs the above fact. A better observation of the dependency is obtained by plotting the $C^*_{t=\infty}$ against I.V. of the *m*-PBI for all the gelation temperature (Figure 6.3). $C^*_{t=\infty}$ decreases with increasing I.V. of the PBI at given temperature and increases with increasing gelation temperature for a given molecular weight (I.V.) of PBI (Figure 6.3 and Table 6.1). Therefore, the above discussion brings two important observations: t_{gel}^{-1} α f(C) f(T) f(I.V.) and $C^*_{t=\infty}$ α f(T) f(I.V.); where f(C), f(T) and f(I.V.)are the concentration, temperature and the molecular weight functions, respectively.

Table 6.1. *$C^*_{t=\infty}$ obtained for different I.V polymers at different temperatures from the Figure 6.1.*

I.V(dL/g)	Critical gelation concentration $C^*_{t=\infty}$ (g /dL)				
	30°C	35°C	40°C	45°C	50°C
0.50	9.02	9.38	9.63	10.12	10.77
0.70	8.06	8.50	8.89	9.50	10.02
0.92	5.73	6.29	7.11	7.41	8.11
1.01	5.55	5.86	6.65	7.01	7.71
2.92	1.16	1.14	1.62	2.07	2.33

The dependence of t_{gel}^{-1} on gelation concentration is obvious since the higher polymer concentration allows faster gelation. Similarly, lowering the gelation temperature helps the faster rate and hence we obtain lower $C^*_{t=\infty}$. However, the effect of molecular weight on both t_{gel}^{-1} and $C^*_{t=\infty}$ needs to be addressed. Our results show that the higher I.V. samples yield the gel readily with higher rate of formation. This is because of the size of the molecule; since higher I.V. samples are bigger in size, hence

they produce gel readily. Figure 6.1 and 6.3 attribute that higher I.V *m*-PBI sample has lower critical gelation concentration ($C^*_{t\,=\,\infty}$) compare to low I.V *m*-PBI and $C^*_{t\,=\,\infty}$ varies with temperature. Polymer having low $C^*_{t\,=\,\infty}$ indicates higher I.V polymer chains overlap more easily compare to low I.V polymer to produce gel at similar kinetics condition.
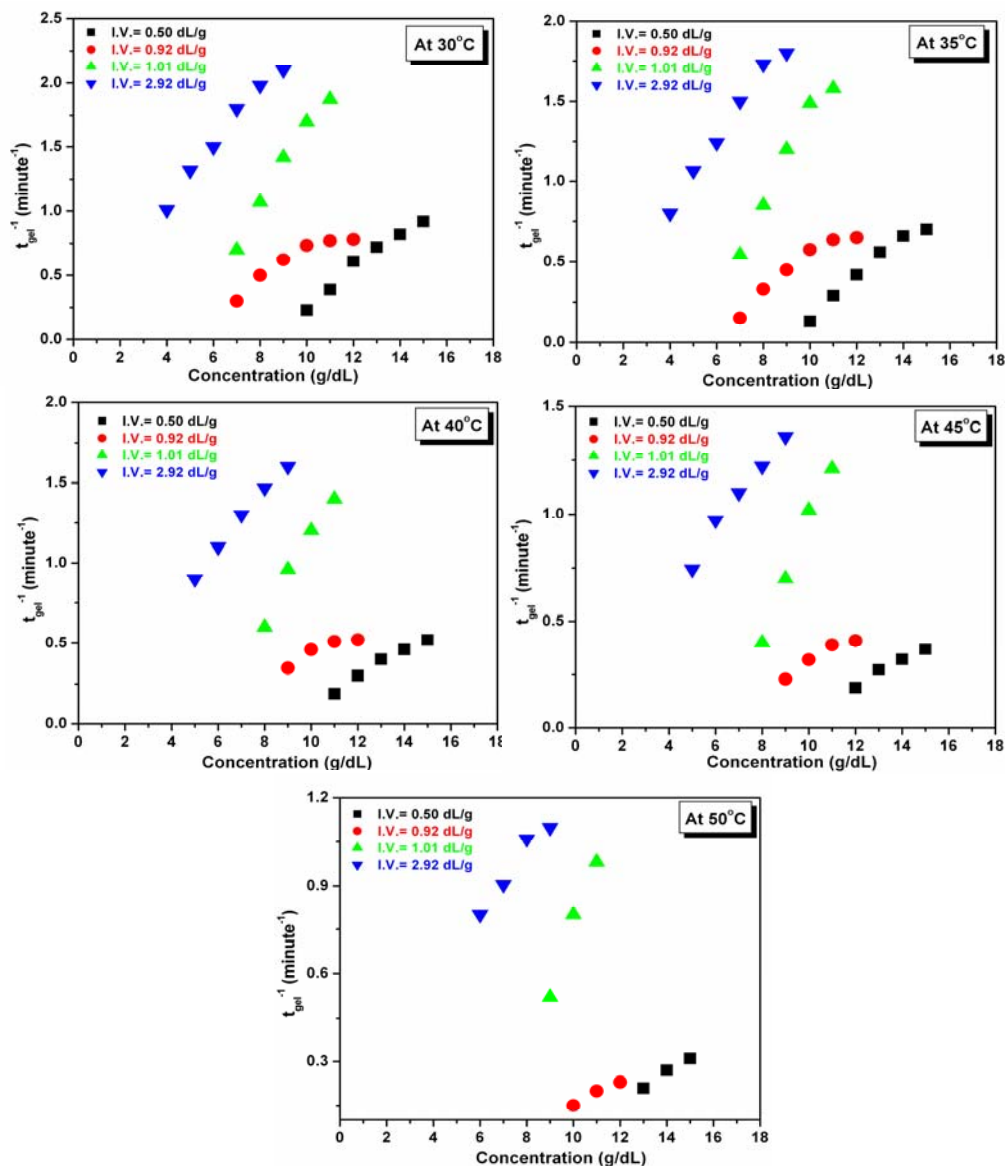
Figure 6.2. *Dependence of gelation kinetics on I.V. of m-PBI polymer at different temperature.*
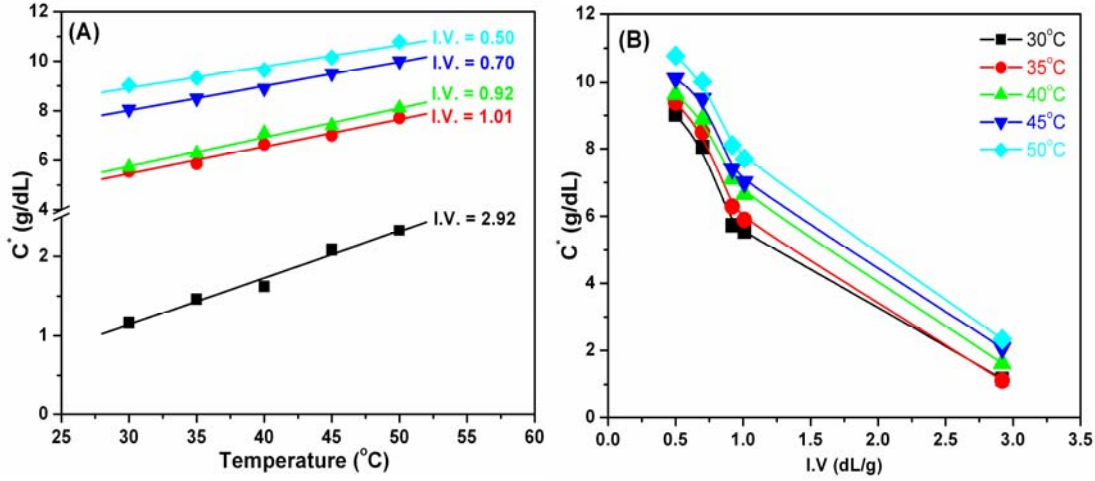
Figure 6.3: $C^*_{t=\infty}$ *vs temperature for different I.V polymers (A) and* $C^*_{t=\infty}$ *vs I.V. at different temperatures (B).*

The critical gelation concentration ($C^*_{t=\infty}$) and the gelation temperature (T_{gel}) can be related using equation (6.1) as proposed earlier by Eldridge and Ferry.[47,48]

$$\log C^* = \frac{\Delta H^o}{2.303 R T_{gel}} + \text{constant} \qquad (6.1)$$

Where, ΔH^o is the heat of reaction for the gelation process to produce 1 mol of cross-link in the gel. We have calculated the values of ΔH^o for different I. V. samples from the slopes of log $C^*_{t=\infty}$ vs. $1/T_{gel}$ plots (Figure 6.4). Data in the Figure 6.4 fit well in a straight line in all the cases. Figure 6.4 also supports our observation that the $C^*_{t=\infty}$ is a function of temperature and it increases with increasing temperature for a fixed I.V. samples. The ΔH^o values are calculated from the least square fitting (slopes) of the straight lines in Figure 6.4 and these values are plotted against the I.V. of the *m*-PBI in Figure 6.5. The values of ΔH^o increases linearly with increasing I.V. of *m*-PBI (Figure 6.5), attributing that higher heat of reaction involves for higher molecular weight *m*-PBI. Earlier, we have shown that the formation of crystalline *m*-PBI in PA is responsible for the thermoreversible gelation of *m*-PBI in PA.[30] These *m*-PBI crystallites act as a

physical junction point (or cross-linking point) for the gelation process. The higher ΔH^o value for higher I.V. *m*-PBI attributes that the higher amount of energy is required to produce the cross-linking junction for higher I.V. polymers. *m*-PBI is an amorphous polymer; however, crystallization can be induced in polyelectrolyte medium such as in PA medium[30] (Chapter 5). Therefore, the bigger *m*-PBI (high I.V.) will be highly amorphous and hence to bring the crystallinity for the gelation, higher heat of reaction is required. Therefore, the ΔH^o value increases with increasing I.V. of the *m*-PBI.
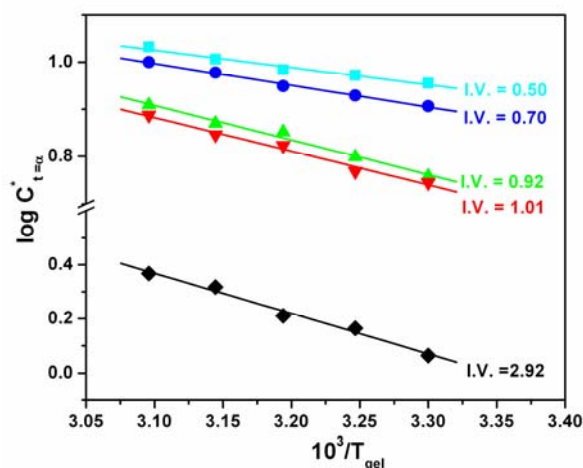

Figure 6.4. *log $C^*_{t=\infty}$ vs. 1/T_{gel} plot for m-PBI gels in PA. Different straight lines are obtained for the indicated I. V. of the m-PBI samples.*
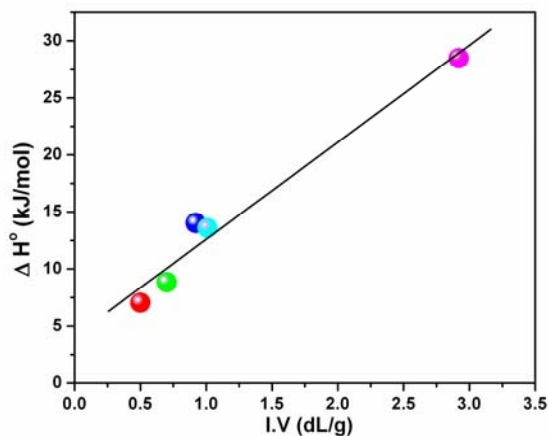

Figure 6.5. *Variation of ΔH^o with the molecular weight (I.V.) of m-PBI polymer in PA gel.*

6.3.2. FT-IR and Raman Spectra. FT-IR spectroscopy is used to understand the interaction between m-PBI and PA molecules in the gel state. The IR spectra of m-PBI and m-PBI gel in PA are presented in the Figure 6.6. Most of the m-PBI stretching bands have been widely discussed earlier by several authors in literature[49-51]. The most prominent bands of m-PBI are located in the 3500 to 3000 cm^{-1} region and these are mostly due to the N – H stretching of imidazole. These region can be divided into three distinct parts as: (i) a relatively sharp peak at 3420 cm^{-1} due to isolated, non hydrogen bonded free N – H groups; (ii) a very broad asymmetric peak centered at around 3161 cm^{-1} owing to self-associated, hydrogen bonded N – H groups; and (iii) a third low intensity peak at 3063 cm^{-1} due to the stretching modes of the aromatic C- H groups. PBI possesses both hydrogen donor (- NH -) and hydrogen acceptor (-N=) sites which can easily take part in hydrogen bonding interaction with suitable solvent molecules[7, 52] and other polymers.[8-10] The hydrogen bonding interaction of m-PBI with variety of polymers forms miscible blends, and with solvents induces the aggregation of *m*-PBI molecules. These are demonstrated in the literature by us and several other groups.[7-10,52] The IR spectral nature of the *m*-PBI and its gel in PA exhibits significant differences as seen in Figure 6.6. The presence of hydrogen bonding in the gel sample is clearly observed from the frequency shifts and peaks broadening in the IR spectra. The N – H stretching band of powder *m*-PBI at about 3420 cm^{-1} display a substantial displacement to lower frequency at about 3402 cm^{-1} in the *m*-PBI – PA gel sample. Also the peak broadening of N-H stretching bands of *m*-PBI in the gel sample is observed (Figure 6.6). These observations are very clear cut proof for the effective hydrogen bonding between *m*-PBI and PA molecules. The stretching band at 2358 cm^{-1} in case of gel sample is attributed to the stretching vibration of NH$^+$ indicating the protonation of *m*-PBI takes place on the imino nitrogen group of the *m*-PBI. The C=C/C=N stretch at 1620 cm^{-1} of *m*-PBI moves to higher wavenumber at 1635 cm^{-1} in gel sample. This is possibly due to the modification of electronic structure and electron delocalization owing to the protonation of imino nitrogen. This is also possible because of the hydrogen bonding interaction between PA molecules and the NH functionality of *m*-PBI. The spectral domains (1550-800 cm^{-1}) corresponding to various ring vibrations of *m*-PBI are not

observed in the gel sample, since the vibrations of PA are overshadowed them owing to the fact that in the gel sample large quantity of PA is present.[53] The stretching bands of m-PBI gel sample originate from both H_3PO_4 and phosphates ($H_2PO_4^-$) species. The bands in *m*-PBI-PA gel sample at 1003 and 887 cm^{-1} are due to free H_3PO_4 molecules. However, 1150 stretching represents the P=O symmetric stretching of $H_2PO_4^-$ species. Hence we can conclude that in the gel sample both ionic species ($H_2PO_4^-$) and pure PA molecule (H_3PO_4) are present and they are in dynamic equalibrium.[53] This equilibrium is established in the gel sample is due to the effective strong hydrogen bonding between the solvent (PA) and polymer (*m*-PBI) molecules.

Raman spectra have been utilized before to establish the physical interaction (hydrogen bonding) of *m*-PBI with PA in the doped state. In the previous section our IR study proved the presence of very strong hydrogen bonding interaction between the *m*-PBI and PA in the gel state. We have used Raman spectra to strengthen our argument further. Raman spectra of *m*-PBI and *m*-PBI gel are shown in Figure 6.7. These Raman bands have been discussed previously.[54-56] Figure 6.7 clearly exhibits significant difference in the spectral nature between PBI powder and gel sample. Band shifting and change in relative intensity are observed for the gel sample. The region 1630 to 1500 cm^{-1} corresponds to the benzimidazole ring vibration. m-PBI shows peak at 1610, 1589, and 1533 cm$^{-1;}$ these peaks are attributed to C=N and C=C vibration. In the gel sample these peaks are shifted towards higher wavenumber and also some of them losses their intensity. Similarly peaks at 1443, 1228, 1000, and 954 of m-PBI powder responsible for various ring vibration are displayed either shifting or reduction in their intensity in the gel sample. All these observations attribute strong physical interactions (hydrogen bonding) between *m*-PBI and PA molecule. The presence of pure PA in gel sample is also proved from the appearance of Raman peaks at 912 cm^{-1}.
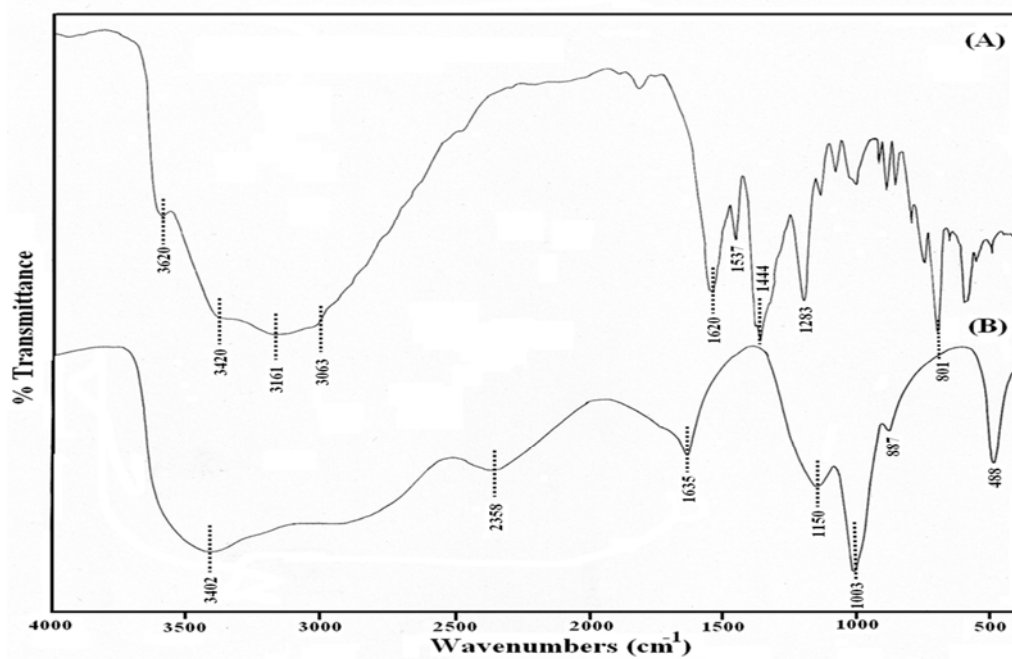
Figure 6.6. *FT-IR spectra of (A) m-PBI polymer and (B) m-PBI gel in PA. The important stretching bands are shown by the dotted lines in the figure.*
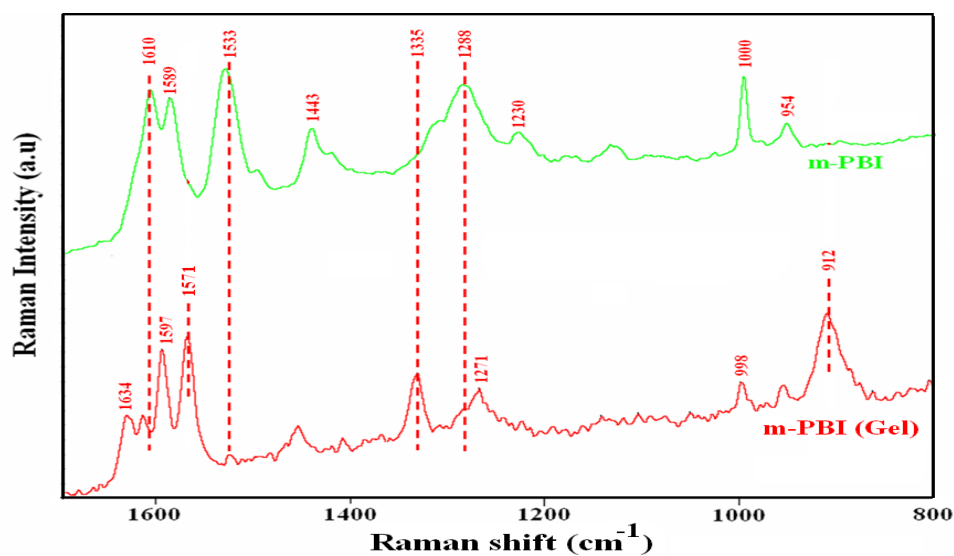

Figure 6.7. *Raman spectra of m-PBI and m-PBI gel in PA. The important peaks which are discussed in the text are shown by dotted lines in the figure.*

6.3.3. Morphology Study. Polymer gels exhibit very distinct morphological features in the gel state and these features differ significantly from the parent polymer morphology. A large number of polymer gels especially gels with thermoreversible characteristic display very unique morphological features. It has been demonstrated in the literature that fibrillar network type morphology is the signature morphology of thermoreversible gels.[30, 42-46] The solid powder *m*-PBI, which is not treated with any solvent, does not show any morphology rather it is almost featureless (Figure 6.8). The morphologies obtained from SEM and TEM studies of dried PBI –PA gels are presented in the Figure 6.8. It must be noted that we have adapted a special drying technique to dry the gel samples without destroying the morphological features of the gel samples. We have used the substitution drying method, in which we have substituted high boiling PA solvent with relatively low boiling solvent water gradually, to retain the morphological features. The removal of PA by freeze drying and simple evaporation was unsuccessful owing to the high boiling point and low volatility of PA.

It is evident from the SEM and TEM pictures (Figure 6.8) that the three dimensional network morphology consisting of fibrils are present in the gel sample. However, the SEM micrograph obtained from the sample with polymer concentration below critical gelation concentration has no such type of fibrils network structure (Figure 6.8B). Although some fibrils with very small length are visible but no network structure is not seen. These above observations clearly demonstrates that the *m*-PBI, which does not have any morphological features in powder state (Figure 6.8A), produces fibrils after treatment with PA and these fibrils form network structure in the higher concentration (gel state). The TEM image also support the fibrillar network morphology formed in the dried gel (Figure 6.8 D).
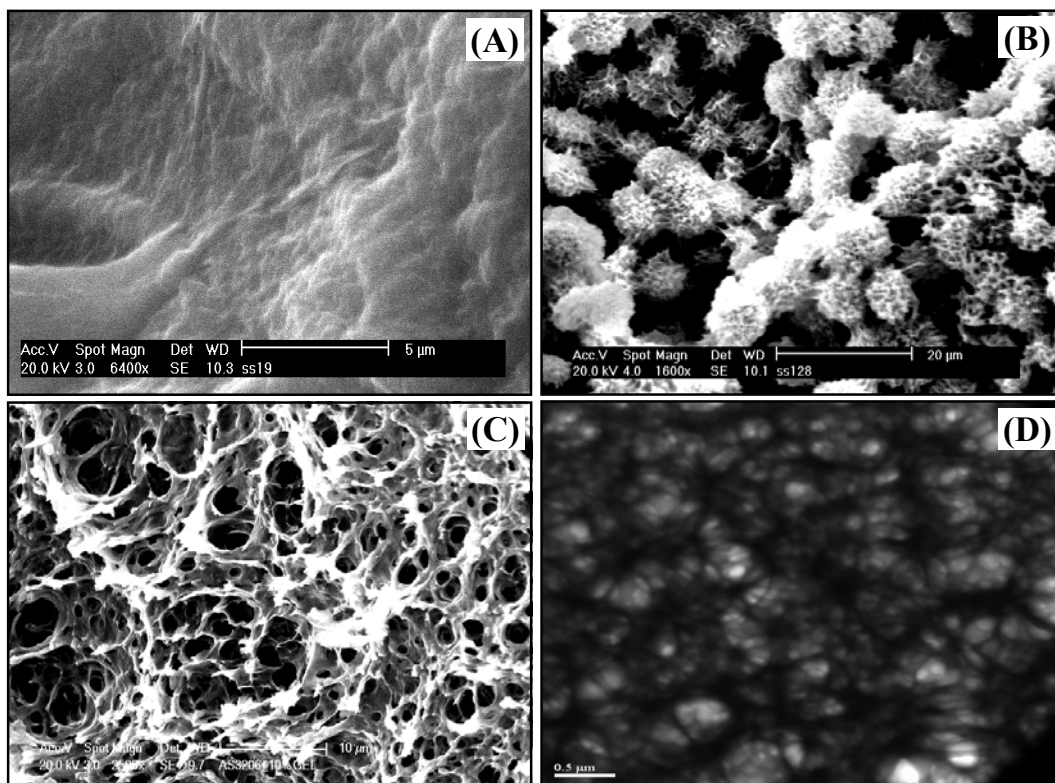
Figure 6.8. *SEM micrographs of (A) m-PBI powder (B) m-PBI sample treated with PA below $C^*_{t\,=\,\infty}$ (C) 10% (w/v) m-PBI-PA gel and (D) TEM micrograph of m-PBI-PA gel. The I.V. of m-PBI sample used here is 1.01 dL/g.*

Figure 6.9 represents the dependence of gel morphological behavior upon the *m*-PBI concentration in the gel sample (gelation concentration) of fixed molecular weight (fixed I.V.) *m*-PBI. The SEM micrographs shown in the Figure 6.9 are obtained from the various gelation concentrations (% w/v) and the drying processes for all the samples are identical. A significant change in the morphological feature is observed with changing the gelation concentration (Figure 6.9). A careful comparison of the micrographs brings the following observations with increasing gelation concentrations: increase in number of fibrils, decrease of fibrils thickness, increase in fibrils length and most importantly significant increase in fibriller network density (number of fibrils crossing each other per unit area). We have observed the similar morphology

dependence repeatedly for various I. V. PBI samples. Also we have noticed that at higher concentration the gels are very stable and the time required for the gelation is very small (discussed previously in the gelation kinetics); thus the morphological study attributes that the polymer concentration (gelation concentration) plays an important role for the gel formation. Higher polymer concentration favors the formation of large number of thinner and longer fibrils. This allows the fibrils to overlap rapidly and strongly resulting faster gelation rate and high network density.
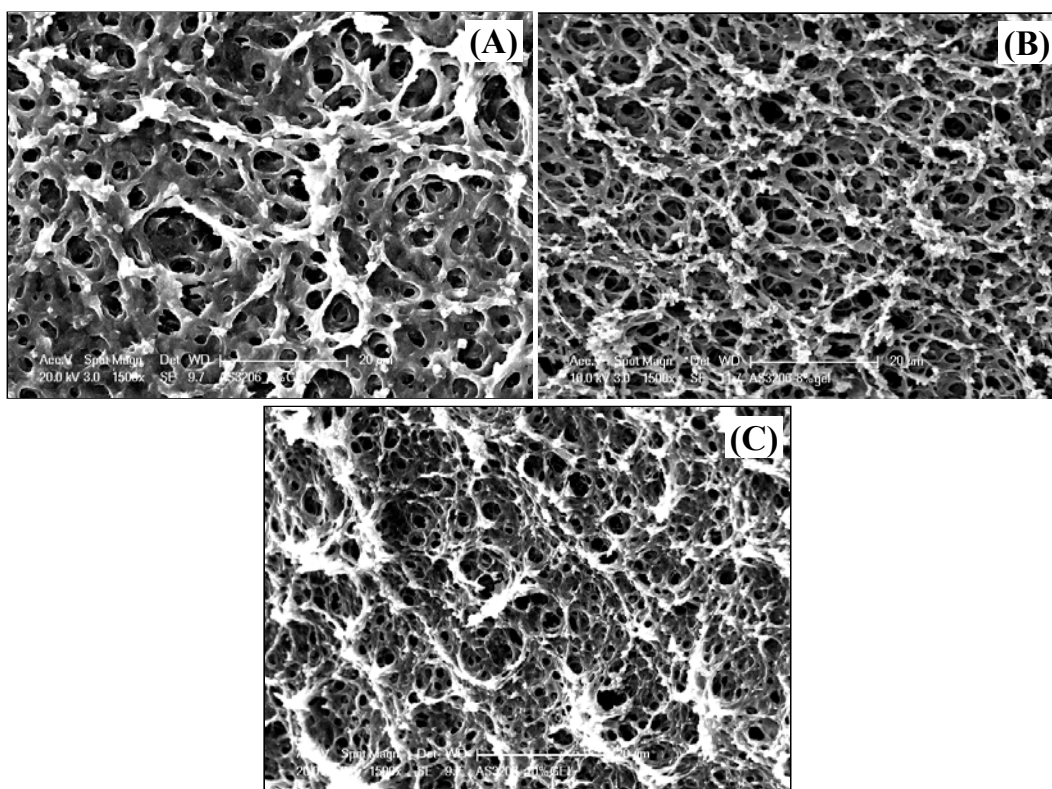
Figure 6.9. *SEM micrographs of m-PBI-PA gels of various m-PBI concentrations (w/v) (A) 6% (B) 8% and (C) 10%. The I.V. of m-PBI sample used here is 1.01 dL/g. Note that all micrographs presented here are in identical magnification (1500X).*

Gelation kinetic studies presented in the previous section demonstrated that the molecular weight of the *m*-PBI influences the gelation rate; higher I.V. *m*-PBI yields gel

in a faster rate. Also, the lower critical gelation concentration ($C^*_{t=\infty}$) is obtained for higher I.V. *m*-PBI (Table 6.1). The faster gelation rate, low $C^*_{t=\infty}$ for higher I.V. *m*-PBI are due to fact that the bigger size of the *m*-PBI can take part in the physical crosslinking readily. Figure 6.10 shows the effect of molecular weight the of *m*-PBI on the gel morphology. The gelation concentration of all the samples is kept fixed at 8%. The fibrils become thinner and longer with increasing I.V. of *m*-PBI. Also the network/crosslinking density increases with increasing I.V. of *m*-PBI (Figure 6.10). Hence the gelation can take place easily for higher I.V. *m*-PBI. These observation provides the justification for the faster gelation rate and lower $C^*_{t=\infty}$ for higher I.V. m-PBI discussed in the gelation kinetics section (6.3.1).

Figure 6.10. *SEM micrographs of 8% (w/v) m-PBI-PA gels of various I.V m-PBI (A) 0.50 dL/g (B) 0.92 dL/g (C) 1.01 dL/g. The magnification for all the image are identical.*

6.3.4. Thermodynamical Study. All the gel samples studied here, exhibit reversible first order phase transition in differential scanning calorimetry (DSC) experiments. Endothermic and exother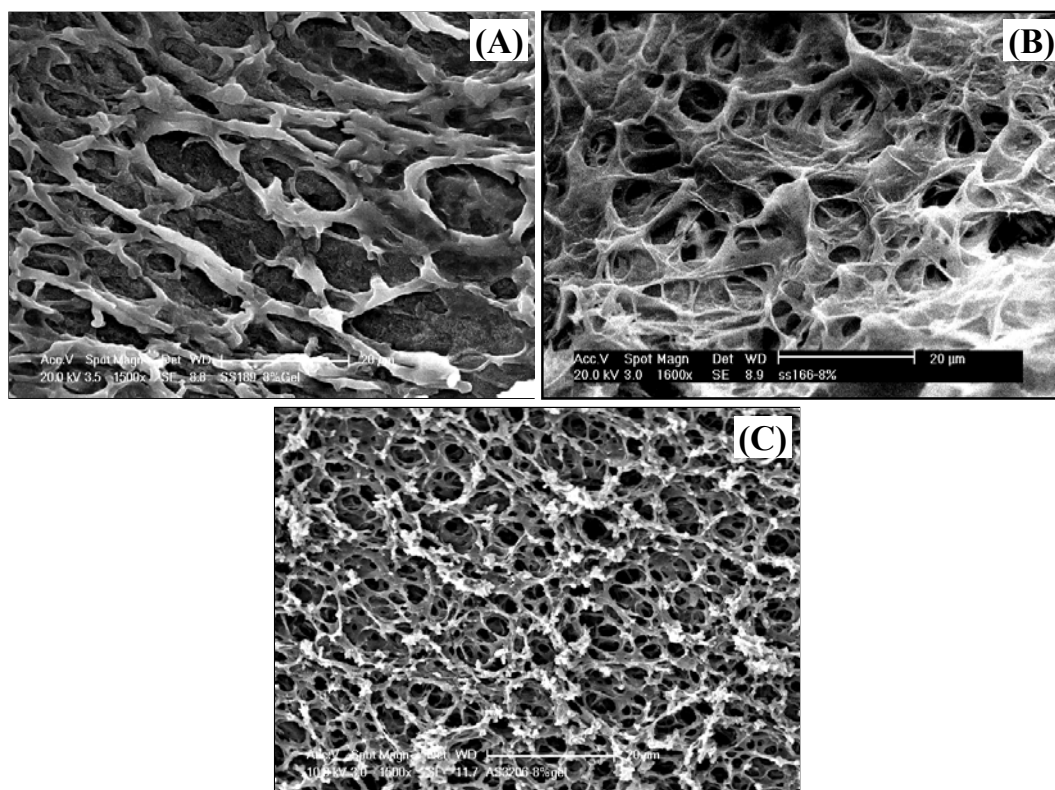mic peaks are obtained reversibly during heating and cooling scans of the gel samples in DSC. These reversible transitions and the fibrillar network morphology of the gel samples provide the evidence of the thermoreversible nature of the gel.[30,42-46] The DSC thermograms of *m*-PBI – PA gel samples of various gelation concentrations are presented in Figure 6.11. Endothermic gel melting temperature (T_{gm}, Figure 6.11 A) and exothermic gelation temperature peak (T_{gel}, Figure 6.11 B) during heating and cooling scan in DSC, respectively, are obtained for all the samples. It must be noted that all the tharmograms particularly endotherms are broad in nature and a shoulder is seen (~ 100ºC) before the gel melting temperature (T_{gm}) in the heating endotherms (Figure 6.11 A). Also, in all the cases the difference in T_{gm} and T_{gel} is observed and this is due to the hysterisis effect of the first order transitions. *m*-PBI is an amorphous polymer and therefore does not exhibit any crystalline melting temperature (T_m) in DSC heating scan. *m*-PBI displays a very high glass transition temperature (T_g) in DSC heating scan. However, the melting endotherm (T_{gm}) is observed for the *m*-PBI-PA gel and this endothermic melting arises due to the formation of crystalline nature of the gel. Earlier (Chapter 5), we have shown that the amorphous *m*-PBI transforms into the partially crystalline in the PA medium due to the strong hydrogen bonding interactions between PA and *m*-PBI.[30] The hydrogen bonding interactions between PA and *m*-PBI has been extensively discussed in the previous section (FT-IR and Raman spectroscopes).
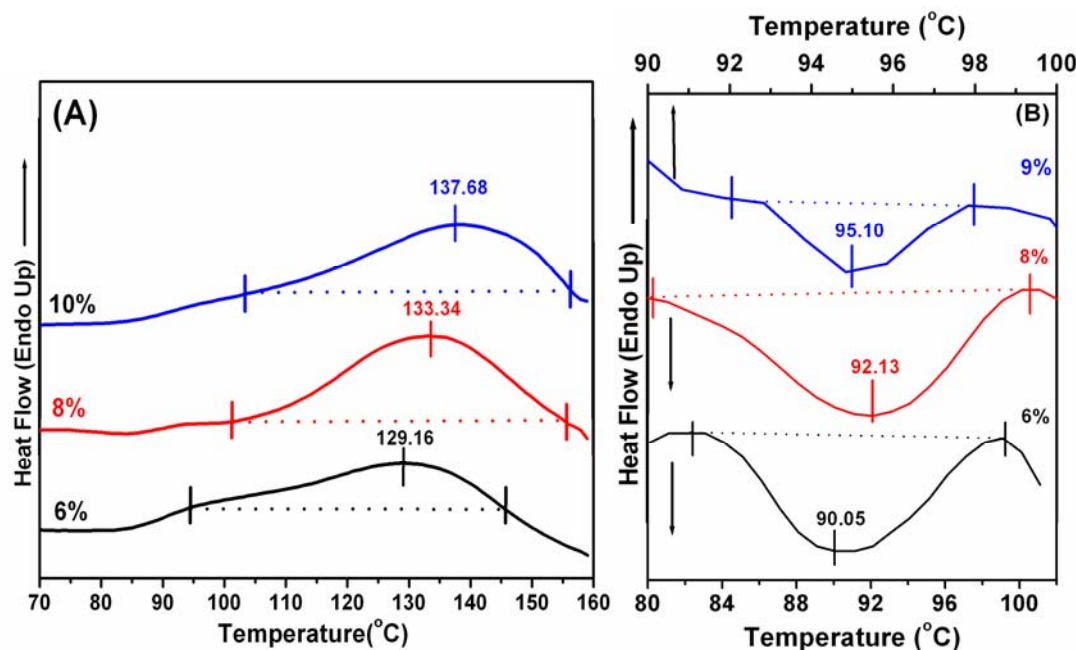
Figure 6.11. *DSC (A) heating and (B) cooling thermograms of m-PBI-PA gel samples at their indicated gelation concentration. The I.V of the m-PBI is 1.01 dL/g.*

A possible schematic model (Figure 6.12) is proposed for the formation of the semicrystalline *m*-PBI in presence of PA using hydrogen bonding as a driving force. The PA molecules self-assemble by the help of hydrogen bonding and reorienting themselves to produce a chain like structure. These PA chains bring different *m*-PBI molecules closer and align more and more *m*-PBI molecules in the gelation concentration which helps to form semicrystalline *m*-PBI (Figure 6.12). A similar type of self-assembly of PA molecules is observed from the single crystal structure analysis of phosphate salt of benzimidazole (Figure 6.13).[57] Imidazole molecule and PA molecule forms a chain type structure, which resembles the scheme shown in Figure 6.12. The gel melting temperature obtained in the DSC heating scan is the melting of this semi-crystalline *m*-PBI-PA complex. The shoulder before T_{gm} is due to the melting of PA chain self-assembly.

Figure 6.12. *Schematic diagram to represent the formation of m-PBI-PA gel through hydrogen bonding.*
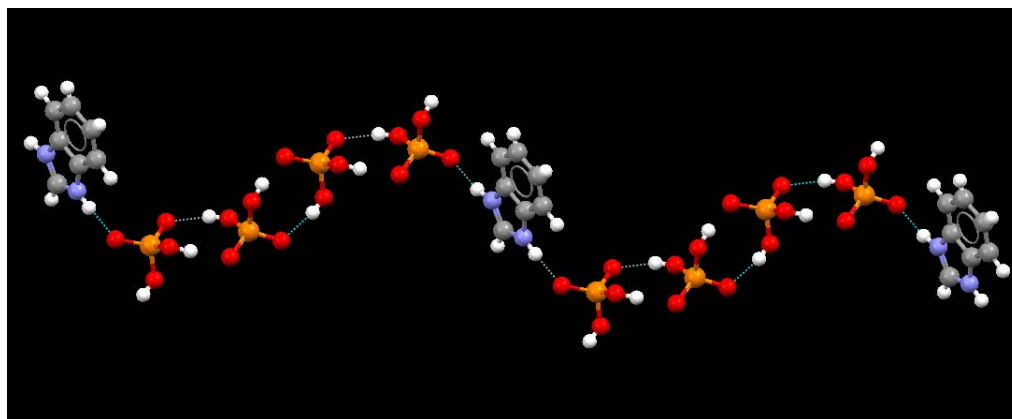
Figure 6.13. *Structural analysis of phosphate salt of benzimidazole. This structure is adapted in reference number* 57. *We have used this structure to compare our model shown in Figure 6.12.*

The T_{gm} and the enthalpy of gel melting (ΔH_{gm}) increase with increasing *m*-PBI concentration in the gel (Figure 6.11 A and Table 6.2). Our morphology studies show that the network density increases with increasing *m*-PBI concentration in the gel. Hence higher temperature is re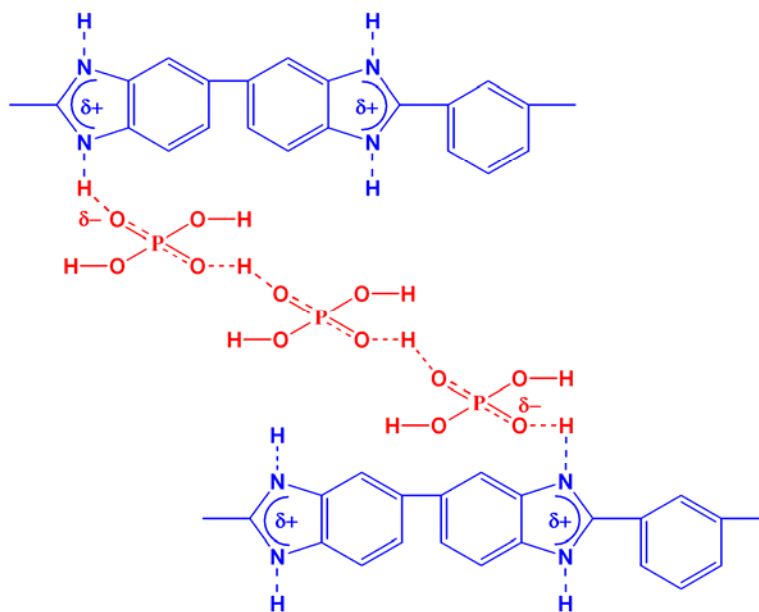quired to melt the gel with higher *m*-PBI concentration which has larger network density. Since network density is high hence more enthalpy change takes place. Similarly the T_{gel} also varies, but the variation of T_{gel} with *m*-PBI concentration is not that prominent as in case of T_{gm} (Table 6.2 and Figure 6.11). This is probably due to the poor crystalline nature of the gel sample.

Table 6.2. *Thermodynamical data obtained from the DSC experiments for various m-PBI-PA gel samples.*

Gel Concentration (w/v)	T_{gm} (^{o}C)	ΔH_{gm} (J/g)	T_{gel} (^{o}C)
I.V. = 1.01 dL/g			
6%	129.16	2.25	90.05
8%	133.34	4.37	92.13
9%	134.38	-	95.10
10%	137.68	7.19	90.18
I.V. = 2.92 dL/g			
2%	121.53	1.83	89.72
4%	132.49	-	90.45
6%	133.63	4.05	92.92
7%	141.82	6.00	94.60

Figure 6.14 represents the heating endotherm of *m*-PBI-PA gel samples in which the PBI has higher I.V. (I.V. = 2.92 dL/g) compare to the gel samples presented in Figure 6.11. The T_{gm} and ΔH_{gm} values are included in the Table 6.2. In this higher I.V. sample also the melting behavior is similar as in the case of lower I.V. sample.

However, the T_{gm} and ΔH_{gm} are higher than the previous low I.V. sample for identical concentration (Table 6.2). T_{gm} and ΔH_{gm} both increase with increasing gel concentration in this case also as in the previous case. The higher T_{gm} and ΔH_{gm} is due to higher network density and better crystallization for higher I.V. *m*-PBI gel sample compare to the lower I.V. *m*-PBI gel sample.
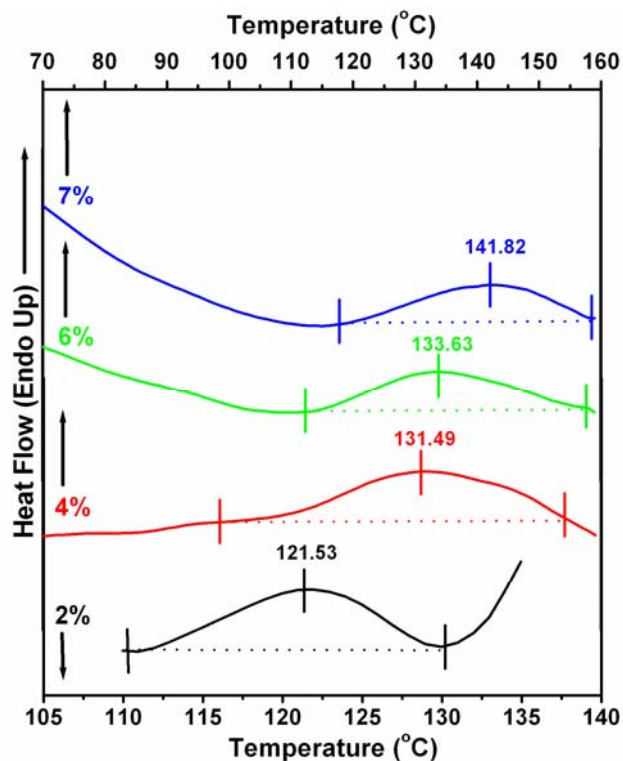
Figure 6.14. *DSC heating thermograms of m-PBI-PA gel samples at their indicated gel concentration (w/v). The I.V. of the m-PBI is 2.92 dL/g.*

6.3.5. UV–VIS Spectroscopic Study. PBI displays interesting photophysical properties both in solution and solid-state.[5] Various spectroscopic techniques especially UV-Vis and fluorescence spectroscopy studies have been used to understand the various solution properties of PBI.[5, 7, 31, 52, 56, 58] We have observed the change in color of *m*-PBI solution from wine red to reddish brown during the sol to gel transformation, indicating the solution process is associated with the visible color change. This allows us to study the gelation process in depth using UV-Vis technique. We have followed the color change

by monitoring the change in absorbance value with time of the dilute *m*-PBI solution by UV-Visible spectroscopy. We are unable to record the absorbance change above critical gelation concentration owing to the fact the *m*-PBI – PA solution has very high absorbance which exceeds the absorption limitation of the instrument. Therefore, we have taken 0.1% (w/v) *m*-PBI in PA and the absorbance of this solution is within the instrument range. The solution was initially kept in an oven at $180^{o}C$ to make homogeneous solution. The hot homogeneous 0.1 % (w/v) solution was transferred into the quartz cell and immediately UV- Vis. spectra from 800 – 400 nm were recorded in every 1 minute time interval for 1 hour at various gelation temperatures (T_{gel}: 30°, 40°, 50ºC).This experiment was carried out with various *m*-PBI samples of different I.V. values. Representative UV-Vis spectra of the above time dependent experiments are shown in Figure 6.15. In addition to the 440 and 480 nm transitions of bibenzimidazole group, a new peak (shoulder) at around 615 nm is developed and the peak gradually shifts towards the higher wavelength with time. Similar observations are obtained for all the samples and at all the gelation temperatures.
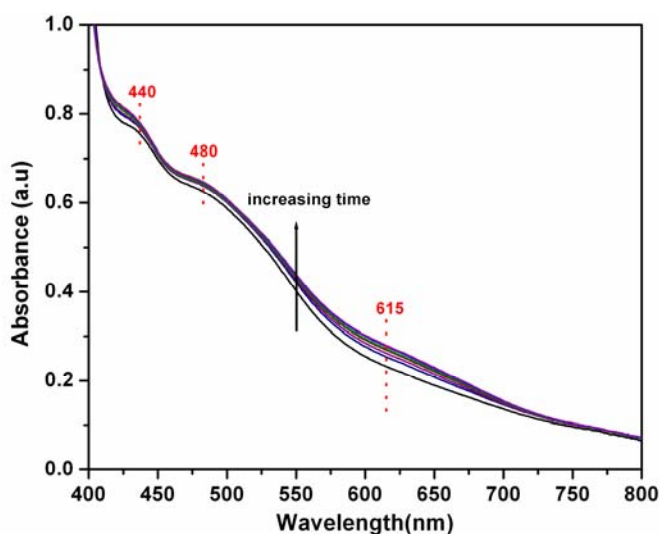

Figure 6.15: *UV – Vis. Spectra of 0.1 %(w/v) m-PBI – PA solution at $30^{º}C$ recorded for 1 hour duration. The I.V. of the polymer is 1.5 dL/g.*

However, we noticed a significant variation in the net increase in absorbance values at 615 nm and the extent of red shifts with change in I.V. of PBI and as well as the T_{gel}. We have plotted the change in absorbance at 615 nm with time for different I.V. samples (Figure 6.16A) for a fixed T_{gel} and for various T_{gel} of a fixed I.V. sample (Figure 6.16B). It is very much clear from the Figure 6.16 that the change in absorbance (change in the color) during sol to gel transformation is a kinetically controlled process. The absorbance gets saturation after the initial induction period. We have fitted the experimental data with non-linear Boltzman type equation and the time constants (time required to achieve the saturation) are shown in the figure. The saturation time or the induction period (time constant) of the color change (absorbance change) decreases with increasing I.V. of the *m*-PBI (Figure 6.16A) but it increases with decreasing the T_{gel} (Figure 6.16B). These observations bring important clues for the understanding of the gelation mechanism of *m*-PBI-PA gel. The former observation (less time required for the gelation of higher I.V. polymer) matches well with our gelation kinetics data presented in the gelation kinetics (section 6.3.1.); however the later observation contradicts our gelation kinetics data presented in section 6.3.1. Gelation kinetic data suggests that the faster gelation takes place when T_{gel} is lowered (Figure 6.1) but Figure 6.16B attributes the faster transformation when T_{gel} is high. This hints that the gelation process must be a two step process. In the first step a conformational transition takes place where the *m*-PBI coils transform into the more ordered rod shaped conformation and in the second step these rods are further aggregated to form the gel through the crystallization of rod and produce the fibrillar network. We have proposed a schematic representation for this gelation process (Figure 6.17). The above analysis provides that the first step is the slowest step and the rate determining step. Hence the gelation process takes place in two step process, where the first step is the slowest step (rate determining step) in which conformational transition takes place and the second step is the aggregation via crystallization of the rod to a fibril like gel structure.
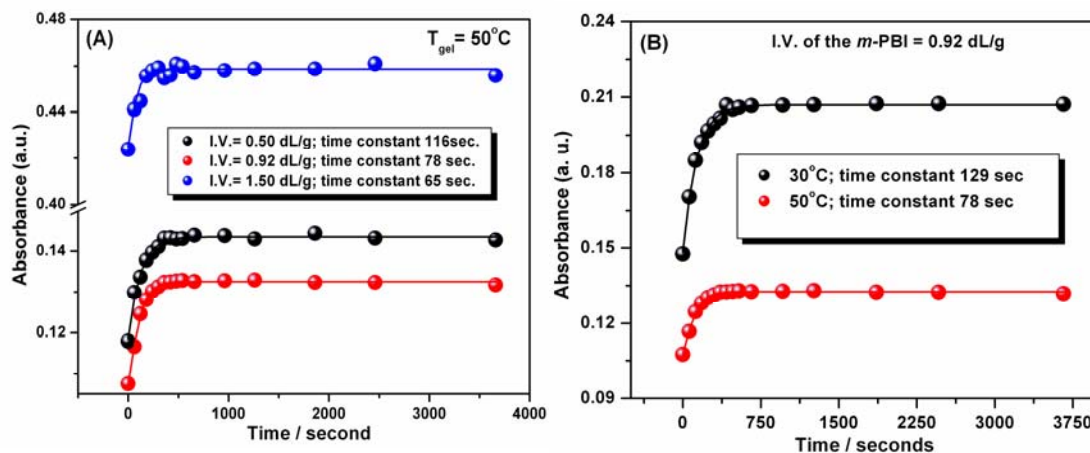
Figure 6.16. *Absorbance at 615 nm vs. time plots (A) for different I.V. of m-PBI at T_{gel} = 50°C. (B) for different T_{gel} of m-PBI (I.V. = 0.92 dL/g).*
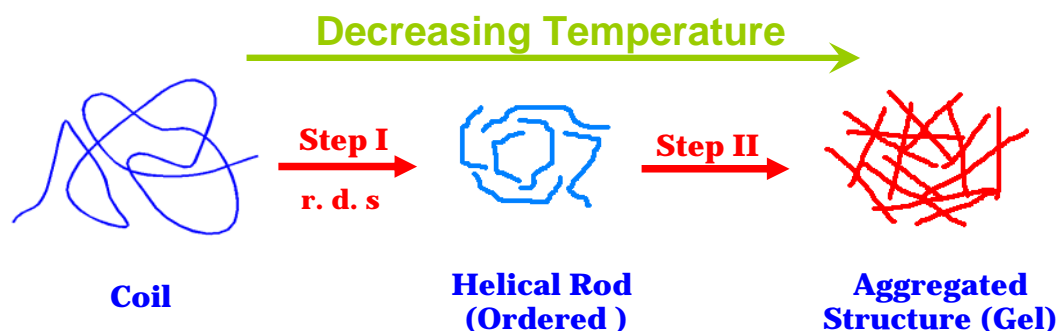
Figure 6.17. *Schematic representation of the gelation mechanism. First step is the slowest step (r.d.s).*

6.3.6. PA Doping Level. The phosphoric acid (PA) loading capacity of the membrane has significant influence on the fuel cell performance. Generally better cell efficiency is expected at high PA loading. Higher acid content facilitates the transport of the protons which significantly enhances the fuel cell efficiency. The PA doping level of the membrane is expressed as the number of PA mols per *m*-PBI repeat unit. The biggest challenge is to prepare a PA doped *m*-PBI membrane with appropriate thermo mechanically stability. It has been shown in the literature that if the acid content of the

membrane is too high it forms soft plastic type material with poor thermo-mechanical stability and which is very difficult to process. The doping level also depends on the molecular weight of the polymer. A large number of efforts have been made to improve the PA doping level of *m*-PBI as discussed in the introduction of this Chapter. Benicewicz et al. showed that PA doping level can be significantly increased by direct casting from the polymerization mixture in polyphosphoric acid.[25] In the present work an effort has been made to prepare the PA doped *m*-PBI membrane from the *m*-PBI-PA gel. We expect to obtain a membrane with high PA loading and moderate thermo-mechanical stability. The reason behind such expectation is because of the fact that the gel can accommodate large quantity of solvent (PA) with excellent thermo-mechanical stability arising due to strong network structure. We have prepared PA doped *m*-PBI membrane from the various gelation concentration of *m*-PBI in PA. The hot solution of *m*-PBI gel in PA poured in the petridish and allowed it to form gel in room temperature (30ºC) in the petridish. Finally we obtained free standing PA doped *m*-PBI membrane. The PA doping level was measured by titrating the PA doped membrane against NaOH and calculated as the number of PA mols per *m*-PBI repeat unit. The acid loading data of various PBI-PA gel samples are shown in Table 6.3. It should be mentioned here that the membrane prepared from a gelation concentration which is below $C^*_{t\,=\,\infty}$ has extremely poor mechanical stability and could not be handled as a free standing membrane. The weight percentage of *m*-PBI obtained in the gel membrane is matching with the gel concentration in all the cases indicating the accuracy of our measurements (Table 6.3). The PA loading varies with both the gelation concentration and the I.V. of the sample. This is controlled by the morphological behavior of the *m*-PBI-PA sample. Earlier, we have seen that as we increase the polymer concentration the network densities increases (Figure 6.9) and hence allow less number of PA molecule to go inside the gel network and hence PA loading decreases (Table 6.3). Similarly, the effect of I.V. can be explained from the morphological structure. The 6% (w/v) gel of higher I.V. sample (2.92 dL/g) holds lesser quantity of PA (29.61 mol/*m*-PBI repeat unit) then the 6% gel of lower I.V. (1.1 dL/g) sample (Table 6.3). Since higher I.V. has higher network density (Figure 6.10) hence it loads less PA molecule. The most significant

observation of Table 6.3 is that the acid loading obtained here is much higher than the already reported data in the literature[15, 24, 26] .Till today this is the highest loading reported in the literature. The reason for high loading is the gel structure of the membrane. Now we need to provide a proof that this gel membrane has enough thermo-mechanical stability and the membrane has the gel type structure.

Table 6.3. *Phosphoric acid loading obtained from different (w/v %)m-PBI-PA gel membrane.*

% Gel membrane (w/v)	% PA (w/w)	% *m*-PBI (w/w)	% H_2O (w/w)	Mols of PA/*m*-PBI repeat unit
I.V.= 2.92 dL/g				
4%	52.68	4.97	42.31	33.37
6%	60.79	6.46	32.74	29.61
I.V.= 1.1 dL/g				
6%	66.61	5.81	27.56	37.21
8%	65.52	8.63	25.83	23.85

6.3.7. Dynamic Mechanical Property. We have carried out the frequency sweep experiments of the PA doped *m*-PBI gel membrane obtained from the *m*-PBI gel in PA to proof that the resultant membrane has gel network structure. The storage (G′) and loss (G″) moduli of *m*-PBI-PA membrane are measured in isothermal condition (40ºC) over a frequency range 1 to 25 Hz using a dynamic mechanical analyzer (DMA). Figure 18 represents the frequency (angular) dependent of moduli of the PBI-PA membrane. Both G′ and G″ values are in the order of MPa indicating very strong mechanical stability of the membrane. The storage modulus (G′) is found to be approximately an order of magnitude larger than the loss modulus (G″) throughout the whole frequency range. Also both G′ and G″ are independent of frequency over the frequency range studied here (Figure 6.18). These observations (G′>G″ and frequency independent moduli) confirm that the *m*-PBI membrane has gel type structure.
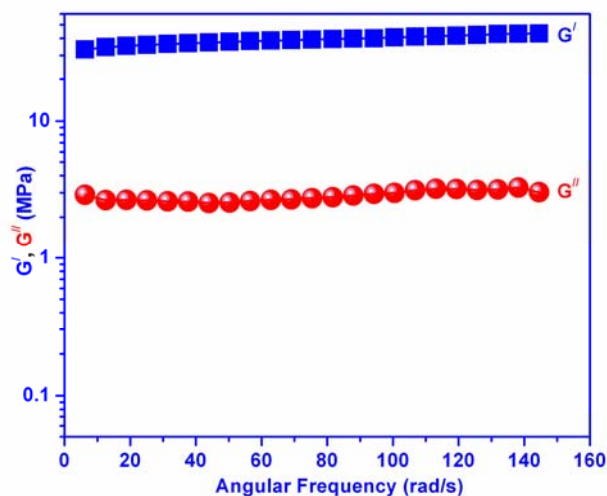
Figure 6.18. *Dependence of moduli on frequency as obtained from DMA. The sample is PA loaded m-PBI membrane obtained from m-PBI gel in PA. I.V. of polymer is 1.1 dL/g.*

6.3.8. Thermal and Mechanical Stability. The thermal and mechanical stabilities of the PA doped *m*-PBI membranes are the most challenging issues and need to be tested before its real application. It has been demonstrated in the literature that the thermal and mechanical stabilities of the PA doped *m*-PBI membrane decrease significantly with increasing PA loading. Large number of efforts has been made to address these issues. The ideal membrane for the fuel cell application would be a membrane with high acid loading and superb thermal and mechanical properties. Unfortunately, none of the method described in the literature solved this problem adequately. We hypothesized that due to network structure of our PA doped *m*-PBI membrane can hold large quantity of PA (solvent) molecule in the network cage without compromising its thermal and mechanical stabilities, owing to the fact that the network structure can provide better strength to this membrane. In the previous section we have shown that our membrane can load large amount (~ 35 mols/ *m*-PBI repeat unit) of PA.

We have carried out thermogravimetric analysis to check the thermal stability of the gel membranes. The thermal stabilities of the *m*-PBI-PA gel membranes are performed under nitrogen atmosphere at a heating rate of 10ºC / minute. The

representative TGA curve for PBI-PA gel membrane is shown in the Figure 6.19. Two distinct different weight losses are observed from the Figure 6.19. An initial weight loss at around 150 – 170ºC and the second weight loss at around 525 - 560ºC are observed. The first 30 - 40 % weight loss is assigned to the loss of loosely bound absorbed water and phosphoric acid molecules. The degradation of the polymer backbone is responsible for the second weight loss at ~ 550ºC. The TGA analysis clearly proofs that the PA doped *m*-PBI gel membrane has remarkably high thermal stability. However, question arises that how long this membrane is stable at temperature above 100ºC? Since long term stability (durability) above 100ºC is very important for real application. Hence, we performed isothermal heating scan (Figure 6.20) for six hours in N_2 atmosphere at 120 and 160ºC for the gel membrane to check the stability and durability of the membrane. We have not found any weight loss after six hours except the initial weight loss for loosely bound water and phosphoric acids (Figure 6.20). These observations proof that our membrane has high thermal stability, durability and appropriate candidate for use in the fuel cell.
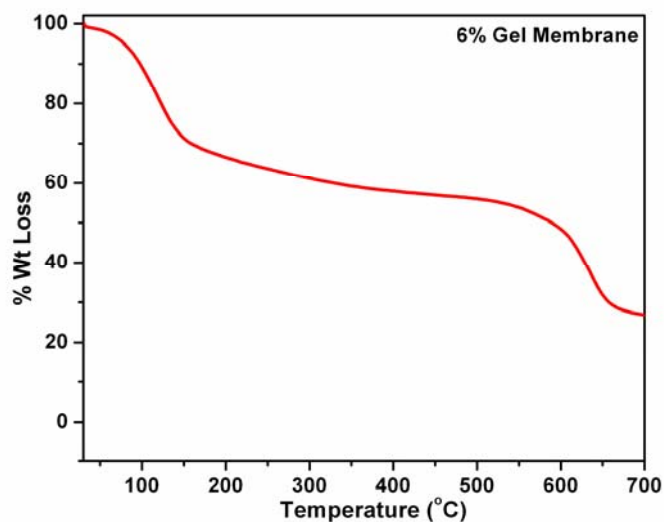
Figure 6.19. *TGA curves of the m-PBI -PA gel membranes. I.V. of the m-PBI is 1.1 dL/g.*
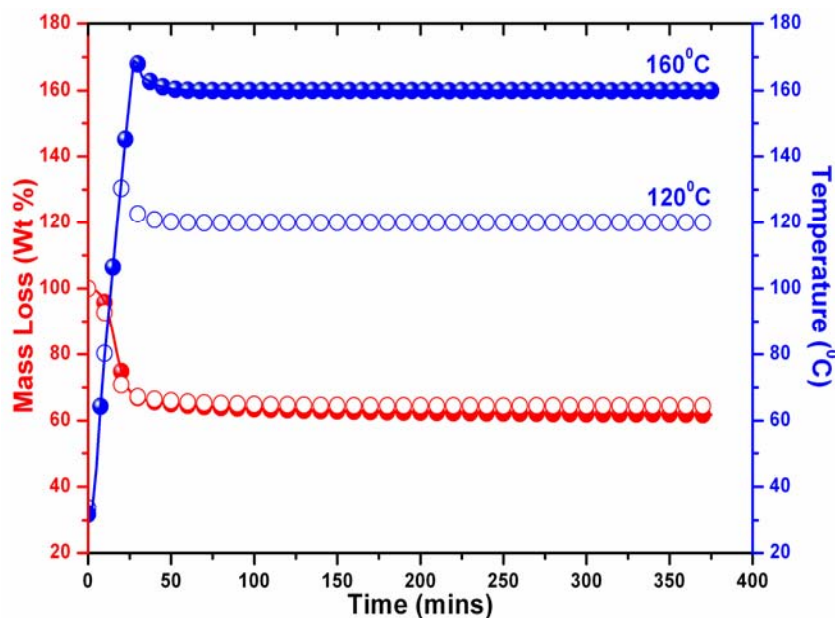
Figure 6.20. *Isothermal TGA curves of the m-PBI-PA gel (8 %) membrane at 120 and 160°C for 6 hours. The I.V of m-PBI is 1.1 dL/g.*

Figure 6.21 represents the stress vs. strain relationship of the PA doped *m*-PBI gel (8%) membrane. The nature of the plot attributes to the elastic nature of the membrane which also supports the gel structure of the membrane. The membrane displays 6.05 MPa tensile strength, 123% elongation at break and 2.2 MPa yield stress. These mechanical stability values are significantly higher compare to the previous reported values of the PA doped m-PBI. It must be noted that the despite of very high PA loading (~24 mols/ *m*-PBI repeat unit) the tensile strength of the membrane is remarkably high. This is due to the network structure (morphology) of the membrane which obtained from the *m*-PBI-PA gel.
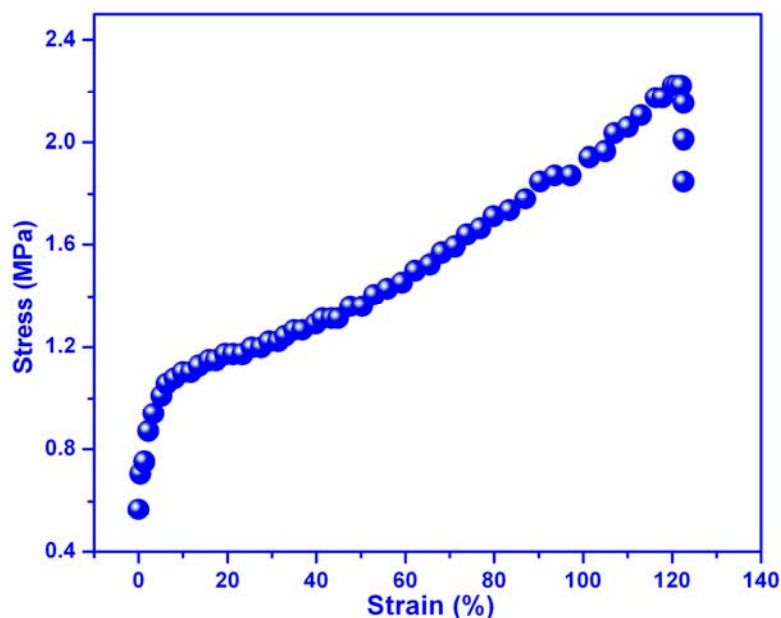
Figure 6.21. *Stress-strain plot of PA doped m-PBI-PA gel (8 %) membrane. The I.V. of m-PBI is 1.1 dL/g.*

6.3.9. Conductivity. The proton conductivity of the membrane is the most crucial parameter for the application in fuel cell. We have measured the proton conductivity of our PA doped *m*-PBI gel membrane by varying the temperature from 30ºC to 160ºC. A home made conductivity cell has been used (Figure 6.22). The membrane resistance data obtained from the impedance measurements are fitted into a two component model with a resistor is parallel with a capacitor across the frequency range (Figure 6.23). The membrane samples are annealed at 100ºC for 2 hours before the measurements to avoid the conduction due to presence of water molecule. It is already known in the literature that the PA doped *m*-PBI has zero osmotic drag coefficient, indicating the fact that the proton conduction can take place in zero humidity condition.
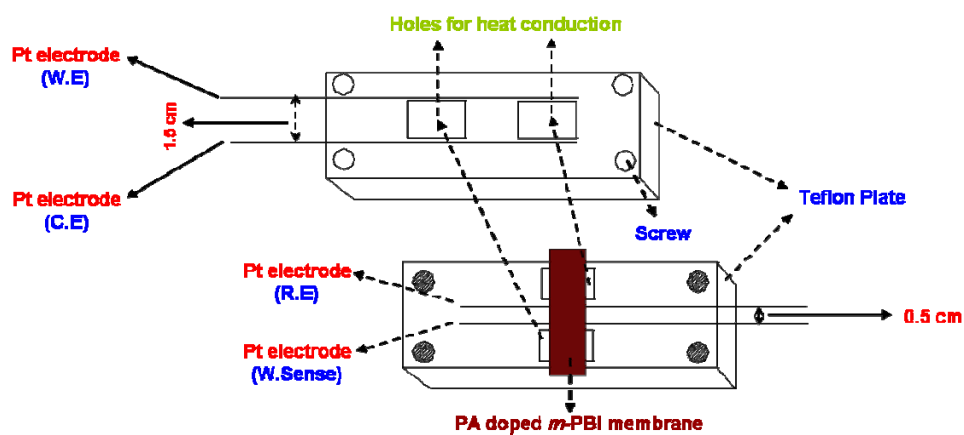
Figure 6.22. *Home made conductivity cell used to measure the proton conductivity of PA doped m-PBI gel membrane. Two parts as shown in the figure are clamped together by the screw and the cell was kept inside a programmable oven to control the temperature.*
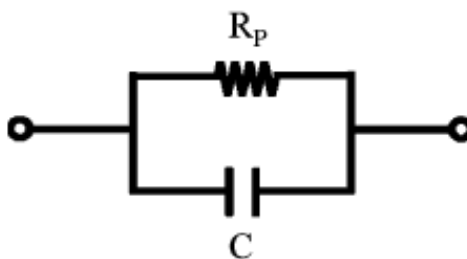
Figure 6.23. *Two components model with a resistor in parallel with capacitor used to fit the impedance data for the PA doped m-PBI gel membrane.*

The Nyquist plot at various temperatures and the proton conductivity as a function of temperature for *m*-PBI-PA gel membrane, are shown in Figure 6.24. All the Nyquist plots perfectly fit into the semicircle at all temperature, attributing that the choice of our two component model is appropriate for this system. As expected the

proton conduction increases with increasing temperature (Figure 6.24B). The proton conduction of our gel membrane at 160ºC is 4.2 x 10^{-2} S/cm. We have prepared and measured the proton conduction of PA doped *m*-PBI membrane obtained from conventional imbibing process using exactly identical I.V. (1.1 dL/g) *m*-PBI. The acid loading of this membrane is 9 mols/*m*-PBI repeat unit. This value is much lower compare to the acid loading of our *m*-PBI-PA gel (Table 6.3) membrane. The proton conductivity of this imbibing process membrane at 160ºC is 8.01 x 10^{-3} S/cm, which is much lower (one order) than our gel membrane conduction value. Hence our membrane is superior compare to the membrane obtained from the conventional imbibing process. Figure 6.25 represents the Nyquist plot and proton conduction as a function of temperature for 6% (w/v) *m*-PBI-PA gel membrane obtained from higher I.V (2.92 dL/g) m-PBI sample. The proton conductivity at 160ºC for this sample is 6.60 x 10^{-2} S/cm.
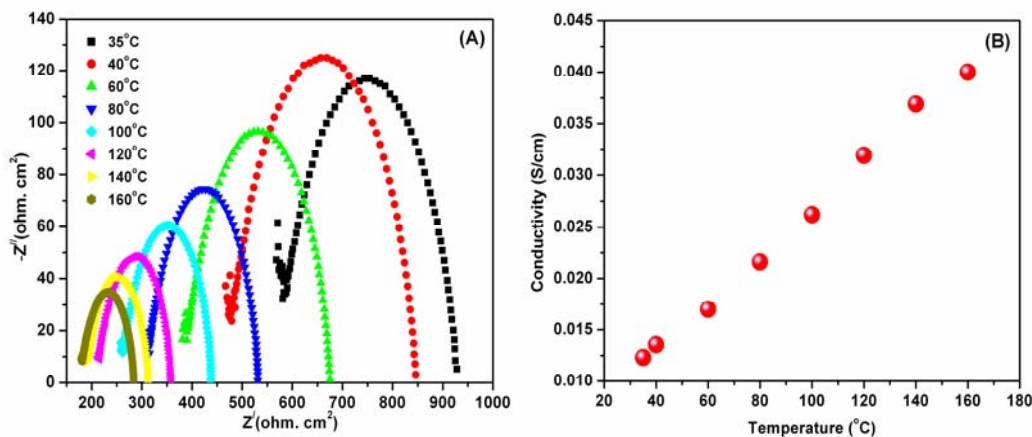
Figure 6.24. *Nyquist plots (A) and proton conduction against temperature (B) for the m-PBI-PA gel membrane. The concentration of gel is 8% (w/v). The PA loading is ~24 mols/PBI repeat unit (Table 6.3). The I.V. of the m-PBI is 1.1dL/g.*
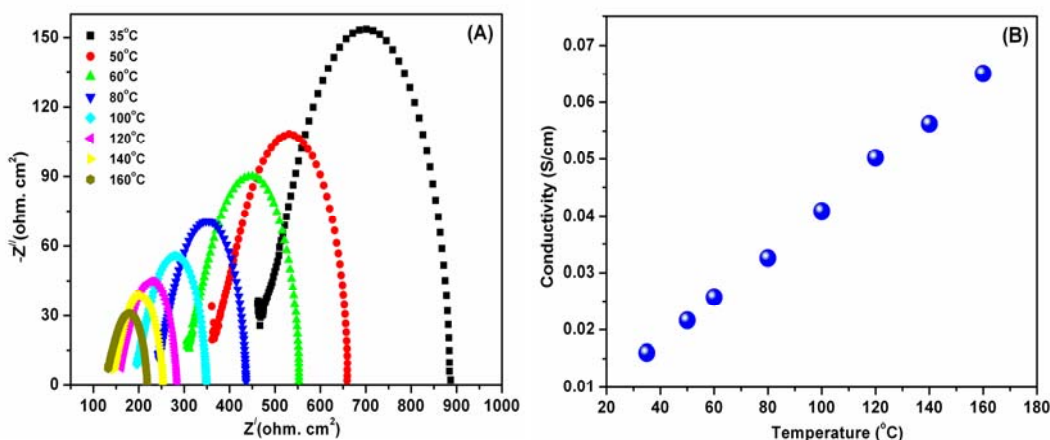
Figure 6.25. *Nyquist plots (A) and proton conduction against temperature (B) for the m-PBI-PA gel membrane. In this case I.V. of m-PBI is 2.92 dL/g. Gel concentration is 6% (w/v) and the PA loading is 29.61 mols/m-PBI repeat unit(Table 6.3).*

Proton conduction mechanism can be better understood from the Arrhenius type plot of conductivity.[59, 60] For a proton hopping dominating mechanism conductivity follows Arrhenius equation (6.2)

$$\sigma = \sigma_o \exp(-\frac{E_a}{RT}) \qquad (6.2)$$

Where σ is the protonic conductivity of the membrane (Scm^{-1}), σ_o is the pre-exponential factor ($S\ K^{-1}\ cm^{-1}$), E_a is the proton conducting activation energy (kJ/mol), R is the ideal gas constant ($J\ mol^{-1}K^{-1}$) and T is the temperature (K). Arrhenius plots of temperature dependent conductivity are shown in the Figure 6.26. We have used hopping mechanism (equation 6.2) to fit the proton conductivity data since in the gel hopping mechanism is always preferred.[61] The data fit very well with the equation 6.2 attributing the hopping mechanism is the mechanism for the proton conduction. The activation energy obtained from the plots are 10.6 and 12.2 kJ/mol for *m*-PBI-PA gel membrane samples with I.V. 1.1dL/g and 2.92 dL/g, respectively. These values are very close to the activation energy obtained for pure H_3PO_4 system (14.29 kJ/mol) as reported in the

literature.[62] Generally, E_a value for PA doped *m*-PBI ranges between from 20-40 kJ/mol are reported in the literature depending on the PA loading. This significantly lower activation energy attributes to the presence of free H_3PO_4 and phosphates species in the membrane and these are involved in the transport process. This is possible since in our gel membrane large quantity of free H_3PO_4 is present as proved from the I.R, Raman and DSC study.
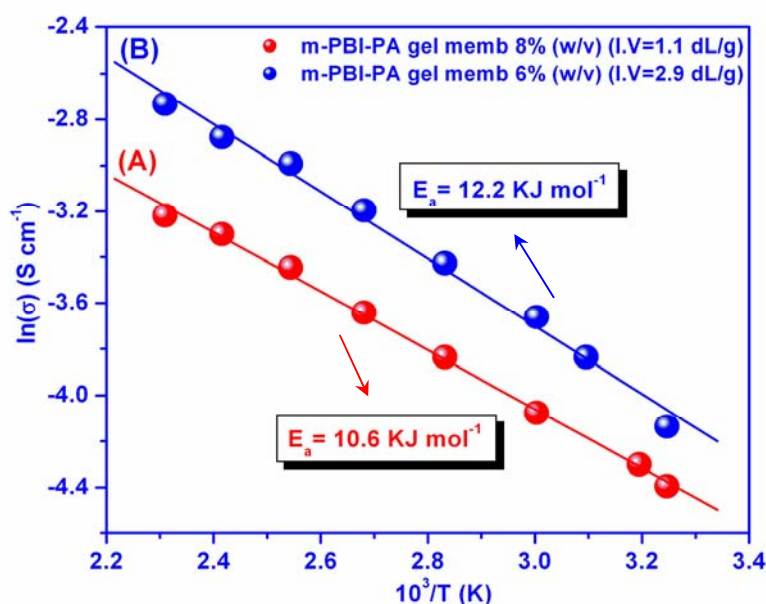
Figure 6.26. *Arrhenius plots for the proton conduction. (A) 8% m-PBI gel membrane, I.V. of m-PBI is 1.1 dL/g, acid loading 23.85 mols PA/ m-PBI repeat unit (B) 6% (w/v) m-PBI gel membrane, I.V. = 2.92 dL/g, acid loading 29.61 mols PA/ m-PBI repeat unit .*

Figure 6.27 and 6.28 represent the time dependent proton conduction behavior of PA doped *m*-PBI gel membrane of two I.V. *m*-PBI sample at 160°C.We have measured impedance of the samples isothermally of 160°C for 15 hours. As seen from the figure the loss of proton conductivity upto 15 hours is almost negligible

indicating the fact that our membrane has better durability. Previous section, we have also shown the long term thermal stability of our membrane using TGA.
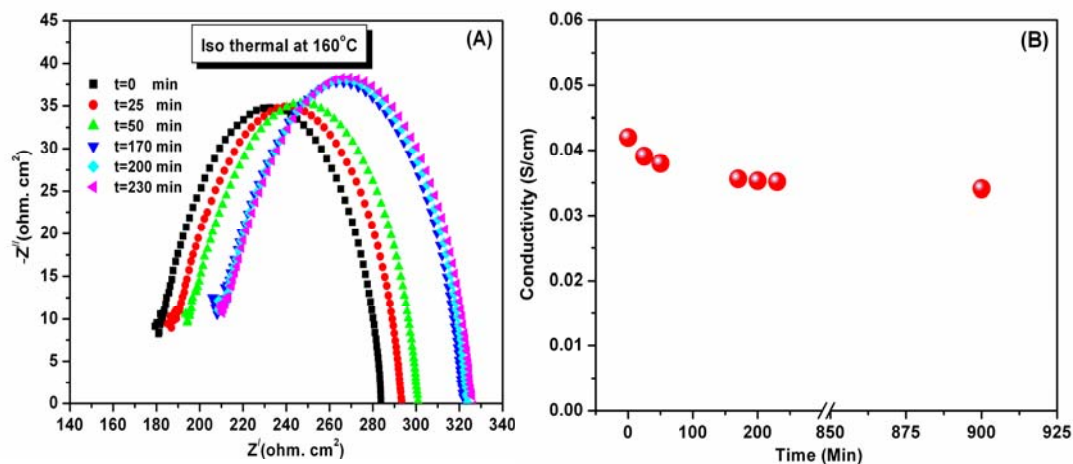
Figure 6.27. Variation of proton conduction (A) *Nyquist plot, (B) proton conduction at 160°C with time for m-PBI-PA gel membrane I.V. of m-PBI is 1.1 dL/g)*
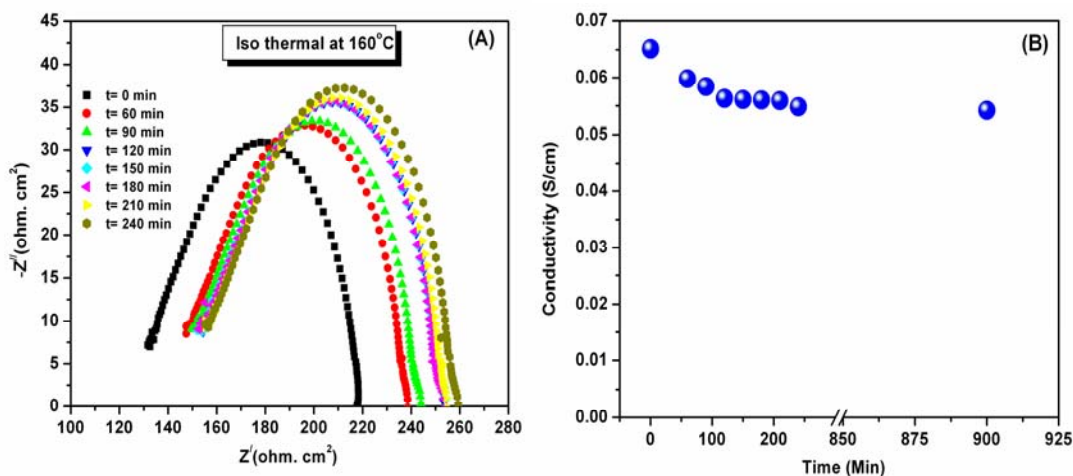
Figure 6.28. Variation of proton conduction (A) *Nyquist plots, (B) proton conduction at 160°C with time for m-PBI-PA gel membrane I.V. of m-PBI is 2.92 dL/g.*

6.4. Conclusion

We have studied thermoreversible gelation of meta polybenzimidazole (*m*-PBI) in phosphoric acid (PA) by varying the gelation concentration and the molecular weight (inherent viscosity) of the *m*-PBI. Morphological investigations, probed by SEM and TEM, show that the large number of longer, thinner fibrils and highly dense fibrillar network morphologies are obtained with increasing gelation concentration and I.V. of the *m*-PBI. A strong hydrogen bonding interaction between *m*-PBI and PA molecules in the gel is observed. The presence of free PA molecules in the gel network is confirmed from the I.R and Raman studies. The gelation rate and critical gelation concentration required for the gelation depend upon the gelation temperature and the I.V of *m*-PBI. We have proposed a two step mechanism; a slow conformational transition followed by a fast aggregation via crystallization, based on the detailed thermodynamical and spectroscopic investigation. We are able to fabricate a superior quality PA doped *m*-PBI membrane with high PA loading and excellent thermo-mechanical stability. The proton conduction of the PA doped *m*-PBI membranes obtained from *m*-PBI-PA gels are much higher than the already reported membranes which are made from the conventional imbibing process. Interestingly, the activation energies (E_a) for the proton conduction for these membranes are in the range of E_a for pure PA supporting the gel structure. In summary, we have developed the PA doped *m*-PBI membrane, which has the remarkably high PA loading with best thermo mechanical stability and durability.

References

(1)   Russo, P. S.; *"Reversible Polymeric Gels and Related Systems"*, Ed, ACS Symposium Series, American Chemical Society, New York, **1986**.

(2)   Guenet, J. M.; *"Thermoreversible Gelation of Polymers and Biopolymers",* Academic Press: London, **1992**.

(3)   Guenet, J. M.; *Macromol. Symp*. **2006**,241,45.

(4)   Berghmans, H. *"Integration of Fundamental Polymer Science and Technology", P. J.* Lemstra, L. A. Kleintjens, Eds, Elsevier Applied Science: London, 1988, Vol. 2, p 195.

(5)   Kojima, T. *J. Polym. Sci.: Polym. Phys. Ed.* **1980**, *18*, 1685.

(6)   Shogbon, C. B.; Brousseau, J.-L.; Zhang, H.; Benicewicz, B. C.; Akpalu, Y. *Macromolecules* **2006,** *39*, 9409.

(7)   Sannigrahi, A.; Arunbabu, D.; Sankar, R. M.; Jana, T. *Macromolecules* **2007**, *40*, 2844.

(8)   Musto, P.; Karasz, F. E., MacKnight, W. J. *Macromolecules* **1991**, *24*, 4762.

(9)   Deimede, V.; Voyiatzis, G. A.; Kallitsis, J. K.; Qingfeng, L.; Bjerrum, N. J. *Macromolecules* **2000**, *33*, 7609.

(10)   Arunbabu,D.; Sannigrahi,A.;Jana,T. *J Phys Chem B* **2008,** *112,* 5305.

(11)   Choe, E. W.; Choe, D. D. In *Polymeric Materials Encyclopedia*; Salamone, J. C., Ed.; CRC Press, New York, 1996

(12)   Tomlina, D.W.; Fratinib, A.V.; Hunsakera, M.; Adamsa W. W.; *Polymer* **2000**,41,9003.

(13)   Hickner, M. A.; Ghassemi, H.; Kim, S. Y.; Einsla, B. R.; McGrath, J. E. *Chem. Rev.* **2004,** *104*, 4587.

(14)   Borup, R.; Meyers, J.; Pivovar, B.; Kim, Y. S.; Mukundan, R.; Garland, N.; Myers, D.; Wilson, M.; Garzon, F.; Wood, D.; Zelenay, P.; More, K.; Stroh, K.; Zawodzinski, T.; Boncella, J.; McGrath, J. E.; Inaba, M.; Miyatake, K.; Hori, M.; Ota, K.; Ogumi, Z.; Miyata, S.; Nishikata, A.; Siroma, Z.; Uchimoto, Y.; Yasuda, K.; Kimijima, Ken-ichi.; Iwashita, N.; *Chem. Rev.* **2007,** *107,* 3904.

(15) Mader, J.; Xiao, L.; Schmidt, T, J.; Benicewicz, B,C; *Adv Polym Sci.* **2008**, 216, 63.

(16) Roziere, J.; Jones, D. J. *Annu. Rev. Mater. Res.* **2003**, *33*, 503.

(17) Kerres, J. *J. Membr. Sci.* **2001**, *185*, 3.

(18) Savinell, R.; Yeager, E.; Tryk, D.; Landau, U.; Wainright, J.; Weng, D.; Lux, K.; Litt, M.; Rogers, C.; *J. Electrochem. Soc.* **1994**, *141*, L46.

(19) Samms, S. R.; Savinell, R. F.; *J. Electrochem. Soc.* **1996,** *143,* 1225.

(20) Weng, D.; Wainright, J.; Landau, S. U.; Savinell, R. F.; *J. Electrochem. Soc.* **1996**, *143*, 1260.

(21) Savinell, R.; Yeager, E.; Tryk, D.; Landau, U.; Wainright, J.; Weng, D.; Lux, K.; Litt, M.; Rogers, C. *J. Electrochem. Soc.* **1994**, *141*, L46.

(22) Samms, S. R.; Wsmus, S.; Savinell, R. F. *J. Electrochem. Soc.* **1996,** *143,* 1225

(23) Weng, D.; Wainright, J.S.; Landau, U.; Savinell, R. F. *J. Electrochem. Soc.* **1996**, *143*, 1260.

(24) Mecerreyes, D.; Grande, H.; Miguel, O.; Ochoteco, E.; Marcilla, R.; Cantero, I. *Chem. Mater.* **2004**, *16,* 604

(25) Xiao, L.; Zhang, H.; Scanlon, E.; Ramanathan, L. S.; Choe, E.-W.; Rogers, D.; Apple, T.; Benicewicz, B. C. *Chem. Mater.* **2005**, *17*, 5328.

(26) Xiao, L.; Zhang, H.; Jana, T.; Scanlon, E.; Chen, R.; Choe, E.-W.; Ramanathan, L. S.; Yu, S.; Benicewicz, B. C. *Fuel Cells* **2005**, *5*, 287.

(27) Mader, J.; Xiao, L.; Schmidt, T, J.; Benicewicz, B,C. *Adv Polym Sci.* **2008**, *216*, 63.

(28) Yu, S.; Benicewicz, B.C. *Macromolecules.* **2009,** *42*, 8640.

(29) Mecerreyes, D.; Grande, H.; Miguel, O.; Ochoteco, E.; Marcilla, R.; Cantero, I.; *Chem. Mater.* **2004**, *16,* 604. Sansone M. J.; Kwiatek M.S.; US patent 4, 933, 397.; 1990.

(30) Sannigrahi, A.; Arunbabu, D.; Jana, T. *Macromol. Rapid Commun.* **2006**, *27*, 1962.

(31) Sannigrahi,A.; Arunbabu,D.; Sankar,R.M.; Jana,T. *J Phys Chem B* **2007**, *111*, 12124

(32) Jouanneau, J.; Mercier, R.; Gonon, L.; Gebel, G. *Macromolecules* **2007**, *40*, 983.

(33) Li, Z. X.; Liu, J. H.; Yang, S. Y.; Huang, S. H.; Lu, J. D.; Pu, J. L.; *J . Polym. Sci.: Part A: Polym. Chem.* **2006**, *44*, 5729.

(34) Chen, C. C.; Wang, L. F.; Wang, J. J.; Hsu, T. C.; Chen, C. F. *J. Mater. Sci* **2002**, *37*, 4109.

(35) Chuang, S-W.; Hsu, S. L-C. *J . Polym. Sci.: Part A: Polym. Chem.* **2006**, *44*, 4508.

(36) Qian, G.; Benicewicz, B. C. *J. Polym. Sci.: Part A: Polym.Chem.***2009**,*47*,4064.

(37) Sansone M. J.; US patent 4,898,917.;1990

(38) Klaehn, J.R.; Luther, T.A.; Orme, C.J.; Jones, M.G.; Wertsching A.K.; Peterson E. S.; *Macromolecules* **2007**;40:7487–92.

(39) Pu, H.T.; Liu, Q.Z.; Liu, G.H.; *J Membr Sci* **2004**;241:169

(40) Li ,Q.; Jensena, J. O.; Savinell, R. F.; Bjerrum, N. J. *Prog. Polym. Sci*. **2009**, 34, 449.

(41) Yu, S.; Xiao, L.;Benicewicz, B. C. *Fuel Cells* **2008**, 3–4, 165.

(42) Dikshit, A. K.; Nandi, A. K, *Macromolecules* **1998**, *31*, 8886.

(43) Malik, S.; Jana, T.; Nandi, A. K, *Macromolecules* **2001**, *34*, 275.

(44) Dikshit, A. K.; Nandi, A. K, *Langmuir* **2001**, *17*, 3607.

(45) Yadav, P. JayPrakash; Aswal, V. K.; Sastry, P. U.; Patra, A, K.; Maity, P. *J Phys Chem B* **2009**, *112*, 13516.

(46) Guenet, J. M, *J. Rheol.* **2000**, *44*, 947.

(47) Eldridge,J.E.; Ferry, J.D.*J. Phys.Chem.***1954**,58,992.

(48) Mal. S.; Maity, P.; Nandi, A. K. *Macromolecules,* **1995**, *28*, 2371.

(49)   Musto, P.; Karasz, F.E.; MacKnight, W. J. *Polymer* **1993,** *34*, 2934.

(50) Lobato, J.; Cañizares , P.; Rodrigo, M. A.; Linares, J. J.; Manjavacas , G. *J. Membr. Sci* **2006***, 280*, 351

(51) Qing, S.; Huang, W.; Yan, D. *Euro Poly J.* **2005,** *41*, 1589.

(52) Ghosh, S.; Sannigrahi, A.; Maity, S.; Jana, T. *J Phys Chem B* **2010**, *114*, 3122.

(53) Glipa, X.; Bonnet, B.; Mula, B. ; Jones, D. J. ; RozieÁre, J. *J. Mater. Chem*, **1999**, *9*, 3045.

(54) Quartarone, E.; Magistris, A.; Mustarelli, P.; Grandi, S.; Carollo, A.;. Zukowska, G.Z.; Garbarczyk, J. E.; Nowinski, J. L.; Gerbaldi, C.; Bodoardo. S.; *Fuel Cells*, **2009**, 4, 349.

(55) Li, Q.;He, R.; Berg, R.W.; Hjuler, H.A.; Bjerrum, N. J.; *Solid State Ionics* **2004**,168,177.

(56) Sannigrahi, A.; Ghosh, S.; Maity, S.; Jana, T. *Polym. Chem*. revised manuscript submitted.

(57) Emsley, J.; Reza, N.M.; Dawes, H.M.; Hursthouse, M.B.; Kuroda, R. *Phosphorus & Sulphur,***1988**,*35,*141.

(58) Sannigrahi, A.; Ghosh, S.; Lalnuntluanga, J.; Jana, T. *J. Appl. Polym. Sci.* **2009**, *111*, 2194.

(59) Bouchet, R.; Siebert, E. *Solid State Ionics.* **1999**, *118*, 287.

(60) He, R.; Li, Q.; Bach, A.; Jensen, J. O.; Bjerrum, N. J. *J. Membr Sci*. **2006**, *277*, 38.

(61) Jana, T.; Nandi, A. K. *Langmuir*, **2001**, *17*, 5768.

(62) Ma, Y-L.; Wainright, J. S.; Litt, M.; Savinell R. F. *J Electrochem Soc*. **2004**, *151*, A8.

Chapter 7

Summary & Conclusions

7.1 Summary

The present thesis entitled "**Copolymerization, Aggregation and Thermoreversible Gelation of Polybenzimidazoles**" describes the synthesis and characterization of polybenzimidazole copolymers with tunable properties. Photo physical properties and the aggregation behavior of *m*-PBI chains in polar aprotic solvent are studied. Formation of *m*-PBI gel in phosphoric acid (PA) by varying the gelation concentration and the polymer molecular weight are investigated. The thesis consists of seven chapters. The summary of the contents of each chapter is given below.

Chapter 1

This chapter deals with a brief introduction of polybenzimidazoles (PBIs) types of polymers, highlighting their synthetic procedure of preparation and giving an overview of how the polymer property changes by changing the microstructure especially focusing on their physical and chemical properties, and versatile applications. In this chapter we have discussed the historical developments on PBI types of polymer and also included acid-base complexation phenomenon which is recently having extra flavors in the high temperature application in polymer electrolyte membrane fuel cell. This chapter provides information about the blending property of PBI polymer due to presence of proton donor (- NH -) and proton acceptor (- N =) hydrogen bonding sites in the backbone. This chapter also describes the most advanced application of phosphoric acid (PA) doped polybenzimidazole in high temperature polymer electrolyte membrane fuel cell.

Chapter 2

A series of novel random polybenzimidazole (PBI) copolymers consisting of *m*- and *p*-phenylene linkages are synthesized from various stoichiometric mixtures of isophthalic acid (IPA) and terephthalic acid (TPA) with 3, 3$^{'}$, 4, 4$^{'}$ – tetraaminobiphenyl (TAB) by solution copolycondensation in polyphosphoric acid (PPA). The resulting copolymers are characterized by different techniques to obtain their molecular

properties parameters. The monomer concentration in the polymerization plays an important role in controlling the molecular weight of the polymer. Surprisingly, a simple change in the dicarboxylic acid architecture from meta (IPA) to para (TPA) increases the molecular weight of the copolymers, which is maximum for the para homopolymer. The low solubility of TPA in PPA is found to be the dominating factor for obtaining the higher molecular weight polymer in the case of the para structure. FT-IR study shows that the introduction of the para structure enhances the conjugation along the polymer chain. The positive deviation of the copolymer composition from the feed ratio is due to the higher reactivity ratio of TPA than IPA, which is obtained from proton NMR studies. The incorporation of the para structure in the chain enhances the thermal stability of the polymers. The para homopolymer shows 59°C lower glass transition temperature compare to the meta homopolymer indicating enhancement of the flexibility of the polymer chain due the introduction of the *p*-phenylene linkage in the backbone. The T_g of the copolymers shows both positive and negative deviation from the expected T_g calculated by the Fox equation. The enhanced conjugation of the polymer chains also influences the photophysical properties of the polymers in solution. All the PBI polymers exhibit strong fluorescence in dimethylacetamide solution. As expected, that all the polymers are amorphous in nature reveals that the copolymerization does not influence the packing characteristics of the PBI chains.

Chapter 3

Three different series of pyridine based polybenzimidazole (PyPBI) random copolymers consisting of meta-para pyridine linkages are synthesized from various stoichiometric mixtures of meta structure pyridine dicarboxylic acids (2,4; 2,6 and 3,5 PDA) and para structure PDA (2,5 PDA) with 3, 3´, 4, 4´- tetraaminobiphenyl (TAB) by solution polycondensation in polyphosphoric acid (PPA). The influences of the structural isomers of PDA on the PyPBI copolymerization and properties are elucidated by characterizing the resulting copolymers using different techniques. The solubility of PDA monomers in PPA and the overall monomer concentration in the polymerization are found to be the deciding factors for controlling the copolymerization and the

molecular weight of the copolymers. The higher molecular weight PyPBI copolymers are obtained for higher para content copolymers due to the low solubility of para PDA (2,5 PDA) in PPA. FT-IR and Raman spectroscopy studies provide the evidence for the enhanced conjugation along the polymer chain due to the introduction of para structure. All the three sets of PyPBI copolymers exhibit positive deviations from the feed because of the higher reactivity of 2,5 PDA (para structure) compare to all other meta structure PDAs. NMR study shows that the reactivity ratio of 2,5 PDA are not identical for all the three sets of PyPBI copolymers, it depends upon the positions of the dicarboxylic acids in the pyridine ring of meta structure PDAs (structural isomeric effect) with which 2,5 PDA is forming the copolymer. Introduction of para structure in the polymeric backbone and meta PDAs structural isomers affect the thermal stability and the flexibility of PyPBI polymers. The glass transition temperature (T_g) decreases with increasing para content in the copolymer attributing the enhancement of flexibility of the polymer chain. The dependence of T_g against the copolymer composition in all the three sets of copolymers exhibit the deviation from the Fox equation. The enhanced conjugation due to the introduction of para in the copolymer and meta PDA structural isomers also influence the photophysical properties of PyPBI copolymers. All the PyPBI polymers exhibit strong fluorescence in dimethyl acetamide solution. All the PyPBI polymers are amorphous in nature attributes that neither copolymerization nor introduction of pyridine moiety in the backbone of PBI can influence the packing characteristics of rigid PBI type polymers.

Chapter 4

This chapter deals with the aggregation behavior of meta polybenzimidazole (*m*-PBI) in polar aprotic solvents such as dimethylacetamide (DMAc). The photophysical studies of the *m*-PBI solution at various concentrations show concentration quenching and reveal that aggregated structures are formed when the polymer concentration is increased. The decay profiles obtained from time-resolved fluorescence study for low (0.00154 g/dL) and high (0.154 g/dL) concentrations of *m*-PBI in DMAc solution fit

into a triexponential decay, surprisingly high concentration shows a growth (negative pre-exponential factor) in the decay profile, providing a support for excimer formation. The excited-state life time for the aggregated/excimer structure is found to be 4.14 ns, longer than that for the free polymer chains for which the life time is 502 ps. The concentration dependence emission spectra attribute that the aggregation/excimer formation is an intermolecular process. An abrupt decrease of Huggins constant and reduced viscosity with increase in concentration indicate the conformational transition of polymer chains of *m*-PBI from compact coil to an extended helical rodlike structure. The NMR and viscosity studies demonstrate that the intra- and intermolecular interactions (interchain hydrogen bonding) play an important role for the conformational transition and aggregation process. Transmission electron microscope images support the conclusion drawn from other studies; show helical rods for high concentration and featureless morphology for low concentration. The circular dichroism spectrum is also in agreement with the helical characteristics of aggregated structure. The temperature-dependent NMR and viscosity studies show that the disruption of interchain hydrogen bonding with increasing temperature destabilizes the aggregated structure at higher temperature.

Chapter 5

This chapter deals with thermoreversible gelation of meta-polybenzimidazole (*m*-PBI) in phosphoric acid (PA). The *m*-PBI gel in PA exhibits fibrillar network morphology and reversible first order phase transition. The gelation rate (t_{gel}^{-1}) is measured by the tube tilting method and found to be depending upon both gelation concentration and gelation temperature. The UV – Vis study demonstrates that the gelation process is a two step process: conformational transformation and aggregation which produces crystallites for the gel formation. The WAXS study supports the presence of crystallites in the gel. The PA doping level of the membrane has increased largely because of gelation.

Chapter 6

In this chapter thermoreversible gelation of meta-polybenzimidazole (*m*-PBI) in phosphoric acid (PA) is investigated thoroughly by studying the gel morphology, thermodynamics of the gelation and gelation kinetics utilizing test tube tilting and UV-Vis spectroscopy technique. The effect of concentration and molecular weight of the *m*-PBI on the gelation process are addressed. Gelation kinetics studies reveal that the both gelation rate and critical gelation concentration ($C^*_{t=\infty}$) are function of gelation temperature (T_{gel}) and the molecular weight of *m*-PBI. The fibrillar network morphology of gel is highly influenced by the gelation concentration and molecular weight of *m*-PBI. Large number of longer, thinner fibrils and dense fibrillar network morphology is obtained for higher gel concentration and higher molecular weight *m*-PBI. Both the gel melting (T_{gm}) and gelation (T_{gel}) temperature depend on gelation concentration and molecular weight of *m*-PBI. The presence of self assembled chain of PA molecules, which helps to produce the *m*-PBI crystallization, is observed from the thermodynamical study. I.R and Raman studies prove the presence of strong hydrogen bonding interaction between the *m*-PBI and PA molecules and free PA molecules in the gel network. Our in depth UV-Visible studies revel that gelation occurs in two step process and these are conformational transition from coil to rod, which is slow rate determining process, followed by aggregation of rod via crystallization. The PA loading of *m*-PBI membrane obtained from the *m*-PBI-PA gel has significantly high loading capacity than the conventional imbibing process membrane. The *m*-PBI gel membrane displays very high thermal and mechanical stabilities. The high acid loading and supub thermo-mechanical stability are due to network structure of the membrane because the gel network structure of the membrane. The proton conductivity of the membrane at 160^oC is ~6.6×10^{-2} Scm^{-1}, which is higher than the reported values in the literature for the *m*-PBI. The activation energy of the proton conduction is 10-12 kJ/mol indicating faster proton transfer by hopping process inside the gel network.

7.2 Conclusions

The following conclusions are drawn from the studies of copolymerization, aggregation and thermoreversible gelation of polybenzimidazoles.

1. A series of random copolymers of polybenzimidazole consisting of *m*- and *p*-phenylene linkage in the backbone are synthesized and characterized.

2. Higher molecular weight polymers are obtained from higher para content copolymer due to the low solubility of the *p*-phenylene dicarboxylic acid (TPA) monomer.

3. The introduction of the *p*-phenylene linkage in the copolymer backbone enhances the flexibility of the polymer chain, increases conjugation along the chain and the thermal stability of the copolymers.

4. The phosphoric acid (PA) loading increases with increasing para content in the PBI copolymer backbone.

5. Polybenzimidazole random copolymers consist of meta and para pyridine linkages in the backbone are synthesized and various molecular properties of three different copolymer pairs are investigated

6. The monomer reactivity ratios of all the pyridine dicarboxylic acids (PDAs) are determined by analyzing the ^{1}H NMR data of the copolymers. The para structure 2,5 PDA has the higher reactivity than all other meta structure PDAs and most importantly the reactivity of 2,5 PDA varies depending upon with which meta PDA it forms the copolymer pair.

7. The T_g of the copolymers decrease and thermal stability increases with increasing para content in all the cases due to the incorporation of conjugated, symmetrical and flexible para structure in the copolymers. The nature of deviations of T_g of copolymers from the expected T_g (as per the Fox equation) are not similar in three cases, attributing the influence of isomeric structures of monomers.

8. *m*-PBI forms aggregated species with increasing concentration in polar aprotic solvents e.g DMAc.These aggregations can be destabilized by increasing the solution temperature.

9. The aggregation of *m*-PBI in DMAc is controlled by a balance between intra and intermolecular interactions.

10. A conformational transition from a compact coil to an extended helical rod likes structure is associated with the aggregation.

11. *m*-PBI produces thermoreversible gel in phosphoric acid (PA).

12. The polyelectrolyte nature of *m*-PBI in PA, strong hydrogen bonding between *m*-PBI and PA molecule induce the crystallinity in the PBI-PA gel, which is the driving force for the gelation.

13. PA doped *m*-PBI membrane obtained from the *m*-PBI-PA gel is superior in acid loading than the reported imbibing process membranes.

14. The gelation rate, critical gelation concentration, morphology and thermodynamical properties depend on the gelation concentration and the molecular weight of *m*-PBI.

15. The *m*-PBI gelation in PA is a two step process; a slow conformational transition followed by a fast aggregation via crystallization.

16. The PA doped *m*-PBI membrane obtained from *m*-PBI-PA gel has very high PA loading with excellent thermal mechanical stabilities and durabilities. The proton conduction of this membrane is significantly higher then the all other reported membranes.

7.3. Scope of Future Work

The present thesis has addressed three important aspects of polybenzimidazoles copolymerization, aggregation and thermoreversible gelation. We believe the findings of this thesis will have great impact on the future development of polybenzimidazole (PBI) chemistry in general, especially the use of PBI in PEMFC application. The thesis put forward and establish novel concept in the PBI chemistry research. The potential and scope of future work of this thesis are enormous. Few of these are listed below

1. Copolymerization of varities of PBI backbone structures can be studied. Effort should be made to understand the polymerization mechanism and establish a correlation between the monomer solubility and reactivity ratios of the monomers.

2. Copolymers with block and graft nature can be explored which may help to control the molecular properties in much higher degree.

3. Efforts should be made for the introduction of organically soluble comonomer in the copolymer backbone so that easily processable PBI can be achieved.

4. The proton conduction behaviors and fuel cell efficiency of the PA doped PBI copolymer membranes require attention.

5. Aggregation of PBI in various solvents can be studied. Effect of PBI molecular structure on the aggregation nature needs to be addressed.

6. Studied of thermoreversible gelation of varities of PBI many be initiated.

7. Finally, the proton conduction and fuel cell testing of the PA doped *m*-PBI membrane obtained from the *m*-PBI –PA gel can be studied.

Publications and Presentations

PUBLICATIONS

1. Tuning the Molecular Properties of Polybenzimidazole by Copolymerization, **Arindam Sannigrahi**, Dhamodaran Arunbabu, R. Murali Sankar, Tushar Jana, *J. Phys. Chem. B* **2007**, *111,* 12124-12132.

2. Monomer Structural Isomer Directed Polybenzimidazole Copolymerization and Their Properties, **Arindam Sannigrahi**, Sandip Ghosh, Sudhangshu Maity, Tushar Jana, *Polym. Chem.* (Revised Manuscript submitted).

3. Aggregation Behavior of Polybenzimidazole in Aprotic Polar Solvent, **Arindam Sannigrahi**, Dhamodaran Arunbabu, R. Murali Sankar, Tushar Jana, *Macromolecule.* **2007**, *40*, 2844-2851.

4. Thermoreversible Gelation of Polybenzimidazole in Phosphoric Acid, **Arindam Sannigrahi**, Dhamodaran Arunbabu, Tushar Jana, *Macromol. Rapid Commun.* **2006**, *27*, 1962-1967.

5. Detailed Insights of meta-Polybenzimidazole Thermoreversible Gelation in Phosphoric acid, **Arindam Sannigrahi**, Sandip Ghosh, Sudhangshu Maity, Tushar Jana, Communicated to *Macromolecules.*

6. Blends of Polybenzimidazole and Poly(vinylidene fluoride) for Use in a Fuel Cell, Dhamodaran Arunbabu, **Arindam Sannigrahi**, Tushar Jana, , *J. Phys. Chem. B* **2008**, *112,* 5305-5310.

7. How the Monomer Concentration of Polymerization Influences Various Properties of Polybenzimidazole: A case Study with Poly (4, $4^{/}$-diphenylether- $5,5^{/}$-

bibenzimidazole), **Arindam Sannigrahi**, Sandip Ghosh, Joseph Lalnuntluanga, Tushar Jana, *J. App. Polym. Sci*. **2009**, *111*, 2194-2203.

8. Role of Solvents Protic Character on the Aggregation Behavior of Polybenzimidazole in Solution, Sandip Ghosh, **Arindam Sannigrahi**, Sudhangshu Maity, Tushar Jana, *J. Phys. Chem. B* **2010***, 114,* 3122–3132.

9. Aggregation of meta-Polybenzimidazole in phosphoric acid, **Arindam Sannigrahi**, Sandip Ghosh, Sudhangshu Maity, Tushar Jana, manuscript under preparation.

10. Tuning the Particle Size and Charge Density of Cross linked Polystyrene Particles, Dhamodaran Arunbabu, **Arindam Sannigrahi**, Tushar Jana, *J. App. Polym. Sci.* **2008**, *108*, 2718-2725.

11. Photonic Crystal Hydrogel Material for the Sensing of Toxic Mercury Ion (Hg^{+2}) in Water, Dhamodaran Arunbabu, **Arindam Sannigrahi**, Tushar Jana, Communicated to *Advanced Functional Material.*

Note: Publications 1-5 are included in this thesis.

CONFERENCE PRESENTATIONS

1. Poster Presented on **"Thermoreversible Gelation of Polybenzimidazole in Phosphoric Acid" Polymer 2006**: *National Conference on Frontiers in Polymer Science and Technology,* February -**2006**, at Indian Association for the Cultivation of Science, Jadavpur, Kolkata, India.

2. Poster Presented on **"Imidazole Based Polymer for Fuel Cell Membranes"** *4th annual in-house symposium CHEMFEST-***2007** of the School of Chemistry, University of Hyderabad, Hyderabad, India.

3. Poster Presented on **"Tuning the Molecular Properties of Polybenzimidazole by Copolymerization for use in Fuel Cell"** *Poly 2008: International Conference on Advances in Polymer Science and Technology*, January 28-31, **2008**, at Indian Institute of Technology, New Delhi, India.

4. Oral presentation on Dr. K. V. Rao 8th Annual Research Award, Hyderabad, March **2008**. "**Novel Polybenzimidazole Membranes for Fuel Cell Applications.**

5. Poster Presented on **"Tuning the Molecular Properties of Polybenzimidazole by Copolymerization for use in Fuel Cell"** *6th annual in-house symposium CHEMFEST* **2009** of the School of Chemistry, University of Hyderabad, Hyderabad, India.

6. Oral Talk and poster presented on "**Synthesis of Polybenzimidazole Copolymers: Isomeric Effect of Pyridine Monomers**" *7 th annual in-house symposium CHEMFEST* **2010** of the School of Chemistry, University of Hyderabad, Hyderabad, India.